STUDIES ON THE STRUCTURES AND PROPERTIES OF BIMETALLIC

URANIUM TRANSITION METAL AND HYBRID

ORGANIC-INORGANIC COMPOUNDS

Except where reference is made to the work of others, the work described in dissertation this is my own or was done in collaboration with my advisory committee. This dissertation does not include proprietary or classified information.

_____

Yaqin Yu

Certificate of Approval:

_____	_____
Andreas J. Illies Professor Chemistry and Biochemistry	Thomas E. Albrecht-Schmitt, Chair Professor Chemistry and Biochemistry
_____	_____
Wei Zhan Assistant Professor Chemistry and Biochemistry	Christian R. Goldsmith Assistant Professor Chemistry and Biochemistry

_____

George T. Flowers
Dean
Graduate School

STUDIES ON THE STRUCTURES AND PROPERTIES OF BIMETALLIC URANIUM TRANSITION METAL AND HYBRID ORGANIC-INORGANIC COMPOUNDS

Yaqin Yu

A Dissertation

Submitted to

the Graduate Faculty of

Auburn University

in Partial Fulfillment of the

Requirements for the

Degree of

Doctor of Philosophy

Auburn, Alabama
August 10, 2009

STUDIES ON THE STRUCTURES AND PROPERTIES OF BIMETALLIC

URANIUM TRANSITION METAL AND HYBRID

ORGANIC-INORGANIC COMPOUNDS

Yaqin Yu

_____
Signature of Author

_____
Date of Graduation

DISSERTATION ABSTRACT

STUDIES ON THE STRUCTURES AND PROPERTIES OF BIMETALLIC URANIUM TRANSITION METAL AND HYBRID ORGANIC-INORGANIC COMPOUNDS

Yaqin Yu

Doctor of Philosophy, August 10, 2009
(M.S., Fujian Normal University, 2001)
(B.S., Fujian Normal University, 1998)

240 Typed Pages

Directed by Thomas E. Albrecht-Schmitt

Hydrothermal synthetic methods have been utilized to synthesize many compounds containing both uranium and transition metals, as well as hybrid organic-inorganic materials. These compounds are found to adopt zero-, one-, two- and three-dimensional structural typologies. Of the 22 compounds covered in this dissertation, seven (31.8%) are based upon sheets of polyhedra, two (9.1%) are based upon chains of polyhedra, and three (13.6%) are based upon limited cluster polyhedra. There are ten (45.5%) structures based upon three-dimensional frameworks. Single crystal diffraction experiments reveal

that the seven sheet structures contain transition metal cations (Ag^{+}, Co^{2+}, Mn^{2+}, Cu^{2+}). The ten three-dimensional frameworks contain transition metal substructures (Ag^{+}, Hg^{2+}, Ni^{2+}, Co^{2+}, Zn^{2+}), metal-organic framework (MOF) structures and porous low-valence uranium framework.

There are two chain structures containing bimetallic metal-organic hybrids and single metal-organic hybrids. Three limited polyhedra structures contain mononuclear and binuclear clusters are also described. All structures were determined through the use of single crystal X-ray diffraction with the aid of EDAX and X-ray powder diffraction analysis. Addition characterization includes Raman spectroscopy, fluorescent spectroscopy, ion-exchange, and thermal stability.

ACKNOWLEDGEMENTS

Although there are many people that I feel that I need to thank for their help during this work, I wish to first thank the Department of Energy, Heavy Elements Program, for providing the funding for this research. I could not have imagined working for a better, more understanding, or friendlier person than Thomas Albrecht-Schmitt. The entire process could have been excruciating without him. I wish to thank my parents for their love and support throughout all of this. The peoples that I have worked together in Lab, Tanya, Jin, Lin, Travis, Anna, Andrea, have given me valuable hands. The classmates that I have studied together, Wu, Sun, Chen, Li, have made my years at Auburn bearable, with a few nights at library that were way too much fun. Most importantly, I appreciated lots of pioneers who made great contribution in this research area, Prof. Burns, Prof. Nakamoto, and Prof. Denning for their great work in uranium geochemistry and spectroscopy studies.

Style manual or journal used:

American Chemical Society

Computer softwares used:

Microsoft Word 2000, Microsoft Excel, Microcal Origin 6.0, Atoms v. 5.0, CorelDRAW 9

TABLE OF CONTENTS

LIST OF FIGURES

Chapter I: Reviews on the Uranyl Transition Metals, Organic Ligands Hybrid Materials and Low-valence Uranium Compounds

1.1 Introduction.

Compounds containing U^{6+} have been the focus of extensive research for many decades.[1-5] During the last 20 years, there has been a massive expansion in the structural chemistry of uranium,[5-8] as shown in Figure 1.1.1 and Figure 1.1.2.[9] These materials exhibit fascinating and complex atomic arrangements between uranyl polyhedra and transition metals or organic ligands as well as polyhedra containing other higher-valence cations.[5,8,10-28] Current research concerning uranyl compounds is driven by the search for novel solids with important physical properties,[29-34] and their importance in the environment.[35-48]

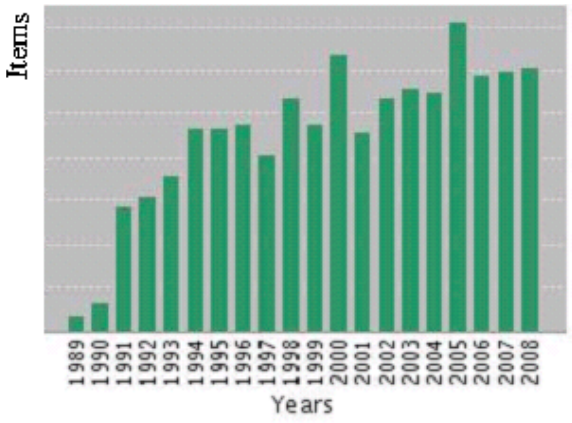

Figure 1.1.1. Published items in each year.

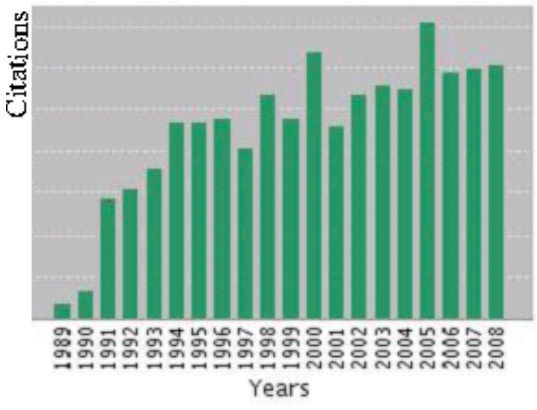

Figure 1.1.2. Citations in each year.

They are significant reasons for understanding water-rock interactions for U-rich minerals because this impacts the mobility of actinides in the environment especially at sites like the Hanford and Svanna River in the U. S. A. [5] Precipitation of uranyl phosphate minerals in the vadose zone of contaminated sites by the addition of phosphate has been proposed as a means to mitigate U^{6+} plums in groundwater.[45,47,48] Uranyl mineral can be bio-precipitated provide sources of phosphate for biological consumption, as well as redox-active U to serve as an electron acceptor needed for metabolism for bacteria.[49] Uranyl minerals are important products of alteration of nuclear waste forms under simulated conditions of geological repositories, in Yucca Moutain, Nevada.[3,5,48,50]

Almost all U^{6+} in crystal structures contain an approximately linear UO_2^{2+} uranyl ion.[51,52] The formal valence of the uranyl ion is 2+, so it must be coordinated by anions in a stable crystal structure. The uranyl ion is typically coordinated by four, five or six ligands, arranged at the equatorial vertices of square, pentagonal and hexagonal bipyramids, respectively. [2-5,53] The bipyramids are capped by the O atoms of the uranyl ions.

Burns *et. al*. provided U^{6+}-O bond-length and uranyl ion bond-angle data for ~100 crystal structures.[4,5] The bond and angle distribution for uranyl polyhedra have been revised to incorporate data for most of uranyl minerals have been provided by Burns et. al.[2,5,8,53] Using the bond-valence parameters provided by Burns et. al., the crystal bond-valences of the U^{6+}-O_{Ur} and U^{6+}-O_{eq} bonds of each coordination polyhedron are: U^{6+}-O_{Ur} = 1.59 valence units (*vu*). U^{6+}-O_{eq} = 0.71 *vu*, U^{6+}-O_{Ur} = 1.64 *vu*, U^{6+}-O_{eq} = 0.53 *vu*, U^{6+}-O_{Ur} = 1.67 *vu*, U^{6+}-O_{eq} = 0.44 *vu*. These values are consistent with extensive linkage of uranyl polyhedra through equatorial ligands, either with other uranyl polyhedra or other

polyhedra containing higher-valence cations. The bond-valences incident upon the O_{Ur} atoms, due to the bond to U^{6+} alone, range from 1.59 to 1.67 *vu*. Thus, the apical (uranyl) vertices of the uranyl bipyramids are seldom shared with polyhedra containing higher-valence cations, as this would overbond the O position.[4,5,54] The two-dimensional polymerization of uranyl polyhedra mandated by the distribition of bond strengths within the polyhedra favors the formation of sheets of polyhedra.

In some cases, the solid state and solution chemistry of actinyl ions involves significant cation-cation interactions in which an O atom of an actinyl ion is also an equatorial ligand of a neighboring polyhedron.[22,55-61] The cation-cation designation arises from the formal valences of actinyl ions, both of which are cations. Such interactions are relatively common for Np^{5+}, but are rather unusually in the case of U^{6+}.[55,57]

1.2 Structure Hierarchy of uranyl minerals.

Structures naturally fall into five categories corresponding to isolated polyhedra, finite clusters of polyhedra, chains of polyhedra, sheets of polyhedra, and frameworks of polyhedra.

1.2.1 Structures containing zero-dimensional polyhedra constructed from $[(UO_2)(XO_4)_4]$.

In isolated polyhedra structures, there are no direct linkages between the U^{6+} polyhedra.[2,62-67] There are 43 compounds based upon finite clusters of polyhedra of higher bond-valence.[2-4,53] A uranyl square bipyramid shares each equatorial vertex with a

different tetrahedron in the cluster with composition $[(UO_2)(XO_4)_4]^{68\text{-}71}$ shown in Figure 1.2.1.

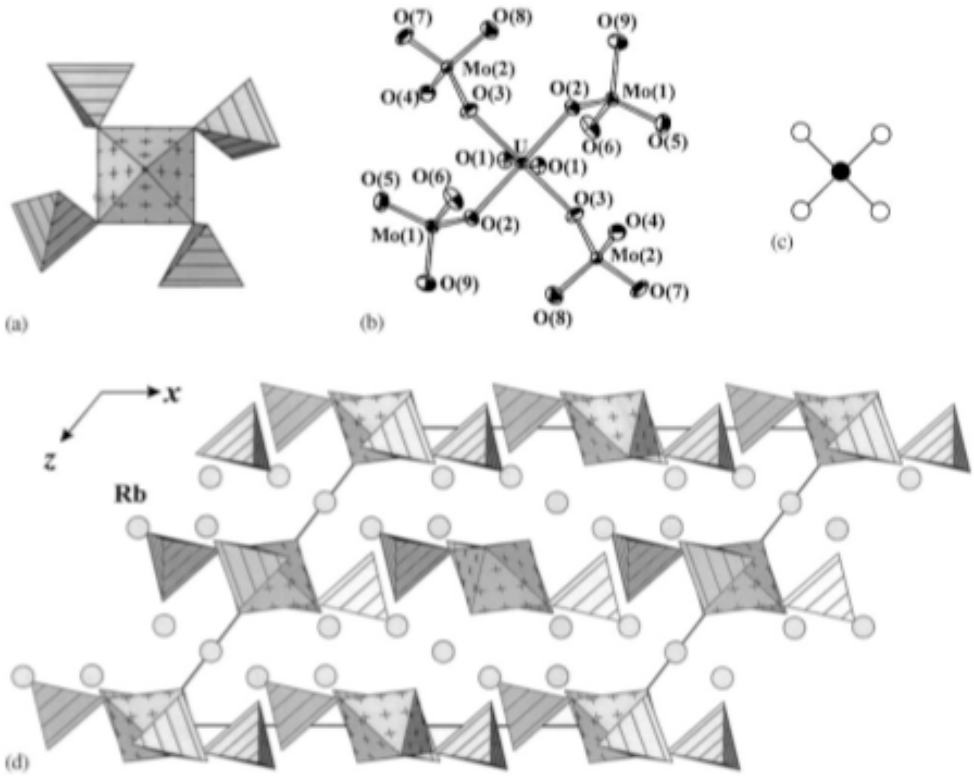

Figure 1.2.1. The $[(UO_2)(MoO_4)_4]^{6-}$ cluster shown in polyhedra representation (a) ball-and-stick representation, (b) (ellipsoids are drawn at the 50% probability level), and (c) nodal representation (insets: U=black, Mo=white). (d) Projection of the structure of $Rb_6[(UO_2)(MoO_4)_4]$ along [010]. Uranyl and molybdate polyhedra are shaded with crosses and parallel lines, respectively.

This cluster was recently found in three compounds, with the X cation being Mo^{6+} in two structures and Cr^{6+} in the other. A more complex uranyl molybdate cluster composed of two uranyl pentagonal bipyramids and eight MoO_4 tetrahedra is kown from $Na_6[(UO_2)(MoO_4)_4]$ and $Na_3Tl_3[(UO_2)(MoO_4)_4]$.[68] Each equatorial ligand of each uranyl

pentagonal bipyramid is shared with a tetrahedron, and two tetrahedra provide a bridge between the uranyl pentagonal bipyramids. A remarkable cluster of uranyl pentagonal bipyramids and sulfate tetrahedra occurs in $Na_6[(UO_2)(SO_4)_4](H_2O)_2$, $Na_{10}[(UO_2)(SO_4)_4](SO_4)_2(H_2O)_3$, and $KNa_5[(UO_2)(SO_4)_4](H_2O)$ (shown in Figure 1.2.2).[72-74] One sulfate tetrahedron shares an edge with the bipyramid, a connectivity that had not been previously observed in hydrous uranyl sulfate. Three additional sulfate tetrahedra are linked to the other three equatorial vertices of the bipyramid. The sharing of edges between polyhedra containing U^{6+} and S^{6+} cations presumably entails significant cation-cation repulsion.

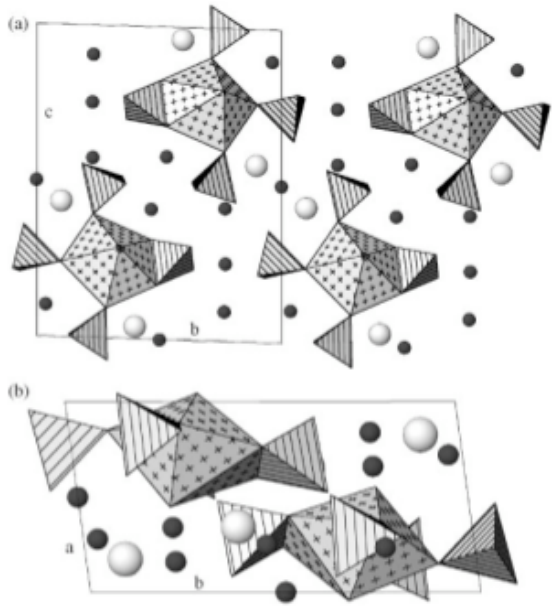

Figure 1.2.2. Polyhedra representations of the structure of the $[(UO_2)(SO_4)_4]^{6-}$ anion.

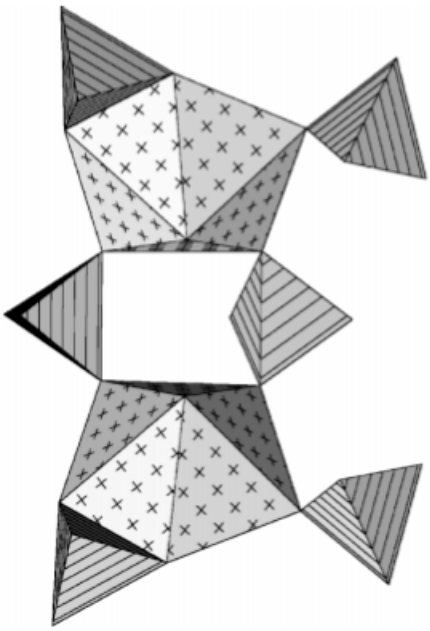

Figure 1.2.3. Crystal structure of $K_4[(UO_2)(SO_4)_3]$.

The structure of the anhydrous compound $K_4[(UO_2)(SO_4)_3]$ possesses a remarkable cluster, in which two uranyl pentagonal bipyramids are bridged by sharing vertices with two sulfate tetrahedra, and each bipyramid also shares an additional vertex with another

sulfate tetrahedron, and an edge with a fourth sulfate tetrahedron, as shown in Figure 1.2.3.[72] This is the only example in which a sulfate tetrahedron shares an edge with a uranyl bipyramid. This phase was grown at elevated temperature, and its stability under ambient conditions is uncertain.

1.2.2 Structures containing infinite chains of polyhedra constructed from $[(UO_2)(XO_4)]$.

The remarkable expansion of this structural class is largely attributable to research focused on understanding linkages between uranyl polyhedra and tetrahedra containing Mo^{6+}, S^{6+} or Cr^{6+}, as well as various polyhedra containing cations with a stereoactive lone-electon pairs such as Se^{4+} and I^{5+}, which occur in 16 of the new structures.[2-5,53] Thirty-nine structures containing uranyl polyhedra and any of the lone-pair stereoactive cation Te^{4+}, Se^{4+} and I^{5+} are known. [2-5]

The chains contain either uranyl square bipyramids or pentagonal bipyramids and each is four-connected within the chain as shown in Figure 1.2.4. Bipyramids are linked through either tetrahedra or pyramids, each of which is two-connected within the chain. The chain structure in Figure 1.2.4 constructs from either arsenate, molybdate, or phosphate tetrahedra.[75]

Uranyl pentagonal bipyramids are bridged through two tetrahedra by the sharing of vertices, such that four equatorial vertices of the bipyramids are also tetrahedra vertices of bridging (two-connected) tetrahedra. The fifth equatorial vertex of the bipyramid is shared with a non-bridging tetrahedron that decorates the side of the chain.

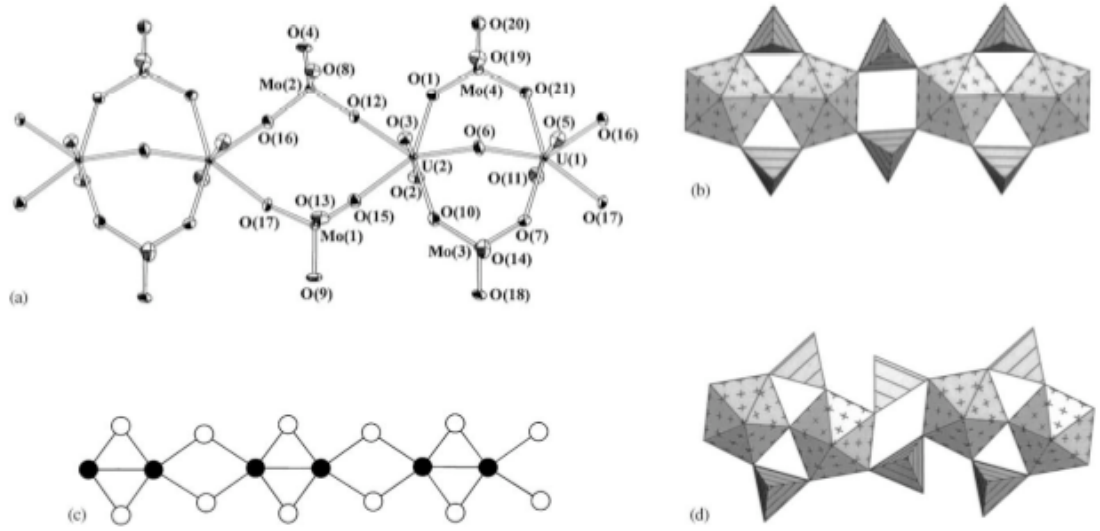

Figure 1.2.4. The $[(UO_2)_2O(MoO_4)_4]^{6-}$ chain in the structure of $Rb_6[(UO_2)_2O(MoO_4)_4]$. (a) ball-and-stick representation (ellipsoids are drawn at the 50% probability level), (b) polyhedra representation, (c) nodal representation (insets: U=black, Mo=white). (d) The $[(UO_2)_2O(MoO_4)_4]^{6-}$ chain in the structure of $Na_6[UO_2)_2O(MoO_4)_4]$.

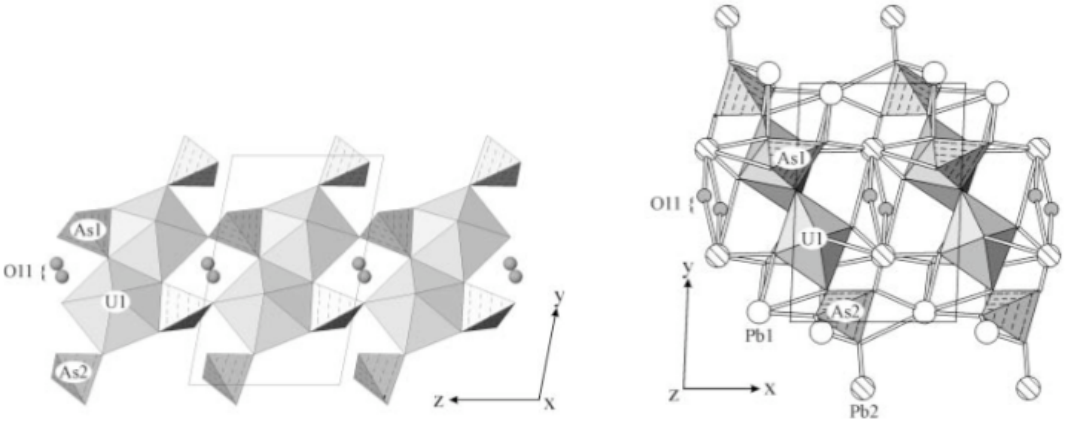

Figure 1.2.5. Anion topologic structure of parsonsite and hallimondite.

The chain structures shown in Figure 1.2.5 are from the structures of parsonsite[2,5,8] and hallimondite,[76] and are composed of uranyl pentagonal bipyramids and phosphate or arsenate tetrahedra. Bipyramids share an edge, forming a dimer, and dimers are linked into chains by sharing edges and vertices with tetrahedra. Additional tetrahedra decorate the edge of the chains by sharing vertices with the polyhedra.

1.2.3 Structures with infinite sheets of polyhedra with the Autunite anionic topology, expanded Autunite topology, zippeite anion-topology, and phosphuranylite anion-topology.

The sheet anion-topology approach works well for most sheets that are dominated by the sharing of edges between polyhedra of higher bond-valence. However, sheets connected only by the sharing of vertices between polyhedra correspond to a series of complex anion-topologies that defy usefulness.

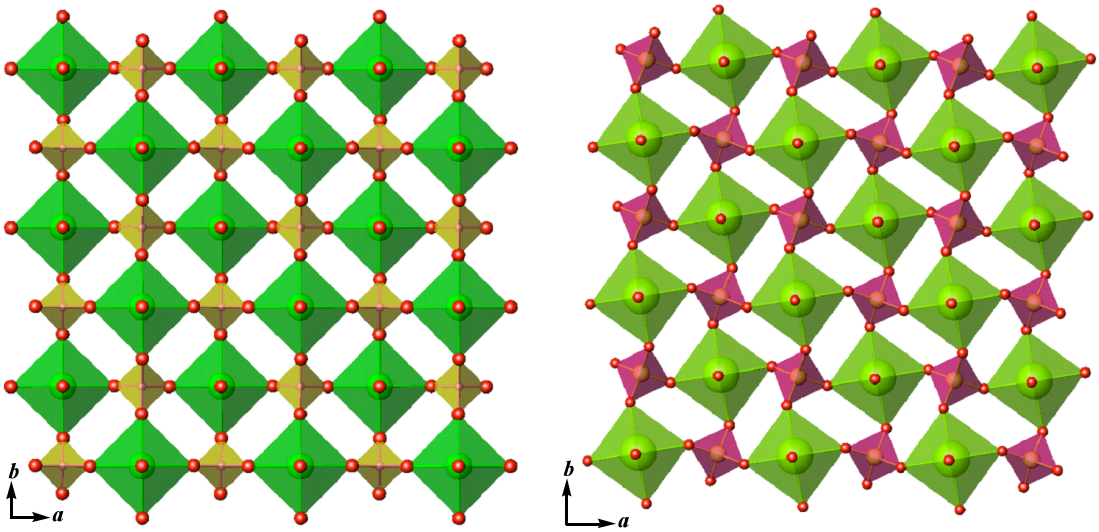

Figure 1.2.6. Meta-autunite and autunite anion topologic structures constructed from $[(UO_2)(XO_4)]^{2-}$ (X = P, As).

The {4,4,4,4} graph shown in Figure 1.2.6 corresponds to the autunite[2,3,5,51-53,77] and meta-autunite[51,78] anion-topology is formed by uranyl square bipyramids and tetrahedra that are connected by sharing vertices, such that each bipyramid is connected to four tetrahedra, and each tetrahedron is linked to four bipyramids. Structures of the autunite and meta-autunite groups contain this sheet, with either phosphate or arsenate tetrahedra. The sheet is based upon the autunite anion-topology that is composed of squares that share vertices and edges.

The structure of $K_4[(UO_2)(PO_4)_2]$ contains the unusual sheet of uranyl square bipyramids and phosphate tetrahedra shown in Figure 1.2.7.[79] This sheet can be obtained from the autunite sheet by deleting every second bipyramid. The sheet contains twice as many tetrahedra as bipyramids, each bipyramid is linked through its equatorial vertices to four tetrahedra, but the tetrahedra are only connected to two bipyramids.

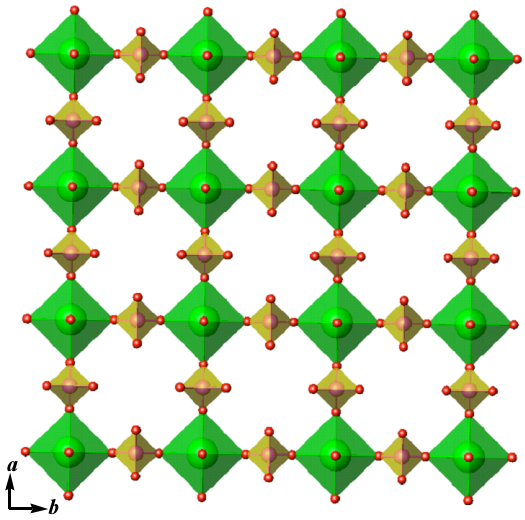

Figure 1.2.7. Expanded autunite anion topologic structure constructed from $[(UO_2)(PO_4)_2]^{4-}$.

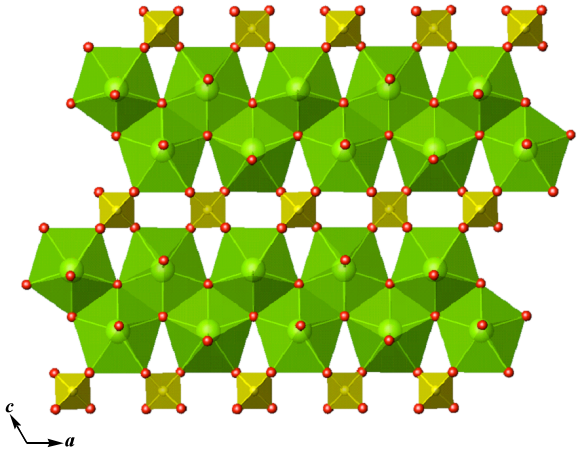

Figure 1.2.8. Zippeite anion-topology constructed from $[(UO_2)_4(SO_4)_2O_4]^{4-}$.

The zippeite anion-topology and corresponding sheet are shown in Figure 1.2.8.[2,3,5,53,80] The sheet contains zig-zag chains of edge-sharing uranyl pentagonal bipyramids, and the chains are connected by the sharing of vertices between the bipyramids and sulfate tetrahedra, such that each sulfate tetrahdron is linked to four different bipyramids, Vochten et. al. reported the first structure of a zippeite-structure material for the synthetic analogue of zippeite, the K-bearing mineral.[81] Although the uranyl sulfate sheets are topologically identical in each zipperte-group structure studied, the sheets in some are anhydrous, whereas in other they may contain hydroxyl groups located at equatorial vertices of the uranyl pentagonal bipyramids. The interlayer configurations of zippeite-group phases are diverse, and include either monovalent or divalent cations as well as H_2O groups.[5,81]

The uranophane anion-topology is elegant in its simplicity (Figure 1.2.9).[3-5,82] It contains chains of edge-sharing pentagons that are separated by chains of edge-sharing triangles and squares. This anion topology is the basis for the chemically diverse uranophane minerals. In all but two of the representative structures, the pentagons are populated by uranyl ions, giving pentagonal bipyramids. In the case of ulrichite, half of the pentagons are populated by Ca, and half of the pentagons contain Na in $Na_{5.5}(UO_2)_3(H_{0.5}PO_4)(PO_4)_3$, but the Na is not considered to be part of the structure.[83]

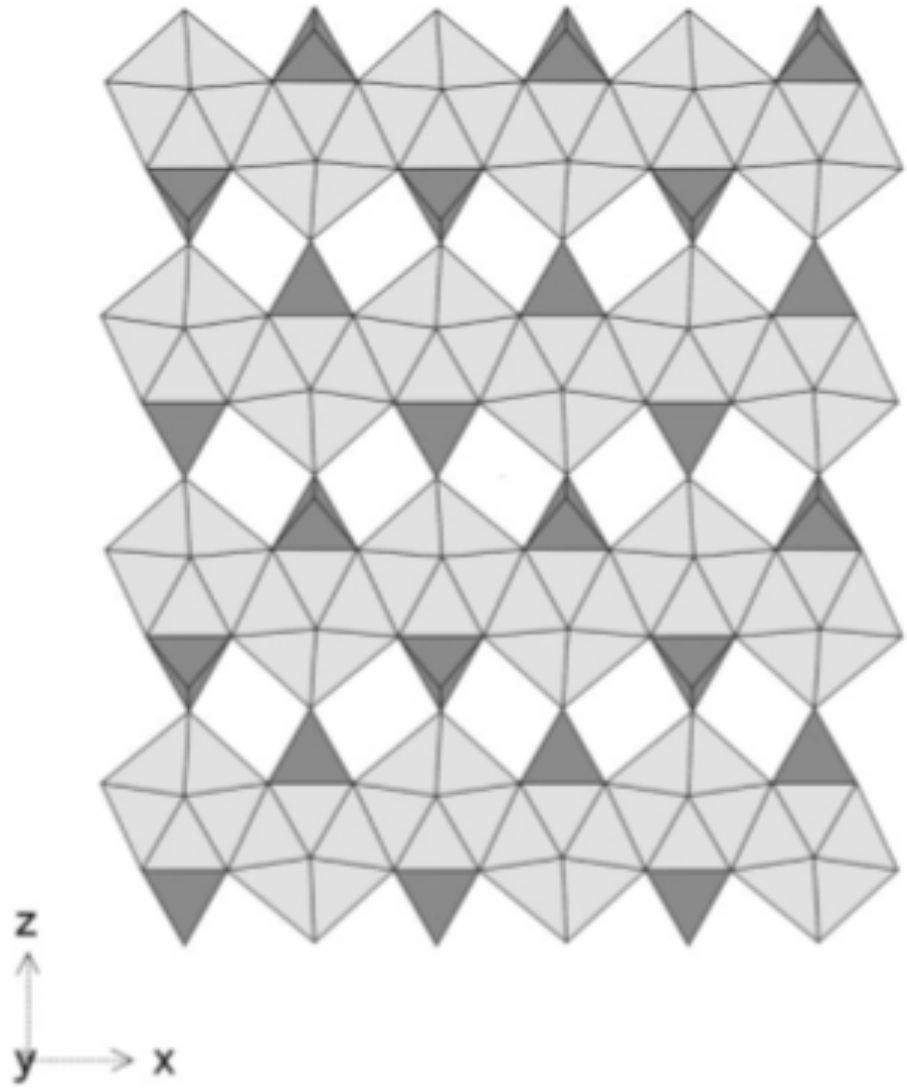

Figure 1.2.9. The uranophane anion-topology constructed from $(UO_2)_3(PO_4)_2(H_2O)_4$.

Phosphuranylite,[84] Upalite,[85] Françoisite-(Nd),[86] Dewindtite,[87] Vanmeersscheite,[88] Dumontite,[89] Hügelite,[90] Phurcalite,[91] Phuralumite,[92] Althupite,[93] Bergenite,[94] and Fontanite[95] share a common anion-topology, shown in Figure 1.2.10, contain pentagons that share edges, resulting in dimers, which are in turn linked into chains by sharing edges with hexagons.[5] These chains are linked through chains of edge-sharing triangles and squares, arranged such that the triangles and squares alternate along the chain length.

Several populations of this anion topology are known, but none involve occupancy of the square sites. In most cases, both the pentagonal and hexagons are populated by uranyl ions, resulting in chains of edge-sharing pentagonal and hexagonal bipyramids. Population of the triangles of the anion topology by phosphate tetrahedra, such that a face of the tetrahedron corresponds to the triangle of the topology, results in the uranyl phosphate sheets of the phosphuranylite group. Along the side of a chain of uranyl polyhedra, the tetrahedra alternate up and down.

The interlayers of the structures of minerals of the phosphuranylite group are complex, and some contain more than one type of cation, as well as H_2O groups. The structures of phosphuranylite and vanmeersscheite are unusual in that both contain uranyl ions in all three common coordination modes square bipyramids are located between the sheets in each structure, with the uranyl ions extending roughly parallel to the sheets. In phosphuranylite, all four of the equatorial ligands of the square bipyramid are apical vertices of the phosphate tetrahedra of sheets on either side. In contrast, the uranyl square bipyramid in the vanmeersscheite interlayer shares vertices only two phosphate tetrahedra, one from each adjacent sheet. Linkage of the uranyl phosphate sheets through interlayer uranyl polyhedra results in open three-dimensional structures in phosphuranylite and vanmeersscheite.

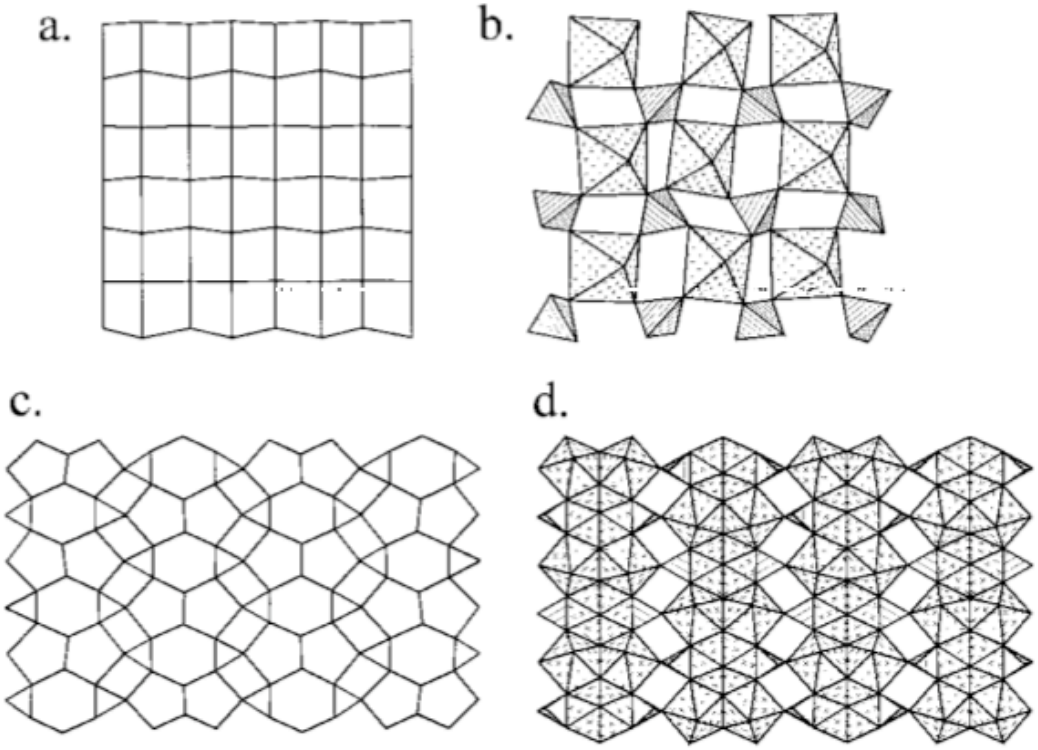

Figure 1.2.10. Uranyl phosphate sheets that are common in minerals. (a) autunite anion-topology, (b) autunite-type sheet, (c) phosphuranylite anion-topology, (d) phosphuranylite-type sheet. The uranyl polyhedra and phosphate tetrahedra are shaded with crosses and parallel lines, respectively.

1.2.4 Framework of uranyl pentagonal bipyramids and phosphate, arsenate tetrahedra.

The compounds $[(UO_2)_3(PO_4)_2](H_2O)_4$,[29] $(UO_2)[(UO_2)(AsO_4)]_2(H_2O)_4$,[96] and $(UO_2)[(UO_2)(AsO_4)]_2(H_2O)_5$,[97] each contain topologically identical sheets of uranyl pentagonal bipyramids and tetrahedra, shown in Figure 1.2.11. The sheet is based upon the uranophane anion-topology (Figure 1.2.9), but is a novel graphical isomer.[82] Note that all of the tetrahedra that share edges with bipyramids of any given chain of bipyramids are oriented in the same direction. In all four structures, adjacent sheets are connected through uranyl pentagonal bipyramids located between the sheets, resulting in

frameworks. Each of the bipyramids between the sheets shares one of its equatorial vertices with a tetrahedron in the sheets, resulting in frameworks. Each of the bipyramids between the sheets shares one of its equatorial vertices with a tetrahedron in the sheet on either side, and the remaining three equatorial vertices are H_2O. In cases of $[(UO_2)_3(PO_4)_2](H_2O)_4$ and $(UO_2)[(UO_2)(AsO_4)]_2(H_2O)_4$, the sheets of polyhedra are relatively flat. In the case of $(UO_2)[(UO_2)(AsO_4)]_2(H_2O)_5$, the sheets are strongly corrugated.

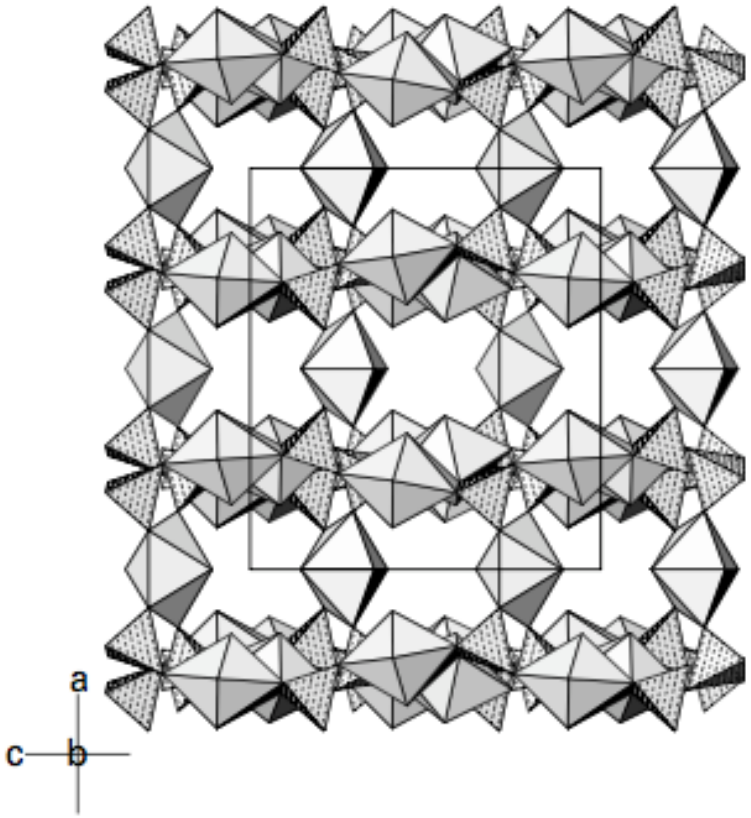

Figure 1.2.11. Polyhedra representation of the structure of $(UO_2)[(UO_2)(PO_4)]_4^{2-}$ projected along [010]. The uranyl polyhedra are shown in shades of gray and the phosphate tetrahedra are stippled.

The compounds $Cs_2(UO_2)[(UO_2)(PO_4)]_4(H_2O)_2$, $Rb_2(UO_2)[(UO_2)(PO_4)]_4(H_2O)_2$, $K_2(UO_2)[(UO_2)(PO_4)]_4(H_2O)_2$, $Cs_2(UO_2)[(UO_2)(AsO_4)]_4(H_2O)_2$, and

$Rb_2(UO_2)[(UO_2)(AsO_4)]_4(H_2O)_{4.5}$ possess homotypic framework structures.[98,99] Each has sheets of uranyl pentagonal bipyramids and tetrahedra that are based upon the underlying uranophane anion-topology graphical isomer as found in ß-uranophane. Adjacent sheets are connected into a framework by sharing vertices with uranyl pentagonal bipyramids located between the sheets. Each interlayer bipyramid shares four of its equatorial vertices with tetrahedra, two from each of the adjacent sheets. The remaining equatorial vertex of the bipyramid is H_2O. The low-valence cations and additional H_2O are located in channels extending through the framework.

1.2.5 Nanoparticals and nanospheres constructed from uranyl selenates.

Nanostructure materials exhibit important properties with promise for many potential applications.[100-104] Such materials also provide unique opportunities to study fundamental structure-property relationships, and the properties of many nanoscale materials are measurably particle-size dependent.[105-107] Following the discovery of carbon nanotubes, considerable attention has also been devoted to synthesizing a range of oxidic nano materials formed by linear UO_2^{2+}, which also have tremendous potential in materials applications.[22,54,61,108,109] Prior to 2005, no materials have been reported with nanoscale aggregates or tubules of higher-valence actinide ions.

Burns et. al. described an unprecedented family of actinyl peroxide nanoclusters.[108] These chemically and structurally elegant spherical clusters were obtained from alkaline solutions containing peroxide under ambient conditions. The clusters are assembled from topologically identical uranyl peroxide polyhedra with the clusters. Burns et. al. provided evidence for the self-assembly and persistence of the some of these clusters in alkaline

solutions, prior to crystallization in complex molecular crystals.[54,108] The assembly and persistence of these nanoclusters in solution suggest that they may influence the mobility of actinides in the environment, such as where highly alkaline nuclear wastes leak into the vadose zone. The complexity of the clusters, which constitute a new class of polyoxometalates, is in sharp contrast to other cluster of cation polyhedra of higher bond-valence in uranyl compounds that are illustrated in Figure 1.2.11.

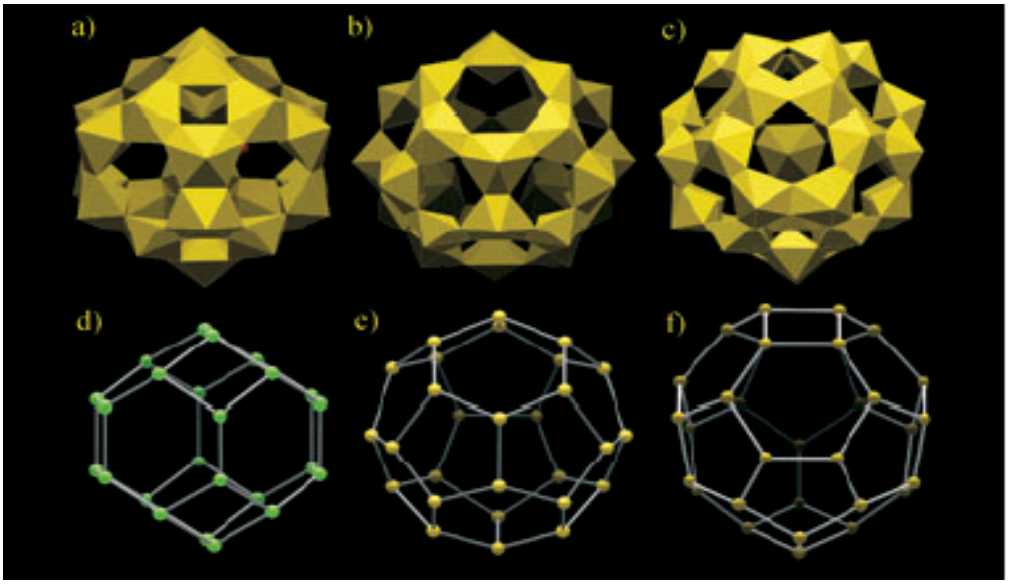

Figure 1.2.12. Polyhedra representations of actinyl peroxide nanoclusters found in a) U-24 and Np-24. b) U-28, and c) U-32 and Ac-Ac connectivity diagrams for d) Np-24, e) U-28 and f) U-32.

Krivovichev et. al. reported the synthesis and structures of two remarkable new uranyl selenate compounds that contain nanoscale tubules, shown in Figure 1.2.12.[61] In each case, uranyl pentagonal bipyramids share vertices with selenate tetrahedra, resulting in open sheets that are rolled into single-walled tubes, with external diameters of 17 and 25 Å, and inner crystallographically free diameters of 4.7 and 12.6 Å. This discovery presents the fascinating possibility that many of the myriad of sheets containing uranyl

polyhedra may be able to form nanoscale tubules.[22] The range of sheet topologies and compositions suggests many potential applications of such materials.

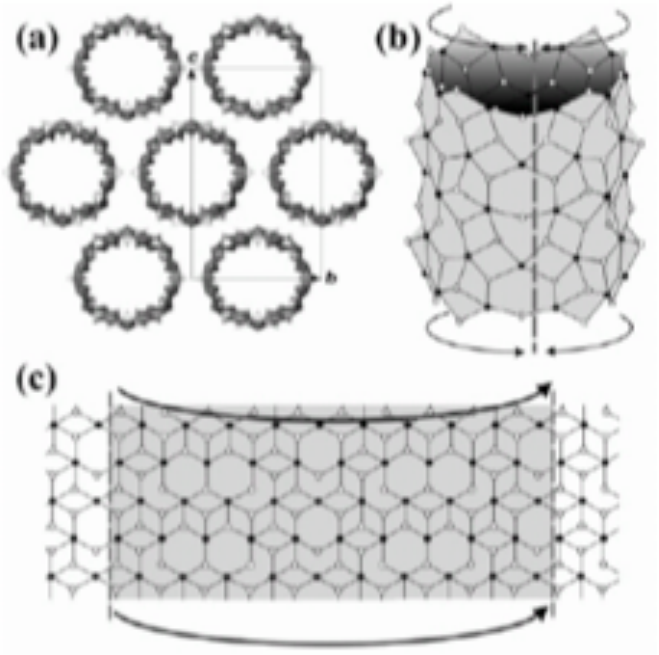

Figure 1.2.13. Crystal structure of $(C_4H_{12}N)_{14}[(UO_2)_{10}(SeO_4)_{17}(H_2O)]$ projected along [100].

1.3 Bimetallic Open-framework Compounds Constructed From Uranyl Phosphates.

Of late there has been an interest in preparing mixed-metal uranyl framework compounds that incorporate transition metals into the three-dimensional lattice.[110-113] A series of uranyl/M/phosphates (M = main group or transition metal) now exist that include the Ga^{3+} compounds $Cs[UO_2Ga(PO_4)_2]$ and $Cs_4[(UO_2)_2(GaOH)_2(PO_4)_4]\cdot H_2O$, which undergo selective ion-exchange of Cs^+ for alkaline-earth metal cations.[114] In addition there are several transition metal compounds including the nonstoichiometric

Cu^{2+} material, $Cs_{3+x}[(UO_2)_3CuH_{4-x}(PO_4)_5]\cdot H_2O$,[115] and the polar, V^{5+} solid, $Cs_2[(UO_2(VO_2)_2(PO_4)_2]\cdot 0.59H_2O$,[116] that shows nonlinear optical properties. Two mixed-metal phosphates have also been reported to contain octahedral Co^{2+} or V^{4+} in $Cs_2\{(UO_2)_4[Co(H_2O)_2]_2(HPO_4)(PO_4)_4\}$,[115] and $A_{3.48}[(UO_2)(VO)_4H_{1.52}(PO_4)_5]$ (A = K, Rb), respectively.[117] The latter compound has been shown to be a Cs^+-selective ion-exchange material and undergoes both antiferromagnetic and ferromagnetic ordering at low temperatures.

1.3.1 Compounds $Cs[UO_2Ga(PO_4)_2]$ and $Cs_4[(UO_2)_2(GaOH)_2(PO_4)_4]\cdot H_2O$.

The structure of $Cs[UO_2Ga(PO_4)_2]$ is three-dimensional,[114] being constructed from one-dimensional $[Ga(PO_4)]^{3-}$ gallium phosphate chains and one-dimensional uranyl phosphate chains, the former of which extend down the *a* axis. These gallium phosphate chains are formed from fused eight-membered rings of alternating corner-shared GaO_4 and PO_4 tetrahedra, shown in Figure 1.3.1.[114] The gallium phosphate and uranyl phosphate chains run approximately perpendicular to one another to create a three-dimensional $[UO_2Ga(PO_4)_2]^-$ framework with intersecting channels running down the *a* and *b* axis, one view of which is shown in Figure 1.3.2.[114]

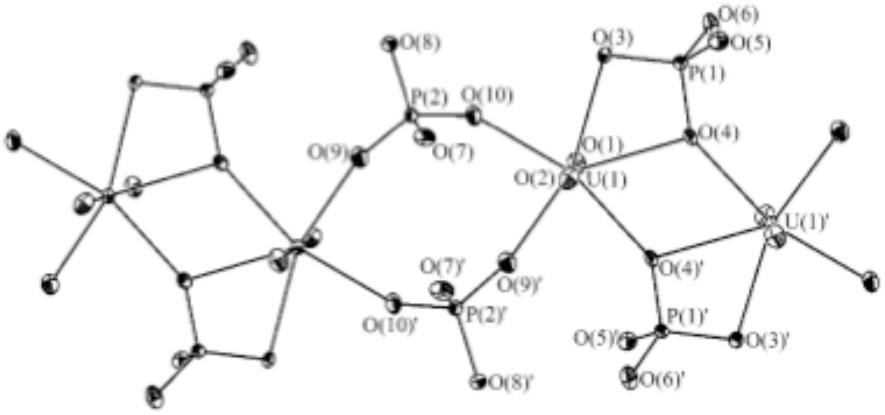

Figure 1.3.1. An illustration of the one-dimensional $[UO_2(PO_4)_2]^{4-}$ chains in $Cs[UO_2Ga(PO_4)_2]$.

The structure of $Cs_4[(UO_2)_2(GaOH)_2(PO_4)_4]\cdot H_2O$ was solved to reveal a three-dimensional framework of interconnected one-dimensional gallium phosphate and uranyl phosphate chains that run approximately perpendicular to one another. The gallium phosphate chain is composed of corner-sharing GaO_6 octahedra and bridging PO_4 tetrahedra that extend along the *c* axis, can be formulated as $[Ga(OH)(PO_4)_2]^{4-,}$ and are depicted in Figure 1.3.3.

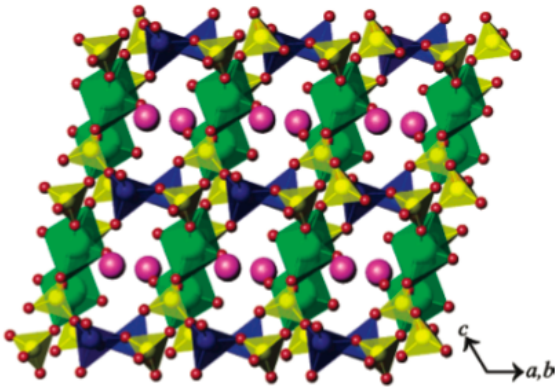

Figure 1.3.2. A depiction of the three-dimensional $[UO_2Ga(PO_4)_2]^-$ framework in $Cs[UO_2Ga(PO_4)_2]$ with intersecting channels running down the *a* and *b* axis.

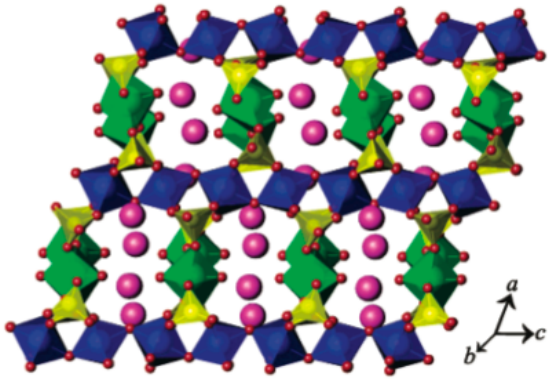

Figure 1.3.3. An illustration of the three-dimensional $[(UO_2)_2(GaOH)_2(PO_4)_4]^{4-}$ anionic lattice of $Cs_4[(UO_2)_2(GaOH)_2(PO_4)_4]\cdot H_2O$.

1.3.2 Compounds $Cs_2\{(UO_2)_4[Co(H_2O)_2]_2(HPO_4)(PO_4)_4\}$ and $Cs_{3+x}[(UO_2)_3CuH_{4-x}(PO_4)_5]\cdot H_2O$.

The interaction of the uranyl cations and phosphate units in $Cs_2\{(UO_2)_4[Co(H_2O)_2]_2(HPO_4)(PO_4)_4\}$ creates layers in the [*ab*] plane that are depicted in Figure 1.3.4.[115] This layer is a new topology for a uranium oxide. Other than the disordered phosphate anion, the phosphate units are approximately tetrahedra with normal P-O bond distances. The Co centers form dimers via two μ_3-oxo atoms from two phosphate anions. The presence of these octahedra building units stitches the structure

together into a three-dimensional framework where void spaces are filled by Cs^+ cations. There are channels in this structures that extend down in *b* axis, as is shown in Figure 1.3.5.

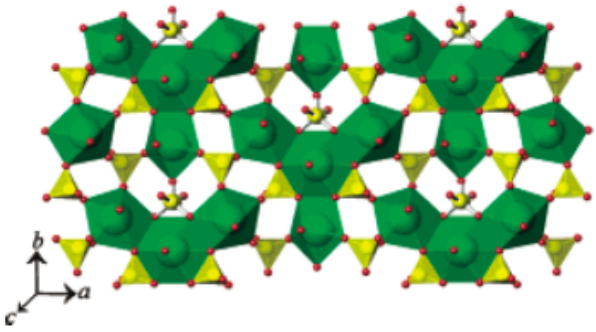

Figure 1.3.4. View down the *c* axis of the uranyl phosphate layers. One of the phosphate anions is disordered and is shown in ball-and-stick format. Uranium polyhedra are in green and phosphate in yellow.

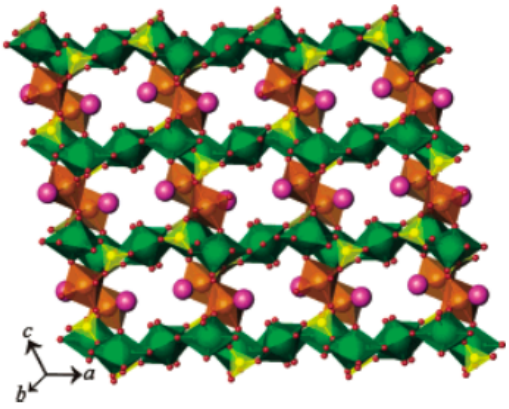

Figure 1.3.5. Illustration of the three-dimensional structure as viewed down the *b* axis. Uranium polyhedra are in green, phosphate in yellow, and cobalt in orange.

The uranyl moieties in $Cs_{3+x}[(UO_2)_3CuH_{4-x}(PO_4)_5]\cdot H_2O$ structure are bridged by phosphate anions into sinusoidal sheets that extend into the [*bc*] plane. These sheets are shown in Figure 1.3.6.[115] Again, this is apparently a new layered topology for a uranium oxide compound. The uranyl phosphate layers in $Cs_{3+x}[(UO_2)_3CuH_{4-x}(PO_4)_5]\cdot H_2O$ structure are interconnected by Cu centers that reside in square planar environments, being bound by four phosphate anions with two Cu-O bond distances. The overall structure is three-dimensional, as can be seen in Figure 1.3.7.

1.3.3 Compounds $Cs_2[(UO_2(VO_2)_2(PO_4)_2]\cdot 0.59H_2O$ and $A_{3.48}[(UO_2)(VO)_4H_{1.52}(PO_4)_5]$ (A = K, Rb).

The structure of $Cs_2[(UO_2(VO_2)_2(PO_4)_2]\cdot 0.59H_2O$ consists of uranyl cations bound by phosphate to yield UO_6 tetragonal bipyramids.[116] These units are bridged by phosphate to yield one-dimensional chains that run down the *c* axis. This basic one-dimensional topology is recognized to occur in several uranyl phases including $Cu_2[UO_2(PO_4)_2]$. The uranyl phosphate chains are fused with chains of corner-sharing VO_5 distorted square pyramids that run down the *b* axis into a novel open-framework structure. There are intersecting channels that occur along the *b* and *c* axes as is shown in Figure 1.3.8. The channels running down the *b* axis are approximately 5.5 × 10.9 Å, whereas those running down the *c* axis are 5.0 × 9.5 Å. These channels are occupied by Cs^+ cations and water molecules. One the most apparent features of this structure is that the VO_5 units are oriented so that the single terminal oxo atoms of these polyhedra are all alighed along the *c* axis. The fundamental building units are shown in Figure 1.3.9.

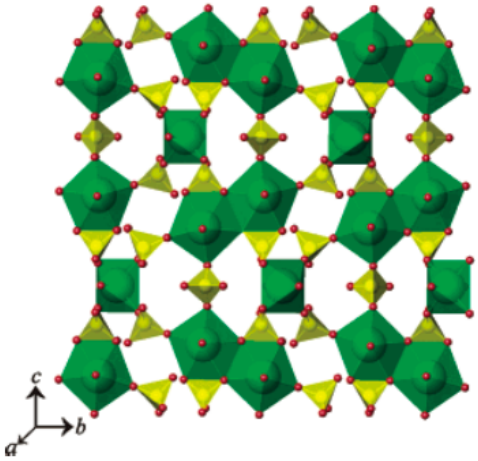

Figure 1.3.6. Depiction of uranyl phosphate layers. Uranium polyhedra are in green and phosphate in yellow.

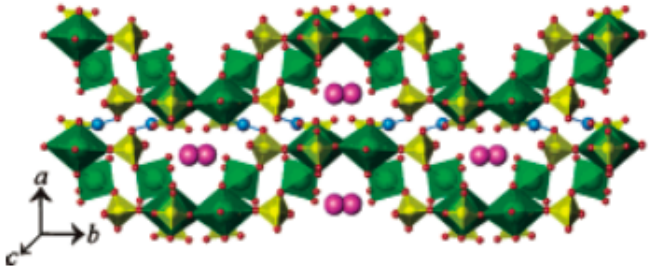

Figure 1.3.7. View of the three-dimensional structure wherein the Cu^{II} centers link uranyl phosphate layers together. Uranium polyhedra are in green, phosphate in yellow, and copper in blue. Some of the Cs^{+} sites have been omitted for clarity.

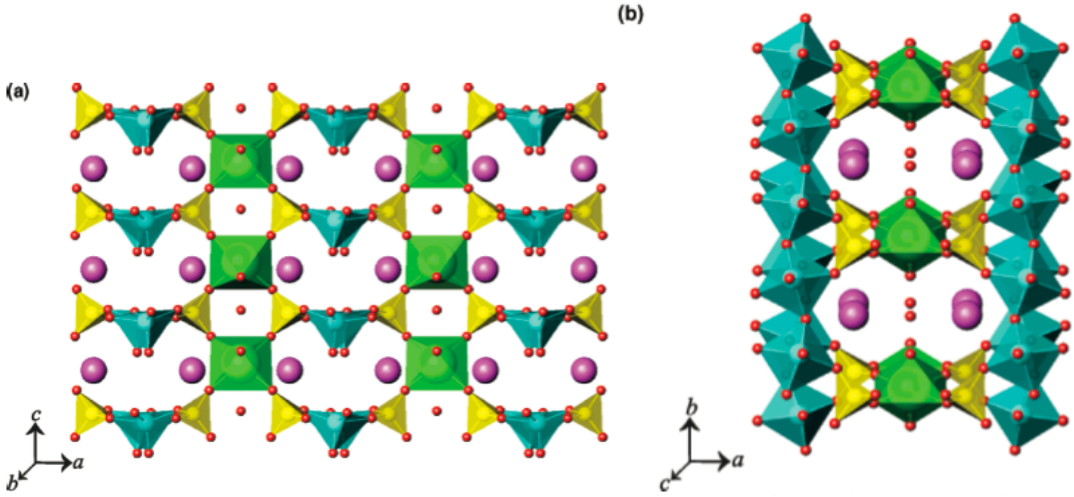

Figure 1.3.8. Two views of the structure of $Cs_2[UO_2(VO_2)_2(PO_4)_2]\cdot 0.59H_2O$ that consist of uranyl cations bound by phosphate (shown in yellow) to yield UO_6 tetragonal bipyramids (shown in green). These channels that occur along the *b* (a) and *c* (b) axis.

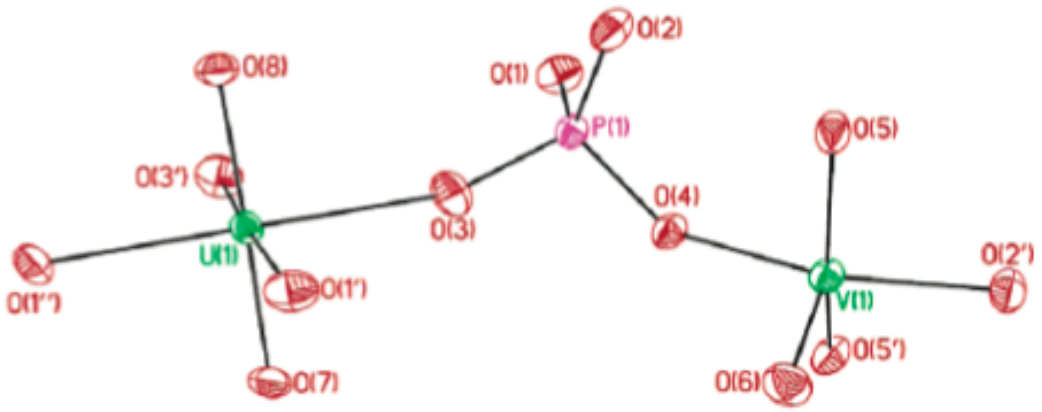

Figure 1.3.9. View of the fundamental building units in $Cs_2[UO_2(VO_2)_2(PO_4)_2]\cdot 0.59H_2O$.

The structures of $A_{3.48}[(UO_2)(VO)_4H_{1.52}(PO_4)_5]$ consists of two-dimensional vanadyl phosphate layers in the [*ab*] plane, depicted in Figure 1.3.10, that are joined by UO_6 tetragonal bipyramids in the *c* direction into a three-dimensional framework structure.[117] The structure has small channels extending down the *c*-axis that are filled by K^+/Rb^+ cations. The individual layers are complex and consist of distorted octahedra VO_6 units that share faces to form dimers, which are in turn bridged by phosphate anions into a 2D network.

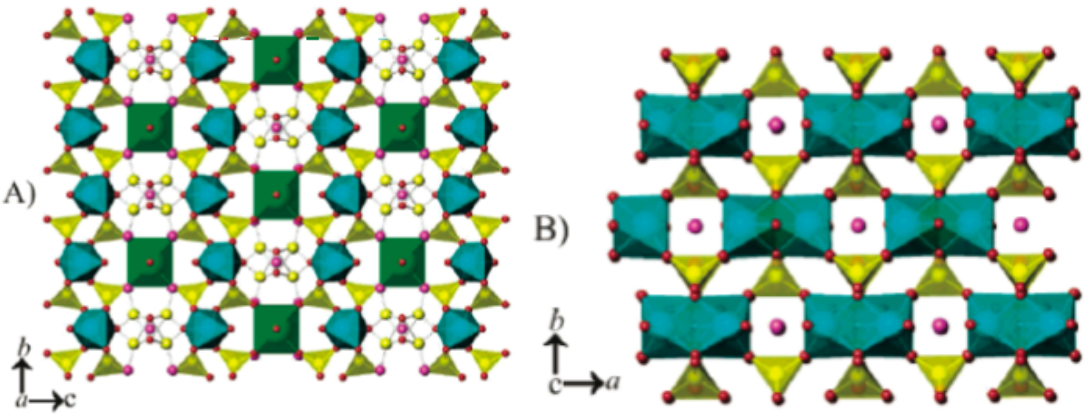

Figure 1.3.10. (a) View down the *a*-axis of two-dimensional vanadyl phosphate layers that extend in the [*ab*] plane (b) Depiction of the small channels that extend along the *c*-axis.

1.4 Metal-organic Frameworks Constructed From UO_2^{2+}.

A fundamental structural component of uranyl carboxylates is the linear UO_2^{2+} cation, a species that when coordinated to carboxylate groups forms square, pentagonal, or hexagonal bipyramids with polymerization occurring solely through the equatorial positions. The apical oxygen atoms (often referred to as the "uranyl oxygens") are bound to the central uranium atom only and show no tendency to bridge to other species. The maturity of uranyl carboxylate chemistry actually makes this system ideal for exploring structures of higher dimensionality (i.e., MOFs) as synthetic investigations can harness the local structural features and thus focus on polymerization efforts by employing multifunctional ligands.

1.4.1 Structures of novel zero-, one-, and two-dimensional uranium isonicotinate framework: $UO_2(C_5H_5NCO_2)(CH_3CO_2)_2$, $[UO_2F][C_5H_5NCO_2]$, $[UO_2F_3][C_5H_6NCO_2]\cdot 0.5H_2O$, and $[UO_2F_2]_2[C_5H_5NCO_2]\cdot H_2O$.

Compound $UO_2(C_5H_5NCO_2)(CH_3CO_2)_2$ is a molecular (zero-dimensional) phase consisting of UO_8 hexagonal bipyramids in which U^{VI} is coordinated by two acetate ligands and an isonicotinate ligand, shown in Figure 1.4.1.[118] Compound $[UO_2F][C_5H_5NCO_2]$ contains a one-dimensional structure with a uranium oxyfluoride chain built up from edge-sharing $[UO_3F_4]$ pentagonal bipyramid polyhedra, shown in Figure 1.4.2.[118] Compound $[UO_2F_3][C_5H_6NCO_2]\cdot 0.5H_2O$ exhibits another one-dimensional chain structure consisting of the edge-sharing chain of $[UO_2F_5]$ pentagonal bipyramids and a hydrogen-bonding network of isonicotinic acid, shown in Figure 1.4.3.[118] A single-crystal X-ray diffraction study of $[UO_2F_2]_2[C_5H_5NCO_2]\ ]\cdot H_2O$ revealed

a two-dimensional layered structure containing two unique uranium pentagonal bipyramids, shown in Figure 1.4.4.[118]

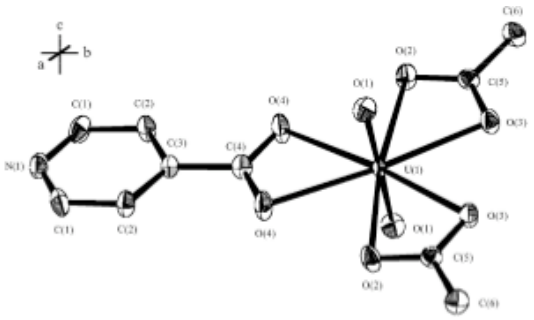

Figure 1.4.1. Thermal ellipsoid plot (50% probability) of $UO_2(C_5H_5NCO_2)(CH_3CO_2)_2$.

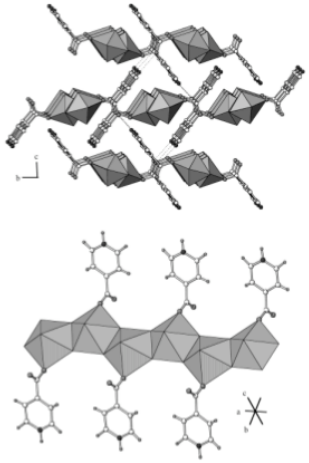

Figure 1.4.2. Crystal structure of $[UO_2F][C_5H_5NCO_2]$.

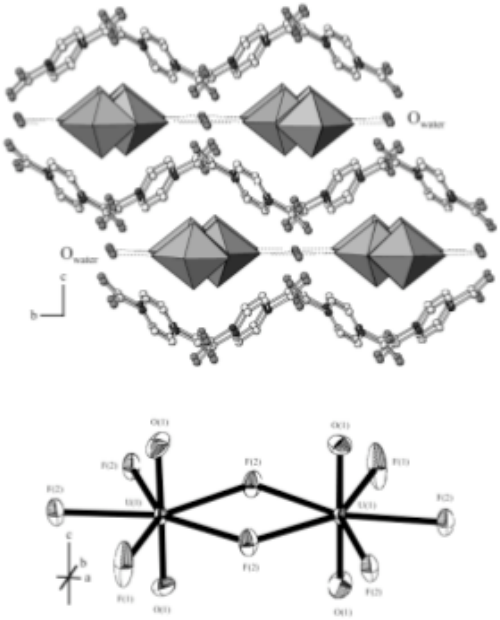

Figure 1.4.3. Crystal structure of $[UO_2F_3][C_5H_6NCO_2]\cdot 0.5H_2O$.

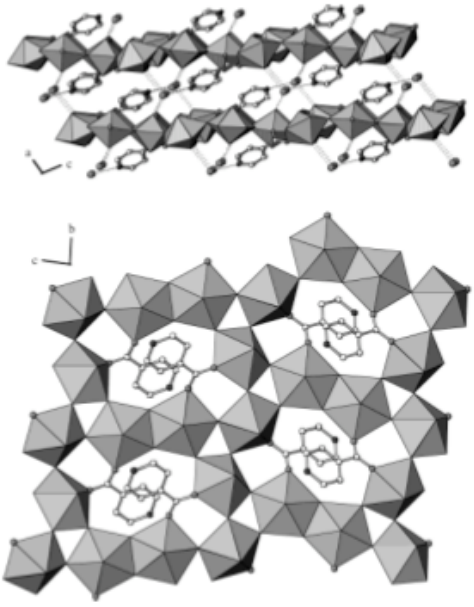

Figure 1.4.4. Crystal structure of $[UO_2F_2]_2[C_5H_5NCO_2]\ ]\cdot H_2O$.

1.4.2 Novel structures constructed from di- and tri- carboxylates ligands coordinated to UO_2^{2+}: $UO_2(opyca)_2$, uranyl-bis[(S)-lactate], $[(UO_2)_3(Hcit)_2(H_2O)_3] \cdot 2H_2O$, $[(UO_2)Na(tca)(H_2O)_4]$, $K[(UO_2)_3(\mu_3\text{-}OH)_3(\mu_2\text{-}OH)(C_7H_4O_4N)_2]OH$, $[UO_2(C_4H_4O_5)_2]^{2-}$, $UO_2(C_6H_8O_4)(H_2O)_2$, $UO_2(C_6H_8O_4)$, $[UO_2(C_4H_4O_4)] \cdot H_2O$, $[UO_2F(C_5H_6O_4)] \cdot 2H_2O$ and $[(UO_2)_{1.5}(C_8H_4O_4)_2]_2[(CH_3)_2NCOH_2] \cdot H_2O$.

The solid-state structure of $UO_2(opyca)_2$ has a slightly distorted pentagonal bipyramid as the local coordination geometry around each U atom center, defined by seven oxygen atoms from two carboxylate groups, two N-oxide, and two oxo groups.[119] Thus, there are two kinds of opyca ligands, one serves as tridentate spacer, and the other acts as bidentate linker. Overall each opyca ligand bridges two U atom centers, resulting in the formation of a 2D square grid network with dimensions of 10.07 × 10.04 Å, shown in Figure 1.4.5. The local coordination geometry around each U atom center in uranyl-bis[(S)-lactate can best be described as a distorted pentagonal bipyramid.[119] The coordination results in the formation of a 2D brick-wall type grid network with approximate dimensions of 3 × 6.04 Å, shown in Figure 1.4.6.

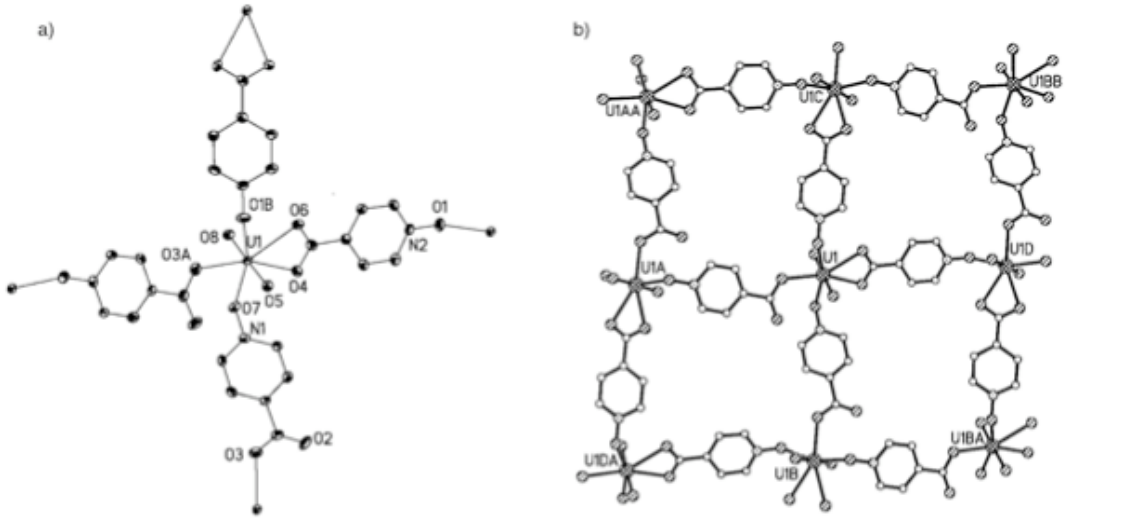

Figure 1.4.5. (a) An asymmetric unit of $UO_2(opyca)_2$ in which thermal ellipsoids are drawn at the 30% probability level; (b) a 2D square grid representation of $UO_2(opyca)_2$.

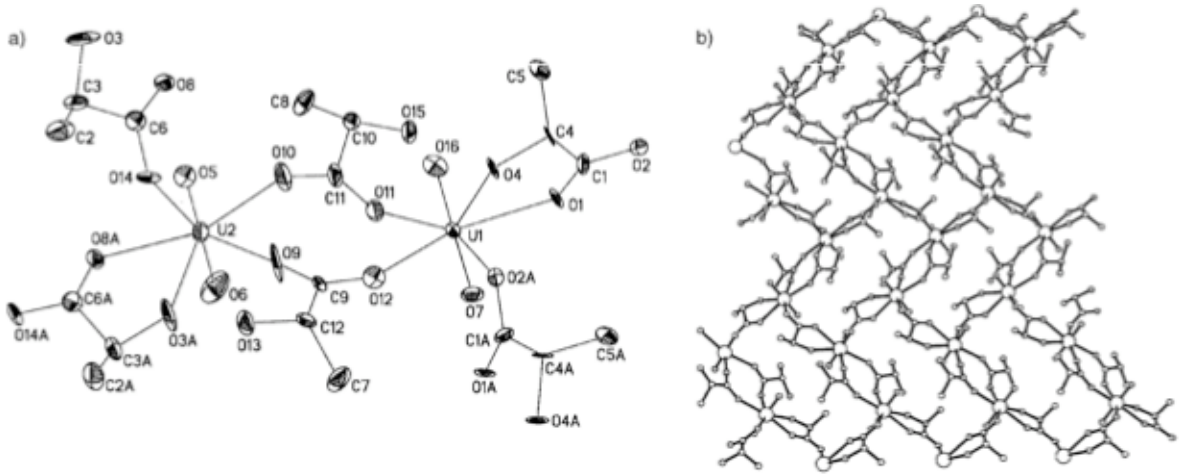

Figure 1.4.6. (a) An asymmetric unit of uranyl-bis[(S)-lactate] in which thermal ellipsoids are drawn at 30% probability level; (b) a 2D brick-wall representation of uranyl-bis[(S)-lactate].

The first crystal structure of uranyl citrate is reported, as well as that of uranyl sodium tricarboxylate; both compounds are polymeric, with all acid groups coordinated, but they are differ strongly in their coordination modes; the resulting assembly architecture is

either three-dimensional with $[(UO_2)_2(Hcit)_2]^{2-}$ metallacycle subunits with citrate or two-dimensional with tricarballylate.[120] The asymmetric unit in compound $[(UO_2)_3(Hcit)_2(H_2O)_3] \cdot 2H_2O$, comprises three uranyl ions and two citrate ligands (Figure 1.4.7).

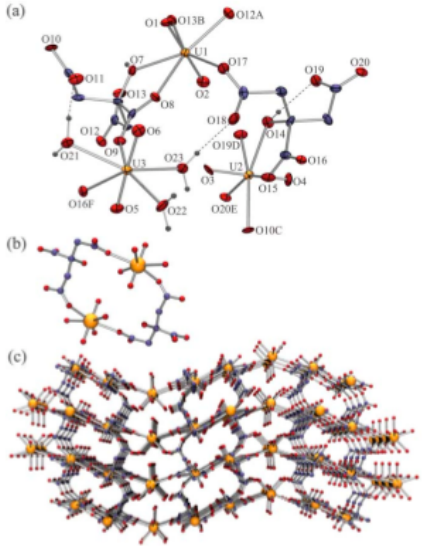

Figure 1.4.7. Crystal structure of $[(UO_2)_3(Hcit)_2(H_2O)_3]\cdot 2H_2O$.

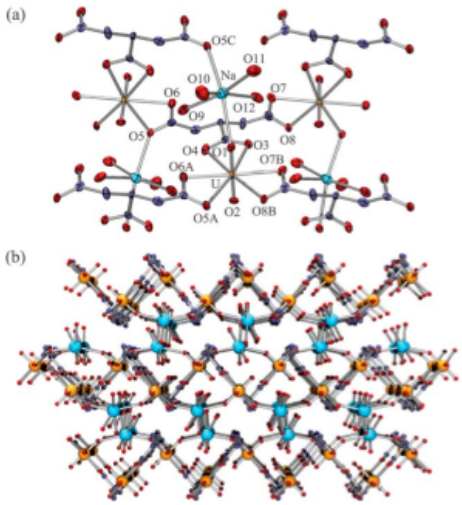

Figure 1.4.8. Crystal structure of $[(UO_2)Na(tca)(H_2O)_4]$.

Due to the twisted citrate conformation, $[(UO_2)(Hcit)_2]^{2-}$ 2:2 metallacycles are formed, which are further bound to neighboring ones to form adjacent very narrow channels directed along *a* axis.[120] These channels are arranged in layers parallel to the [*ab*] plane and are bridged by $[UO_2(H_2O)_3]^{2+}$ units to give a three-dimensional polymer. An extend hydrogen bonding network links the coordinated and solvent water molecules and the hydroxyl and acid groups of the citrate ligands. $[(UO_2)Na(tca)(H_2O)_4]$ includes both uranium and sodium ions. The uranium atom is bound to three chelating carboxylate

groups pertaining to three different molecules, which gives a hexagonal bipyramidal enviroment with the oxo atoms in axial positions (Figure 1.4.8).

The basic unit of compound $K[(UO_2)_3(\mu_3\text{-}OH)_3(\mu_2\text{-}OH)(C_7H_4O_4N)_2]OH$ is presented in Figure 1.4.9.[121] The uranium polyhedron forms an infinite one-dimensional ribbon along the *b*-axis, which is constructed by numerous edge-sharing uranium pentagonal bipramids. The edge of the ribbon is terminated by *p*-nitrobenzoic acid and μ_2-OH that arrange in AABAAB fashion along the ribbon. The ribbons are linked to form a two-dimensional layer structure by the potassium ion that serves to bridge between the two adjacent ribbons as shown in Figure 1.4.9.

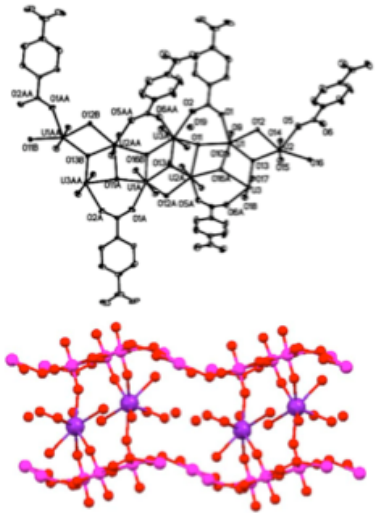

Figure 1.4.9. Structure of $K[(UO_2)_3(\mu_3\text{-}OH)_3(\mu_2\text{-}OH)(C_7H_4O_4N)_2]OH$. It show the infinite one-dimensional ribbons.

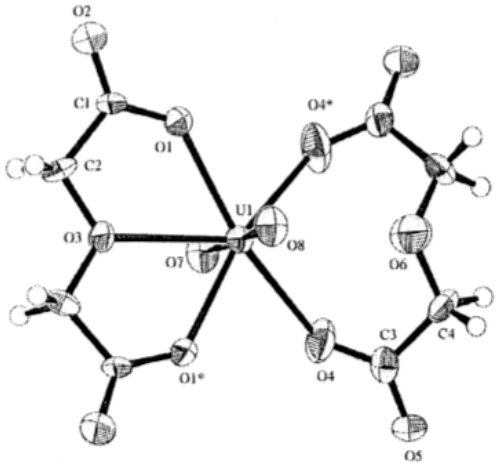

Figure 1.4.10. Dimeric anion in $[UO_2(C_4H_4O_5)_2]^{2-}$.

The anion structure of $[UO_2(C_4H_4O_5)_2]^{2-}$ is a centrosymmetric dimer, whose structure is shown in Figure 1.4.10.[122] The two uranyl groups are bonded by two μ_2-

bridging hydroxo groups, in which the hydrogen atoms are required for charge balancing. The uranium atoms are at the centers of neighboring pentagonal bipyramids with one common edge.

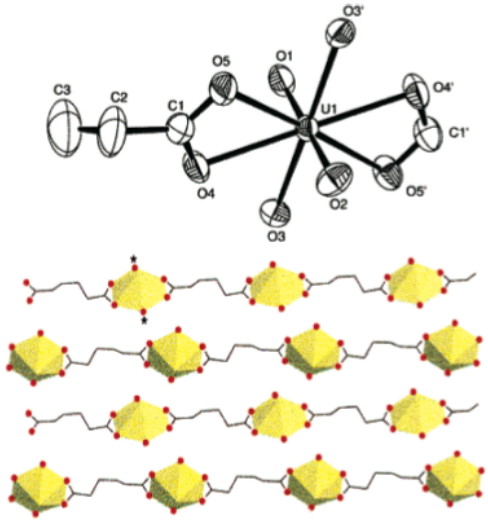

Figure 1.4.11. Polyhedra representation of $UO_2(C_6H_8O_4)(H_2O)_2$.

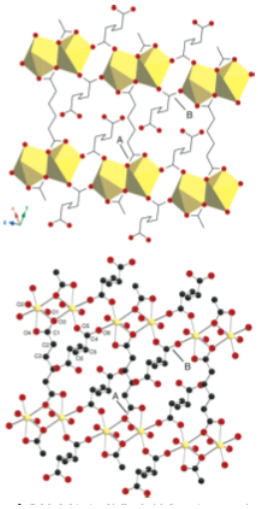

Figure 1.4.12. Chains of edge-shared $[(UO_2)_2O_8]$ dimers of $UO_2(C_6H_8O_4)$ run along [0 0 1].

The structure of $UO_2(C_6H_8O_4)(H_2O)_2$ consists of chains of dehydrated UO_2^{2+} cations tethered through an adipic acid backbone (Figure 1.4.11).[123] Within the hexagonal bipyramidal coordination sphere of the uranium, there are three distinct types of oxygens. The uranyl oxygen atoms are bonded to the central uranium atom at the average distance of 1.74 Å to form the linear UO_2^{2+} cation. The structure of $UO_2(C_6H_8O_4)$ (Figure 1.4.12) consists of $[(UO_2)_2O_8]$ dimers cross-linked through adipic acid groups to form a neutral three-dimensional framework.[123] Each dimer contains two edge-shared U pentagonal bipyramids constructed from linear UO_2^{2+} cations coordinated to five equatorial carboxylate oxygens donated from four unique adipic acid molecules. The dimers are linked through bridging carboxylate groups to form chains running along, which are then

cross-linked by additional adipic acid groups to form channels parallel to the chain direction. The adipic acid groups occur in two distinct enviroments, and thus, there are two modes of cross-linking the dimmer chains.

The structure of $[UO_2(C_4H_4O_4)]\cdot H_2O$ is composed of uranium pentagonal bipyramid (PBs) and succinate anions connected in a three-dimensional network (Figure 1.4.13).[124] The uranium polyhedra form a layer in the ac plane, which is constructed by uranium PBs and dicarboxylate group linking each PBs. The three dimensional architecture of $[UO_2(C_4H_4O_4)]\cdot H_2O$ is completed by the bridging of the 2D-uranium layer by bidentate succinate units. The alkyl chains act as spacers between the layers.

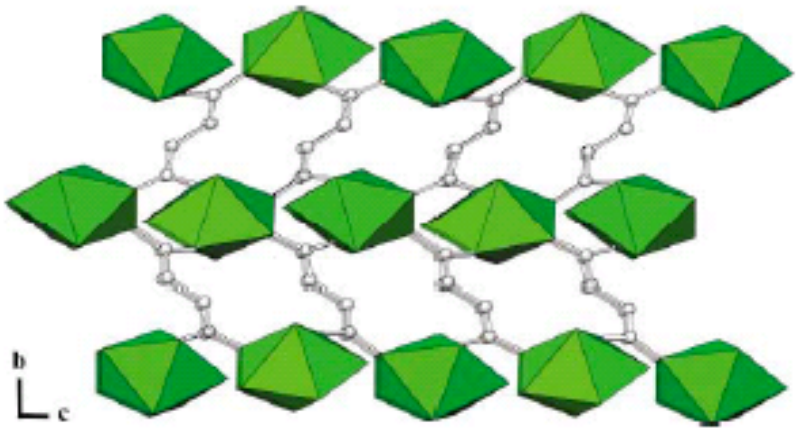

Figure 1.4.13. The structure of $[UO_2(C_4H_4O_4)]\cdot H_2O$.

$[UO_2F(C_5H_6O_4)]\cdot 2H_2O$ exhibits a one-dimensional chain structure consisting of uranium oxyfluoride dimers and cross-linking glutarate units. The neutral $[UO_2F][C_5O_4H_6]$ chain, which runs along [100] direction and the occluded water molecule in the cavity within the chain are shown in Figure 1.4.14.[124] As shown in Figure 1.4.15, the linkages between the anionic glutarates and the uranium oxyfluoride

dimers in compound $[UO_2F(C_5H_6O_4)]\cdot 2H_2O$ create a channel of width 3.4 × 2.0 Å along [0 0 1] direction.[124] Compound $[(UO_2)_{1.5}(C_8H_4O_4)_2]_2[(CH_3)_2NCOH_2]\cdot H_2O$ has a one-dimensional chain structure consisting of uranium hexagonal bipyramids (HPs) and anionic bridges of 1,3-benzenedicarboxylate (BDC). The uranium-BDC chain running along [1 0 0] direction is shown in Figure 1.4.16. The uranium-BDC chains stack along the b axis as shown in Figure 1.4.16.[124]

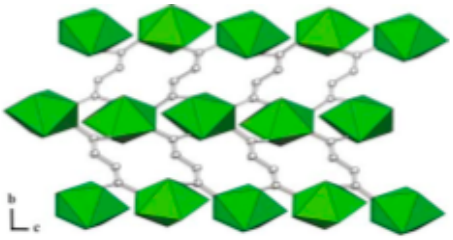

Figure 1.4.14. View of $[UO_2F(C_5H_6O_4)]\cdot 2H_2O$. Inorganic layers built up from uranium pentagonal bipyramids are linked by the organic group of succinate.

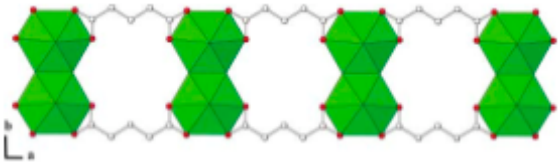

Figure 1.4.15. Uranium glutarate chain of $[UO_2F(C_5H_6O_4)]\cdot 2H_2O$.

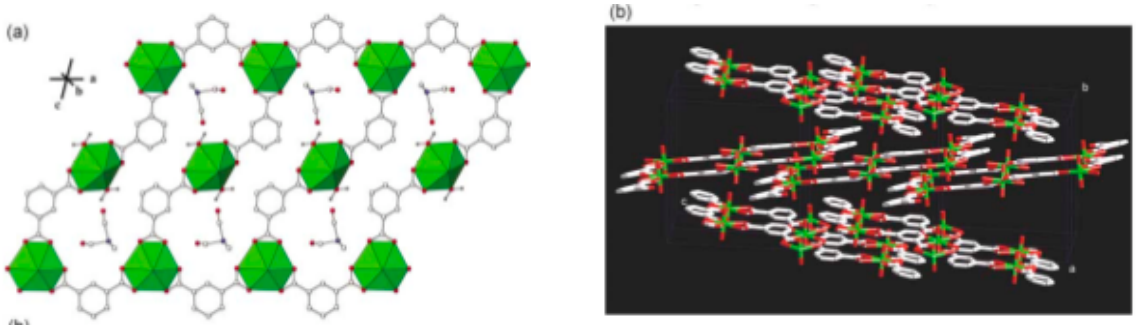

Figure 1.4.16. Crystal structure of $[(UO_2)_{1.5}(C_8H_4O_4)_2]_2[(CH_3)_2NCOH_2]\cdot H_2O$.

1.4.3 Bimetallic-organic molecular compounds: $(ZnO)_2(UO_2)_3(NA)_4(OAc)_2$ (HNA = nicotinic acid; HOAc = acetic acid); $[Ag(bipy)(UO_2)_2(bdc)_{1.5}]$ (bipy = 2,2'-bipyridyl, bdc = 1,4-benzenedicarboxylate); and $[Ag_2(phen)_2UO_2(btec)]$ (phen = 1,10-phenanthroline; btec = 1,2,4,5-benzenetetracarboxylate).

X-ray single-crystal diffraction analysis reveals that the structure of $(ZnO)_2(UO_2)_3(NA)_4(OAc)_2$ possesses a three-dimensional structure with rich coordination, including eight-coordinate hexagonal bipyramidal and seven-coordinate pentagonal bipyramid U cations, six-coordinate octahedra and five-coordinate trigonal bipramidal Zn cations (Shown in Figure 1.4.17).[125] The inorganic double sheets are further interconnected *via* Zn and O by the metal-organic layers resulting from the cross-linkage of zinc ions and tridentate NA ligands to construct a three-dimensional sandwich uranium-zinc-organic polymeric network.

In $[Ag(bipy)(UO_2)_2(bdc)_{1.5}]$, each uranium atom is located in a pentagonal-bipyramidal enviroment, surrounded by seven oxygen atoms, five of which are in the equatorial plane and are from three bdc ligands.[126] As shown in Figure 1.4.18, the structure of $[Ag(bipy)(UO_2)_2(bdc)_{1.5}]$ comprises bridging bdc ligands, $[Ag(bipy)]^+$ units, and uranyl ions, which form a neutral 2D layer in the [*ac*] plane. The 2D layers stack along the *b* axis through edge-to-face π- π interactions between bdc and bipy ligands in neighboring layers.

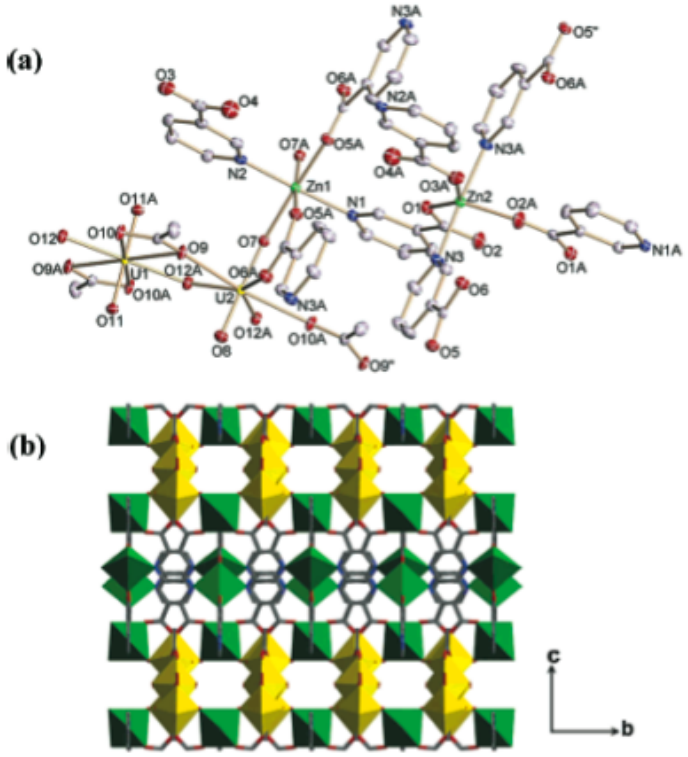

Figure 1.4.17. The structure of $(ZnO)_2(UO_2)_3(NA)_4(OAc)_2$: (a) the Zn and U coordination environment represented by thermal ellipsoids drawn to encompass 30% of their electron density; (b) the three-dimensional framework viewed along the [100] direction. Green: ZnO_5 or ZnO_6 units; yellow: UO_7 or UO_8 units.

The coordination sphere at the uranium site of $[Ag_2(phen)_2UO_2(btec)]$ is defined by two axial oxygen donors and an equatorial plane occupied by six oxygen donors form two chelating and two monodentate carboxyl groups of btec ligands.[126] The extended structure of $[Ag_2(phen)_2UO_2(btec)]$ consists of a 2D layered network with Ag-UO_8-Ag trinuclear cores as building units, which are linked by the bridging btec ligands (Figure 1.4.18).

(a) **(b)**

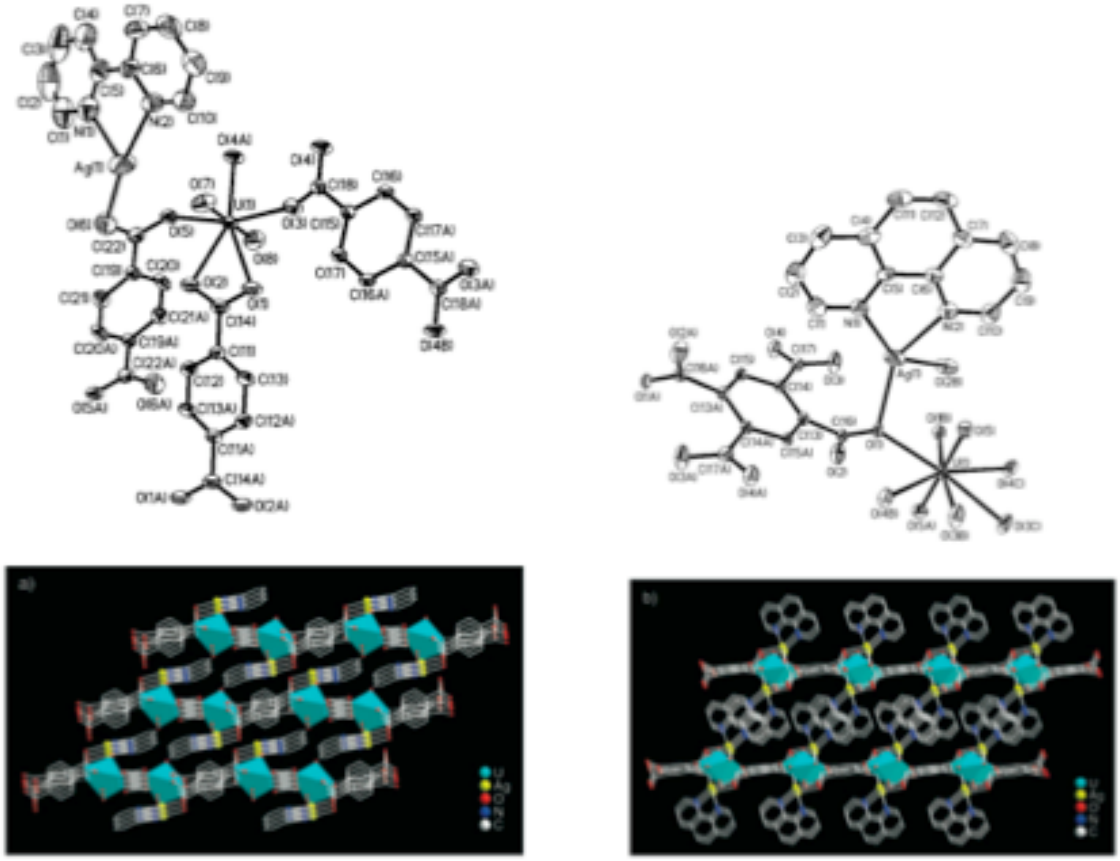

Figure 1.4.18. (a) The building block including the asymmetric unit present in $[Ag(bipy)(UO_2)_2(bdc)_{1.5}]$ with packing view. (b) The building block including the asymmetric unit present in $[Ag_2(phen)_2UO_2(btec)]$ with packing view.

1.5 Low-valence Uranium Compounds.

While alkaline peroxide conditions have allowed the isolation of uranium nanoclusters containing the diamagnetic $U^{VI}O^{2+}$ group, the access to clusters containing U^{IV} ($5f^2$) or U^{V} ($5f^1$), which are more attractive for the design of new magnetic materials,

requires the development of different synthetic conditions.[127-133] Successful work showed that the oxidation of an unidentified low-valent uranium species with pyridine N-oxide (PyNO) leads to the isolation of an organometallic U_6O_{13} cluster.[127] The controlled oxidation of low-valent uranium species in non-aqueous conditions might be the key to the synthesis of uranium oxoclusters. The use of non-aqueous conditions prevents the formation of uranyl cations, which are the most stable form of uranium in aqueous media.[134]

1.5.1 Compounds $[U_{12}(\mu_3\text{-}OH)_8(\mu_3\text{-}O)_{12}I_2(\mu_2\text{-}OTf)_{16}(CHCN)_8]\cdot 2CH_3CN_2H_2O$, $[K_4(\mu_2\text{-}H_2O)_2(H_2O)_4][U_6((\mu_3\text{-}O)_8(\mu_2\text{-}OTf)_{12}(H_2O)_{3.5}]\cdot 4.5H_2O$, $K_2[U_6((\mu_3\text{-}O)_8(\mu_2\text{-}OTf)_8(\eta 2\text{-}OTf)_4]$ and $[U_6((\mu_3\text{-}O)_8(\mu_2\text{-}OTf)_{12}(H_2O)_3]\cdot 23H_2O$.

Controlled hydrolysis of trivalent uranium in acetonitrile can indeed lead to the self-assembly of a large dodecanuclear discrete oxide cluster in a pure form or to mixtures of discrete clusters and extended networks depending on the ligand (iodide or trifluoromethanesulfonate) and on the reaction time. A series of mixed-valence uranium oxo clusters were structurally characterized, anticipating the fascinating structural variety of this chemistry. It has been found four remarkably different structures resulting from this process: 1) a discrete mixed-valence ($10U^{IV}/2U^{V}$) dodecanuclear clusters with an unprecedented $U_{12}O_{20}$ core formulated as $[U_{12}(\mu_3\text{-}OH)_8(\mu_3\text{-}O)_{12}I_2(\mu_2\text{-}OTf)_{16}(CHCN)_8]\cdot 2CH_3CN_2H_2O$, (shown in Figure 1.5.1); 2) an unprecedented 3D framework with zeolite-like topology composed of U^{IV} hexanuclear clustrs and potassium ions namely the 3D $[K_4(\mu_2\text{-}H_2O)_2(H_2O)_4][U_6((\mu_3\text{-}O)_8(\mu_2\text{-}OTf)_{12}(H_2O)_{3.5}]\cdot 4.5H_2O$, (shown in Figure 1.5.2); 3) a 2D array of mixed-valence ($4U^{IV}/2U^{V}$) hexanuclear clusters namely

the 2D $K_2U_6[(\mu_3\text{-}O)_8(\mu_2\text{-}OTf)_8(\eta 2\text{-}OTf)_4]$, (shown in Figure 1.5.3); and 4) a discrete mixed-valence ($2U^{IV}/4U^{V}$) hexanuclear cluster, (shown in Figure 1.5.4).[135]

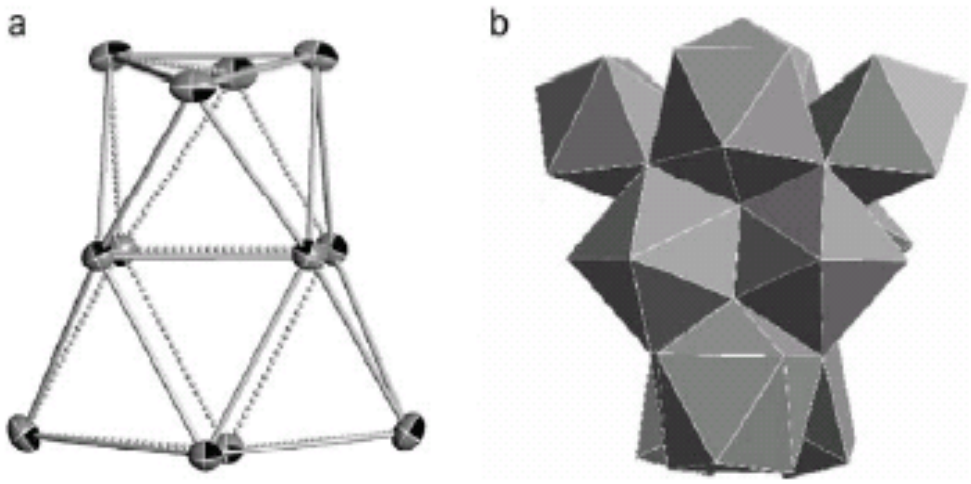

Figure 1.5.1. a) ORTEP view of the polyhedron (two adjacent square antiprisms) formed by the 12 uranium atoms. b) Polyhedral presentation of the cluster.

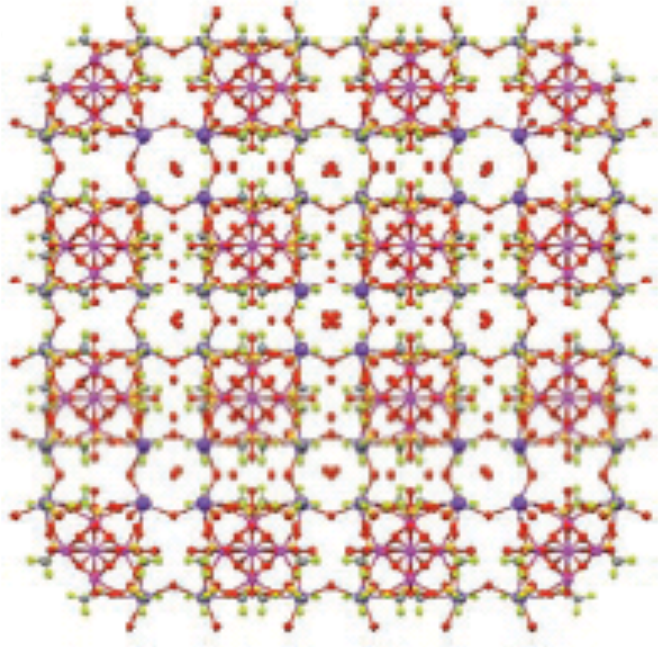

Figure 1.5.2. Extended 3D framework formed by complex $[U_6((\mu_3\text{-}O)_8(\mu_2\text{-}OTf)_{12}(H_2O)_{3.5}][K_4(\mu_2\text{-}H_2O)_2(H_2O)_4]\cdot 4.5H_2O$.

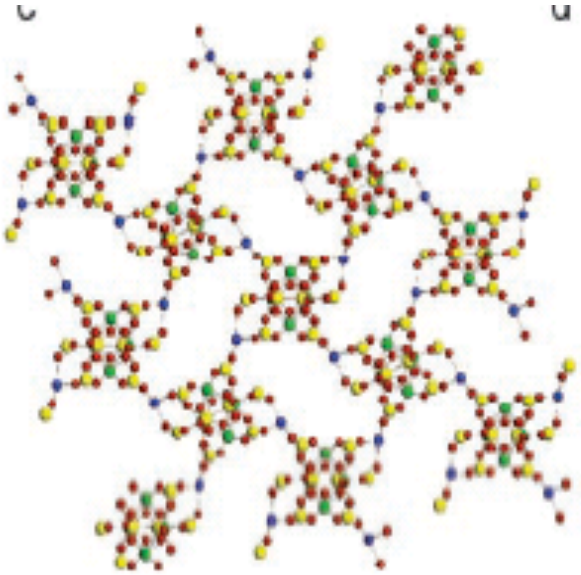

Figure 1.5.3. Extended 2D framework formed by complex $K_2U_6[(\mu_3\text{-}O)_8(\mu_2\text{-}OTf)_8(\eta_2\text{-}OTf)_4]$.

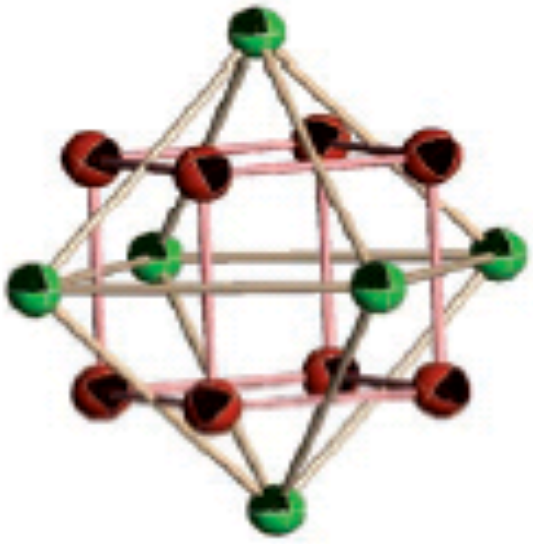

Figure 1.5.4. ORTEP view of the O_h-symmetric U_6O_8 core found in the compound $[U_6((\mu_3\text{-}O)_8(\mu_2\text{-}OTf)_{12}(H_2O)_3]\cdot 23H_2O$.

1.5.2 $M_7(\mu_3\text{-}N)_6(\mu_3\text{-}N)_6$ core analogous to the Anderson-type polyoxometalate motif: $[U_4(NPh)_6Cl_4(Ph)_8]$, $[U_4(NPh)_6Cl_4(ph)_6]$, $[Mg(THF)_5][U_7(NPh)_{12}Cl_6(THF)_6]$, $[Mg_2Cl_3(THF)_6][U_7(NPh)_{12}Cl_5(THF)_6]\cdot 2THF$.

Views of the centrosymmetric tetranuclear cluster $[U_4(NPh)_6Cl_4(Ph)_8]$, $[U_4(NPh)_6Cl_4(Ph)_6]$, are shown in Figure 1.5.5;[128] the structures differ by the distinct number of pyridine molecules coordinated to U1 and the presence in $[U_4(NPh)_6Cl_4(Ph)_6]$ of an additional U1···*Cipso* interaction.[128] Both complexes possess a central U_4N_6 core that can be described as "deck chair" or as two *seco*-heterocubes sharing a U_2N_2 face.

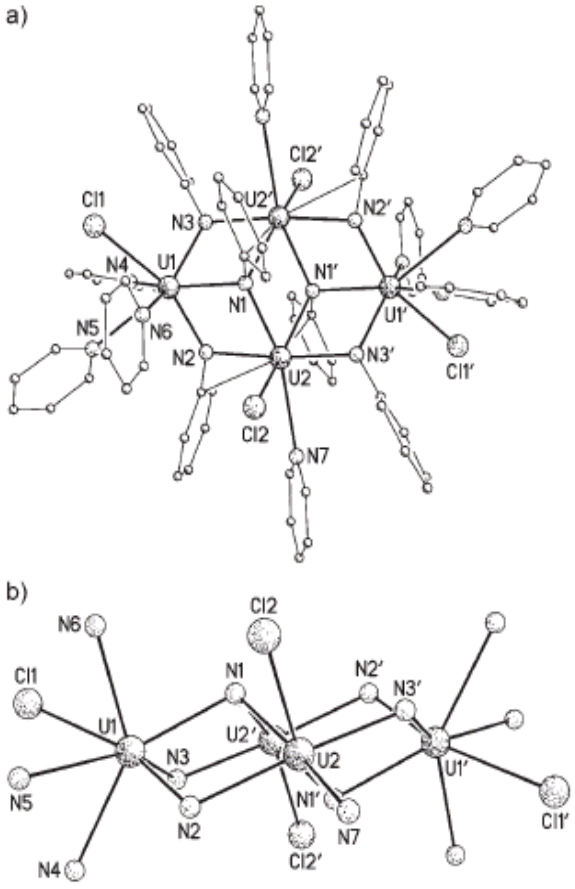

Figure 1.5.5. Core structure of $[U_4(NPh)_6Cl_4(ph)_8]$, $[U_4(NPh)_6Cl_4(ph)_6]$.

While homo- and hetermetallic compounds containing the symmetrical M_7O_{12} or $M_6M'O_{12}$ core are well documented, in particular the hetero-polyoxometalates of the Anderson type, $[Mg(THF)_5][U_7(NPh)_{12}Cl_6(THF)_6]$ is the first complex exhibiting the analogue $M_7(\mu_3\text{-}N)_6(\mu_3\text{-}N)_6$ structural motif, shown in Figure 1.5.6.[128] The structure of the anion $[Mg_2Cl_3(THF)_6][U_7(NPh)_{12}Cl_5(THF)_6]\cdot 2THF$, exhibits the same $M_7(\mu_3\text{-}N)_6(\mu_3\text{-}N)_6$ core but is devoid of any even approximate symmetry element.

The formation of these polynuclear complexes demonstrates the potential of the imido ligand to expand the molecule chemistry of actinides with attractive perspectives for the synthesis of clusters. Further work, including theoretical studies, is in progress to extend the variety of imido polynuclear compounds of uranium either by changing the nature of R in RN^{2-}, the ancillary ligands, and the oxidation state of the metal center.

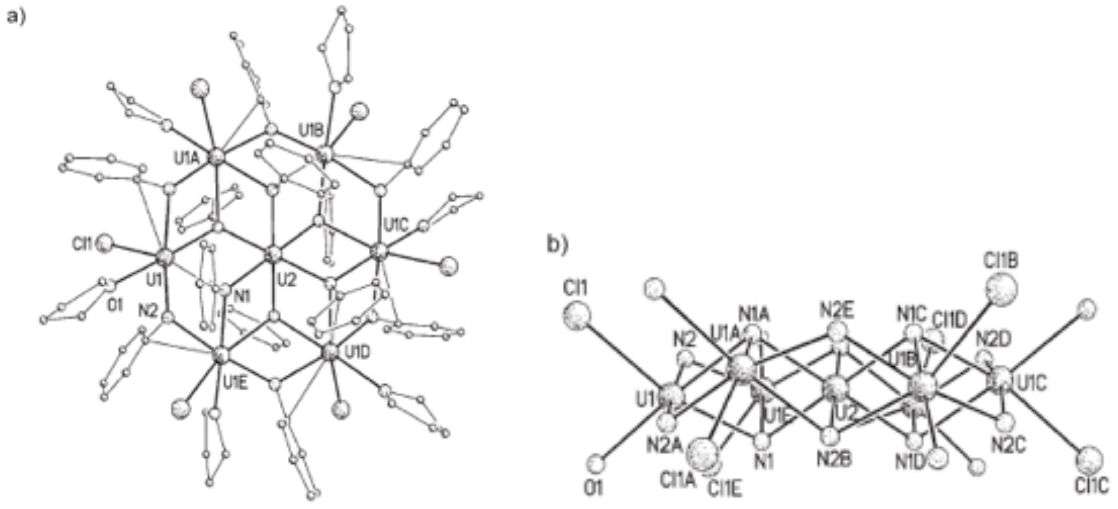

Figure 1.5.6. Core structure of $[Mg(THF)_5][U_7(NPh)_{12}Cl_6(THF)_6]$, $[Mg_2Cl_3(THF)_6][U_7(NPh)_{12}Cl_5(THF)_6]\cdot 2THF$.

1.5.3 Lindqvist-type $[Cp^{\neq}_4U_6O_{13}(bipy)_2]$ ($Cp^{\neq}$=1,2,4-*t*$Bu_3C_5H_2$; bipy=2,2'-bipyridine).

The X-ray crystal structure for $[Cp^{\neq}_4U_6O_{13}(bipy)_2]$ reveals six uranium atoms arranged in approximate octahedral symmecenter of the cluster, shown in Figure 1.5.7.[127] Tetragonal compression of the uranium octahedron is observed along the U(1)-O(7)-U(1A) axis. Twelve other oxo ligands form μ_2-O bridging interactions to uranium centers around the cluster framework to furnish the $[U_6O_{13}]$ core that mimics the isopolyoxometalate. Lindqvist structure, however, a terminal oxo ligand on each metal center would normally complete the coordination sphere, whereas in $[Cp^{\neq}_4U_6O_{13}(bipy)_2]$ these terminal sites are occupied instead by either an η^5-$Cp^{\neq}$ ligand (on the "equatorial" uranium atoms or a chelating bipyridine (bpy) ligand (on the "axial" uranium atoms). The presence of terminal ligands other than oxo groups has been noted in isopolyoxometalates ions, but with the notable exception of organoimido functionalities, only one terminal oxo ligand is typically substituted.

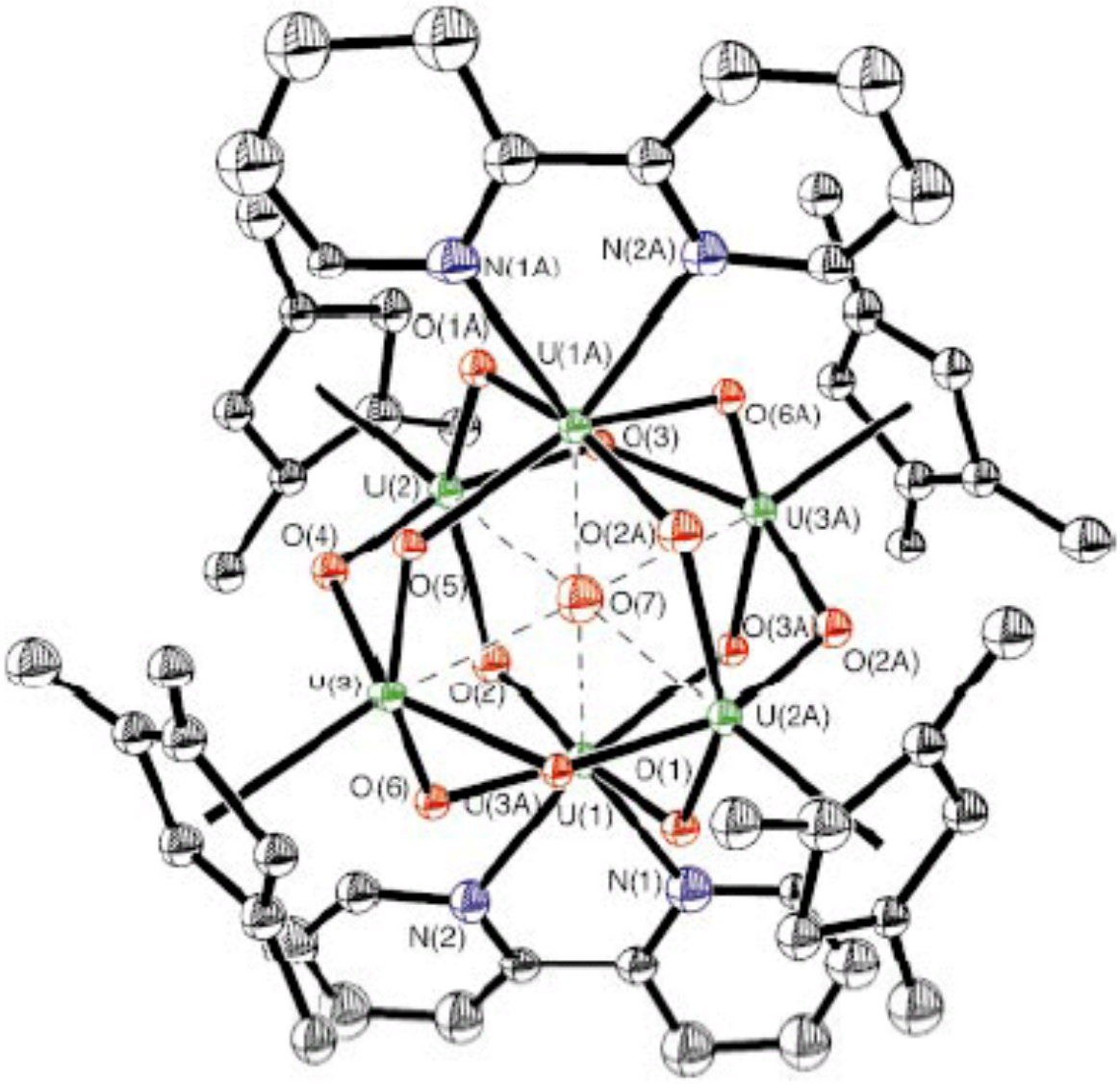

Figure 1.5.7. Molecular structure of Lindqvist-type $[Cp^{\neq}{}_4U_6O_{13}(bipy)_2]$ ($Cp^{\neq}$=1,2,4-tBu$_3$C$_5$H$_2$; bipy=2,2'-bipyridine)

1.6 Studies on Structural-properties relationships.

1.6.1 Uranyl vibrational modes (fundamental vibrations).[53]

A free uranyl, UO_2^{2+}, point symmetry $D_{\infty h}$, should exhibit three fundamental modes: symmetric stretching vibration ν_1; bending vibration ν_2 (δ); and antisymmetric stretching vibration ν_3. The bending mode is doubly degenerate since it can occur in two mutually perpendicular planes. It can split into its two components when the uranyl ion is placed in an external force field. Thus, the linear uranyl group, point symmetry $D_{\infty h}$, has four normal vibrational modes, but only three fundamentals.

Uranyl stretching vibrations, ν_1 UO_2^{2+} and ν_3 UO_2^{2+}

In linearly symmetry uranyl ions belonging to the $D_{\infty h}$ point group, the symmetric strectching vibration, ν_1 UO_2^{2+}, exhibits in the region 900-750 cm^{-1} and is Raman active, whereas, ν_1 UO_2^{2+} appears in the IR spectrum only in the case of substantial symmetry lowering. The antisymmetric stretching vibration, ν_3 UO_2^{2+} (1000-850 cm-1), is active in the infrared and inactive Raman and is sensitive to isotopic exchange. A lowering of symmetry ($D_{\infty h} \rightarrow C_{\infty v}$, C_{2v} or C_s) causes both the activation of all three fundamentals in the infrared and Raman spectra and the activation of their overtones and combination vibrations.

If the uranyl group is linear, but not symmetric, all three vibrational modes ν_1, ν_2 and ν_3 UO_2^{2+} show vibrational activity in Raman as well as in IR spectra. In this case the intensities of ν_2 and ν_3 UO_2^{2+} in Raman spectra are lower than that of ν_1 UO_2^{2+}. If uranyl ion is linear, then the frequencies $2\nu_3$, $4\nu_3$, $6\nu_3$ etc. $3\nu_1$, $5\nu_1$, $7\nu_1$ etc. should be IR-forbidden but Raman-allowed whereas $3\nu_3$, $5\nu_3$, $7\nu_3$ etc. $2\nu_1$, $4\nu_1$, $6\nu_1$ etc. should be IR-allowed but Raman-forbidden. A combination band $\nu_1 + \nu_3$ is also IR-allowed. In contrast

to this, in the case of $D_{\infty h}$ symmetry, only those overtones and combinations should be IR-active which makes the resultant vibration effectively antisymmetric (e.g. ($v_1 + v_3$), ($2v_2 + v_3$), $3v_2$, $3v_3$. etc). The site symmetry for the symmetric linear ion is likely to be D_{nh} or lower (n is the number of ligands in the equatorial plane), ($2 \leq n \geq 6$), depending upon the number and manner in which the ligands (L) are coordinated to the uranyl ion. Under these circumstances, the UO_2L_n will have a number of vibrations v_1 and v_3.

Several bands attributed to the v_1 and v_3 UO_2^{2+} vibrations and correlated with crystal structure data are interpreted as indicating either several structurally nonequivalent uranyl groups in the unit cell or the co-existence of different crystal modifications in the mineral studied.

Relations between a free UO_2^{2+} group stretching and bending vibrations and their corresponding force constants can be calculated using the following equations:

$v_1 = 1303\ [(f+f')/m_o]^{1/2}\ cm^{-1}$

$v_2 = 1303\ [2d\ (2/m_u + 1/m_o)]^{1/2}\ cm^{-1}$

$v_3 = 1303\ [(f-f')\ (2/m_u + 1/m_o)]^{1/2}\ cm^{-1}$

Where m_u and m_o are expressed in atomic mass units (amu), f (stretching f_{uo}), f' (interaction $f_{uo,uo'}$) and d (bending) force constants in N cm^{-1}. In a simple valence force field, and assuming harmonic vibrations characteristic of a linear ion, the f' interaction force constant can be omitted and the relation between v_1 and v_3 is

$v_3 = v_1\ (2m_o/m_u)^{1/2}$

Under these conditions, the v_3/v_1 ratio is ~1.065. If the f' interaction force constant is respected, the v_3/v_1 may decrease or increase depending upon the sign of f'. The intensity of the antisymmetric stretching vibration v_1 (if IR active) is usually low. The v_1 UO_2^{2+}

vibration is located in the region of oxyanion skeletal vibrations or δ UOH vibrations, and some coincidences are possible. This may cause a wrong tentative assignment of the vibration.

The character of IR spectra of uranyl minerals (wavenumbers of ν_1 UO_2^{2+} and ν_3 UO_2^{2+} vibrations) may be influenced by conditions under which the minerals formed and the stability of their crystal structures.

Uranyl bending vibration ν_2 (δ) UO_2^{2+}

The doubly degenerate bending vibration, ν_2 UO_2^{2+} (δ UO_2^{2+}), (approximately 300-200 cm^{-1}) is IR active, and a decrease of symmetry can cause splitting if this vibration into two IR and Raman active components. Coincidences between uranyl bending vibrations and U-O_{ligand} vibrations are possible.

The large amounts of works on the Raman spectroscopy of uranyl minerals,[136-163] including in compreignacite ($K_2[(UO_2)_3O_2(OH)_3]_2 \cdot 7H_2O$);[162] molybdate-containing calcurmolite;[164] nullaginite and zaratite;[163] phosphuranyllite;[164] yingjiangite;[164] uranopilite of different origins;[150] multi-anion schroeckingerite;[153] rutherfordine;[149] zippeite;[152] bergenite;[156] dewindtite;[141] threadgoldite;[142] parsonsite;[143] phurcalite[144] and autunite,[139,140] gave us the similar results, listed below. In a linear symmetric uranyl ion belonging to the $D_{\infty h}$ point group to the ν_1 band is found in the 900-750 cm^{-1} region and is Raman active but only appears in the infrared spectrum in the case of substantial symmetry lowering. The antisymmetric stretching vibration is active in the infrared and inactive in the Raman. Lowering of the symmetry results in the activation of all fundamentals. The ν_1 mode of PO_4 was given at 920 cm^{-1}, ν_2 at 472 and 435 cm^{-1}, ν_3 at 1115 and 1023 cm^{-1} and ν_4 at 615 and 550 cm^{-1} for autunite. The position of the $(UO_2)^{2+}$

bands as v_1 located at 805 cm^{-1} for torbernite and v_3 at 915 cm^{-1}. The interpretation of this assignment is open to question. Cejka et al. reported the infrared spectrum of sabugalite and suggested that the weak absorption band a 810 cm^{-1} was attributable to the symmetric stretching mode of the $(UO_2)^{2+}$ unit and that the band at 915 cm^{-1} was attributable to the antisymmetric stretching vibration of the $(UO_2)^{2+}$ unit. The v_2 bands of the $(UO_2)^{2+}$ units were found at 298 and 254 cm^{-1}. Herein lie the difficulty in that both the v_1 bands of PO_4 and $(UO_2)^{2+}$ is found at the same spectral positions making interpretation by infrared spectroscopy difficult.

1.6.2 Fluorescence Spectroscopy of Uranyl Vibronic Emission.

When the UO_2^{2+} ion is present in minerals, a transition occurs between the free UO_2^{2+} ion and the UO_2^{2+} ion bonded in a crystal structure.[53,165-167] This results in a decrease in site symmetry of the UO_2^{2+} ion from $D_{\infty h}$ to D_{6h} or lower symmetry.[53] This change in symmetry leads to a rearrangement in molecular orbitals. The features of the absorption and luminescent spectra of UO_2^{2+} minerals is a function of transitions between different energy levels.[53] These differences are equal to the vibrational energy of the UO_2^{2+} and are characteristic properties of the material.[166] Each of the broad bands of electronic transitions of the UO_2^{2+} ion represents one series of vibrational transitions.[166]

A characteristic property of UO_2^{2+} luminescence emission is that the luminescence bands are narrower than transition-metal activators.[3,165-167] The energy levels of UO_2^{2+} can be described by using molecular orbital theory; however, the energy is not yet available.[165,166] The luminescent emission spectra of most UO_2^{2+} minerals are generally similar.[128,168-174] It has been suggested that some features of the optical spectrum of the

uranyl (VI) ion in the solid state can be explained by considering the properties of anharmonic charge-transfer vibronic excitons (CTVEs).[165,166,175] The idea underlying the CTVE is that the energy associated with interatomic charge transfer can be modified by strong coupling to local vibrational displacements.

As a result of strong coupling between charge transfer excitons and ligand (or local lattice) vibration, formation of anharmonic CTVEs along with harmonic CTVEs is expected in covalent systems such as actinyl ions.[3,165,166] In fact, some intriguing spectroscopic behaviors of uranyl might be as well due to the anharmonic nature of charge transfer and vibronic coupling. The first treatment of a charge transfer exciton interacting with a lattice was performed in the pioneering work of Agranovich and Zakhidov.[176] For a uranyl ion as shown in Figure 1.6.1, the primary vibrations of the linear O-U-O structure include a symmetric stretching mode and an asymmetric stretching mode.[167] Of course, in crystals and complexes, a uranyl ion may couple with ligands (lattice) in a variety of other vibrational modes, the ligand-ion charge transfer involves the 2p orbital's of O^{2-} and the 5f and 6d orbitals of U^{6+}.[167,177] Depending strongly on ligands, the first excited CTVE state of uranyl could be metastable and many systems its relaxation (charge transfer recombination) is dominantly a radiative process and emits photons in visible region.[168,169] As a general characteristic of uranyl luminescence, the charge transfer vibronic transitions always progression with the vibrational frequency of the symmetric stretching mode with frequency around 800 cm^{-1}.[166] Because of the complexity of charge transfer vibronic interaction, the electronic and vibronic origins and dynamics of uranyl luminescence have not been well understood even though they have been topical subjects of studies for more than 50 years.[165,166]

It has been reported that the present work focuses on modeling CTVE structure of uranyl and provides a theoretical interpretation to the anomalous hot bands previously observed in crystals doped with uranyl ions.[167] Based on the co-exitence anharmonic CTVE-II and harmonic CTVE-I, calculations have been perfomed for simulating the temperature dependent spectrum of the uranyl luminescence spectrum.[167] In addition, the proposed model allows explaining the origin of weakly splitted uncommon doublet in uranyl absorption spectrum as a result of tunneling between CTVE-I and CTVE-II states.[167,177]

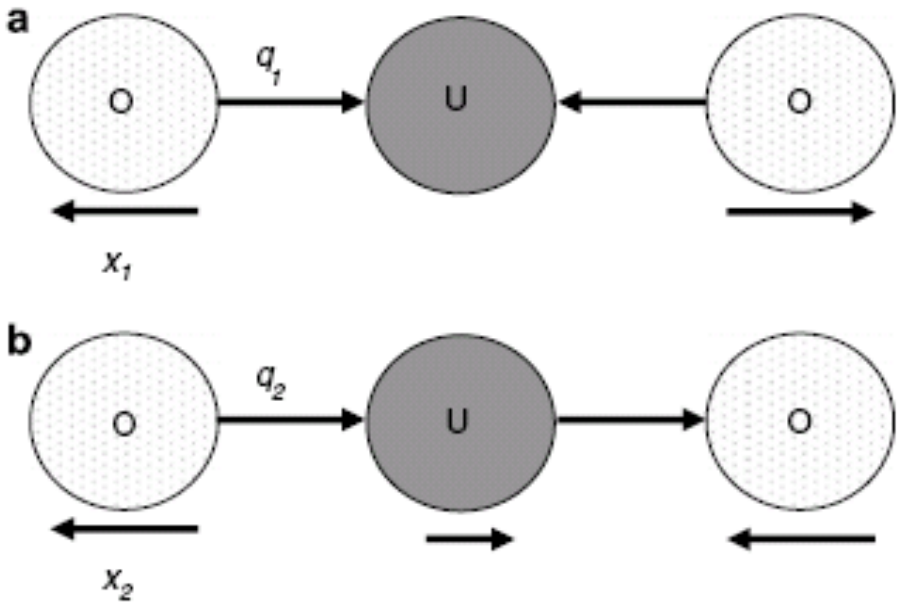

Figure 1.6.1. A scheme of uranyl charge transfer and vibronic excitons in (a) symmetry starching mode, and (b) asymmetric stretching mode, x1, q1 and x2 and q2 are ion displacements and charge transfer coordinates, respectively for the symmetric and asymmetric modes.

To elucidate the excitation and luminescence associated with vibronic transitions, the shape of CTVE-II potential well, the shape of CTVE-I potential well and vibronic

transitions, basing on the reported equations, are plotted in Figure 1.6.2.[167] An optical excitation thus leads coordinate distortion and occupation of both CTVE-1 and CTVE-II of the lowest charge transfer states, from which radiative relaxation, namely, fluorescence emission occurs as a result of charge recombination.

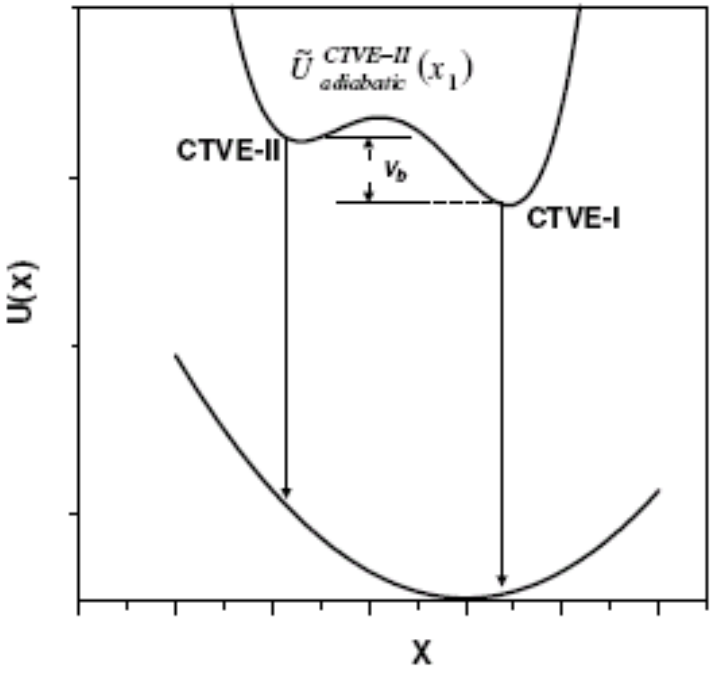

Figure 1.6.2. Configurations of uranyl harmonic CTVE-I and anharmonic CTVE-II with respect to the ground state potential well. A hot band is expected to appear in the CTVE-I luminescence spectrum of the uranyl ion.

The luminescence of uranyl ion in compounds exhibits intriguing dynamics because of its origin in terms of charge transfer and vibronic excitons. Once we expand the adiabatic Hamiltonian from the conventional harmonic terms of charge transfer and coordinate displacements to inclusion of higher orders of charge transfer and coordinate displacements, it would lead to a potential of multiple wells from which luminescence emmision could be originated if these wells are isolated form non-radiative relaxation

channels of ligand states. It is shown that an anharmonic potential well, CTVE-II may appear along with the harmonic CTVE-I at a higher energy. However, the luminescence emission from the CTVE-II have lower energy than that from the CTVE-I. Such simulation may also be used in resolving uranyl species in different local environments and determining the ion-ligand coupling mechanisms.

Research Motivation.

Uranyl phosphates and arsenates have been the subject of intense interest for many decades for a variety of reasons, a partial list of which includes their importance in the transport of uranium in the environment, the abundance and diversity of uranium phosphate minerals, the unique structures that these compounds adopt, their use as long-term storage waste forms for radioactive materials, their use as ion-exchange materials, and their use as proton conductors. Of late, there has been interest in expanding structural diversity and physicochemical properties of uranyl phosphates through the incorporation of main group elements and transition metals. These uranyl/M/phosphates have displayed a variety of properties including second-harmonic generation, magnetic ordering, and ion exchange with promising selectivity.

At the heart of uranyl phosphate chemistry is the phenomenal richness of the observed crystal chemistry that can be attributed in part to the structural versatility of U(VI), which generally occurs as tetragonal, pentagonal, and hexagonal bipyramids. Less obvious influencers of structure include the cations that are used to maintain charge balance with the anionic lattices that are adopted by uranyl compounds. Organoammonium cations have played an important role in directing the structures of novel anionic uranyl phosphate topologies A number of open-framework uranyl phosphates have been prepared using cyclic amines as structure-directing agents in hydrothermal syntheses. The goal of the dissertation is the utilize both transition metal polyhedra as structural building units and the organic amines as templates to form the new topologic structures uranyl/transiton metal/phosphate that can be tested in variety of applications including ion exchange and luminescence. This strategy has proven to be

successful. The synthesis method, structures, Raman spectroscopy, Fluorescent spectroscopy and ion-exchange properties will be discussed in detailed.

References:

1 Burns, P. C.; Ewing, R. C.; Hawthrone, F. C. *Canadian Mineralogist* **1997**, *35*, 1551.

2 Burns, P. C.; Miller, M. L.; Ewing, R. C. *Canadian Mineralogist* **1996**, *34*, 845-880.

3 Burns, P. C.; Uranium: Mineralogy, Georchemistry and the Environment, 1999.

4 Burns, P. C.; Ewing, R. C.; Hawthorne, F. C. *Canadian Mineralogist* **1997**, *35*, 1551-1570.

5 Burns, P. C. *Canadian Mineralogist* **2005**, *43*, 1839-1894.

6 Liebe, D.; Eberhardt, K.; Hartmann, W.; Hager, T.; Hubner, A.; Kratz, J. V.; Kindler, B.; Lommel, B.; Thoerle, P.; Schadel, M.; Steiner, J. *Nuclear Instruments & Methods in Physics Research Section a-Accelerators Spectrometers Detectors and Associated Equipment* **2008**, *590*, 145-150.

7 von Zweidorf, A.; Angert, R.; Bruchle, W.; Burger, S.; Eberhardt, K.; Eichler, R.; Hummrich, H.; Jager, E.; Kling, H. O.; Kratz, J. V.; Kuczewski, B.; Langrock, G.; Mendel, M.; Rieth, U.; Schadel, M.; Schausten, B.; Schimpf, E.; Thorle, P.; Trautmann, N.; Tsukada, K.; Wiehl, N.; Wirth, G. *Radiochimica Acta* **2004**, *92*, 855-861.

8 Burns, P. C. *American Mineralogist* **2000**, *85*, 801-805.

9 ISI Web of Knowledge, v.4.0.

10 Ok, K. M.; Doran, M. B.; O'Hare, D. *Journal of Materials Chemistry* **2006**, *16*, 3366-3368.

11 Wang, C. M.; Liao, C. H.; Lin, H. M.; Lii, K. H. *Inorganic Chemistry* **2004**, *43*, 8239-8241.

12 Almond, P. M.; Deakin, L.; Porter, M. J.; Mar, A.; Albrecht-Schmitt, T. E. *Chemistry of Materials* **2000**, *12*, 3208-3213.

13 Walker, S. M.; Halasyamani, P. S.; Allen, S.; O'Hare, D. *Journal of the American Chemical Society* **1999**, *121*, 10513-10521.

14 Doran, M. B.; Norquist, A. J.; O'Hare, D. *Acta Crystallographica Section E-Structure Reports Online* **2005**, *61*, M881-M884.

15 Francis, R. J.; Halasyamani, P. S.; O'Hare, D. *Angewandte Chemie-International Edition* **1998**, *37*, 2214-2217.

16 Francis, R. J.; Halasyamani, P. S.; O'Hare, D. *Chemistry of Materials* **1998**, *10*, 3131-3139.

17 Doran, M. B.; Cockbain, B. E.; O'Hare, D. *Dalton Transactions* **2005**, 1774-1780.

18 Norquist, A. J.; Doran, M. B.; O'Hare, D. *Acta Crystallographica Section E-Structure Reports Online* **2005**, *61*, M807-M810.

19 Norquist, A. J.; Doran, M. B.; O'Hare, D. *Inorganic Chemistry* **2005**, *44*, 3837-3843.

20 Doran, M. B.; Cockbain, B. E.; Norquist, A. J.; O'Hare, D. *Dalton Transactions* **2004**, 3810-3814.

21 Doran, M. B.; Norquist, A. J.; O'Hare, D. *Inorganic Chemistry* **2003**, *42*, 6989-6995.

22 Krivovichev, S. V.; Kahlenberg, V.; Kaindl, R.; Mersdorf, E.; Tananaev, I. G.; Myasoedov, B. F. *Angewandte Chemie-International Edition* **2005**, *44*, 1134-1136.

23 Krivovichev, S. V.; Armbruster, T.; Chernyshov, D. Y.; Burns, P. C.; Nazarchuk, E. V.; Depmeier, W. *Microporous and Mesoporous Materials* **2005**, *78*, 225-234.

24 Krivovichev, S. V.; Burns, P. C.; Armbruster, T.; Nazarchuk, E. V.; Depmeier, W. *Microporous and Mesoporous Materials* **2005**, *78*, 217-224.

25 Krivovichev, S. V.; Cahill, C. L.; Nazarchuk, E. V.; Burns, P. C.; Armbruster, T.; Depmeier, W. *Microporous and Mesoporous Materials* **2005**, *78*, 209-215.

26 Danis, J. A.; Runde, W. H.; Scott, B.; Fettinger, J.; Eichhorn, B. *Chemical Communications* **2001**, 2378-2379.

27 Doran, M. B.; Stuart, C. L.; Norquist, A. J.; O'Hare, D. *Chemistry of Materials* **2004**, *16*, 565-566.

28 Locock, A. J.; Burns, P. C. *Journal of Solid State Chemistry* **2004**, *177*, 2675-2684.

29 Locock, A. J.; Burns, P. C. *Journal of Solid State Chemistry* **2002**, *163*, 275-280.

30 Krivovichev, S. V.; Burns, P. C. *Canadian Mineralogist* **2000**, *38*, 717-726.

31 Almond, P. M.; Albrecht-Schmitt, T. E. *Inorganic Chemistry* **2002**, *41*, 1177-1183.

32 Wallez, G.; Clavier, N.; Dacheux, N.; Quarton, M.; van Beek, W. *Journal of Solid State Chemistry* **2006**, *179*, 3007-3016.

33 Terra, O.; Clavier, N.; Dacheux, N.; Podor, R. *New Journal of Chemistry* **2003**, *27*, 957-967.

34 Brandel, V.; Clavier, N.; Dacheux, N. *Radiochimica Acta* **2006**, *94*, 461-464.

35 Li, Y. P.; Burns, P. C. *Journal of Nuclear Materials* **2001**, *299*, 219-226.

36 Zeggar, F.; Halilou, A.; Meftah, B.; Mokeddem, M. Y.; Letaim, F.; Bousbia-Salah, A. *Nuclear Technology & Radiation Protection* **2008**, *23*, 11-18.

37 War, S. A.; Nongkynrih, P.; Khathing, D. T.; Iongwai, P. S.; Jha, S. K. *Journal of Environmental Radioactivity* **2008**, *99*, 1665-1670.

38 Wan, J. M.; Tokunaga, T. K.; Kim, Y. M.; Brodie, E.; Daly, R.; Hazen, T. C.; Firestone, M. K. *Environmental Science & Technology* **2008**, *42*, 7573-7579.

39 Simsek, C. *Environmental Geology* **2008**, *55*, 1637-1646.

40 Sidborn, M.; Neretnieks, I. *Journal of Contaminant Hydrology* **2008**, *100*, 72-89.

41 Risso, C.; Methe, B. A.; Elifantz, H.; Holmes, D. E.; Lovley, D. R. *Microbiology-Sgm* **2008**, *154*, 2589-2599.

42 Popovic, D.; Todorovic, D.; Frontasyeva, M.; Ajtic, J.; Tasic, M.; Rajsic, S. *Environmental Science and Pollution Research* **2008**, *15*, 509-520.

43 Moreels, D.; Crosson, G.; Garafola, C.; Monteleone, D.; Taghavi, S.; Fitts, J. P.; van der Lelie, D. *Environmental Science and Pollution Research* **2008**, *15*, 481-491.

44 Marmolejo-Rodriguez, A. J.; Caetano, M.; Prego, R.; Vale, C. *Journal of Environmental Radioactivity* **2008**, *99*, 1631-1635.

45 Fuller, C. C.; Bargar, J. R.; Davis, J. A.; Piana, M. J. *Environmental Science & Technology* **2002**, *36*, 158-165.

46 Francis, A. J.; Dodge, C. J. *Environmental Science & Technology* **2008**, *42*, 8277-8282.

47 Buck, E. C.; Brown, N. R.; Dietz, N. L. *Environmental Science & Technology* **1996**, *30*, 81-88.

48 Wronkiewicz, D. J.; Bates, J. K.; Wolf, S. F.; Buck, E. C. *Journal of Nuclear Materials* **1996**, *238*, 78-95.

49 Macaskie, L. E.; Bonthrone, K. M.; Yong, P.; Goddard, D. T. *Microbiology-Uk* **2000**, *146*, 1855-1867.

50 Finn, P. A.; Hoh, J. C.; Wolf, S. F.; Slater, S. A.; Bates, J. K. *Radiochimica Acta* **1996**, *74*, 65-71.

51 Locock, A. J.; Burns, P. C. *Canadian Mineralogist* **2003**, *41*, 489-502.

52 Locock, A. J.; Burns, P. C.; Flynn, T. M. *Canadian Mineralogist* **2004**, *42*, 1699-1718.

53 Burns, P. C. B., P. C.. Finch, R., Eds.; *Mineralogical Society of America: Washington, DC, ; Chapter I.* **1999**.

54 Soderholm, L.; Almond, P. M.; Skanthakumar, S.; Wilson, R. E.; Burns, P. C. *Angewandte Chemie-International Edition* **2008**, *47*, 298-302.

55 Sullens, T. A.; Jensen, R. A.; Shvareva, T. Y.; Albrecht-Schmitt, T. E. *Journal of the American Chemical Society* **2004**, *126*, 2676-2677.

56 McKee, M. L.; Swart, M. *Inorganic Chemistry* **2005**, *44*, 6975-6982.

57 Bean, A. C.; Albrecht-Schmitt, T. E. *Journal of Solid State Chemistry* **2001**, *161*, 416-423.

58 Charushnikova, I. A.; Krot, N. N.; Starikova, Z. A. *Radiochimica Acta* **2007**, *95*, 495-499.

59 Almond, P. M.; Skanthakumar, S.; Soderholm, L.; Burns, P. C. *Chemistry of Materials* **2007**, *19*, 280-285.

60 Krot, N. N.; Grigoriev, M. S. *Uspekhi Khimii* **2004**, *73*, 94-106.

61 Krivovichev, S. V.; Kahlenberg, V.; Tananaev, I. G.; Kaindil, R.; Mersdorf, E.; Myasoedov, B. F. *Journal of the American Chemical Society* **2005**, *127*, 1072-1073.

62 Vanduivenboden, H. C.; Ijdo, D. J. W. *Acta Crystallographica Section C-Crystal Structure Communications* **1986**, *42*, 523-525.

63 Ijdo, D. J. W. *Acta Crystallographica Section C-Crystal Structure Communications* **1993**, *49*, 650-652.

64 Wolf, R.; Hoppe, R. *Zeitschrift Fur Anorganische Und Allgemeine Chemie* **1985**, *528*, 129-137.

65 Wolf, R.; Hoppe, R. *Zeitschrift Fur Anorganische Und Allgemeine Chemie* **1987**, *554*, 34-42.

66 Debets, P. C. *Acta Crystallographica* **1966**, *21*, 589-&.

67 Fischer, A. *Zeitschrift Fur Anorganische Und Allgemeine Chemie* **2003**, *629*, 1012-1016.

68 Krivovichev, S. V.; Burns, P. C. *Canadian Mineralogist* **2001**, *39*, 197-206.

69 Krivovichev, S. V.; Burns, P. C. *Journal of Solid State Chemistry* **2002**, *168*, 245-258.

70 Krivovichev, S. V.; Finch, R. J.; Burns, P. C. *Canadian Mineralogist* **2002**, *40*, 193-200.

71 Krivovichev, S. V.; Burns, P. C. *Canadian Mineralogist* **2002**, *40*, 201-209.

72 Hayden, L. A.; Burns, P. C. *Journal of Solid State Chemistry* **2002**, *163*, 313-318.

73 Hayden, L. A.; Burns, P. C. *Canadian Mineralogist* **2002**, *40*, 211-216.

74 Burns, P. C.; Hayden, L. A. *Acta Crystallographica Section C-Crystal Structure Communications* **2002**, *58*, I121-I123.

75 Krause, W.; Effenberger, H.; Brandstatter, F. *European Journal of Mineralogy* **1995**, *7*, 1313-1324.

76 Locock, A. J.; Burns, P. C.; Flynn, T. M. *American Mineralogist* **2005**, *90*, 240-246.

77 Locock, A. J.; Burns, P. C. *American Mineralogist* **2003**, *88*, 240-244.

78 Makarov, E. S.; Ivanov, V. I. *Doklady Akademii Nauk Sssr* **1960**, *132*, 673-676.

79 Linde, S. A.; Gorbunova, Y. E.; Lavrov, A. V. *Zhurnal Neorganicheskoi Khimii* **1980**, *25*, 1992-1994.

80 Burns, P. C.; Deely, K. M.; Hayden, L. A. *Canadian Mineralogist* **2003**, *41*, 687-706.

81 Vochten, R.; Vanhaverbeke, L.; Vanspringel, K.; Blaton, N.; Peeters, O. M. *Canadian Mineralogist* **1995**, *33*, 1091-1101.

82 Viswanathan, K.; Harneit, O. *American Mineralogist* **1986**, *71*, 1489-1493.

83 Kolitsch, U.; Giester, G. *Mineralogical Magazine* **2001**, *65*, 717-724.

84 Demartin, F.; Diella, V.; Donzelli, S.; Gramaccioli, C. M.; Pilati, T. *Acta Crystallographica Section B-Structural Science* **1991**, *47*, 439-446.

85 Piret, P.; Declercq, J. P. *Bulletin De Mineralogie* **1983**, *106*, 383-389.

86 Piret, P.; Deliens, M.; Piretmeunier, J. *Bulletin De Mineralogie* **1988**, *111*, 443-449.

87 Piret, P.; Piretmeunier, J.; Deliens, M. *European Journal of Mineralogy* **1990**, *2*, 399-405.

88 Piret, P.; Deliens, M. *Bulletin De Mineralogie* **1982**, *105*, 125-128.

89 Piret, P.; Piretmeunier, J. *Bulletin De Mineralogie* **1988**, *111*, 439-442.

90 Locock, A. J.; Burns, P. C. *Mineralogical Magazine* **2003**, *67*, 1109-1120.

91 Atencio, D.; Neumann, R.; Silva, A. J. G. C.; Mascarenhas, Y. P. *Canadian Mineralogist* **1991**, *29*, 95-105.

92 Piret, P.; Piretmeunier, J.; Declercq, J. P. *Acta Crystallographica Section B-Structural Science* **1979**, *35*, 1880-1882.

93 Piret, P.; Deliens, M. *Bulletin De Mineralogie* **1987**, *110*, 65-72.

94 Locock, A. J.; Burns, P. C. *Canadian Mineralogist* **2003**, *41*, 91-101.

95 Hughes, K. A.; Burns, P. C. *American Mineralogist* **2003**, *88*, 962-966.

96 Locock, A. J.; Burns, P. C. *Journal of Solid State Chemistry* **2003**, *176*, 18-26.

97 Saadi, M.; Dion, C.; Abraham, F. *Journal of Solid State Chemistry* **2000**, *150*, 72-80.

98 Locock, A. J.; Burns, P. C. *Journal of Solid State Chemistry* **2002**, *167*, 226-236.

99 Locock, A. J.; Burns, P. C. *Journal of Solid State Chemistry* **2003**, *175*, 372-379.

100 Tenne, R.; Margulis, L.; Genut, M.; Hodes, G. *Nature* **1992**, *360*, 444-446.

101 Margulis, L.; Salitra, G.; Tenne, R.; Talianker, M. *Nature* **1993**, *365*, 113-114.

102 Tenne, R.; Homyonfer, M.; Feldman, Y. *Chemistry of Materials* **1998**, *10*, 3225-3238.

103 Tremel, W. *Angewandte Chemie-International Edition* **1999**, *38*, 2175-2179.

104 Rao, C. N. R.; Nath, M. *Dalton Transactions* **2003**, 1-24.

105 Krumeich, F.; Muhr, H. J.; Niederberger, M.; Bieri, F.; Schnyder, B.; Nesper, R. *Journal of the American Chemical Society* **1999**, *121*, 8324-8331.

106 Patzke, G. R.; Krumeich, F.; Nesper, R. *Angewandte Chemie-International Edition* **2002**, *41*, 2446-2461.

107 Krusin-Elbaum, L.; Newns, D. M.; Zeng, H.; Derycke, V.; Sun, J. Z.; Sandstrom, R. *Nature* **2004**, *431*, 672-676.

108 Burns, P. C.; Kubatko, K. A.; Sigmon, G.; Fryer, B. J.; Gagnon, J. E.; Antonio, M. R.; Soderholm, L. *Angewandte Chemie-International Edition* **2005**, *44*, 2135-2139.

109 Albrecht-Schmitt, T. E. *Angewandte Chemie-International Edition* **2005**, *44*, 4836-4838.

110 Cheetham, A. K.; Ferey, G.; Loiseau, T. *Angewandte Chemie-International Edition* **1999**, *38*, 3268-3292.

111 Wilson, S. T.; Lok, B. M.; Messina, C. A.; Cannan, T. R.; Flanigen, E. M. *Journal of the American Chemical Society* **1982**, *104*, 1146-1147.

112 Parise, J. B. *Journal of the Chemical Society-Chemical Communications* **1985**, 606-607.

113 Obbade, S.; Dion, C.; Rivenet, M.; Saadi, M.; Abraham, F. *Journal of Solid State Chemistry* **2004**, *177*, 2058-2067.

114 Shvareva, T. Y.; Sullens, T. A.; Shehee, T. C.; Albrecht-Schmitt, T. E. *Inorganic Chemistry* **2005**, *44*, 300-305.

115 Shvareva, T. Y.; Albrecht-Schmitt, T. E. *Inorganic Chemistry* **2006**, *45*, 1900-1902.

116 Shvareva, T. Y.; Beitz, J. V.; Duin, E. C.; Albrecht-Schmitt, T. E. *Chemistry of Materials* **2005**, *17*, 6219-6222.

117 Shvareva, T. Y.; Skanthakumar, S.; Soderholm, L.; Clearfield, A.; Albrecht-Schmitt, T. E. *Chemistry of Materials* **2007**, *19*, 132-134.

118 Kim, J. Y.; Norquist, A. J.; O'Hare, D. *Chemistry of Materials* **2003**, *15*, 1970-1975.

119 Xie, Y. R.; Zhao, H.; Wang, X. S.; Qu, Z. R.; Xiong, R. G.; Xue, X. A.; Xue, Z. L.; You, X. Z. *European Journal of Inorganic Chemistry* **2003**, 3712-3715.

120 Thuery, P. *Chemical Communications* **2006**, 853-855.

121 Jiang, J.; Sarsfield, M. J.; Renshaw, J. C.; Livens, F. R.; Collison, D.; Charnock, J. M.; Helliwell, M.; Eccles, H. *Inorganic Chemistry* **2002**, *41*, 2799-2806.

122 Borkowski, L. A.; Cahill, C. L. *Inorganic Chemistry* **2003**, *42*, 7041-7045.

123 Zhang, W. H.; Zhao, J. S. *Inorganic Chemistry Communications* **2006**, *9*, 397-399.

124 Kim, J. Y.; Norquist, A. J.; O'Hare, D. *Dalton Transactions* **2003**, 2813-2814.

125 Yu, Z. T.; Liao, Z. L.; Jiang, Y. S.; Li, G. H.; Chen, J. S. *Chemistry-a European Journal* **2005**, *11*, 2642-2650.

126 Chen, W.; Yuan, H. M.; Wang, J. Y.; Liu, Z. Y.; Xu, J. J.; Yang, M.; Chen, J. S. *Journal of the American Chemical Society* **2003**, *125*, 9266-9267.

127 Duval, P. B.; Burns, C. J.; Clark, D. L.; Morris, D. E.; Scott, B. L.; Thompson, J. D.; Werkema, E. L.; Jia, L.; Andersen, R. A. *Angewandte Chemie-International Edition* **2001**, *40*, 3358-+.

128 Berthet, J. C.; Thuery, P.; Ephritikhine, M. *Angewandte Chemie-International Edition* **2008**, *47*, 5586-5589.

129 Berthet, J. C.; Thuery, P.; Ephritikhine, M. *Organometallics* **2008**, *27*, 1664-1666.

130 Mokry, L. M.; Dean, N. S.; Carrano, C. J. *Angewandte Chemie-International Edition in English* **1996**, *35*, 1497-1498.

131 Berthet, J. C.; Thuery, P.; Ephritikhine, M. *Chemical Communications* **2005**, 3415-3417.

132 Berthet, J. C.; Siffredi, G.; Thuery, P.; Ephritikhine, M. *Chemical Communications* **2006**, 3184-3186.

133 Berthet, J. C.; Thuery, P.; Ephritikhine, M. *Polyhedron* **2006**, *25*, 1700-1706.

134 Natrajan, L.; Burdet, F.; Pecaut, J.; Mazzanti, M. *Journal of the American Chemical Society* **2006**, *128*, 7152-7153.

135 Nocton, G.; Burdet, F.; Pecaut, J.; Mazzanti, M. *Angewandte Chemie-International Edition* **2007**, *46*, 7574-7578.

136 Lehmann, S.; Geipel, G.; Foerstendorf, H.; Bernhard, G. *Journal of Radioanalytical and Nuclear Chemistry* **2008**, *275*, 633-642.

137 Ruan, C. M.; Luo, W. S.; Wang, W.; Gu, B. H. *Analytica Chimica Acta* **2007**, *605*, 80-86.

138 Ling, M. X.; Yang, X. Y. *Geochimica Et Cosmochimica Acta* **2007**, *71*, A583-A583.

139 Frost, R. L.; Weier, M. *Spectrochimica Acta Part a-Molecular and Biomolecular Spectroscopy* **2004**, *60*, 2399-2409.

140 Frost, R. L. *Spectrochimica Acta Part a-Molecular and Biomolecular Spectroscopy* **2004**, *60*, 1469-1480.

141 Frost, R. L.; Cejka, J.; Weier, M.; Ayoko, G. A. *Journal of Raman Spectroscopy* **2006**, *37*, 1362-1367.

142 Frost, R. L.; Cejka, J.; Weier, M. *Spectrochimica Acta Part a-Molecular and Biomolecular Spectroscopy* **2006**, *65*, 797-801.

143 Frost, R. L.; Cejka, J.; Weier, M.; Martens, W. N. *Journal of Raman Spectroscopy* **2006**, *37*, 879-891.

144 Frost, R. L.; Weier, M. L.; Martens, W.; Cejka, J. *Vibrational Spectroscopy* **2006**, *41*, 205-212.

145 Frost, R. L.; Weier, M. L.; Williams, P. A.; Leverett, P.; Kloprogge, J. T. *Journal of Raman Spectroscopy* **2007**, *38*, 574-583.

146 Frost, R. L.; Pinto, C. *Journal of Raman Spectroscopy* **2007**, *38*, 841-845.

147 Frost, R. L.; Palmer, S. J.; Bouzaid, J. M.; Reddy, B. J. *Journal of Raman Spectroscopy* **2007**, *38*, 68-77.

148 Frost, R. L.; Dickfos, M. J. *Journal of Raman Spectroscopy* **2007**, *38*, 1516-1522.

149 Frost, R. L.; Cejkal, J. *Journal of Raman Spectroscopy* **2007**, *38*, 1488-1493.

150 Frost, R. L.; Cejka, J.; Weier, M. L.; Martens, W. N.; Ayoko, G. A. *Journal of Raman Spectroscopy* **2007**, *38*, 398-409.

151 Frost, R. L.; Cejka, J.; Weier, M. L. *Journal of Raman Spectroscopy* **2007**, *38*, 460-466.

152 Frost, R. L.; Cejka, J.; Ayokol, G. A.; Weier, M. L. *Journal of Raman Spectroscopy* **2007**, *38*, 1311-1319.

153 Frost, R. L.; Cejka, J.; Ayokol, G. A.; Dickfos, M. J. *Journal of Raman Spectroscopy* **2007**, *38*, 1609-1614.

154 Frost, R. L.; Bouzaid, J. M.; Martens, W. N.; Reddy, B. J. *Journal of Raman Spectroscopy* **2007**, *38*, 135-141.

155 Frost, R. L.; Bouzaid, J. M. *Journal of Raman Spectroscopy* **2007**, *38*, 873-879.

156 Frost, R. L.; Cejka, J.; Ayoko, G. A.; Weier, M. *Spectrochimica Acta Part a-Molecular and Biomolecular Spectroscopy* **2007**, *66*, 979-984.

157 Frost, R. L.; Wain, D. L. *Spectrochimica Acta Part a-Molecular and Biomolecular Spectroscopy* **2008**, *71*, 490-495.

158 Frost, R. L.; Keefe, E. C. *Journal of Raman Spectroscopy* **2008**, *39*, 1408-1412.

159 Frost, R. L.; Cejka, J.; Keefe, E. C.; Dickfos, M. J. *Journal of Raman Spectroscopy* **2008**, *39*, 1413-1418.

160 Frost, R. L.; Locke, A. J.; Hales, M. C.; Martens, W. N. *Journal of Thermal Analysis and Calorimetry* **2008**, *94*, 203-208.

161 Frost, R. L.; Bahfenne, S.; Graham, J.; Martens, W. N. *Thermochimica Acta* **2008**, *475*, 39-43.

162 Frost, R. L.; Dickfos, M. J.; Cejka, J. *Journal of Raman Spectroscopy* **2008**, *39*, 1158-1161.

163 Frost, R. L.; Dickfos, M. J.; Reddy, B. J. *Journal of Raman Spectroscopy* **2008**, *39*, 1250-1256.

164 Frost, R. L.; Cejka, J.; Ayoko, G. *Journal of Raman Spectroscopy* **2008**, *39*, 495-502.

165 Denning, R. G. *Chemical Physics Letters* **2007**, *449*, 365-366.

166 Denning, R. G. *Journal of Luminescence* **2008**, *128*, 1745-1747.

167 Liu, G. K.; Vikhnin, V. S. *Chemical Physics Letters* **2007**, *437*, 56-60.

168 Frisch, M.; Borkowski, L. A.; Cahill, C. L. *Abstracts of Papers of the American Chemical Society* **2004**, *228*, U812-U812.

169 Frisch, M.; Cahill, C. L. *Dalton Transactions* **2005**, 1518-1523.

170 Frisch, M.; Cahill, C. L. *Dalton Transactions* **2006**, 4679-4690.

171 Frisch, M.; Cahill, C. L. *Journal of Solid State Chemistry* **2007**, *180*, 2597-2602.

172 Knope, K. E.; Cahill, C. L. *Inorganic Chemistry* **2008**, *47*, 7660-7672.

173 Thuery, P. *Crystal Growth & Design* **2008**, *8*, 4132-4143.

174 Thuery, P.; Masci, B. *Crystal Growth & Design* **2008**, *8*, 3430-3436.

175 Wilkerson, M. P.; Berg, J. M.; Hopkins, T. A.; Dewey, H. J. *Journal of Solid State Chemistry* **2005**, *178*, 584-588.

176 Agranovich, V. M.; Zakhidov, A. A. *Chemical Physics Letters* **1977**, *50*, 278-281.

177 Liu, G. K.; Vikhnin, V. S. *Chemical Physics Letters* **2007**, *449*, 367-368.

Chapter II: Studies on Hydrothermal methods in Crystal Design and Synthesis

2.1 Introduction.

Defined as a chemical process that involves the use of water as a solvent and reaction conditions at a temperature in excess of 100 ^{o}C and pressure above 1 bar,[1] the mild hydrothermal synthetic method has been proven as an effective rout for chemistry and geochemistry.[2-4] The ability to mimic natural geological processes is ideal for recreating the conditions under which minerals are formed.[3-9] This technique can thus be used to synthesize the minerals in the laboratory.[10-19] When attempting to understand the types of compounds that are formed by the actinides in the environment, whether the actinides are deposited through natural source or because of fission reactor waste, the hydrothermal method can bring insight into the interactions these elements and other components in the mixture through the manufacture of crystalline solids.[20] This, as well as other mineral structures, can be synthesized using this method, which therefore mimic natural geological processes. The study of such naturally occurring actinide compounds may lead to the eventual discovery of cleaning processes or storage mechanisms for the radioactive elements.

Each of the mild hydrothermal reactions in this report was carried out in a PARR 4749 autoclave which consists of a 23-mL PTFE liner encapsulated by a stainless steel

reaction bomb.[1] The reactants were loaded into the liner with the water added drop-wise to the solid reactants. Any acid or base solutions were then added drop-wise to the re action mixture. The autoclave was then sealed and placed in a box oven preheated to 100 to 230 ^{o}C. Temperatures above that range risk the break-down of the PTFE liner. Autogenetic pressure created within the liner is proportional to the amount of water in and temperature of the autoclave. The reaction mixture was heated for a number of days, usually between one and six days, and then cooled to room temperature. The rate of cooling can have a high impact on not only the size of crystals,[21] but the product itself.[22]

The compounds synthesized can be extremely sensitive to temperature, volume of water, pH, stoichiometry of reactants, and rate of cooling. Solvation of reactants that are rather insoluble in aqueous media can be achieved under these conditions. The addition of mineralizing agents, such as F^{-},[11,23-25] Cl^{-},[2,26,27] OH^{-},[2,26,28-31] and NO_3^{-},[2] into the reaction mixture can also aid in the dissolution of the reactants, whereas without these agents, no reaction would occur. Due to the sensitivity of the reactions conditions, the use of a modified compositional diagram is necessary to vary these conditions in order to synthesize crystalline phases.[2,32-39] Hydrothermal method has been proven to an effective to synthesized uanyl transition metal phosphates and inorganic-organic hybrid framework containing uranyl cations.[14-17,40,41] Previous reports show that oxalate anion formation under hydrothermal conditions is one such example and several pathways for its formation have been proposed, including the reductive coupling of carbon dioxide, the decomposition or oxidation of an organic compound, and decarboxylation of an organic species.[42-47] The infinite structures including one-dimensional chains, two-dimensional sheets and three-dimensional frameworks constructed uranyl, UO_2^{2+} cations,[2,14-18,40,41]

have been widely reported with the potential application in radioactivity materials,[48,49] new selective ion-exchange materials,[16,17,50] proton conductors[51-53] and luminescence.[15,17] It is well-known that HCN is thermodynamically unstable, could be hydrolyzed by H_2O and $[CN]^-$ are kinetically stable enough for them to well-established. As shown by Scheme 2.1, HCN behaves as a weak acid (p*Ka*= 9.31) and is hydrolyzed in aqueous solution to $[HCO_2]^-$ which could be further coupling t o oxalate anions under hydrothermal reaction.

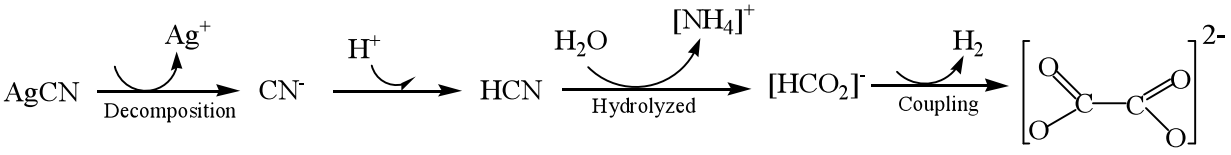

Scheme 2.1. The process of *in situ* synthesized oxalate anions

2.1 Chemical Reagents in Dissertation

Company	Formula	M.W.	
Alfa-Aesar	$UO_2(NO_3)_2 \cdot 6H_2O$	502	98%
Baker	$UO_2(AC)_2 \cdot 2H_2O$	424.15	98%
Alfa-Aesar	UO_2	270.03	99.8%
Aldrich	H_3PO_4	98	98%
Baker	$Na_2HAsO_4 \cdot 7H_2O$	312.01	99.9%
Alfa-Aesar	H_5IO_6	227.94	NA
Alfa-Aesar	CuCN	89.56	NA
Alfa-Aesar	$Ni(CN)_2 \cdot 4H_2O$	182.79	NA
Alfa-Aesar	$K_2[Ni(CN)_4] \cdot 6H_2O$	349.05	NA
Alfa-Aesar	$K_3[Co(CN)_6]$	332.33	90+%
Alfa-Aesar	AgCN	133.89	99%
Alfa-Aesar	$KAg(CN)_2$	199	99.9%
Alfa-Aesar	$Zn(CN)_2$	117.42	98%
Baker	$AgNO_3$	169.87	99.7%
Chemical MFG. Corp.	$Co(NO_3)_2 \cdot 6H_2O$	291.03	98%
Mallinckrodt	$Cu(NO_3)_2 \cdot 2.5H_2O$	187.56	98.2%
Baker	$Hg_2(NO_3)_2 \cdot 2H_2O$	561.22	98.5%
Fisher	$MnCl_2 \cdot 4H_2O$	197.91	99.9%
Alfa-Aesar	NaCl	58.44	99.0%
Alfa-Aesar	CsCl	168.36	99%

Avocado	4,4´-bipyridyl	156	98%
Alfa-Aesar	2,2´-bipyridyl	156	98%
Aldrich	1,2-Bis(4-pyridyl)-ethane	184.24	99%
Aldrich	4,4'-Dimethyl-2,2'-dipyradyl	184.24	99%
Aldrich	5,5'-Dimethyl-2,2'-dipyradyl	184.24	98%
Aldrich	6,6'-Dimethyl-2,2'-dipyradyl	184.24	98%
Aldrich	$(CH_3)_4NCl$	109.60	97%

2.2 Instruments and Data Collection.

2.2.1 Crystallographic Studies.

Single crystals were mounted on a thin glass fibers and optically aligned on a Bruker APEX CCD X-ray diffractometer using a digital camera. Initial intensity measurements were performed using graphite monochromated Mo Kα (λ = 0.71073 Å) radiation from a sealed tube and monocapillary collimator. SMART (v 5.624) was used for preliminary determination of the cell constants and data collection control. The intensities of reflections of a sphere were collected by a combination of 3 sets of exposures (frames). Each set had a different ϕ angle for the crystal and each exposure covered a range of 0.3° in ω. A total of 1800 frames were collected with an exposure time per frame from 30 to 60 s and 10 s for CuUAs-1.

Determination of integrated intensities and global refinement were performed with the Bruker SAINT (v 6.02) software package using a narrow-frame integration algorithm. The data were treated with a semi-empirical absorption correction by SADABS.[54] The

program SHELXTL (v 6.12) was used for space group determination (XPREP), direct methods structure solution or Patterson method (XS), and least-squares refinement (XL).[55] The final refinement included anisotropic displacement parameters for all atoms. Some crystallographic details are given in Appendix I. The details of bond length and bond angles are listed in Appendix II. Thermal parameters for each compound are listed in Appendix III.

2.2.2 Raman Spectroscopy.

The Raman spectra of compounds were acquired from single crystals using a Renishaw inVia Confocal Raman microscope with a 514 nm Ar^+ laser.

2.2.3 Fluorescence Spectroscopy.

The fluorescence emission spectra of compounds were acquired using a PI Acton spectrometer (SpectraPro SP 2356, Acton, NJ) that is connected to the side port of an epi-fluorescence microscope (Nikon TE-2000U, Japan). The emission signal was recorded by a back-illuminated digital CCD camera (PI Acton PIXIS:400B, Acton, NJ) operated by a PC. The excitation was generated by a mercury lamp (X-Cite 120, EXFO, Ontario, Canada) filtered by a band-pass filter at 450-490 nm. The emission signal was filtered by a long-pass filter with a cutoff wavelength of 515 nm.

2.3 Hydrothermal methods used to synthesize compounds.

Reactions were run in PTFE-lined Parr 4749 autoclaves with a 23 mL internal volume. Distilled and Millopore filtered water with a resistance of 18.2 MΩ·cm was used in all reactions. Standard precautions were performed for handling radioactive materials during work with $UO_2(NO_3)_2{\cdot}6H_2O$, $UO_2(Ac)_2{\cdot}2H_2O$, UO_2 and the products of the reactions.

$(H_3O)U_2(PO_4)_3$ (U^{IV}P-1).

UO_2 (0.1633 g, 0.605 mmol), 4,4′-dimethyl-2,2'-bipyridly (0.0557 g, 0.303 mmol), AgCN (0.0810 g, 0.604 mmol) and H_3PO_4 (2 mL, pH = 1.3) were loaded into a 23 mL autoclave. The autoclave was sealed and heated to 200 ^oC in a box furnace for 3 days. The autoclave was then cooled at an average rate of 9 ^oC/h to 35 ^oC. Green plate crystals fragment which grow with unidentified grey precipitation, were recovered and thoroughly washed with water, then rinsed with methanol, and allowed to dry.

$[[Ni(2,2'\text{-bpy})_3](UO_2)(NO_3)(H_2PO_4)_2](NO_3){\cdot}3.25(H_2O)$ (NiUP-1).

$UO_2(NO_3)_2{\cdot}6H_2O$ (0.3350 g, 0.667 mmol), 2,2'-bipyridyl (0.1041 g, 0.667 mmol), $Ni(CN)_2{\cdot}4H_2O$ (0.0610 g, 0.334 mmol) and H_3PO_4 (2 mL, pH = 1.3) were loaded into a 23 mL autoclave. The autoclave was sealed and heated to 180 ^oC in a box furnace for 3 d. The autoclave was then cooled at an average rate of 9 ^oC/h to 35 ^oC. Pink crystals of NiUP-1 were thoroughly washed with water then rinsed with methanol, and allowed to dry.

$[(UO_2)(NO_3)_2(H_2O)][C_6H_6N]$ (UNO_3-1).

$UO_2(NO_3)_2{\cdot}6H_2O$ (0.3231 g, 0.644 mmol), 1,2-bis(4-pyridyl)-ethane (0.0593 g, 0.322 mmol), $Ni(CN)_2{\cdot}4H_2O$ (0.1176 g, 0.644 mmol) and 2 mL distilled water were loaded into

a 23 mL autoclave. The autoclave was sealed and heated to 180 ^{o}C in a box furnace for 4.5 days. The autoclave was then cooled at an average rate of 9 ^{o}C/h to 35 ^{o}C. Yellow plates crystal were recovered and thoroughly washed with water, then rinsed with methanol, and allowed to dry. Powder X-ray diffraction data were collected and compared to a simulated diffraction pattern indicating a pure phase. Yield: 37.2 mg (7.4% based on UO_2^{2+}).

$(UO_2)(Ac)_2$(2,2'-bpy) (UAc-1).

$UO_2(Ac)_2{\cdot}2H_2O$ (0.3277 g, 0.773 mmol), 2,2'-bipyridyl (0.1205 g, 0.772 mmol), AgCN (0.0517 g, 0.386 mmol) and H_2SO_4 (2 mL, pH = 1.3) were loaded into a 23 mL autoclave. The autoclave was sealed and heated to 180 ^{o}C in a box furnace for 6 days. The autoclave was then cooled at an average rate of 9 ^{o}C/h to 35 ^{o}C. The product consisted of yellow plates of UAc-1 and unidentified yellow precipitate. Yellow plates crystal were recovered and thoroughly washed with water, then rinsed with methanol, and allowed to dry.

$[Ag(4,4'\text{-bipy})]_2[(UO_2)_2H_3(PO_4)_3]$ (AgUP-1).

UO_2 (164 mg, 0.607 mmol), 4,4'-bipyridyl (95 mg, 0.609 mmol), AgCN (41 mg, 0.304 mmol), and H_3PO_4 (2 mL, pH = 1.3) were loaded into a 23 mL autoclave. The autoclave was sealed and heated to 160 °C in a box furnace for 3 d. The autoclave was then cooled at an average rate of 9 °C/h to 35 °C. The product consisted of yellow prisms of AgUP-1 and an unidentified black precipitate. The product was thoroughly washed with water, then rinsed with methanol, and allowed to dry.

$Ag(2,2'\text{-bipy})(UO_2)_2(HPO_4)(PO_4)$ (AgUP-2).

$UO_2(C_2H_3O_2)_2 \cdot 2H_2O$ (187 mg, 0.441 mmol), 2,2'-bipyridyl (69 mg, 0.441 mmol), $KAg(CN)_2$ (44 mg, 0.221 mmol), and H_3PO_4 (2 mL, pH = 1.37) were loaded into a 23 mL autoclave. The autoclave was sealed and heated to 180 °C in a box furnace for 3 d. The autoclave was then cooled at an average rate of 9 °C/h to 35 °C. The product consisted of yellow prisms of AgUP-2 and a pale-yellow gel. The product was thoroughly washed with water, then rinsed with methanol, and allowed to dry.

$Na_2Ag_6[(AgO)_2(UO_2)_3(AsO_4)_4]$ (AgUAs-1)

UO_2 (0.1255 g, 0.464 mmol), AgCN (0.1245 g, 0.930 mmol), and Na_2HAsO_4/HNO_3 (2 mL, pH = 0.5) were loaded into a 23 mL autoclave. The autoclave was sealed and heated to 200 °C in a box furnace for 5.5 d. The autoclave was then cooled at an average rate of 9 °C/h to 35 °C. The product consisted of green prisms of AgUAs-1 and yellow precipitation. The product was thoroughly washed with water, then rinsed with methanol, and allowed to dry.

$Ag(UO_2)(AsO_4)$ (AgUAs-2)

$UO_2(NO_3)_2 \cdot 6H_2O$ (0.2176 g, 0.433 mmol), $Na_2HAsO_4 \cdot 7H_2O$ (0.1352 g, 0.433 mmol), $AgNO_3$ (0.1472 g, 0.867 mmol), and 2 mL H_2O were loaded into a 23 mL autoclave. The autoclave was sealed and heated to 200 °C in a box furnace for 4 d. The autoclave was then cooled at an average rate of 9 °C/h to 35 °C. The product consisted of yellow plates of AgUAs-2. The product was thoroughly washed with water, then rinsed with methanol, and allowed to dry.

$[Hg_5O_2(OH)_5][(UO_2)_2(AsO_4)_2]$ (HgUAs-1)

$UO_2(NO_3)_2 \cdot 6H_2O$ (0.194 g, 0.388 mmol), $Na_2HAsO_4 \cdot 7H_2O$ (0.0612 g, 0.196 mmol), $HgNO_3 \cdot H_2O$ (0.220 g, 0.695 mmol), $(CH_3)_4NCl$ (0.0215 g, 0.196 mmol), and 2 mL of

water were loaded into a 23 mL autoclave. The autoclave was sealed and heated to 200 ^{o}C in a box furnace for 3 days. The autoclave was then cooled at an average rate of 9 ^{o}C/h to 35 ^{o}C. Yellow blocks were recovered and thoroughly washed with water, then rinsed with methanol, and allowed to dry. Yield: 146 mg, 19.4% based on uranium. EDX analysis confirmed the presence of Hg, U, and As in the crystals.

$[Zn(2,2'\text{-bpy})]_2[UO_2(HPO_4)_3]$ (ZnUP-1)

UO_2 (167 mg, 0.619 mmol), 2,2'-bipyridyl (97 mg, 0.618 mmol), $Zn(CN)_2$ (36 mg, 0.309 mmol), and H_3PO_4 (2 mL, pH = 1.3) were loaded into a 23 mL autoclave. The autoclave was sealed and heated to 180 °C in a box furnace for 3 d. The autoclave was then cooled at an average rate of 9 °C/h to 35 °C. The product consisted of yellow plates of ZnUP-1 and a black precipitate. The product was thoroughly washed with water, then rinsed with methanol, and allowed to dry.

$[H_2bipy]_2[(UO_2)_6Zn_2(PO_3OH)_4(PO_4)_4]\cdot H_2O$ (ZnUP-2).

$UO_2(C_2H_3O_2)_2\cdot 2H_2O$ (0.2269 g, 0.535 mmol), 4,4'-bipyridyl (0.0417 g, 0.267 mmol), $Zn(CN)_2$ (0.0314 g, 0.267 mmol) and H_3PO_4 (2 mL, pH = 1.3) were loaded into a 23 mL autoclave. The autoclave was sealed and heated to 180 ^{o}C in a box furnace for 3 days. The autoclave was then cooled at an average rate of 9 ^{o}C/h to 35 ^{o}C. Yellow tablets were recovered and thoroughly washed with water, then rinsed with methanol, and allowed to dry. Powder X-ray diffraction data were collected and compared to a simulated diffraction pattern indicating a pure phase. Yield: 133.8 mg (8.8% based on $UO_2(C_2H_3O_2)_2\cdot 2H_2O$)

$K_2[UO_2Co(PO_4)_2]\cdot H_2O$ (CoUP-1).

UO_2 (0.152 g, 0.562 mmol), $K_3[Co(CN)_6]$ (0.085 g, 0.256 mmol), 2 mL of 85% H_3PO_4 were loaded into a 23 mL autoclave. The autoclave was sealed and heated to 200 ^oC in a box furnace for 5.5 d. The autoclave was then cooled at an average rate of 9 ^oC/h to 35 ^oC. Dark blue crystals of KUCoP-1 were manually isolated from a mixture that also contains pink crystals of $[H_3O][Co(H_2O)PO_4]$. EDX analysis provided K:U:Co:P ratio of approximately 2:1:1:2.

$Zn(OH)_2[(UO_2)_8O_4(SO_4)_4] \cdot 14H_2O$ (ZnUS-1).

$UO_2(C_2H_3O_2)_2 \cdot 2H_2O$ (0.3320 g, 0.783 mmol), 4,4'-bipyridyl (0.1221 g, 0.783 mmol), $Zn(CN)_2$ (46 mg, 0.392 mmol), and H_2SO_4 (2 mL, pH = 1.3) were loaded into a 23 mL autoclave. The autoclave was sealed and heated to 180 °C in a box furnace for 5 d. The autoclave was then cooled at an average rate of 9 °C/h to 35 °C. The product consisted of yellow needle of ZnUS-1 and yellow precipitation. The product was thoroughly washed with water, then rinsed with methanol, and allowed to dry.

$[Co(OH)_2]_3[(UO_2)_8O_4(SO_4)_4] \cdot 2H_2O$ (CoUS-1).

UO_2 (0.1368 g, 0.507 mmol), 2,2'-bipyridyl (0.0790 g, 0.506 mmol), $K_3[Co(CN)_6]$ (0.0842 g, 0.253 mmol), and H_2SO_4 (2 mL, pH = 1.3) were loaded into a 23 mL autoclave. The autoclave was sealed and heated to 200 ^oC in a box furnace for 4 d. The autoclave was then cooled at an average rate of 9 ^oC/h to 35 ^oC. Burgundy crystals of **CoUS-1** were manually isolated from a mixture that also contains gray precipitation.

$[Ni(OH)_2]_3[(UO_2)_8O_4(SO_4)_4] \cdot 10H_2O$ (NiUS-1).

$UO_2(NO_3)_2 \cdot 6H_2O$ (0.3350 g, 0.667 mmol), 2,2'-bipyridyl (0.1041 g, 0.667 mmol), $Ni(CN)_2 \cdot 4H_2O$ (0.0610 g, 0.737 mmol) and H_2SO_4 (2 mL, pH = 1.3) were loaded into a 23 mL autoclave. The autoclave was sealed and heated to 200^{o}C in a box furnace for 7

days. The autoclave was then cooled at an average rate of 9 ^{o}C/h to 35 ^{o}C. Purple prism crystal were recovered and thoroughly washed with water, then rinsed with methanol, and allowed to dry. Powder X-ray diffraction data were collected and compared to a simulated diffraction pattern indicating a pure phase.

$[Ni(OH)_2][(UO_2)_4O_2(SO_4)_2] \cdot 8H_2O$ (NiUS-2).

$UO_2(C_2H_3O_2)_2 \cdot 2H_2O$ (0.3158 mg, 0.745 mmol), 2,2'-bipyridyl (0.1162 g, 0.745 mmol), $Ni(CN)_2 \cdot 4H_2O$ (0.0680 g, 0.372 mmol) and H_2SO_4 (2 mL, pH = 1.3) were loaded into a 23 mL autoclave. The autoclave was sealed and heated to 200^{o}C in a box furnace for 7 days. The autoclave was then cooled at an average rate of 9 ^{o}C/h to 35 ^{o}C. Yellow block crystal were recovered and thoroughly washed with water, then rinsed with methanol, and allowed to dry.

$(UO_2)(OH)(CO_2)(C_5H_4N)$ (Uoxa-1).

$UO_2(NO_3)_2 \cdot 6H_2O$ (0.2462 g, 0.490 mmol), 4,4'-bipyridyl (0.0719 g, 0.461 mmol), AgCN (0.0656 g, 0.490 mmol) and H_5IO_6 (0.1117 g, 0.490 mmol) were loaded into a 23 mL autoclave. The autoclave was sealed and heated to 180 ^{o}C in a box furnace for 5 days. The autoclave was then cooled at an average rate of 9 ^{o}C/h to 35 ^{o}C. Yellow blocks which grow with yellow precipitation, were recovered and thoroughly washed with water, then rinsed with methanol, and allowed to dry.

$(UO_2)(OH)_2(C_5H_4N)_2$ (Ubpy-1).

$UO_2(C_2H_3O_2)_2 \cdot 2H_2O$ (0.3277 g, 0.773 mmol), 4,4'-bipyridyl (0.1205 g, 0.772 mmol), AgCN (0.0517 g, 0.386 mmol) and H_2SO_4 (2 mL, pH = 1.3) were loaded into a 23 mL autoclave. The autoclave was sealed and heated to 180 ^{o}C in a box furnace for 5 days. The autoclave was then cooled at an average rate of 9 ^{o}C/h to 35 ^{o}C. Yellow block

crystals which grow with yellow precipitation, were recovered and thoroughly washed with water, then rinsed with methanol, and allowed to dry.

$(C_6H_5NH)(UO_2)(PO_4)$ (Ubpe-1).

$UO_2(NO_3)_2 \cdot 6H_2O$ (0.3165 g, 0.630 mmol), 1,2-Bis(4-pyridyl)-ethane (0.0581 g, 0.319 mmol), $KAg(CN)_2$ (0.1254 g, 0.630 mmol) and H_3PO_4 (2 mL, pH = 1.3) were loaded into a 23 mL autoclave. The autoclave was sealed and heated to 180 ^oC in a box furnace for 3.5 days. The autoclave was then cooled at an average rate of 9 ^oC/h to 35 ^oC. Yellow Blocks crystals which grow with yellow precipitation, were recovered and thoroughly washed with water, then rinsed with methanol, and allowed to dry.

$Co(UO_2)_2(AsO_4)_2 \cdot 8H_2O$ (CoUAs-1).

$UO_2(NO_3)_2 \cdot 6H_2O$ (0.2128 g, 0.424 mmol), $Na_2HAsO_4 \cdot 7H_2O$ (0.1322 g, 0.424 mmol), $Co(NO_3)_2$ (0.1550 g, 0.847 mmol) and 2 mL of water were loaded into a 23 mL autoclave. The autoclave was sealed and heated to 200 ^oC in a box furnace for 3 days. The autoclave was then cooled at an average rate of 9 ^oC/h to 35 ^oC. Pink plate crystals were recovered and thoroughly washed with water, then rinsed with methanol, and allowed to dry.

$Mn(UO_2)_2(AsO_4)_2 \cdot 8H_2O$ (MnUAs-1).

$UO_2(NO_3)_2 \cdot 6H_2O$ (0.2075 g, 0.413 mmol), $Na_2HAsO_4 \cdot 7H_2O$ (0.1289 g, 0.413 mmol), $MnCl_2 \cdot 4H_2O$ (0.1636 g, 0.827 mmol) and 2 mL of water were loaded into a 23 mL autoclave. The autoclave was sealed and heated to 200 ^oC in a box furnace for 4 days. The autoclave was then cooled at an average rate of 9 ^oC/h to 35 ^oC. Yellow plate crystals were recovered and thoroughly washed with water, then rinsed with methanol, and allowed to dry.

$Cu(UO_2)_2(AsO_4)_2 \cdot 5H_2O$ (CuUAs-1).

$UO_2(NO_3)_2 \cdot 6H_2O$ (0.2679 g, 0.534 mmol), $Na_2HAsO_4 \cdot 7H_2O$ (0.1665 g, 0.534 mmol), $Cu(NO_3)_2$ (0.0501 g, 0.267 mmol), NaCl (0.0156, 0.267 mmol) and 2 mL of water were loaded into a 23 mL autoclave. The autoclave was sealed and heated to 200 ^oC in a box furnace for 3 days. The autoclave was then cooled at an average rate of 9 ^oC/h to 35 ^oC. Green plate crystals were recovered and thoroughly washed with water, then rinsed with methanol, and allowed to dry.

References:

1 Sullens, T. A. Ph. D. Dissertation, Aug. 2005.

2 Burns, P. C. *Canadian Mineralogist* 2005, *43*, 1839-1894.

3 Barsukov, V. L. *Geochemistry International* 2006, *44*, 1191-1214.

4 Barsukov, V. L. *Geochemistry International* 2006, *44*, 591-612.

5 Bach, W.; Peucker-Ehrenbrink, B.; Hart, S. R.; Blusztajn, J. S. *Geochemistry Geophysics Geosystems* 2003, *4*, -.

6 Barsukov, V. L.; Borisov, M. V. *Geokhimiya* 1988, 1429-1446.

7 Barsukov, V. L.; Borisov, M. V. *Geokhimiya* 1989, 68-86.

8 Barsukov, V. L.; Sokolova, N. T.; Knyazeva, S. N.; Shvarov, Y. V. *Geochemistry International* 2000, *38*, 652-675.

9 Barsukov, V. L.; Sokolova, N. T. *Geokhimiya* 2000, 55-77.

10 Almond, P. M.; Deakin, L.; Mar, A.; Albrecht-Schmitt, T. E. *Journal of Solid State Chemistry* 2001, *158*, 87-93.

11 Almond, P. M.; Deakin, L.; Mar, A.; Albrecht-Schmitt, T. E. *Inorganic Chemistry* 2001, *40*, 886-890.

12 Sykora, R. E.; McDaniel, S. M.; Wells, D. M.; Albrecht-Schmitt, T. E. *Inorganic Chemistry* 2002, *41*, 5126-5132.

13 Sykora, R. E.; Wells, D. M.; Albrecht-Schmitt, T. E. *Inorganic Chemistry* 2002, *41*, 2304-2306.

14 Shvareva, T. Y.; Albrecht-Schmitt, T. E. *Inorganic Chemistry* 2006, *45*, 1900-1902.

15 Yu, Y.; Zhan, W.; Albrecht-Schmitt, T. E. *Inorganic Chemistry* 2007, *46*, 10214-10220.

16 Shvareva, T. Y.; Skanthakumar, S.; Soderholm, L.; Clearfield, A.; Albrecht-Schmitt, T. E. *Chemistry of Materials* 2007, *19*, 132-134.

17 Yu, Y. Q.; Zhan, W.; Albrecht-Schmitt, T. E. *Inorganic Chemistry* 2008, *47*, 9050-9054.

18 Yu, Y. Q.; Albrecht-Schmitt, T. E. *Solid State Sciences* 2008, *10*, 821-824.

19 Bray, T. H.; Skanthakumar, S.; Soderholm, L.; Sykora, R. E.; Haire, R. G.; Albrecht-Schmitt, T. E. *Journal of Solid State Chemistry* 2008, *181*, 493-498.

20 Bayushki.Im; Dikov, Y. P. *Geokhimiya* 1974, 1654-1663.

21 Shiraki, T.; Wakihara, T.; Sadakata, M.; Yoshimura, M.; Okubo, T. *Microporous and Mesoporous Materials* 2001, *42*, 229-234.

22 Sullens, T. A.; Jensen, R. A.; Shvareva, T. Y.; Albrecht-Schmitt, T. E. *Journal of the American Chemical Society* 2004, *126*, 2676-2677.

23 Almond, P. M.; Deakin, L.; Porter, M. J.; Mar, A.; Albrecht-Schmitt, T. E. *Chemistry of Materials* 2000, *12*, 3208-3213.

24 Cahill, C. L.; Burns, P. C. *Inorganic Chemistry* 2001, *40*, 1347-1351.

25 Bean, A. C.; Sullens, T. A.; Runde, W.; Albrecht-Schmitt, T. E. *Inorganic Chemistry* 2003, *42*, 2628-2633.

26 Li, Y. P.; Burns, P. C. *Canadian Mineralogist* 2000, *38*, 1433-1441.

27 Bean, A. C.; Xu, Y. W.; Danis, J. A.; Albrecht-Schmitt, T. E.; Scott, B. L.; Runde, W. *Inorganic Chemistry* 2002, *41*, 6775-6779.

28 Li, Y. P.; Burns, P. C. *Canadian Mineralogist* 2000, *38*, 727-735.

29 Li, Y. P.; Cahill, C. L.; Burns, P. C. *Chemistry of Materials* 2001, *13*, 4026-4031.

30 Burns, P. C.; Deely, K. M. *Canadian Mineralogist* 2002, *40*, 1579-1586.

31 Glatz, R. E.; Li, Y. P.; Hughes, K. A.; Cahill, C. L.; Burns, P. C. *Canadian Mineralogist* 2002, *40*, 217-224.

32 Locock, A. J.; Burns, P. C. *Journal of Solid State Chemistry* 2004, *177*, 2675-2684.

33 Giesting, P. A.; Porter, N. J.; Burns, P. C. *Zeitschrift Fur Kristallographie* 2006, *221*, 589-599.

34 Almond, P. M.; Talley, C. E.; Bean, A. C.; Peper, S. M.; Albrecht-Schmitt, T. E. *Journal of Solid State Chemistry* 2000, *154*, 635-641.

35 Talley, C. E.; Bean, A. C.; Albrecht-Schmitt, T. E. *Inorganic Chemistry* 2000, *39*, 5174-+.

36 Bean, A. C.; Albrecht-Schmitt, T. E. *Journal of Solid State Chemistry* 2001, *161*, 416-423.

37 Almond, P. M.; Albrecht-Schmitt, T. E. *Inorganic Chemistry* 2002, *41*, 5495-5501.

38 Almond, P. M.; Albrecht-Schmitt, T. E. *Inorganic Chemistry* 2003, *42*, 5693-5698.

39 Bray, T. H.; Ling, J.; Choi, E. S.; Brooks, J. S.; Beitz, J. V.; Sykora, R. E.; Haire, R. G.; Stanbury, D. M.; Albrecht-Schmitt, T. E. *Inorganic Chemistry* 2007, *46*, 3663-3668.

40 Shvareva, T. Y.; Almond, P. M.; Albrecht-Schmitt, T. E. *Journal of Solid State Chemistry* 2005, *178*, 499-504.

41 Shvareva, T. Y.; Sullens, T. A.; Shehee, T. C.; Albrecht-Schmitt, T. E. *Inorganic Chemistry* 2005, *44*, 300-305.

42 Adams, D. M. Y. B.; Kahwa, I. A.; Mague, J. T. *New Journal of Chemistry* 1998, *22*, 919-921.

43 Farrugia, L. J.; Lopinski, S.; Lovatt, P. A.; Peacock, R. D. *Inorganic Chemistry* 2001, *40*, 558-+.

44 Wong, W. K.; Zhang, L. L.; Xue, F.; Mak, C. W. *Journal of the Chemical Society-Dalton Transactions* 2000, 2245-2246.

45 Baruah, B.; Golub, V. O.; O'Connor, C. J.; Chakravorty, A. *European Journal of Inorganic Chemistry* 2003, 2299-2303.

46 Orioli, P.; Bruni, B.; Di Vaira, M.; Messori, L.; Piccioli, F. *Inorganic Chemistry* 2002, *41*, 4312-4314.

47 Belsky, A. J.; Maiella, P. G.; Brill, T. B. *Journal of Physical Chemistry A* 1999, *103*, 4253-4260.

48 Terra, O.; Clavier, N.; Dacheux, N.; Podor, R. *New Journal of Chemistry* 2003, *27*, 957-967.

49 Brandel, V.; Clavier, N.; Dacheux, N. *Radiochimica Acta* 2006, *94*, 461-464.

50 Sykora, R. E.; Albrecht-Schmitt, T. E. *Chemistry of Materials* 2001, *13*, 4399-+.

51 Gordon, R. E.; Strange, J. H.; Halstead, T. K. *Solid State Communications* 1979, *31*, 995-997.

52 Howe, A. T.; Shilton, M. G. *Journal of Solid State Chemistry* 1980, *34*, 149-155.

53 Childs, P. E.; Howe, A. T.; Shilton, M. G. *Journal of Solid State Chemistry* 1980, *34*, 341-346.

54. Sheldrick, G. M. *SADABS* 2001, Program for absorption correction using SMART CCD based on the method of Blessing: Blessing, R. H. *Acta Crystallogr.* 1995, *A51*, 33.

55. Sheldrick, G. M. SHELXTL PC, Version 6.12, An Integrated System for Solving, Refining, and Displaying Crystal Structures from Diffraction Data; Siemens Analytical X-Ray Instruments, Inc.: Madison, WI 2001.

Chapter III. Studies on Structure and Structure-Properties Relationships

Of the 22 compounds covered in this dissertation, seven (31.8%) are based upon sheets of polyhedra, two (9.1%) are based upon chains of polyhedra, and three (13.6%) are based upon limited cluster polyhedra. There are ten (45.5%) structures based upon three-dimensional frameworks. Single crystal diffraction experiments reveal that the seven sheet structures contain transition metal cations (Ag^{+}, Co^{2+}, Mn^{2+}, Cu^{2+}). The ten three-dimensional frameworks contain transition metal substructures (Ag^{+}, Hg^{2+}, Ni^{2+}, Co^{2+}, Zn^{2+}), metal-organic framework (MOF) structures and porous low-valence uranium framework. There are two chain structures containing bimetallic metal-organic hybrids and single metal-organic hybrids. Three limited polyhedra structures contain mononuclear and binuclear clusters are also described. In each case the structural unit is illustrated, and pertinent crystallographic information are provided in the appendix. Addition characterization includes Raman spectroscopy, fluorescent spectroscopy, ion-exchange, and thermal stability.

Table 3.1 Structures based upon linkage between uranium and

Transition metals, Organic ligands

Name	Formula
Open framework constructed by Low valence U^{4+} phosphate	
$U^{IV}P$-1	$(H_3O)U_2(PO_4)_3$
Limit polyhedra structures	
NiUP-1	$[[Ni(2,2'\text{-bpy})_3](UO_2)(NO_3)(H_2PO_4)_2](NO_3)\cdot 3.25(H_2O)$
UNO_3-1	$[(UO_2)(NO_3)_2(H_2O)][C_6H_6N]$
UAc-1	$(UO_2)(Ac)_2(2,2'\text{-bpy})$
2D and 3D constructed from Uranyl Silver	
AgUP-1	$[Ag(4,4'\text{-bpy})]_2[(UO_2)H_3(PO_4)_3]$
AgUP-2	$Ag(2.2'\text{-bpy})(UO_2)_2(HPO_4)(PO_4)$
AgUAs-1	$Na_2Ag_6[(AgO)_2(UO_2)_3(AsO_4)_4]$
AgUAs-2	$Ag(UO_2)(AsO_4)$
1D and 3D constructed from uranyl mercury and zinc	
HgUAs-1	$[Hg_5O_2(OH)_5][(UO_2)_2(AsO_4)_2]$
ZnUP-1	$[Zn(2,2'\text{-bpy})]_2[UO_2(HPO_4)_3]$
ZnUP-2	$[H_2bipy][(UO_2)_6Zn_2(PO_3OH)_4(PO_4)_4\cdot H_2O$
3D frameworks constructed from uranyl cobalt	
CoUP-1	$K_2[UO_2Co(PO_4)_2]\cdot H_2O$
Transition metal zippeite (Zn^{II}, Co^{II}, Ni^{II})	
ZnUS-1	$[Zn(OH)_2][(UO_2)_8O_4(SO_4)_4]\cdot 14H_2O$
CoUS-1	$[Co(OH)_2]_3[(UO_2)_8O_4(SO_4)_4]\cdot 2H_2O$

NiUS-1	$[Ni(OH)_2]_3[(UO_2)_8O_4(SO_4)_4]\cdot 10H_2O$
NiUS-2	$[Ni(OH)_2][(UO_2)_4O_2(SO_4)_2]\cdot 8H_2O$
1D, 2D and 3D structures constructed by incorporation of bipy ligands	
Uoxa-1	$(UO_2)(OH)(CO_2)(C_5H_4N)$
Ubpy-1	$(UO_2)(OH)_2(C_5H_4N)_2$
Ubpe-1	$(C_6H_5NH)(UO_2)(PO_4)$
2D, 3D constructed from transition metal (Mn, Co, Cu) autunite	
CoUAs-1	$Co(UO_2)_2(AsO_4)_2\cdot 8H_2O$
MnUAs-1	$Mn(UO_2)_2(AsO_4)_2\cdot 8H_2O$
CuUAs-1	$Cu(UO_2)_2(AsO_4)_2\cdot 5H_2O$

3.1 $(H_3O)U_2(PO_4)_3$ (U^{IV}P-1)

3.1.1 Structural features.

U^{IV}P-1 possesses an open-framework structure consisting of nine-coordinated U^{IV} that are linked by edge-sharing and further joined together by PO_4 tetrahedra by corner-sharing. Channels occur along the *c* axis. These channels house the hydration cation, and are approximately 8.548 × 8.548 Å. Various views of this structure are shown in Figure 3.1.1. The basic building units are shown in Figure 3.1.2. The view down the *c* axis shows something peculiar about the channels that extend in this direction in that they appear to be void spaces filled by diprotonated water molecules. The view down the *b* axis shows the three-dimensional structure could be constructed by two-dimensional uranium (IV) phosphates layer further linked each other by tetrahedra PO_4^{3-} bridging by edge-sharing.

There is one crystallographically unique uranium center in the structure of U^{IV}P-1. Each of these units contains nine-coordination uranium (IV). Unlike the most of nine-coordinated geometries which take the tricapped trigonal prism, the uranium center of U^{IV}P-1 locates in the center of distorted tetrahedral which is constructed from the three different tetrahedra edge-sharing each other consisting with the two capped-tetrahedra and one of distorted tetrahedra geometry, as shown in Figure 3.1.2.

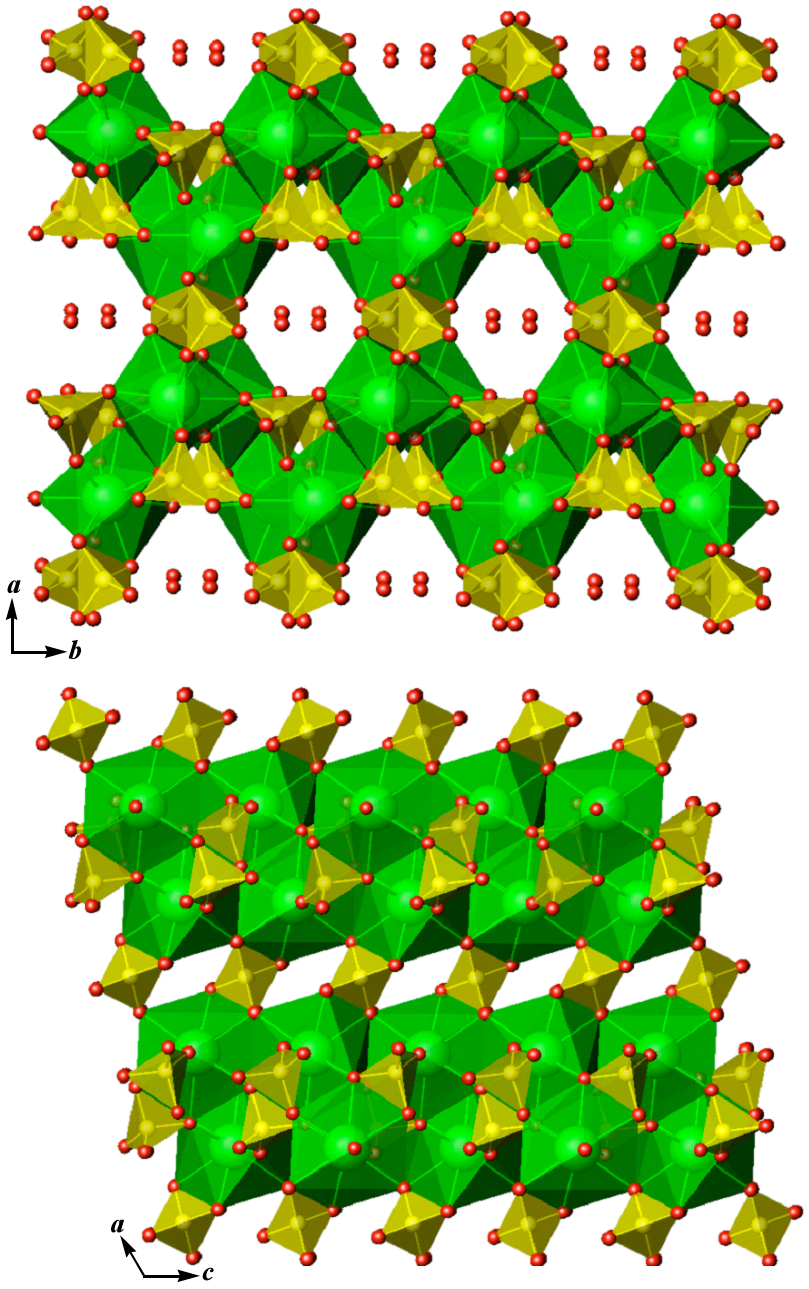

Figure 3.1.1. Two views of the open-framework structure of $(H_3O)U_2(PO_4)_3$ ($U^{IV}P$-1) UO_9 = Green, PO_4 = Yellow.

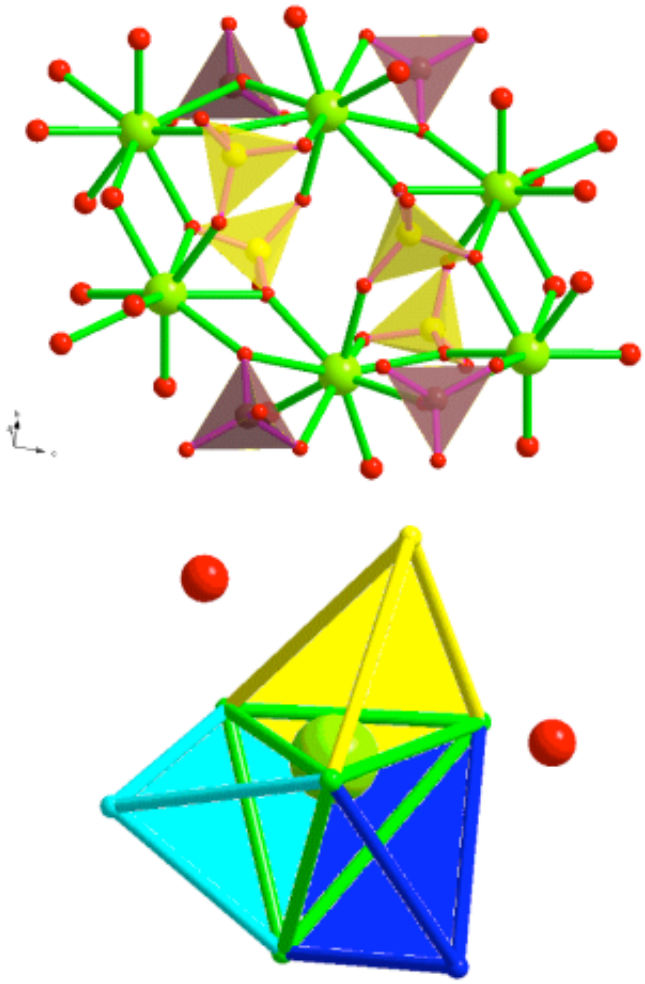

Figure 3.1.2. Depiction of the basic building units and coordination mode of U(IV) in $(H_3O)U_2(PO_4)_3$ ($U^{IV}P$-1).

The U-O distances within the $U^{IV}P$-1 from 2.304(8) to 2.610(8) Å. These bond distances are typical for uranium (IV), and can be used to calculate bond-valence sums of 3.88 for U(1), which is consistent with the expected oxidation state of U(IV) in starting compound UO_2. There are one and half PO_4 tetrahedra with bond distances ranging from 1.506(8) to 1.549(8) Å. However, it encompasses both short and long P–O bonds. For example, the P(1)–O(5) bond length is 1.506(8) Å, and the oxygen atom is terminal.

This linkage and be described as P=O. One of PO_4 tetrahedra can be identified by average P-O bond length due to act as the phosphate bridging connected with two dimensional uranium phosphate planes. The basic building unit is the hexanuclear U(IV) cluster ring which belongs to the center-missing Anderson-type polyoxometalate motif structure type. Six uranium(IV) centers link each other to ring type with the size of 10.077 × 5.460 Å by edge-sharing. Unlike the $U_7N_6N_6$ core analogue Anderson-type structure which six U(IV) atoms surrounding the center U(IV) atom share the same plane in molecular structure, there are two structure features that make the center-missing Anderson-type of basic unit of U^{IV}P-1 identical. On one hand, there are only six U(IV) centers in different planes stabilized by the four capped phosphate tetrahedra in the structure due to the softer U(IV)-O bonding than that of Mo(VI)-O bonding. On the other hand, the shape of hexanuclear U(IV) cluster ring is a eclipsed ring which has 2-fold rotation axis consistent with the one of symmetric components (2) in *C*2/c space group. As shown in Figure 3.1.3, the one-dimensional chains constructed from hexanuclear U(IV) eclipsed rings by edge-sharing each other are parallel each other along the [1 1 0] direction. Further linkage between these parallel one-dimensional chains by edge-sharing each other constructs the $[U^{IV}_2O_7]^{6-}$ anion sheet. Three crystallographic independent phosphates can be divided into two kinds according to different functions in structure. As shown in Figure 3.1.4, two phosphates anions act as decoration and structure stabilization groups located on both sides of the hexanuclear U(IV) eclipsed rings , basic building units, by corner-sharing. The different orientations at both sides basic building units provide the enough space for the hydration cations. The construction mode shows that the active $[U^{IV}_2O_7]^{6-}$ anion sheets are protected by PO_4^{3-} tetrahedra. The other

phosphate acts as bridging group linking two-dimensional sheets constructed from U(IV) phosphates into a three-dimensional framework, as shown in Figure 3.1.4.

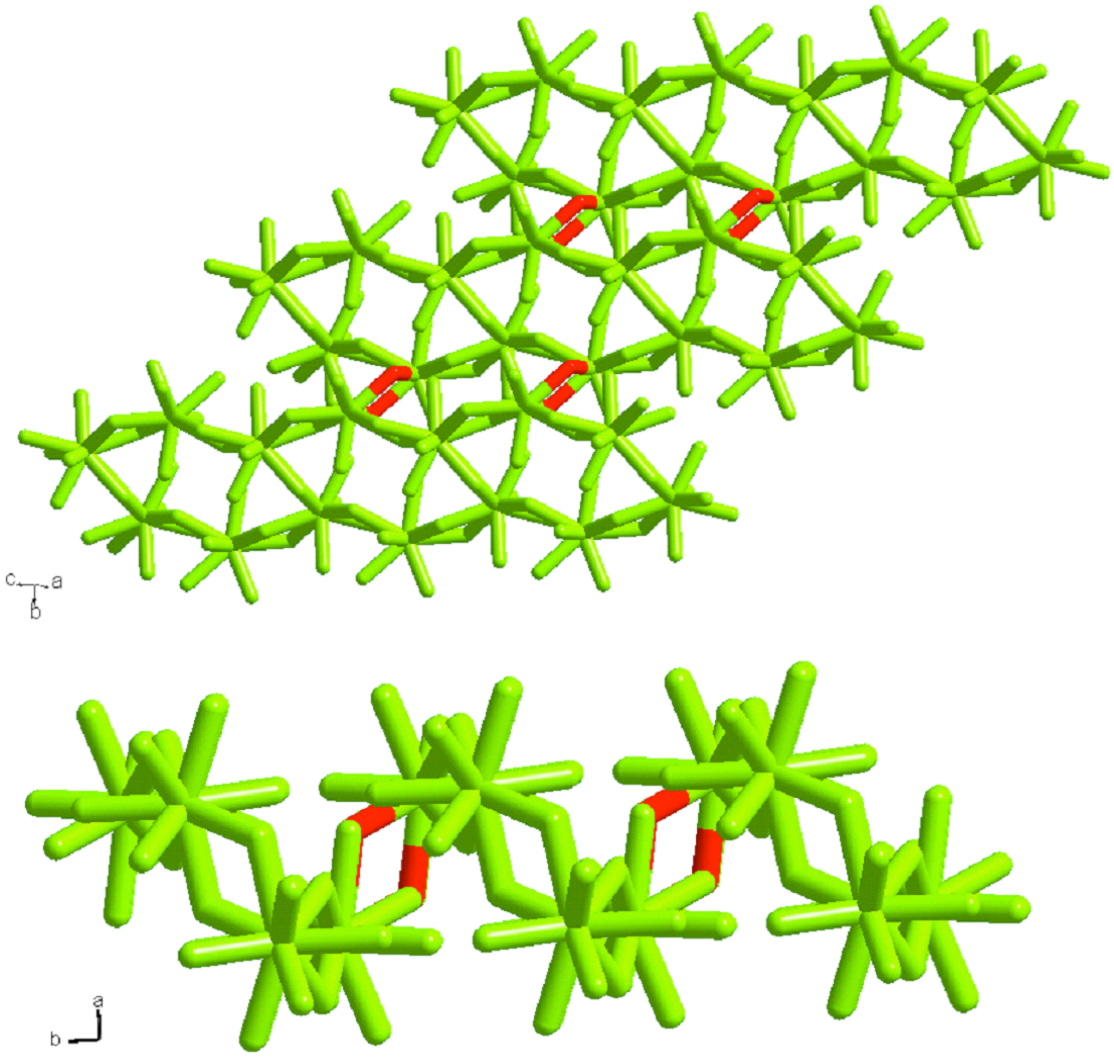

Figure 3.1.3. Two-dimensional anionic sheet constructed from the $[U^{IV}_2O_7]^{6-}$ cluster.

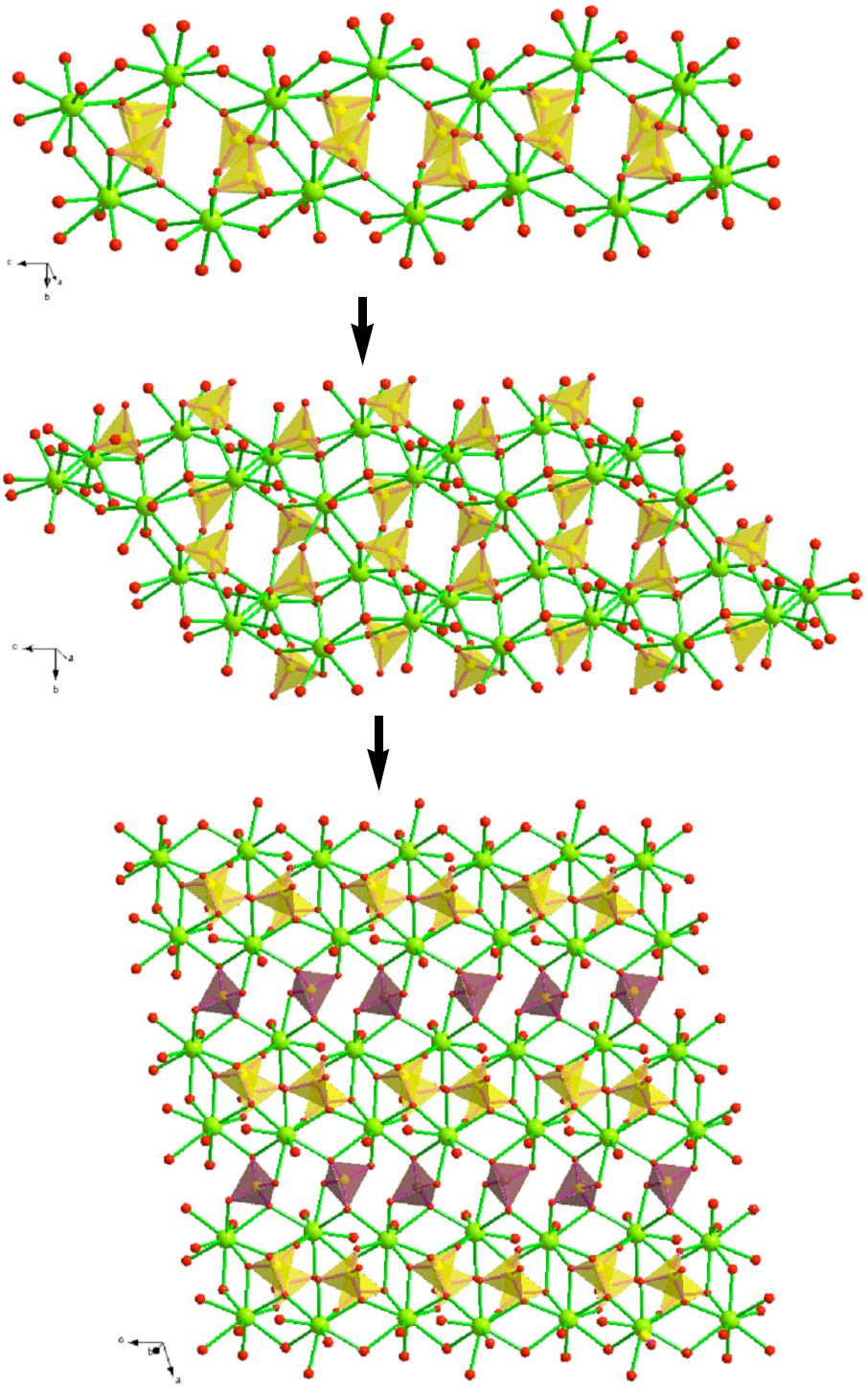

Figure 3.1.4. Structure construction modes of $(H_3O)U_2(PO_4)_3$ ($U^{IV}P$-1)

3.1.2 Raman Spectroscopy

The Raman spectra were collected on a Renishaw inVia Raman microscope spectrometer, as shown in Figure 3.1.5. Missing Raman bands at 840 cm^{-1} which are attributed to the υ_1 symmetric stretching mode for the $(UO_2)^{2+}$ units shows no existence of U^{6+} species in solid state consistence with the single crystal diffraction data. The intensity peaks at 1593.15 and 1377.27 cm^{-1} is attributed to the H_3O^+ bending mode which present the intense peak at 1630-1600 cm^{-1} in most of publications, due to the protonation of lattice water. The weak peak at 939.17 cm^{-1} is assigned to ν_1 symmetric stretching mode of P–O. Another weak peak for lattice water at 660.79 cm^{-1} is attributed to exhibit "librational modes" that are due to rotational oscillations of the water molecules, restricted by hydrogen bonding between O2, O3 and O6 to O1w with distances of 2.719 to 2.845 Å.

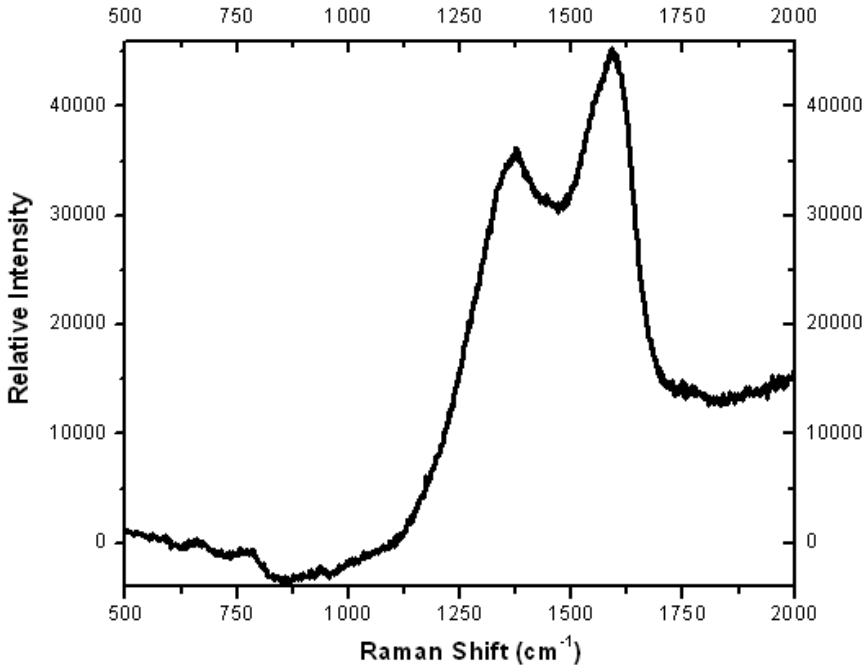

Figure 3.1.5. The Raman Spectrum of $(H_3O)U_2(PO_4)_3$ (U^{IV}P-1).

3.2 $[[Ni(2,2'\text{-bpy})_3](UO_2)(NO_3)(H_2PO_4)_2](NO_3)\cdot 3.25(H_2O)$ (NiUP-1)

3.2.1 Synthesis and Structural features

Synthesis. The methodology of synthesizing new heterobimetallic compounds using $UO_2(NO_3)_2\cdot 6H_2O$ with transition metal and phosphoric acid under mild hydrothermal condition has been proven successful. The infinite structures including one-dimensional chains, two-dimensional sheets and three-dimensional frameworks constructed by uranyl, UO_2^{2+} cations, have been widely reported but it is the research trend to study three-dimensional frameworks constructed by uranyl phases with potential application in the storage of key radionuclides from spent nuclear fuel and as new selective ion-exchange materials. Up to now, few structures containing finite clusters of polyhedra have been reported due to strong coordination tendency of equatorial oxygen atoms. The binuclear structure of NiUP-1 is constructed from pentagonal bipyramidal uranyl units linking by two phosphates tetrahedra. The structure is unusual because it contains the unique bulky cation constructed from octahedra Ni^{2+} coordinated with three 2,2'-bpy ligands.

Structural features of NiUP-1. The bond-valence sum calculations show value of 6.05 for U1 consistence with the expected oxidation state U^{6+} in UO_2^{2+}. The calculation for coordinated octahedra Ni1 is 2.41, which is higher than the expecting value of +2. The reason is that the electronic configuration of Ni^{2+} t_{2g} 6 e_g^* 2 overlapped with π^* orbital of 2,2'-bpy ligands due to similar energy levels and orbital shapes led to the partial charge transfer from center Ni^{2+} to 2,2'-bpy ligands. The calculation values for P1 and P2 are 4.83 and 4.88 respectively, which close to the expecting value of +5.

The binuclear uranium anions constructed from pentagonal bipyramidal uranyl in which the bond lengths of apical vertices are about 1.76 Å with a corresponding typical UO_2^{2+} and the range of bond lengths for equatorial vertices is from 2.28 Å to 2.54 Å. Tetrahedra phosphate anions have P-O bond lengths ranging from 1.57 Å to 1.50 Å, and a terminal nitrate with the distance of 2.96 Å for U1-N2, as shown in Figure 3.2.1. View down [*ab*] plane, each structural motif constructed from pentagonal bipyramidal uranyl geometry bonding to two crystallographic independent corner-sharing $(H_2PO_4)^-$ and one crystallographic independent edge-sharing NO_3^-. Several previous studies of hexavalent uranium containing compounds showed that they exhibit a strong tendency to adopt infinite structures due to the distribution of bond strengths within the polyhedra favors the formation of sheets of polyhedra. Obviously, the edge-sharing NO_3^- groups in **NiUP-1** acts as a terminal group to stop the structure propagation. It is very interesting that the planes of equatorial position of both uranyl groups are offset each other with distance of 1.32 Å, as shown in Figure 3.2.2. The similar plane functions indicate the combination of C glide plane, 2-fold axis and symmetric center located in the six-member ring constructed by P2, O5, O8, P2A, O5A, and O8A, which is consistent with the space group C*2/c* for NiUP-1**.** The unique bulky cation $Ni^{II}(2,2'\text{-bpy})_3$ which is constructed from octahedra Ni^{2+} coordinated to three 2,2'-bpy organic ligands with the Ni-N bond lengths of 2.08 Å are isolated from the uranyl phosphate anion. A packing view, as shown in Figure 3.2.3.

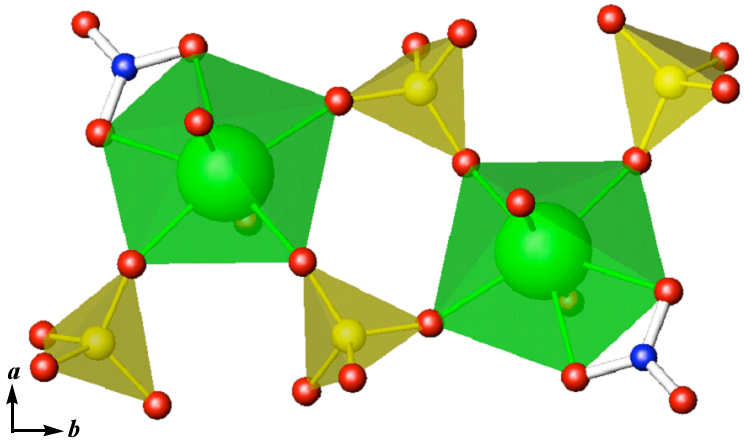

Figure 3.2.1. Structure of binuclear isolated polyhedra [[Ni(2,2'-bpy)$_3$](UO$_2$)(NO$_3$)(H$_2$PO$_4$)$_2$](NO$_3$)·3.25(H$_2$O), view down [*ab*] plane. UO$_7$ = green, PO$_4$ = yellow.

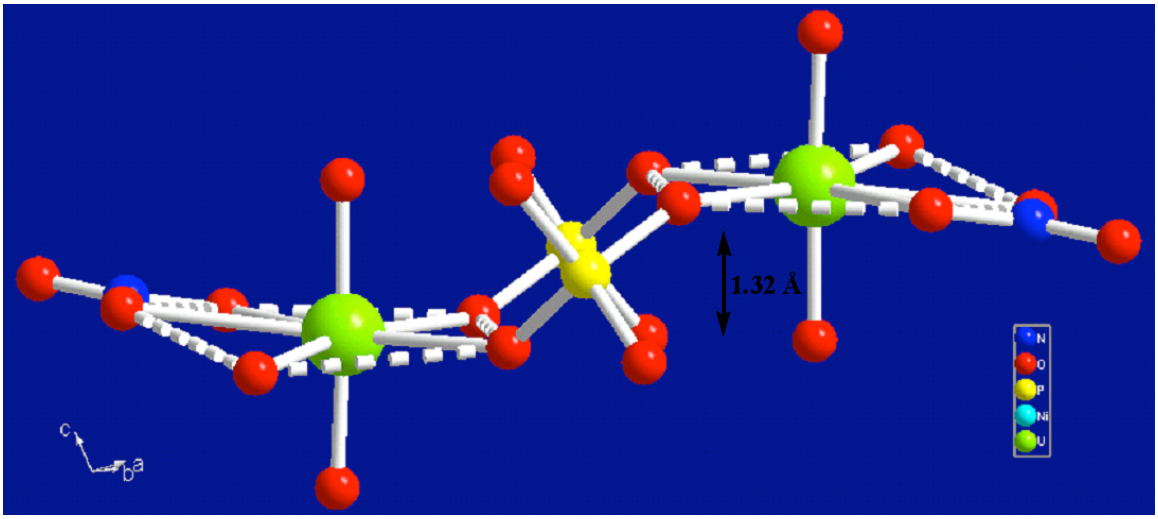

Figure 3.2.2. A view of [[Ni(2,2'-bpy)$_3$](UO$_2$)(NO$_3$)(H$_2$PO$_4$)$_2$](NO$_3$)·3.25(H$_2$O) showing the distance of 1.32 Å for offset planes indicated by dash lines.

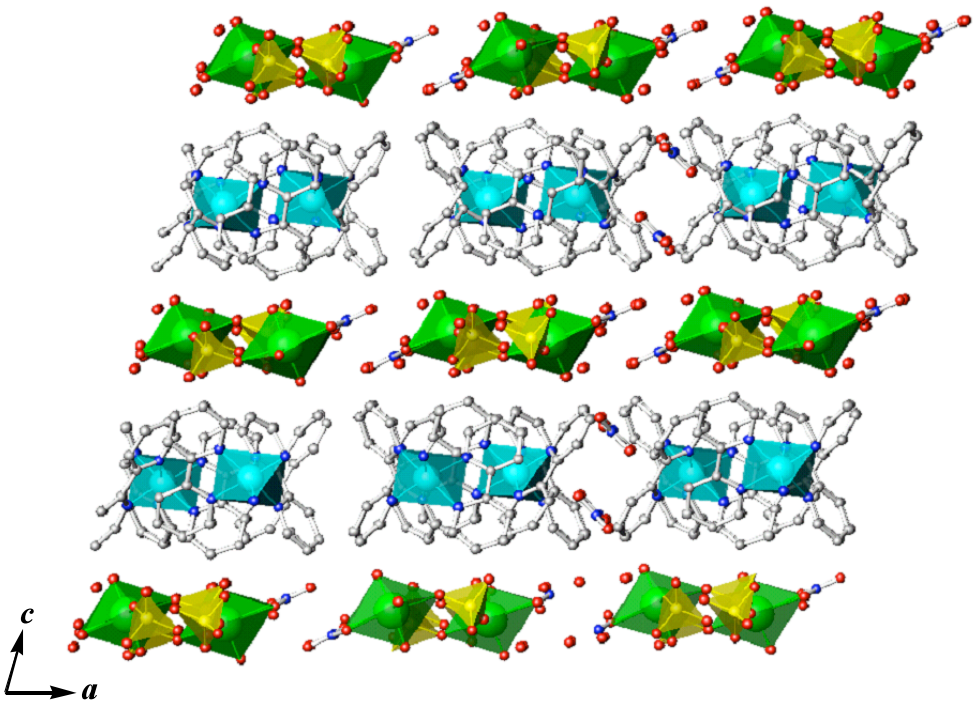

Figure 3.2.3. Packing mode shows the isolated binuclear anion and $Ni^{II}(2,2'\text{-bpy})_3$ cation groups, view down [*ac*] plane. UO_7 = green, PO_4 = yellow.

3.2.2 Raman spectroscopy.

The Raman spectra were collected on a Renishaw inVia Raman microscope spectrometer, as shown in Figure 3.2.4. Raman band at 840 cm^{-1} is attributed to the υ_1 symmetric stretching mode for the $(UO_2)^{2+}$ units. The empirical relation by Bartlett and Cooney ($R = 106.5[\nu_1(UO_2)^{2+}]^{-2/3} + 0.575$ Å) enable us to calculate the U-O bond lengths in uranyl using Raman shift (cm^{-1}) of the uranyl symmetric stretching vibrations [R(Å)/ $\nu_1(cm^{-1})$]: 1.745/840, which is consistence with the single crystal data of 1.769 to 1.774 Å. The bands at 1029 cm^{-1} are assigned to the split ν_1 $(PO_4)^{3-}$ symmetric.

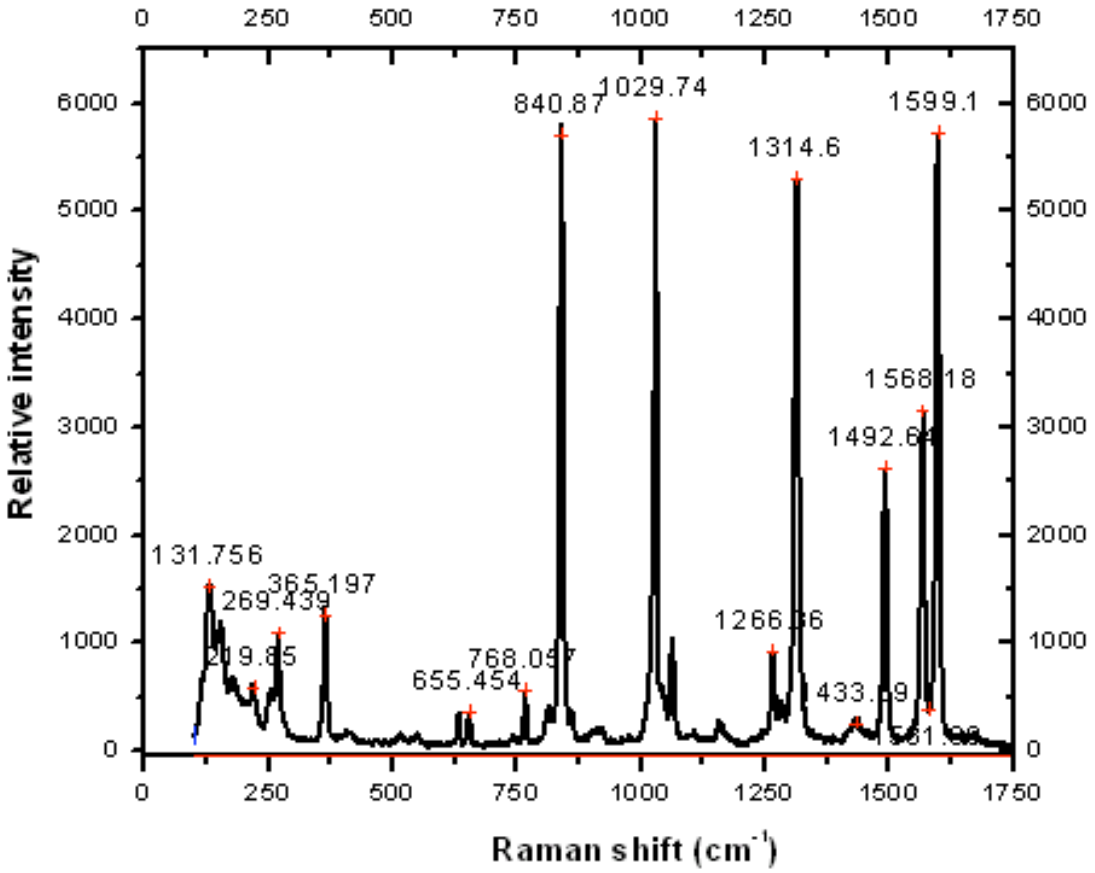

Figure 3.2.4. Raman spectrum for [[Ni(2,2'-bpy)$_3$](UO$_2$)(NO$_3$)(H$_2$PO$_4$)$_2$](NO$_3$)·3.25(H$_2$O).

3.3 $[(UO_2)(NO_3)_2(H_2O)][C_6H_6N]$ (UNO_3-1)

3.3.1 Structure features.

UNO_3-1 possesses a finite structure consisting of UO_8 hexagonal bipyramids that are linked into an edge-sharing dimer. The three-dimensional framework is constructed from covalent-bonding and hydrogen bonding simultaneously as shown in the [*ab*] plane packing view of this structure in Figure 3.3.1. The [*ab*] plane packing view shows inorganic layers constructed from uranyl nitrate and organic layers constructed from 1,2-bis(4-pyridyl)-ethane alternatively. The basic building units are shown in Figure 3.3.2.

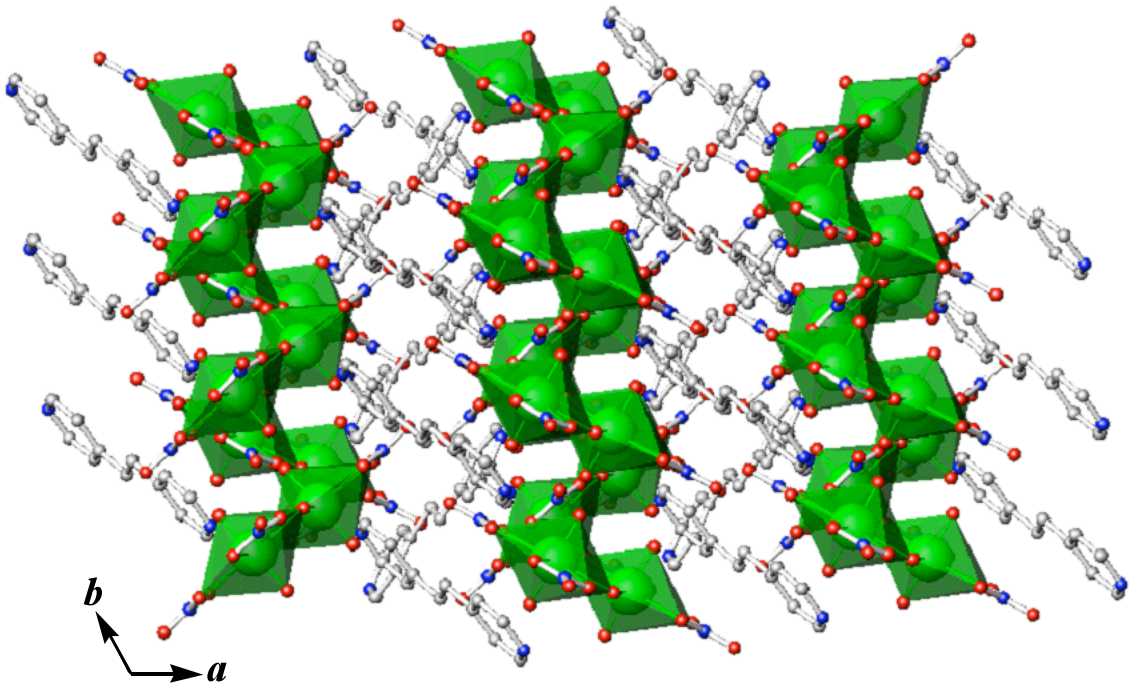

Figure 3.3.1. Packing view of [*ab*] plane UO_8 = green.

There is only one crystallographically unique uranium center in the structure of UNO_3-1. This unit contains a nearly linear uranyl, UO_2^{2+}, core. The U≡O distances within the uranyl cations are 1.771(2) and 1.767(2) Å; whereas those in the equatorial plane are considerably longer are 2.362(3), 2.391(3), 2.496(3), 2.509(3), 2.523(3) and 2.543(3) Å respectively. These bond distances are typical for uranyl polyhedra, and can be used to calculate bond-valence sum of 6.03 for U(1), which is consistent with the expected oxidation state of U(VI) in UO_2^{2+}. Two nitrate anions edge-share with the uranyl hexagonal bipyramids through equatorial positions to stop the structure extension an infinite structure.

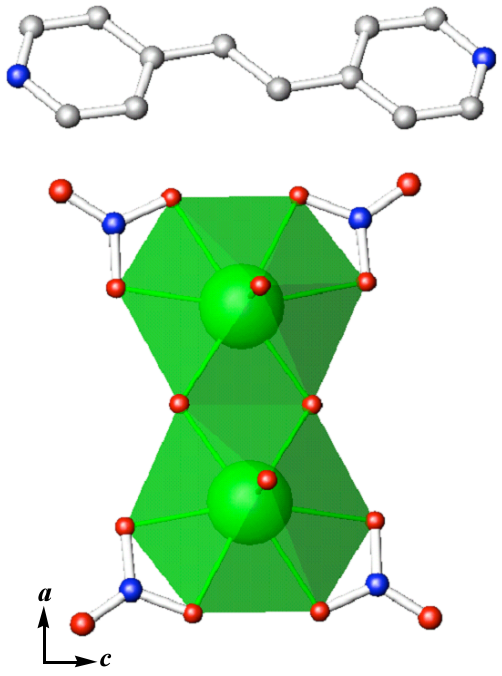

Figure 3.3.2. Depiction of the isolated dimeric structure of $[(UO_2)(NO_3)_2(H_2O)][C_6H_6N]$ (UNO_3-1).

Bond-valence sum calculations for UNO_3-1 show that the valence units for four O_{eq} atoms linked to nitrate anions are U_1-O_2 = 0.397, U_1-O_3 = 0.372, U_1-O_5 = 0.387, U_1-O_6 = 0.408 respectively. The valence unit values are N_1-O_5 = 1.613, N_1-O_6 = 1.592, N_2-O_2 = 1.603, N_2-O_3 = 1.628 respectively. The valence units for nitrate groups should be –0.205 and –0.231 is close to a neutral group after coordinated to hexagonal bipyramids U^{6+}. It is worth mentioning that the valence unit values for water bridging (U_1-O_9 = 0.531 and U_1-O_9#1 = 0.502 respectively) means the stronger bonding energy for U-O bonds, which is consistence with the shorter bond lengths found in X-ray single crystal diffraction data.

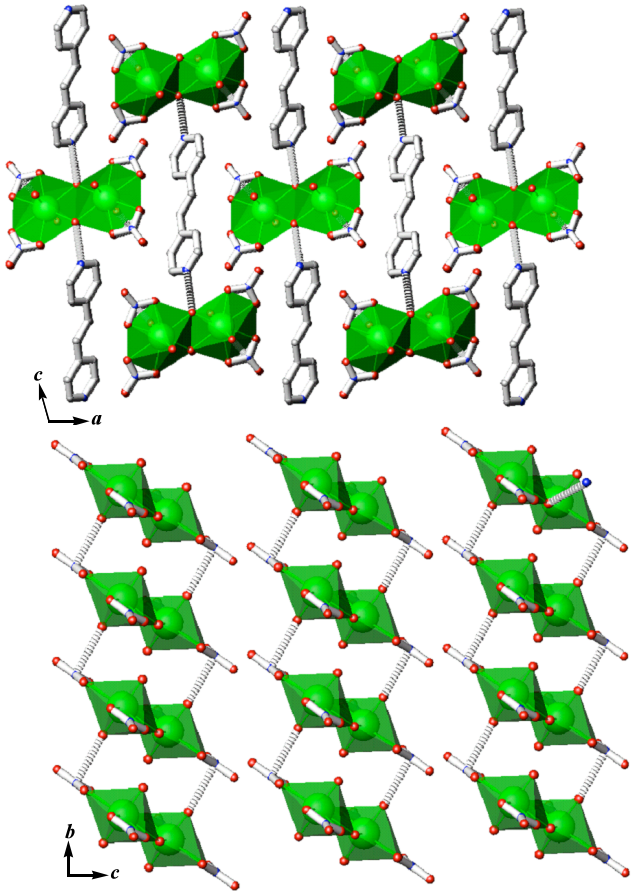

Figure 3.3.3. Intermolecular interactions (Hydrogen bonding and electrostatic interaction) along [*ac*] and [*bc*] planes.

Intermolecular interaction is another important structure feature to constructed three-dimensional framework in UNO_3-1. Two kinds of interactions (hydrogen bonding and electrostatic interaction) can be found in UNO_3-1 in the [*ac*] plane and the [*bc*] plane respectively. As shown in Figure 3.2.3. 1,2-bis(4-pyridyl)-ethane organic compounds act as hydrogen bonding acceptor and bridging oxygen atoms of uranyl hexagonal bipyramids dimer act as hydrogen bonding donor with hydrogen bonding length of 2.848 Å in the [*ac*] plane. The electrostatic interaction between apical atom of uranyl and nitrate anions found in [*bc*] plane donate the binding energy between two independent units with the distance of 2.853 Å.

3.3.2 Raman Spectroscopy.

The Raman spectrum were collected on a Renishaw inVia Raman microscope spectrometer, as shown in Figure 3.3.4. Raman bands at 844 cm^{-1} for UNO_3-1 are attributed to the υ_1 symmetric stretching mode for the $(UO_2)^{2+}$ units. The empirical relation by Bartlett and Cooney ($R = 106.5[\nu_1(UO_2)^{2+}]^{-2/3} + 0.575$ Å) enable us to calculate the U-O bond lengths in uranyl using Raman shift (cm^{-1}) of the uranyl symmetric stretching vibrations [R(Å)/ $\nu_1(cm^{-1})$]: 1.768/844 for UNO_3-1, which are consistence with the corresponding single crystal data of 1.769 Å. Bands observed lower than 300 cm^{-1} for both compounds are assigned to the ν_2 (δ) $(UO_2)^{2+}$ (ν (U-O(N)) and δ (U-O(N))) vibrations. UNO_3-1 has some common bands for organic compounds such as aromatic ring breathing peaks at 652, 747 cm^{-1} for UNO_3-1 respectively.

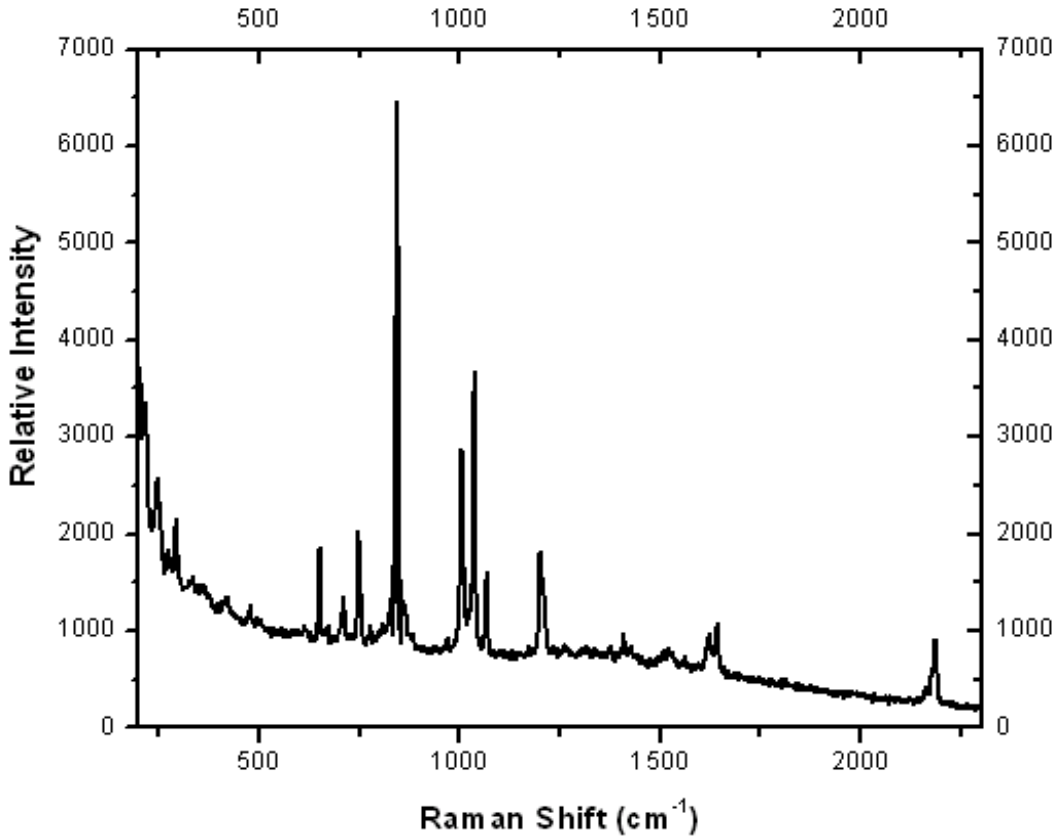

Figure 3.3.4. Raman spectrum of isolated clusters of $[(UO_2)(NO_3)_2(H_2O)][C_6H_6N]$ (UNO_3-1).

3.3.3 Fluorescence Spectroscopy.

The emission of green light from uranyl compounds excited by long-wavelength UV light, ascribed to the vibronic fine-structure characteristic, has been known for centuries. Previously studies on in Chapter I show that uranyl fluorescence typically has a characteristic six peak spectrum relating to the $S_{11} \rightarrow S_{00}$ and $S_{10} \rightarrow S_{0v}$, where v = 0-4, electronic transitions, and for $UO_2(NO_3)_2 \cdot 6H_2O$, the most intense peak ($S_{10} \rightarrow S_{00}$) is positioned at 508 nm. Only one broad fluorescent band at 544 nm in UNO_3-1 could be assigned to $S_{10} \rightarrow S_{00}$ electronic transition due to nitrate ligands. Compared to

$UO_2(NO_3)_2 \cdot 6H_2O$ emission spectrum, the red shift indicates that there is little energy loss from radiationless dacay resulting from formation of more stable binuclear compound.

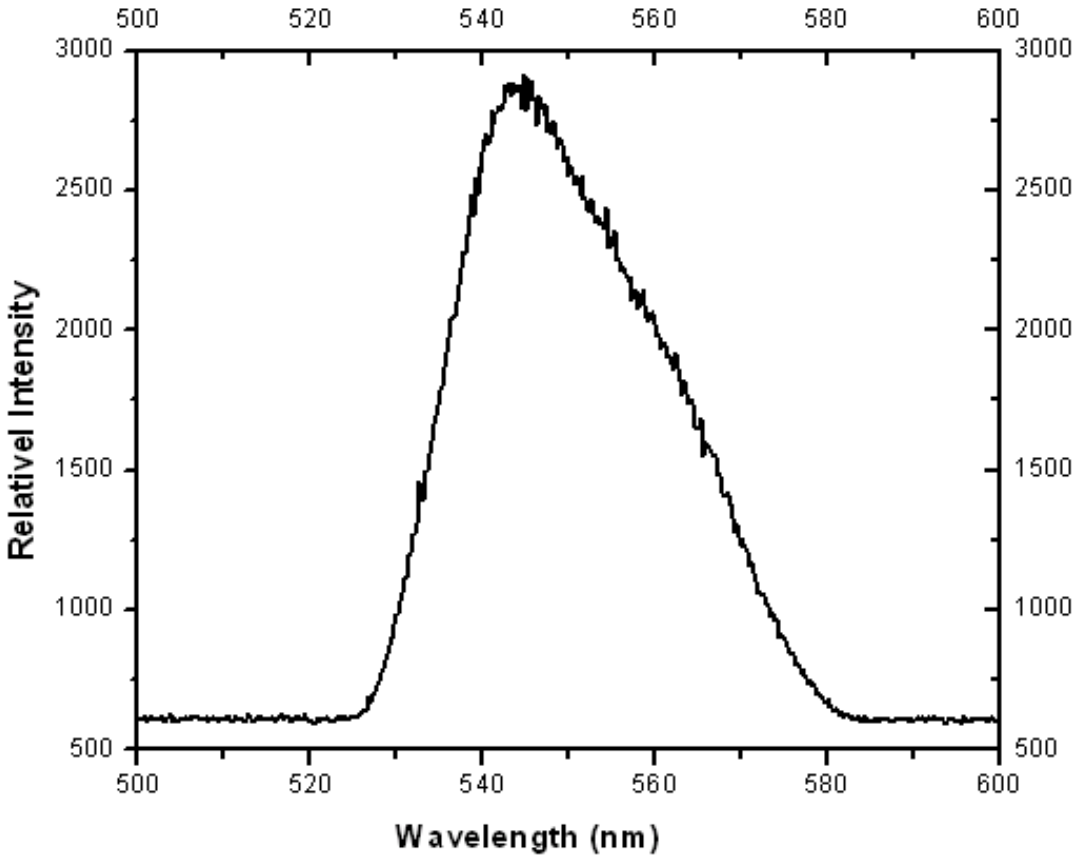

Figure 3.3.5. The fluorescence spectrum of $[(UO_2)(NO_3)_2(H_2O)][C_6H_6N]$ (**UNO_3-1**).

3.4 $(UO_2)(Ac)_2(2,2'\text{-bpy})$ (UAc-1)

3.4.1 Structural features

UAc-1 possesses a finite structure consisting of UO_6N_2 distorted hexagonal bipyramids edge sharing with acetate and 2,2'-bpy ligands, belonging to the inorganic-organic hybrid structure. The three-dimensional framework is constructed from covalent-bonding and aromatic interactions simultaneously as shown in the [*ab*] and [*bc*] planes packing views of this structure in Figure 3.4.1. The [*ab*] plane packing view shows mononuclear UO_6N_2 hexagonal bipyramids constructed from uranyl acetate and edge-sharing 2.2'-bpy ligand independent each other. The [*bc*] plane packing view shows the aromatic rings of 2.2'-bpy from different UO_6N_2 distorted hexagonal bipyramids moieties overlapped each other. The basic building units are shown in Figure 3.4.2.

There is only one crystallographically unique uranium center in the structure of UAc-1. This unit contains a nearly linear uranyl, UO_2^{2+}, core. The U≡O distances within the uranyl cations with bond lengths of 1.772(4) and 1.776(4) Å; whereas those oxygen atoms or nitrogen atoms in the equatorial plane are considerably longer with bond lengths of 2.435(4), 2.471(4), 2.443(4), 2.456(4), 2.639(4) and 2.620(4) Å respectively. These bond distances are typical for uranyl polyhedra, and can be used to calculate bond-valence sum of 5.80 for U(1), which is consistent with the expected oxidation state of U(VI) in UO_2^{2+}. Two acetate anions act as the bidentate ligands coordinated to UO_6N_2 hexagonal bipyramid along equatorial positions. Another bidentate ligand is 2,2'-bpy which has been found as a terminal ligand in many MOF structures. This is the first case for U(VI) coordination geometry determined by electronic factors and spatial

requirements, as shown in Figure 3.4.2. The six equatorial coordination atoms, which should be in same plane in most of cases determined by the electronic factors, belong to two isolated planes with 30° plane angle due to the two coordinated nitrogen atoms coming from the bulky 2,2'-bpy group.

Intermolecular interactions play important roles in constructing the one-dimensional chain for UAc-1. The aromatic interaction between adjacent uranyl moieties link each other through the 2,2'-bpy face to face interaction with the distance of 3.02 Å as shown in Figure 3.4.3.

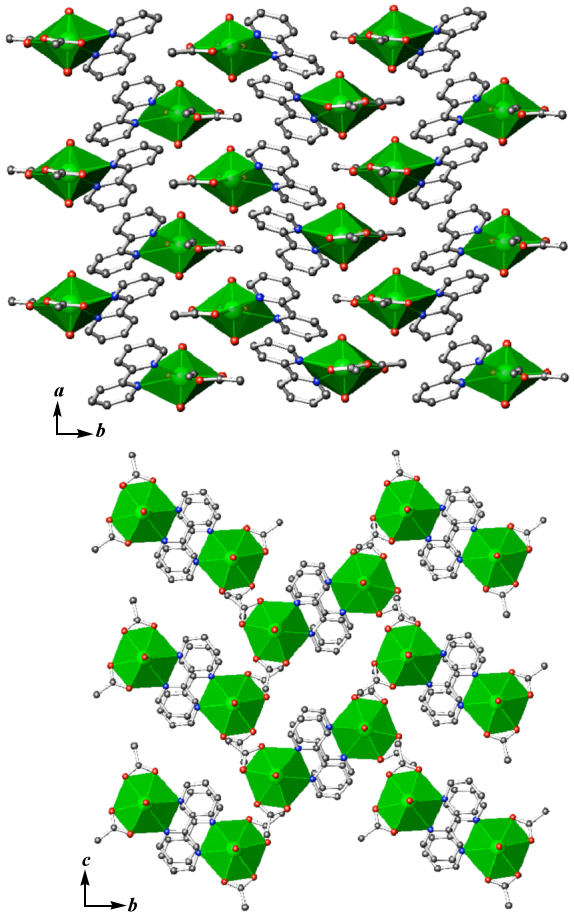

Figure 3.4.1. Various packing views of $(UO_2)(Ac)_2$(2,2'-bpy) **(**UAc-1**)** along the [*ab*] and [*bc*] planes.

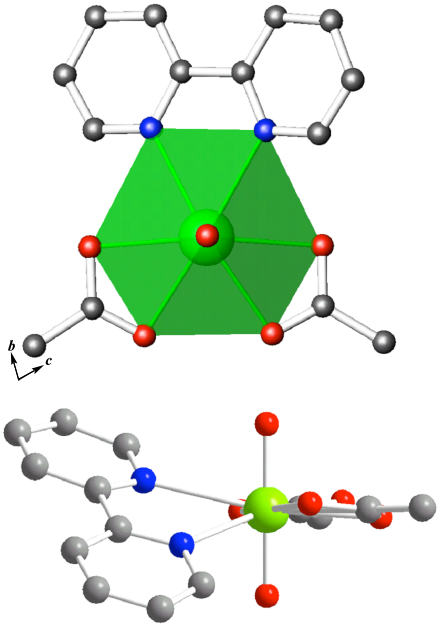

Figure 3.4.2. Various views of distorted pentagonal bipyramidal structure of $(UO_2)(Ac)_2(2,2'\text{-bpy})$ (UAc-1).

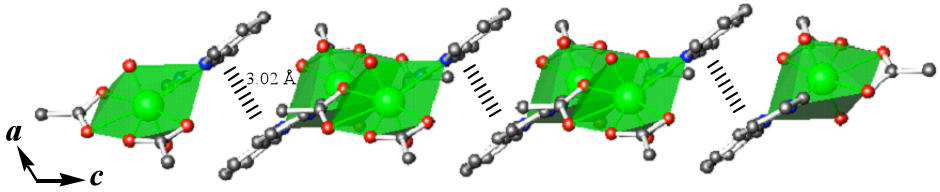

Figure 3.4.3. Short distance of face to face aromatic interactions between each UAc-1 molecule.

3.4.2 Raman Spectroscopy.

The Raman spectra were collected on a Renishaw inVia Raman microscope spectrometer, as shown in Figure 3.4.4. Raman bands at 840 cm^{-1} for UAc-1 are attributed to the υ_1 symmetric stretching mode for the $(UO_2)^{2+}$ units. The empirical relation by Bartlett and Cooney ($R = 106.5[\nu_1(UO_2)^{2+}]^{-2/3} + 0.575$ Å) enable us to calculate the U-O bond lengths in uranyl using Raman shift (cm^{-1}) of the uranyl

symmetric stretching vibrations [R(Å)/ $\nu_1(cm^{-1})$]: 1.745/840 for UAc-1, which are consistence with the corresponding single crystal data of 1.772 and 1.776 Å. Bands observed lower than 300 cm^{-1} for UAc-1 are assigned to the ν_2 (δ) $(UO_2)^{2+}$ (ν (U-O(N)) and δ (U-O(N))) vibrations. Both compounds share some common bands for organic compounds such as aromatic ring breathing peaks at 652, 747 cm^{-1} for UNO_3-1 and 767cm^{-1} for UAc-1 respectively. Obviously, peak shift in Raman spectroscopy because the covalent bond between 2,2'-bpy and UO_2^{2+} core is much stronger than that of hydrogen bonding between 1,2-bis(4-pyridyl)-ethane and UO_8 hexagonal bipyramidal in UNO_3-1.

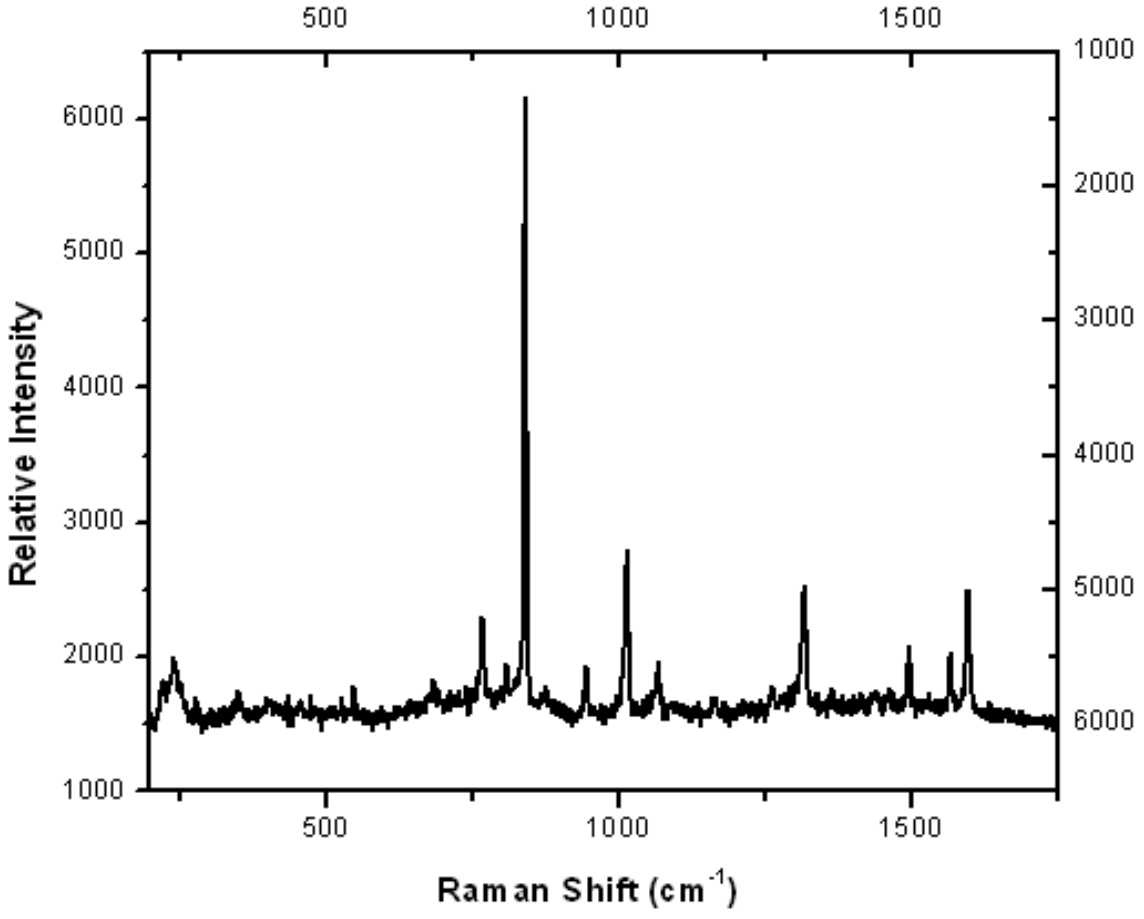

Figure 3.4.4. Raman spectrum of $(UO_2)(Ac)_2$(2,2'-bpy) (UAc-1).

3.4.3 Fluorescence Spectroscopy.

Similar to UNO_3-1, the intensity band at 552 nm of emission spectrum in UAc-1, which shows the red shift, is the results of vibronic electronic transitions and 2,2'-bpy ligand excitation. More recently it has been demonstrated uranyl compounds containing aromatic organic moieties can exhibit the antenna effect, yielding enhanced emission by the uranyl cation. The more intensity emission band for UAc-1 shows the antenna ligand effect for coordinated 2,2'-bpy, which is consistent with the X-ray single crystal structure.

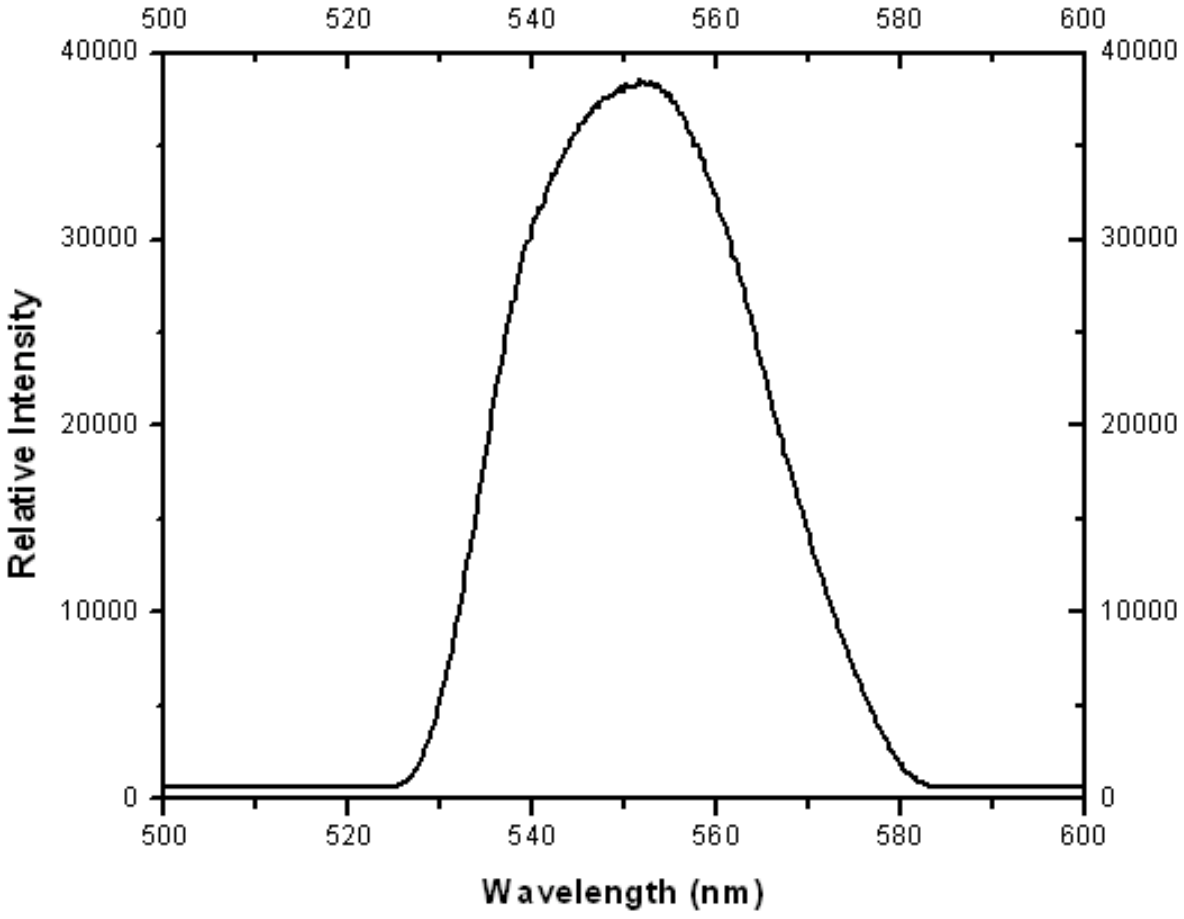

Figure 3.4.5. The fluorescence spectrum of $(UO_2)(Ac)_2$(2,2'-bpy) (UAc-1).

Conclusions for 3.2-3.3

Hydrothermal methods have proven to effective for synthesizing uanyl transition metal phosphates and inorganic-organic hybrid frameworks containing uranyl cations. The infinite structures including one-dimensional chain, two-dimensional sheets and three-dimensional frameworks constructed uranyl, UO_2^{2+} cations, have been widely reported with the potential application in radioactive materials, new selective ion-exchange materials, proton conductors and fluorescent material. Up to date, the only seven structures containing isolated U^{6+} polyhedra (shown in Chapter 1.2.1) have been synthesis by solid-state method with reaction temperature over 1000 ^oC. Two isolated structures $[(UO_2)(NO_3)_2(H_2O)][C_6H_6N]$ (UNO_3-1) and $(UO_2)(Ac)_2$(2,2'-bpy) (UAc-1), which belong to binuclear UO_2^{2+} and mono-nuclear UO_2^{2+} respectively, have been synthesized by mild hydrothermal synthesis. In UNO_3-1 compound, 1,2-bis(4-pyridyl)-ethane, which becomes diprotonated by the HCN, was employed to direct the formation of the anionic lattice. While the yield was low for UNO_3-1, the product is surprisingly pure according to PXRD measurements. But in UAc-1, which belongs to the inorganic-organic hybrid class of material, contains 2,2'-bipyradyl ligand which acts as terminal group to stop the structure infinite extension along equatorial positions of UO_2^{2+} cation.

The difference with the aforementioned mono-nuclear isolated structures, nitrate or acetate anions in two adjacent positions of equatorial plane provide the sufficient space for edge-sharing dimer formation or bulky organic substitutive groups for compounds UNO_3-1 and UAc-1 respectively. Each of these compounds exhibits different fluorescence properties, indicating that the organic emission and antenna ligand effect affect the vibronic transition from the uranyl cations.

3.5 $[Ag(4,4'\text{-bpy})]_2[(UO_2)H_3(PO_4)_3]$(AgUP-1)

3.5.1 Structural features.

The description of the structure of AgUP-1 begins with the presence of a classical uranyl, UO_2^{2+}, unit that is nearly linear with a O(9)-U1-O(8) bond angle of 179.3(2)° and normal U≡O bond distances of 1.788(5) and 1.791(5) Å. Four oxygen atoms are found approximately perpendicular to the uranyl axis, creating an environment that is best described as a tetragonal bipyramid. These donor atoms belong to phosphate anions found within the structure, and the U-O bond distances range from 2.261(5) to 2.313(6) Å. Using these distances, a bond-valence sum of 6.1 was arrived at for U(1), which is consistent with this compound containing uranium(VI).

The phosphate anions bridge uranyl cations to create ribbons that extend in the *a* axis direction. These ribbons are similar to those found in compounds and minerals with the autunite-layered topology (shown in Chapter 1.2.3). The ribbons are in turn linked to one another through phosphate anions to create $[(UO_2)_2H_3(PO_4)_3]^{2-}$ layers in the [*ac*] plane that are shown in Figure 3.5.1. One of the phosphate anions is disordered with two different, but equally occupied, orientations being present. The P-O distances can be distinguished from the P-OH distances on the basis of the bond length and whether or not they are terminal or bridging oxygen atoms. For P(1), the longest P-O bond distance of 1.551(6) Å also corresponds to a terminal oxygen atom, and this therefore is likely to the site of protonation. For P(2), there are two such terminal oxygen atoms; however, owing to the disorder of this anion, the P-O bond distances are

irregular, and bond distance analysis is not possible. Small channels through the sheets are formed where there are appropriate distances between protonated phosphate anions to create hydrogen bonding interactions. These interactions might be the source of the novel sheet topology observed for AgUP-1.

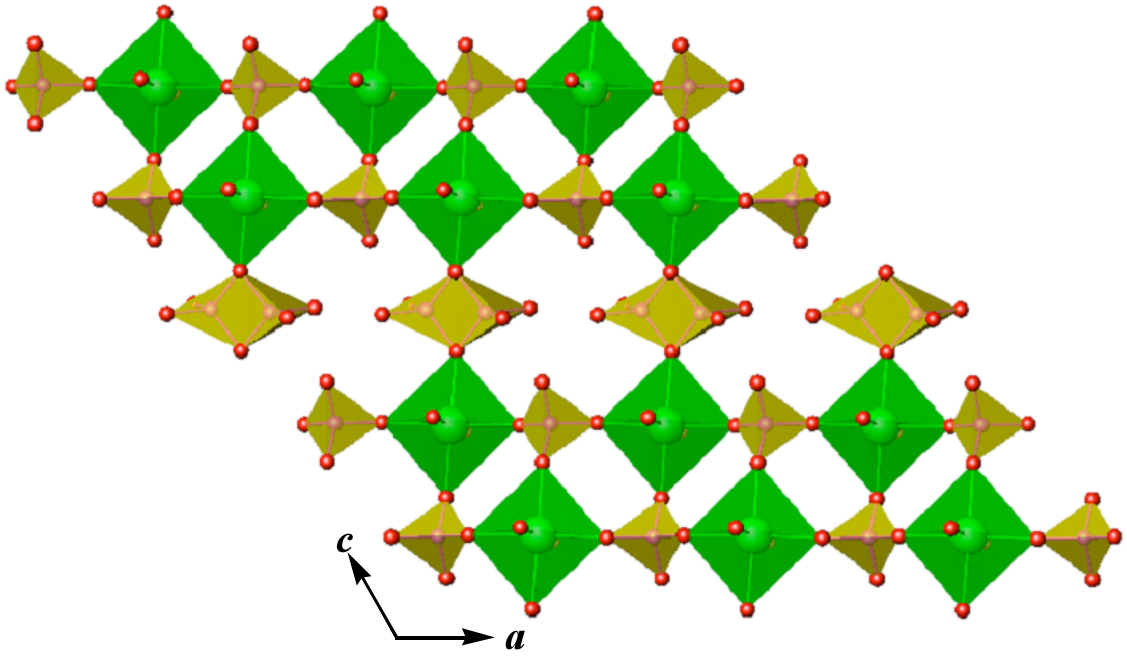

Figure 3.5.1. A view of the $^{2}_{\infty}[(UO_2)_2H_3(PO_4)_3]^{2-}$ layers that extend in the [*ac*] plane in the structure of $[Ag(4,4'\text{-bipy})]_2[(UO_2)_2H_3(PO_4)_3]$ (AgUP-1).

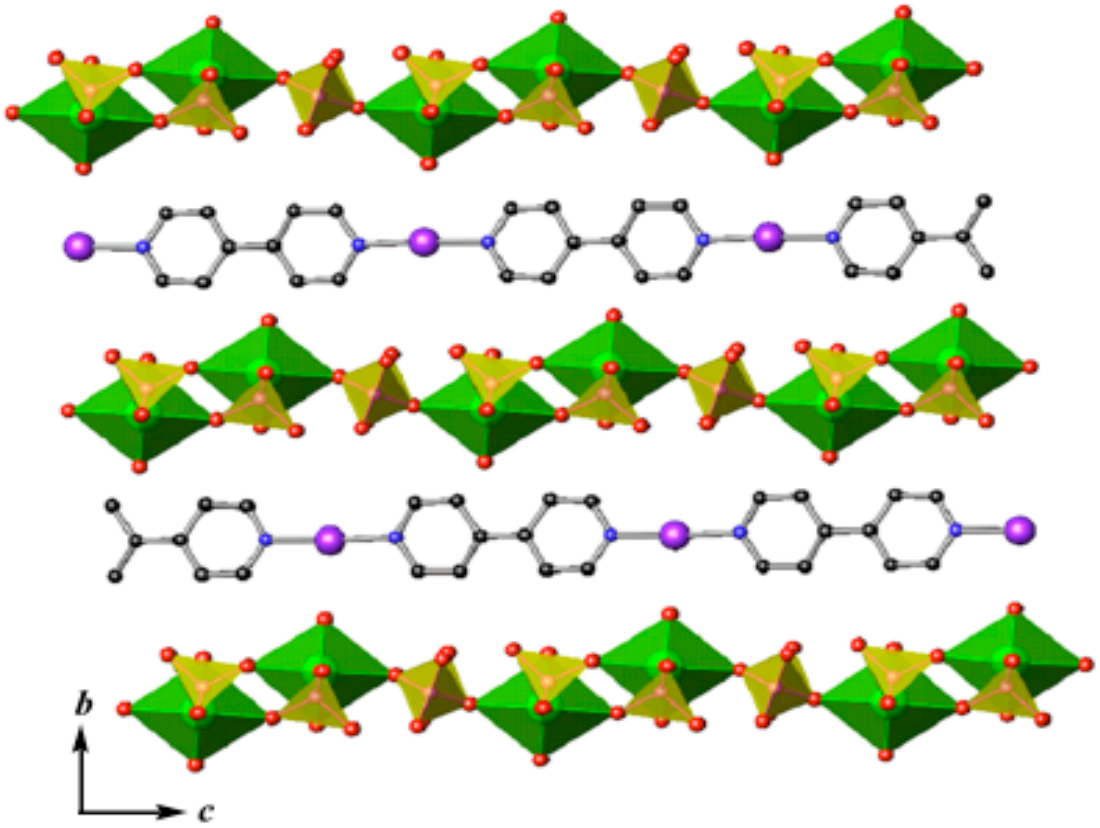

Figure 3.5.2. A depiction of the separation of uranyl phosphate layers are from one another by $^{1}_{\infty}$[Ag(4,4′-bipy)]$^{+}$ chains formed from two-coordinate Ag^{+} bridged by 4,4′-bipy in $[Ag(4,4'\text{-bipy})]_2[(UO_2)_2H_3(PO_4)_3]$ (AgUP-1).

The uranyl phosphate layers are separated from one another by [Ag(4,4-bipy)]$^{+}$ chains formed from two coordinate Ag^{+} cations bridged by 4,4-bipy, as is shown in Figure 3.5.2. The Ag-N distances of 2.100(6) and 2.123(6) Å are normal. The N(1)-Ag(1)-N(2) angle is nearly linear with an angle of 176.3(2)^{o}. This is apparently the first example of uranyl-containing layers being separated by a coordination polymer.

3.5.2 Raman Spectroscopy.

The Raman spectra were collected on a Renishaw inVia Raman microscope spectrometer, as shown in Figure 3.5.3. Raman band at 813 cm^{-1} is attributed to the υ_1 symmetric stretching mode for the $(UO_2)^{2+}$ units. The empirical relation by Bartlett and Cooney ($R = 106.5[\nu_1(UO_2)^{2+}]^{-2/3} + 0.575$ Å) enable us to calculate the U-O bond lengths in uranyl using Raman shift (cm^{-1}) of the uranyl symmetric stretching vibrations [R(Å)/ $\nu_1(cm^{-1})$]: 1.798 Å /814, which is consistence with the single crystal data of 1.788 to 1.791 Å. The bands at 1032 cm^{-1} are assigned to the split ν_1 $(PO_4)^{3-}$ symmetric stretching vibration and ν_3 antisymmetric stretching vibration respectively. Bands of very low intensity in the 575-655 cm^{-1} region are attributed to the split, triple degenerate ν_4 $(PO_4)^{3-}$ bending modes. Bands observed lower than 300 cm^{-1} are assigned to the ν_2 (δ) $(UO_2)^{2+}$ (ν (U-O) and δ (U-O)) vibrations.

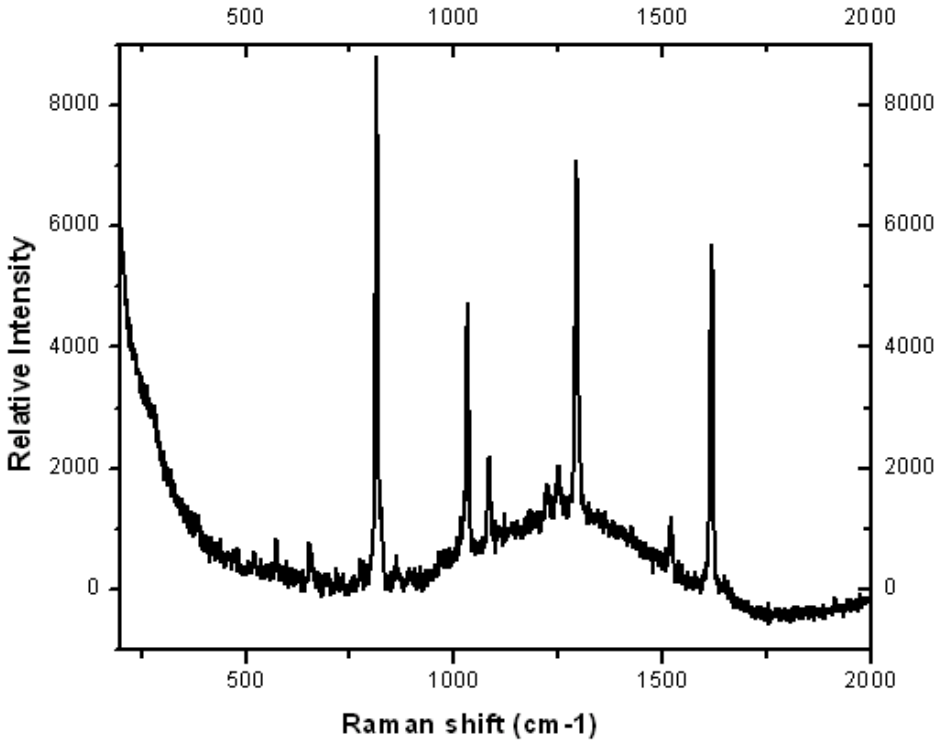

Figure 3.5.3. Raman spectrum of $[Ag(4,4'\text{-bipy})]_2[(UO_2)_2H_3(PO_4)_3]$ (AgUP-1).

3.5.3 Fluorescence Spectroscopy.

Emission from uranyl containing networks is complex and easily influenced by subtle changes in bonding, as indicated by Grohol and Clearfield's report on the luminescent properties of two closely related uranyl phosphonates, $[UO_2(HO_3PC_6H_5)_2(H_2O)]_2 \cdot 8H_2O$ and $UO_2(HO_3PC_6H_5)_2(H_2O) \cdot 2H_2O$, whose structural differences are based largely on conformational changes in the phosphonate anions (shown in Chapter 1.6.2). More recently it has been demonstrated uranyl compounds containing aromatic organic moieties can exhibit the antenna effect, yielding enhanced emission by the uranyl cations (shown in Chapter 1.6.2). The fluorescence spectrscopy of $[Ag(4,4\text{-bipy})]_2[(UO_2)_2H_3(PO_4)_3]$ (AgUP-1) shows in Figure 3.5.4. The intensity peak at 558 nm ascribed to the vibronic of uranyl cation.

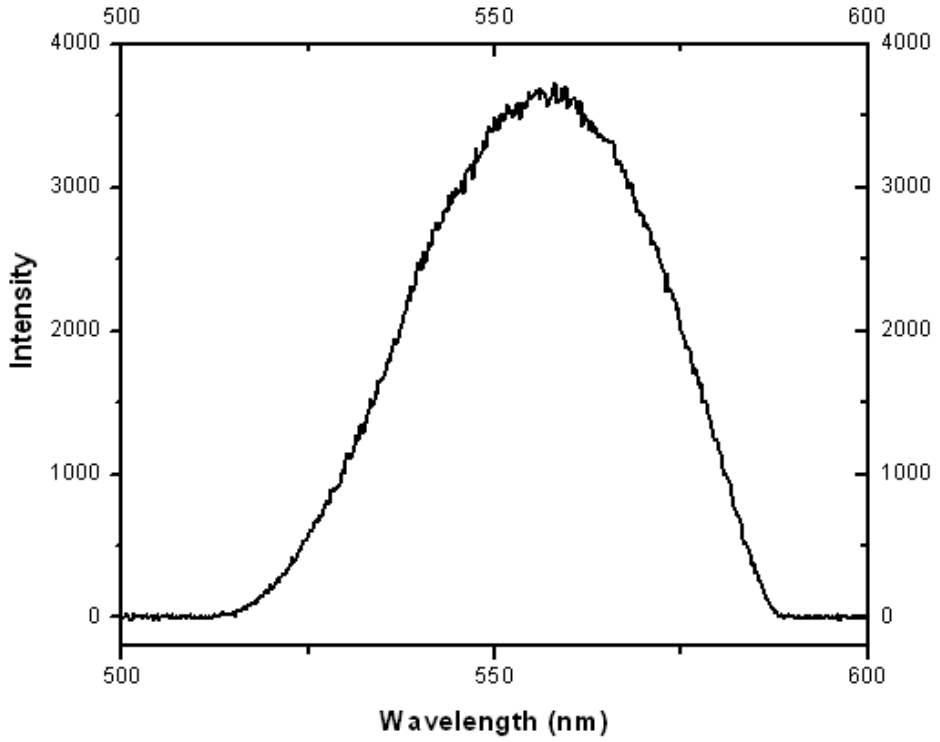

Figure 3.5.4. The fluorescence spectrum of $[Ag(4,4\text{-bipy})]_2[(UO_2)_2H_3(PO_4)_3]$ (**AgUP-1**) showing fine-structure in its emission peaks assigned to vibronic coupling for the UO_2^{2+} moiety.

3.6 $Ag(2.2'\text{-bpy})(UO_2)_2(HPO_4)(PO_4)$(AgUP-2)

3.6.1 Structural features.

Whereas the structure of AgUP-2 also contains 2D uranyl phosphate layers (shown in Chapter 1.2.3), Ag^+, and bipy ligands, its structure is substantially different from that of AgUP-1 for a number of reasons. Foremost among these is that 4,4'- bipy has been exchanged for 2,2'-bipy, and this prevents the formation of a $Ag(bipy)^+$ extended substructure, owing to the chelating nature of 2,2'-bipy. Additionally, the fundamental uranyl-containing building units found here are the more common UO_7 pentagonal bipyramids.

There are two crystallographically unique building units with U≡O bond distances being slightly shorter than normal at 1.737(5) to1.766(5) Å. Both units are also nearly linear with bond angles of 178.0(2) and 179.4(2)° for U(1) and U(2), respectively. The five equatorial distances range from 2.282(4) to 2.555(4) Å for U(1) and from 2.311(4) to 2.526(4) Å for U(2). This allows for the determination of the bond-valence sums for U(1) and U(2) of 5.9 and 6.0, respectively. The UO_7 units share two opposite edges, to create 1D chains that are joined to one another by phosphate and hydrogen phosphate anions to yield $[(UO_2)_2(HPO_4)(PO_4)]^-$ sheets with the β-uranophane topology that extend in the [*ab*] plane as is shown in Figure 3.6.1.

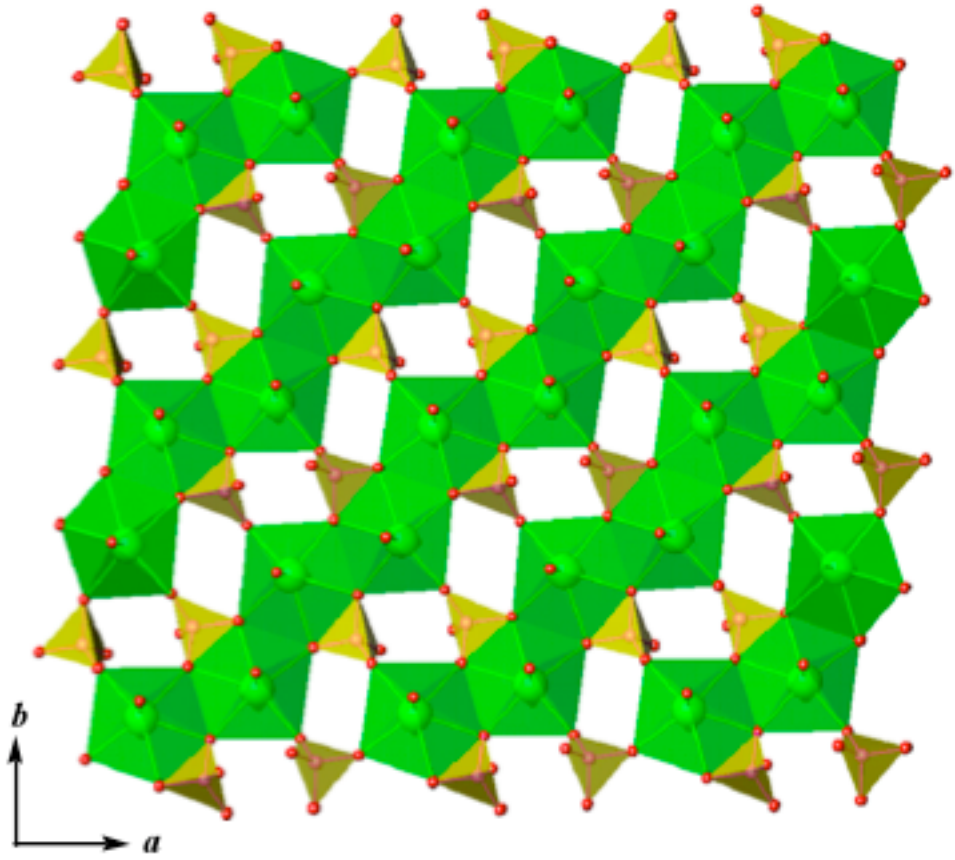

Figure 3.6.1. An illustration of the $[(UO_2)_2(HPO_4)(PO_4)]^-$ sheets with the β-uranophan topology that extend in the [*ab*] plane in structure of Ag(2,2′-bipy)$(UO_2)_2(HPO_4)(PO_4)$ (AgUP-2).

Fortunately there is no disorder in the structure of AgUP-2, and the longest terminal P(2)-O bond distance of 1.561(5) Å likely corresponds to the site of protonation. P(1) also possesses an oxo atom that is directed between the layers, much like the P(2)-OH group. However, here the O(1) atom bridges between P(1) and Ag(1). Therefore, there is direct coordination by the Ag^+ centers to the $[(UO_2)_2(HPO_4)(PO_4)]^-$ sheets, making AgUP-2 fundamentally different in construction from AgUP-1. The coordination sphere

of the Ag^{+} center is completed by one chelating 2,2'-bipy ligand, making the silver atom three coordinate with a distorted trigonal-planar environment with Ag-O and Ag-N (×2) distances of 2.185(4), 2.259(6), and 2.318(7) Å. The $[Ag(2,2'\text{-bipy})]^{+}$ moieties can be thought of as decorating the top and bottom of the uranyl phosphate layers in AgUP-2, as is depicted in Figure 3.6.2.

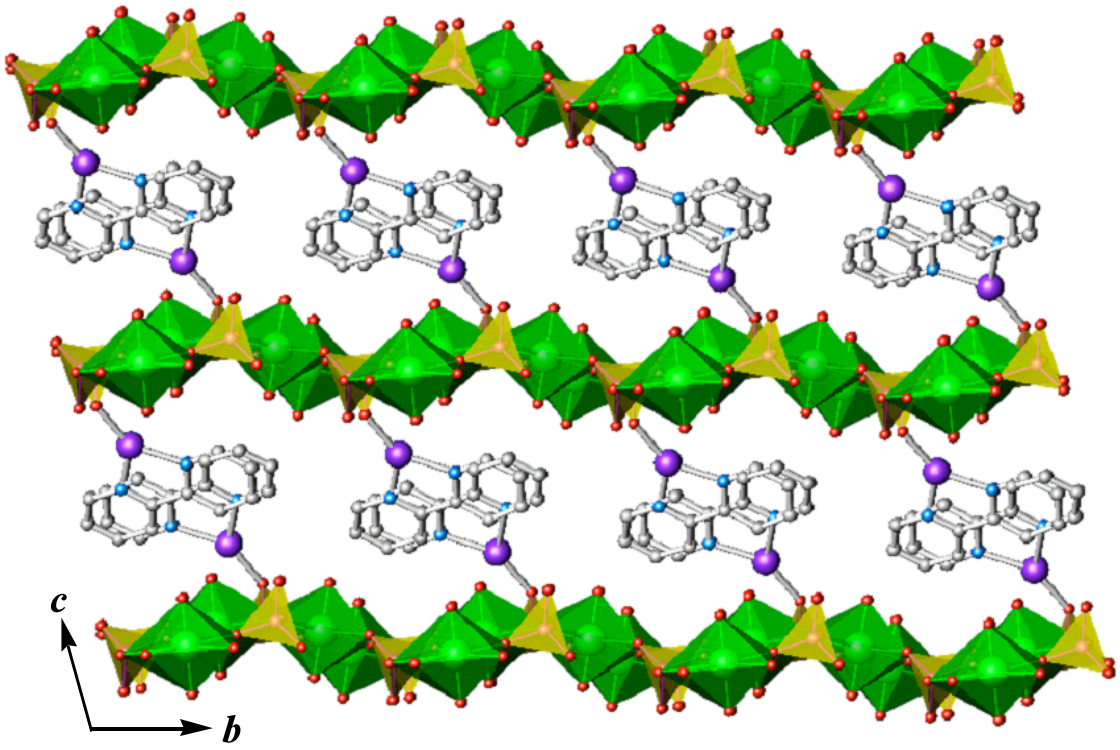

Figure 3.6.2. A view of the decoration of $[(UO_2)_2(HPO_4)(PO_4)]^{-}$ sheets by $[Ag(2,2'\text{-bipy})]^{+}$ moieties in $Ag(2,2'\text{-bipy})(UO_2)_2(HPO_4)(PO_4)$ (AgUP-2).

3.6.2 Raman Spectroscopy.

The Raman spectra were collected on a Renishaw inVia Raman microscope spectrometer, as shown in Figure 3.6.3. Raman band at 837.8 cm^{-1} is attributed to the υ_1 symmetric stretching mode for the $(UO_2)^{2+}$ units. The empirical relation by Bartlett and

Cooney ($R = 106.5[\nu_1(UO_2)^{2+}]^{-2/3} + 0.575$ Å) enable us to calculate the U-O bond lengths in uranyl using Raman shift (cm^{-1}) of the uranyl symmetric stretching vibrations [R(Å)/ $\nu_1(cm^{-1})$]: 1.773 Å /837.8, which is consistence with the single crystal data of 1.753 to 1.766 Å. The bands at 1008cm^{-1} are assigned to the split ν_1 $(PO_4)^{3-}$ symmetric stretching vibration and ν_3 antisymmetric stretching vibration respectively. Bands of very low intensity in the 575-655 cm^{-1} region are attributed to the split, triple degenerate ν_4 $(PO_4)^{3-}$ bending modes. Bands observed lower than 300 cm^{-1} are assigned to the ν_2 (δ) $(UO_2)^{2+}$ (ν (U-O) and δ (U-O)) vibrations.

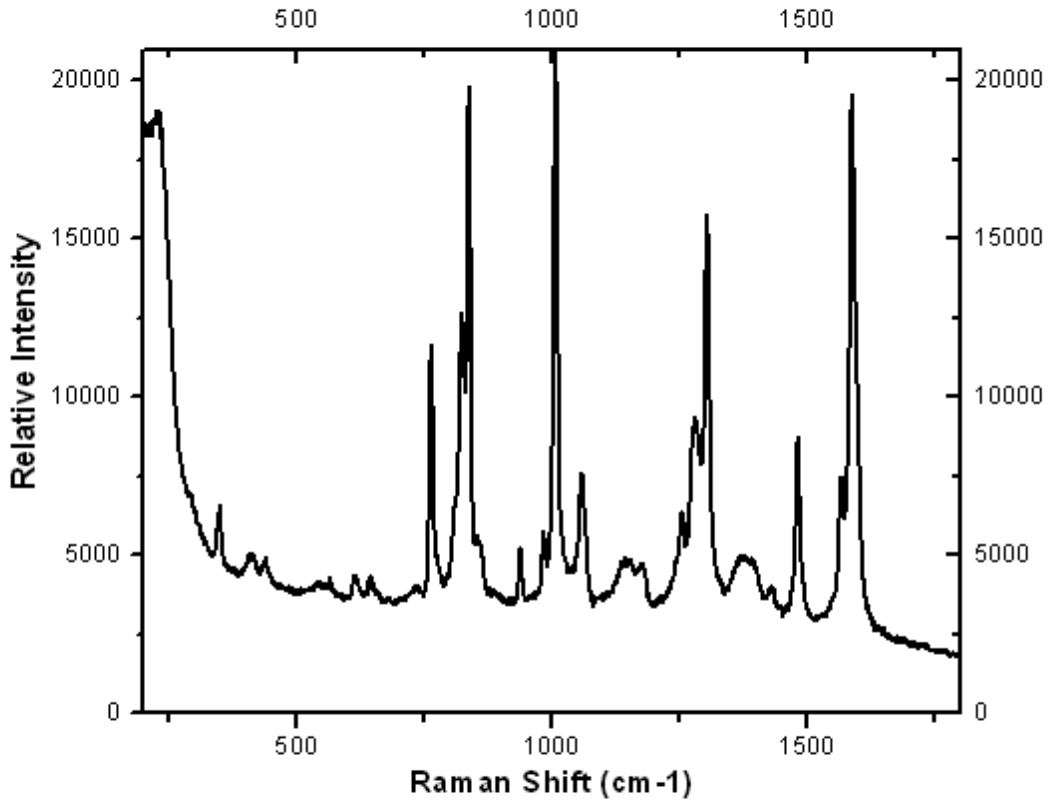

Figure 3.6.3. Raman spectrum of Ag(2,2′-bipy)$(UO_2)_2(HPO_4)(PO_4)$ (**AgUP-2**)

3.6.3 Fluorescence Spectroscopy.

The fluorescence spectroscopy of $Ag(2,2'\text{-bipy})(UO_2)_2(HPO_4)(PO_4)$ (AgUP-2) shows in Figure 3.6.4. The intensity peaks at 530 and 550 nm ascribed to the vibronic of uranyl cation. There are two different aspects in fluorescent spectra for AgUP-1 and AgUP-2**.** First, whereas the fluorescence of AgUP-1 is observed, all of the fine structure is lost. Second, AgUP-2 whereas the emission from is quite strong, again much of the fine structure is lost.

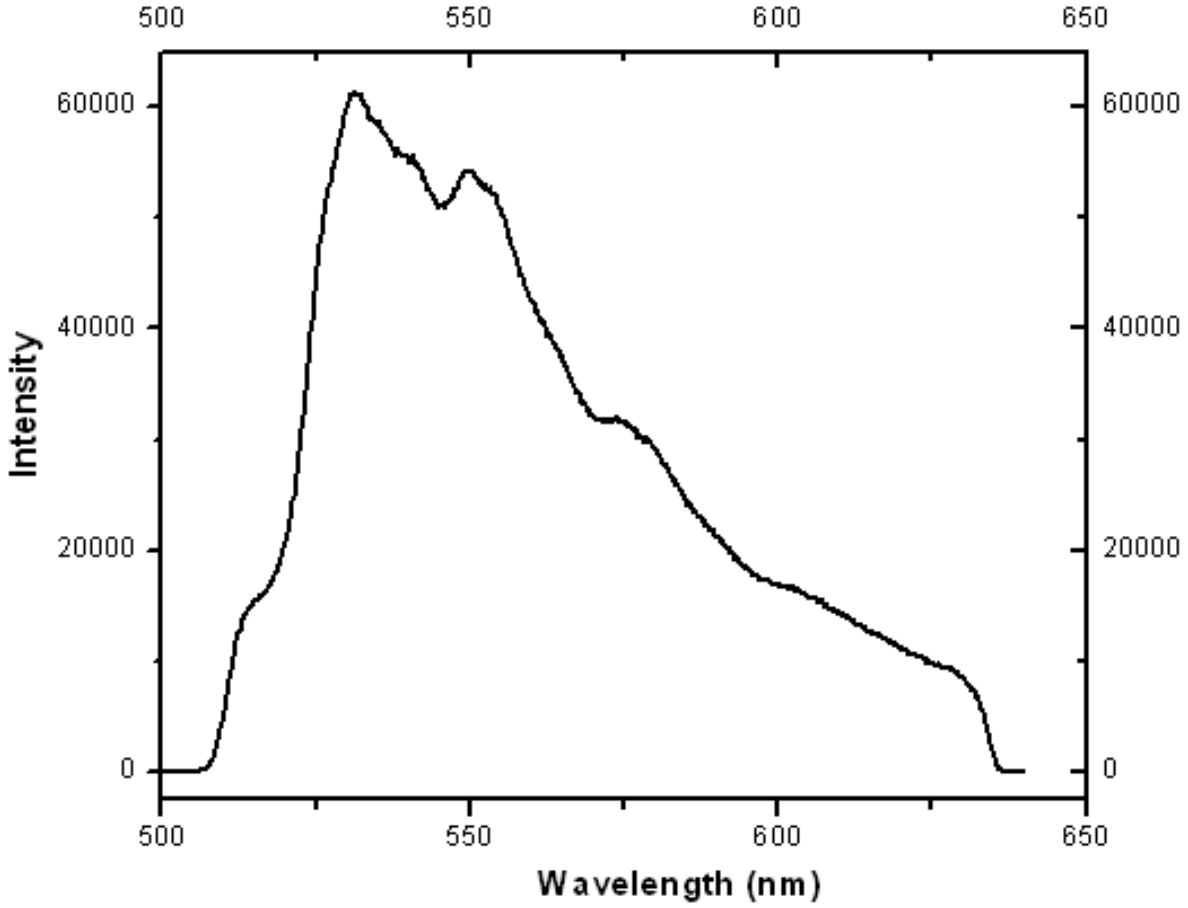

Figure 3.6.4. The fluorescence spectrum of $Ag(2,2'\text{-bipy})(UO_2)_2(HPO_4)(PO_4)$ (AgUP-2) showing fine-structure in its emission peaks assigned to vibronic coupling for the UO_2^{2+} moiety.

3.7 $Na_2Ag_6[(AgO)_2(UO_2)_3(AsO_4)_4]$ (AgUAs-1)

3.7.1 Structural features.

AgUAs-1 possesses an open-framework structure consisting of UO_6 tetragonal bipyramids that are joined together by PO_4 tetrahedra by edge-sharing through the equatorial positions of UO_6 tetragonal bipyramids. Ellipsed channels occur along *b* axis. These channels house the Ag^+, Na^+ cations, and water molecules with the size of approximately 11.37 × 7.50 Å. Various views of this structure are shown in Figure 3.7.1. The view down the *a* axis shows something peculiar about the channels in that there appears to be void spaces. We suspect that disordered water resides in these channels, but these are not resolved in the structure.

There are three crystallographically independent uranium centers in the structure of AgUAs-1. Each unit contains a nearly linear uranyl, UO_2^{2+}, core. The U≡O distances within the uranyl cations range of 1.775(8) to 1.792(12) Å; whereas those in the equatorial plane are considerably longer and within the range of 2.273(8) to 2.353 (9) Å. These bond distances are typical for uranyl polyhedra, and can be used to calculate bond-valence sums of 6.12, 5.85, and 5.82 for U(1), U(2), and U(2a), respectively, which is consistent with the expected oxidation state of U(VI) in UO_2^{2+}. The As–O bond distances within the range 1.677(8) to 1.690(9) Å are consistent with the expected value for tetrahedra arsenates.

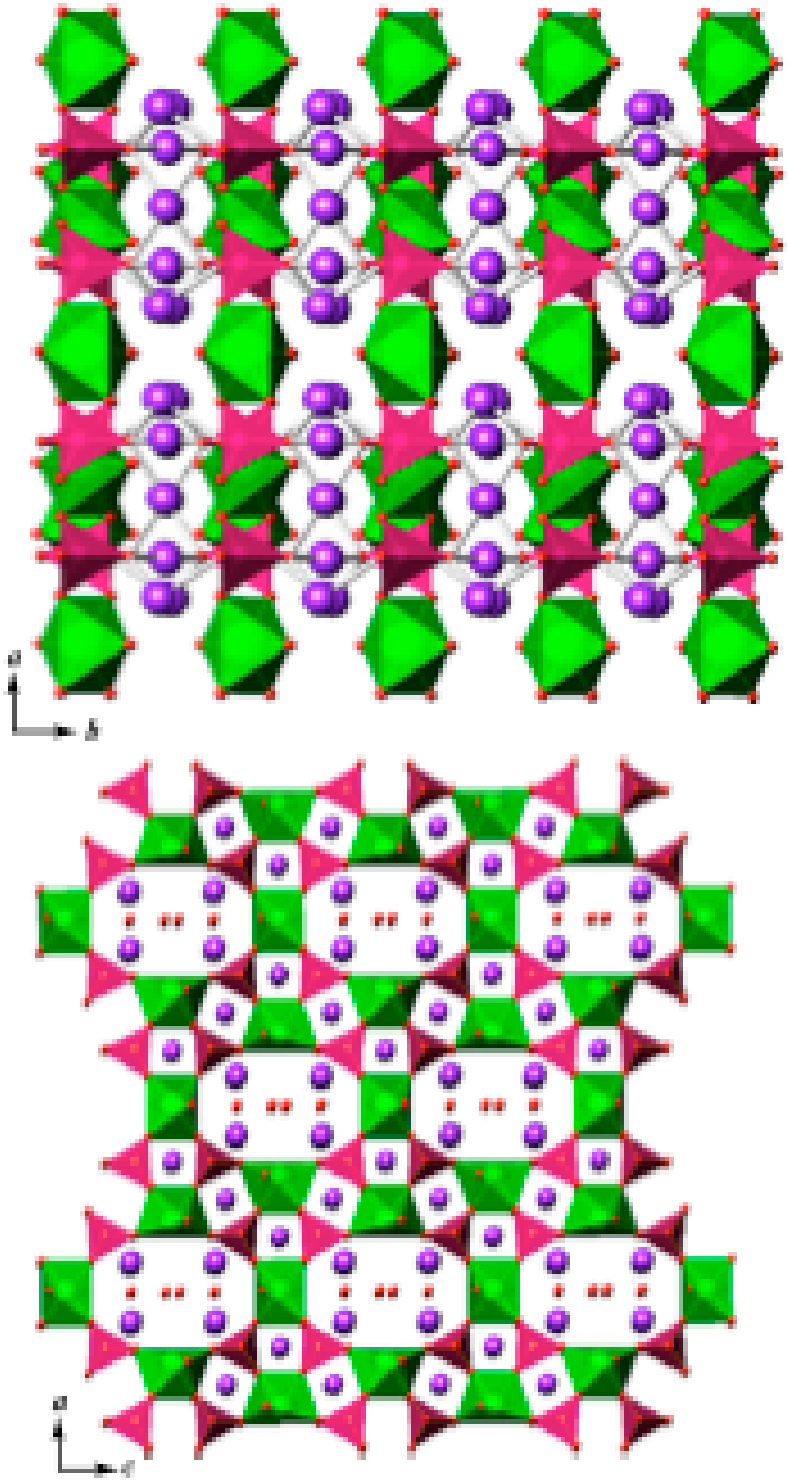

Figure 3.7.1. Two views of the open-framework structure of $Na_2Ag_6[(AgO)_2(UO_2)_3(AsO_4)_4]$ (AgUAs-1) UO_6 = green, AsO_4 = Pink.

The structure of AgUAs-1 shares some common structural building features with previous members of the UO_2^{2+}/M/AsO_4 series (show in Chapter 1.2.3 and 1.2.4). Each uranium center takes distorted tetragonal bipyramidal coordination geometry, which links with the arsenate tetrahedra along the equatorial positions by corner-sharing, building units. These building units further link each other through the other distorted tetragonal bipyramidal uranyl to form the two-dimensional porous sheets, as shown in Figure 3.7.2.

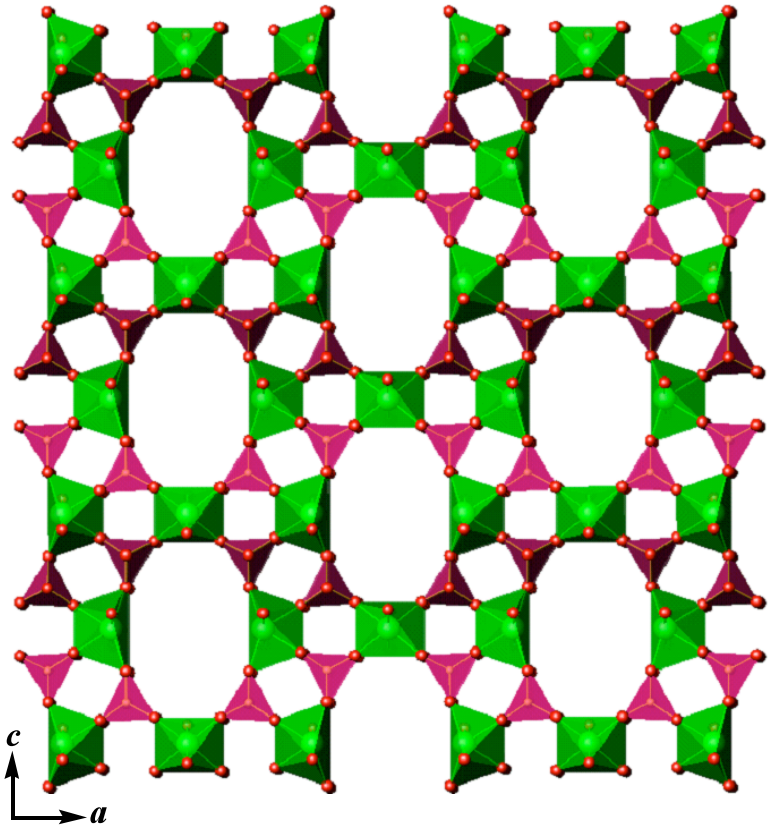

Figure 3.7.2. The new topologic sheet found in AgUAs-1**,** formed by the sharing of vertices between uranyl tetragonal bipyramids and phosphate tetrahedra.

The other structure features, which make the compound AgUAs-1 unique, are the new topologic structure constructed by Ag^{+} and water molecules. There are eight crystallographic independent Ag centers in AgUAs-1, which can be divided into two categories according to the different coordination number. As shown in Figure 3.7.3, the coordination number for Ag centers could be 2 and 3, which is consistent with the typical Ag^{+} coordination environment. The ten-membered rings constructed by connection two-coordinated Ag and three-coordinated Ag alternatively, are the basic units, which could be further linked each other by two-coordinated Ag bridging.

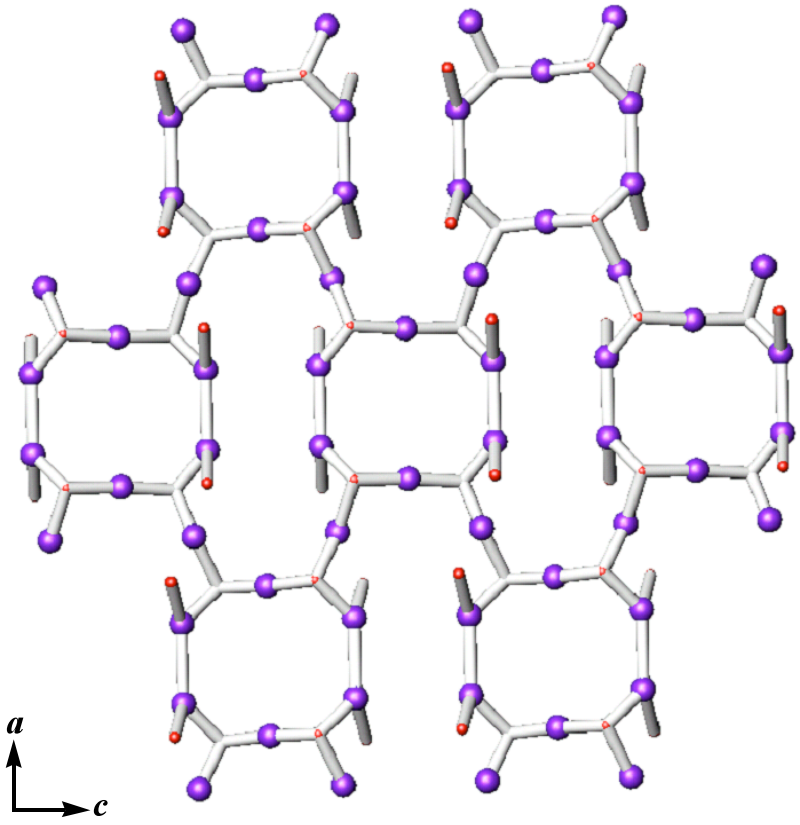

Figure 3.7.3. Two-dimensional layer constructed by Ag^{+} in $Na_2Ag_6[(AgO)_2(UO_2)_3(AsO_4)_4]$ (AgUAs-1).

3.8 $Ag(UO_2)(AsO_4)$ (AgUAs-2)

3.8.1 Structural features.

AgUAs-2 is isostructural with its K^+, NH_4^+, and H_3O^+ analogues listed in Table 3.8.1 (shown in Chapter 1.2.3).

Table 3.8.1: Unit Cell Parameters of meta-autunite group compounds that contain monovalent cations.

Formula	Space group	a (Å)	c (Å)	Mineral
$Li[(UO_2)(AsO_4)](H_2O)_4$	*P*4/n	7.097	9.190	
$H_3O[(UO_2)(PO_4)](H_2O)_3$	*P*4/ncc	6.995	17.491	chemikovite
$H_3O[(UO_2)(AsO_4)](H_2O)_3$	*P*4/ncc	7.162	17.639	trögerite
$K[(UO_2)(PO_4)](H_2O)_3$	*P*4/ncc	6.994	17.784	meta-ankoleite
$K[(UO_2)(AsO_4)](H_2O)_3$	*P*4/ncc	7.176	18.126	abernathyite
$K(H_3O)[(UO_2)(AsO_4)]_2(H_2O)_6$	*P*4/ncc	7.171	18.048	
$NH_4[(UO_2)(PO_4)](H_2O)_3$	*P*4/ncc	7.03	18.09	uramphite
$NH_4[(UO_2)(PO_4)](H_2O)_3$	*P*4/ncc	7.022	18.091	uramphite
$NH_4[(UO_2)(PO_4)](H_2O)_3$	*P*4/ncc	7.189	18.191	

In this structure type (Figure 3.8.1), first described by Ross & Evans (1964), the autunite-type sheet consists of uranyl square bipyramids and either phosphate or arsenate

tetrahedra, and the acute angles of the parallelograms formed between the tetrahedral and square bipyramids change slightly because of the rotation of the polyhedra (the axis of rotation is normal to the plane of the sheet, along [0 0 1]), and depend on the nature of the interlayer cation and the type of tetrahedron present.

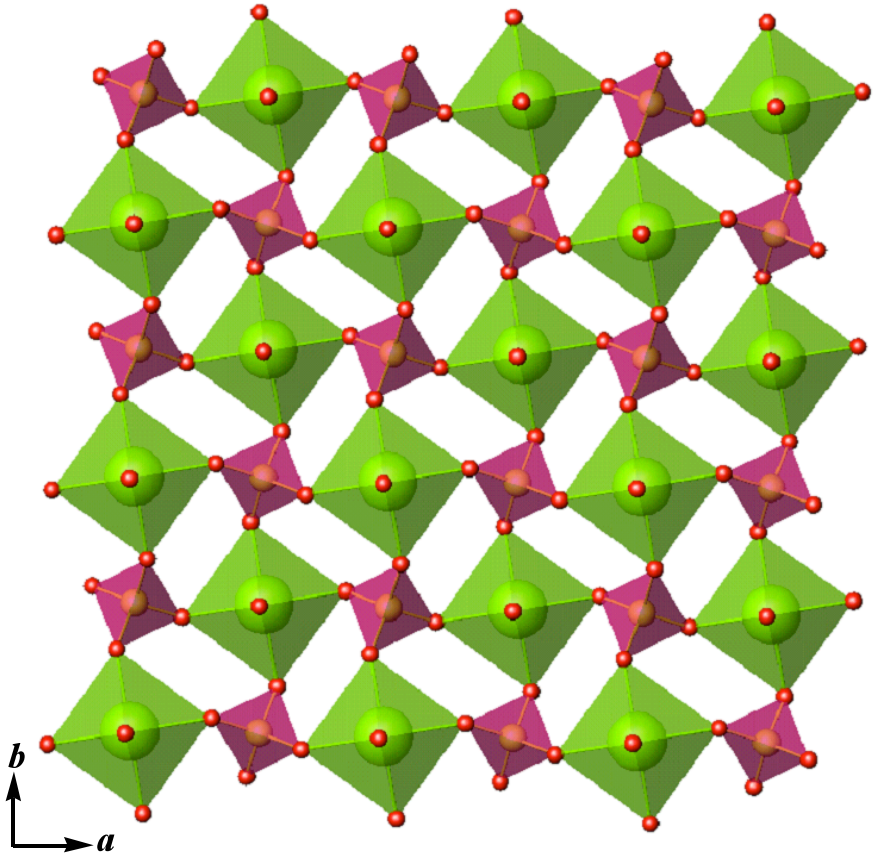

Figure 3.8.1. The autunite-type sheet found in AgUAs-2**,** formed by the sharing of vertices between uranyl square bipyramids and phosphate tetrahedra.

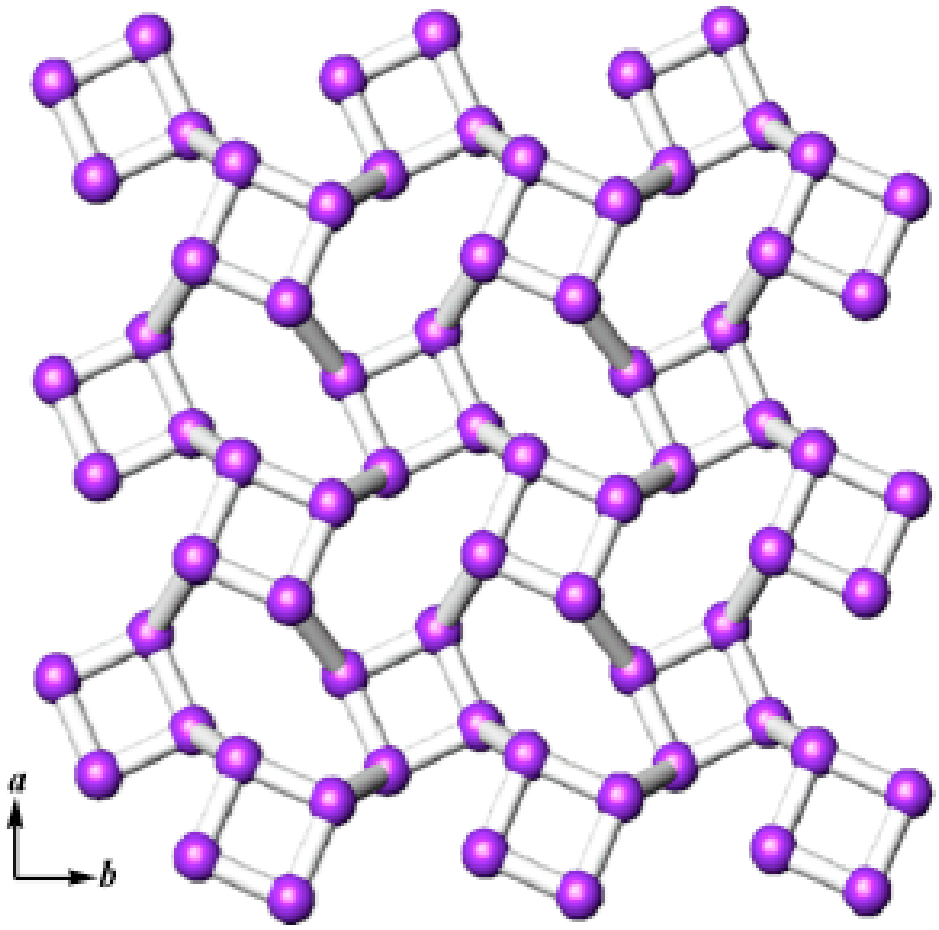

Figure 3.8.2. Two-dimensional layer constructed from Ag^{+} in $Ag(UO_2)(AsO_4)$ (AgUAs-2).

There is only one crystallographically unique Ag^{+} acting as the charge balance for meta-autunite constructed by uranyl arsenates. As shown in Figure 3.8.2, the silver cation planes constructed from metal-metal bonding between the Ag^{+} atoms with bond distance range from 2.511(9) to 2.923(14) Å are the two-dimensional cluster sheets. Each silver atom has three coordination number connected to distorted tetrahedra that are further linked to each other through corner-sharing. Three-dimensional packing view shows that

there are no any interactions between the meta-autunite layers and silver cluster layers, as shown in Figure 3.8.3.

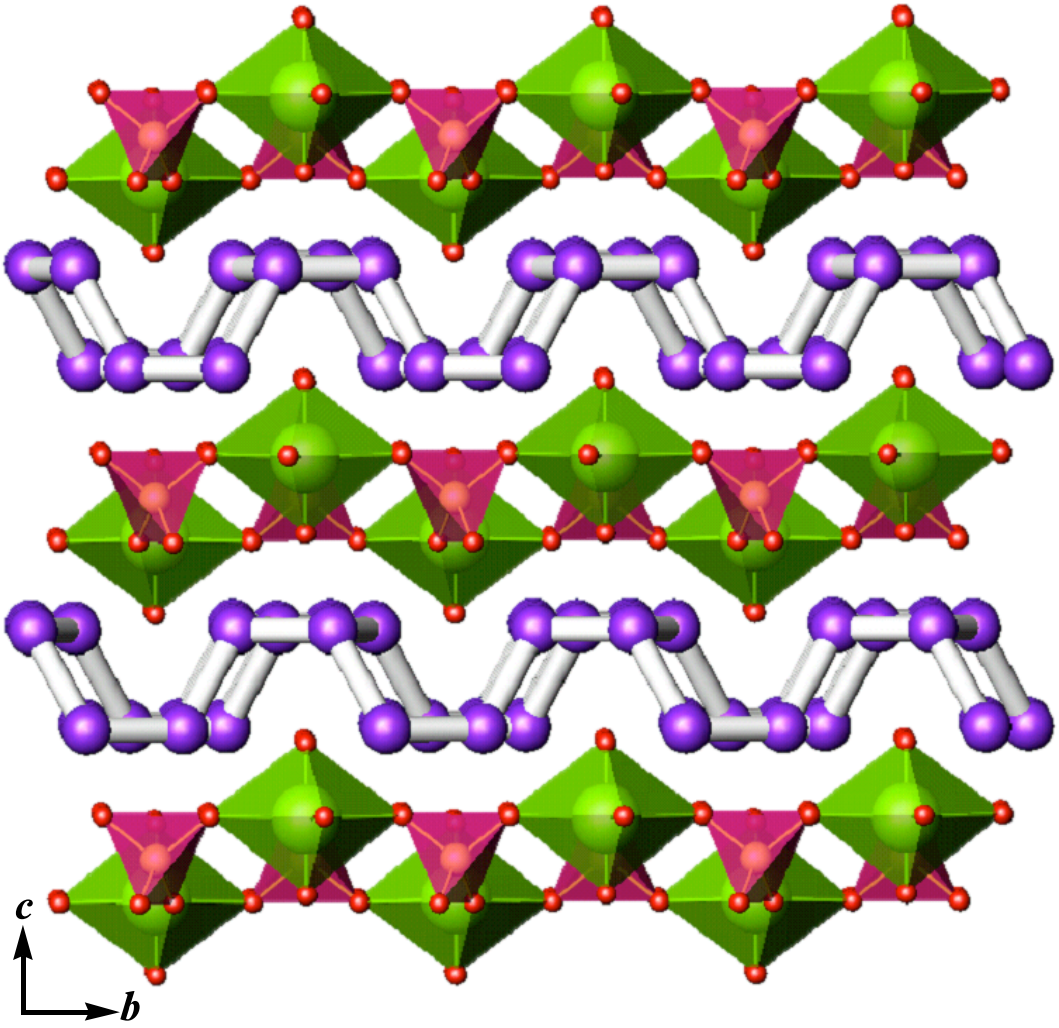

Figure 3.8.3. Three-dimensional structure of $Ag(UO_2)(AsO_4)$ (AgUAs-2), along *a* axis.

3.9 $[Hg_5O_2(OH)_5][(UO_2)_2(AsO_4)_2]$ (HgUAs-1)

3.9.1 Structural features.

HgUAs-1 possesses a pseudo-layered structure with $^2_\infty[Hg_5O_2(OH)_5]^{2+}$ and $^2_\infty[(UO_2)_2(AsO_4)_2]^{2-}$ layers. The latter layers consist of UO_7 pentagonal bipyramids that are linked into edge-sharing dimers that are joined together by AsO_4^{3-} tetrahedra. The former layer formulated as $^2_\infty[Hg_5O_2(OH)_5]^{2+}$ consists of three crystallographically unique mercury centers. As shown in Figure 3.9.1, the compact three-dimensional structure is constructed from the joining of these layers by bridging oxo atoms, which provide linkage for As(1)···Hg(3), Hg(2)···U(1), As(1)···Hg(3), and U(1)···Hg(3). Figure 3.9.2 shows the interactions of the UO_2^{2+} cations and Hg(1) that provides one method for interconnecting the layers. Previous reports show that the apical (uranyl) vertices of the uranyl bipyramids can be shared with polyhedra containing higher-valence cations, even though this would over-bond the oxygen position. However, long uranyl oxo interactions with interlayer cations are well represented. The apical (uranyl) oxygen O(9) provides the μ_2 oxygen atom that bridges to Hg(1).

There is only one crystallographically unique uranium center contained in a nearly linear uranyl, UO_2^{2+}, core in the structure of HgUAs-1. The U≡O bond lengths are 1.804(14) and 1.835 (15) Å, whereas those in the equatorial plane range from 2.270(13) to 2.371(12) Å. These distances can be used to determine the bond-valence sum of U(1) to be 6.02, which is consistent with the expected oxidation state of U(VI) in UO_2^{2+}. The two-dimensional uranyl arsenate plane of HgUAs-1 shares some common structural building features with previous members of the Johannite-class of uranyl minerals that are constructed from $UO_2^{2+}/M/SO_4(CrO_4)$ (Shown in Chapter 1.2.3). The most obvious

similarity is found in the edge-sharing dimers of UO_7 pentagonal bipyramids that are linked by anions, as shown in Figure 3.9.3. This unit is also found in $Cu[(UO_2)_2(SO_4)_2(OH)_2](H_2O)_8$ and $Sr[(UO_2)_2(CrO_4)_2(OH)_2](H_2O)_8$ (Shown in Chapter 1.2.3).

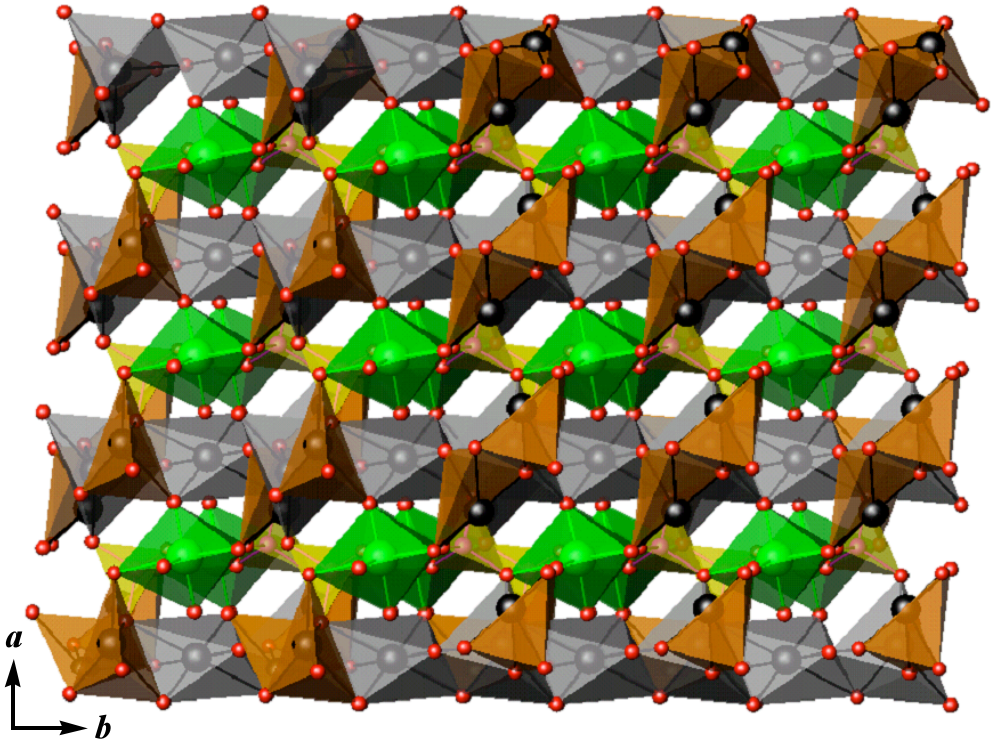

Figure 3.9.1. Three-dimensional structure of $[Hg_5O_2(OH)_5][(UO_2)_2(AsO_4)_2]$ (HgUAs-1).

The single arsenic center is found as an AsO_4^{3-} distorted tetrahedron; yielding a reasonable value for As(V) of 4.95. The As–O bond distances average is 1.689(13) Å. However, this average encompasses both short and long As–O bonds. An As-OH moiety is typically indicated by longer, terminal As–O bonds; these are not present. Three oxygen vertices of the AsO_4 tetrahedron are shared with uranyl or mercury. The

remaining As(1)–O(1) bond is terminal and short, with a bond distance of 1.661(12) Å indicating an As=O unit.

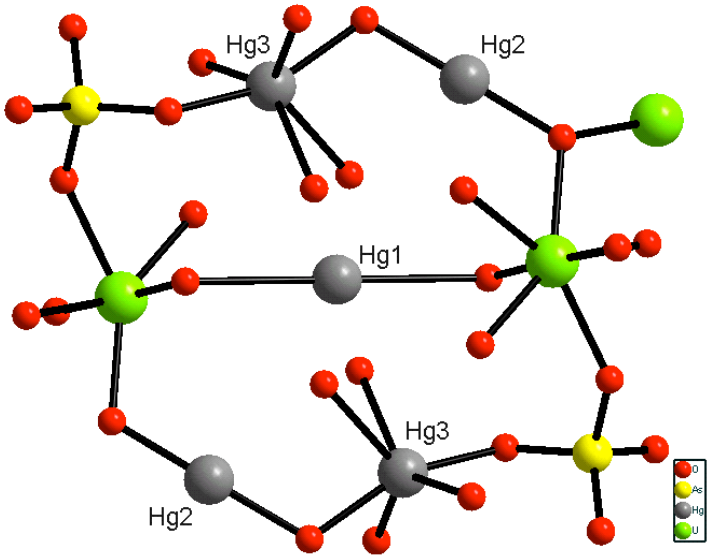

Figure 3.9.2. Basic unit of $[Hg_5O_2(OH)_5][(UO_2)_2(AsO_4)_2]$ (HgUAs-1).

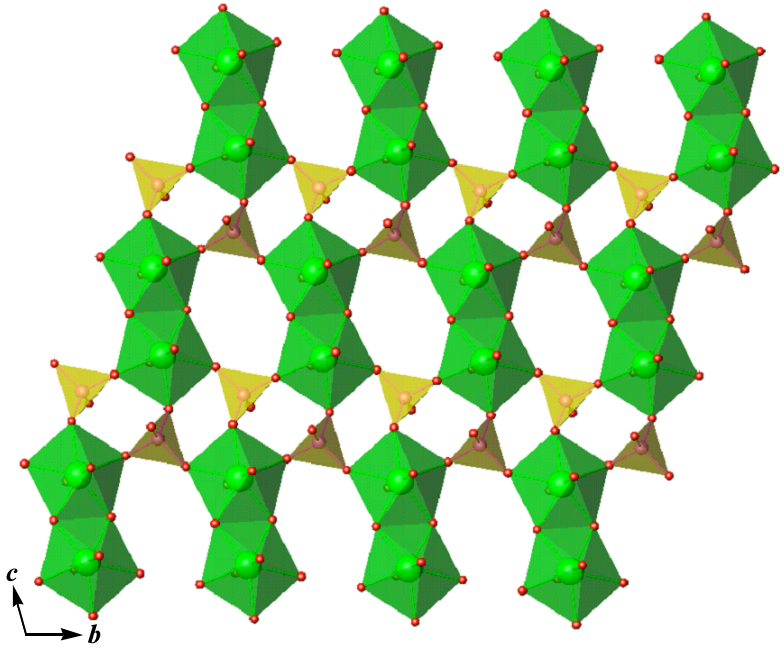

Figure 3.9.3. Johannite layer constructed by $^{2}_{\infty}[(UO_2)_2(AsO_4)_2]^{2-}$.

The most intriguing feature of this compound is the $^{2}_{\infty}[Hg_5O_2(OH)_5]^{2+}$ layer shown in Figure 3.9.4. There are three crystallographically unique mercury centers. Hg(1) and Hg(2) can be described as linear if these longer interactions are excluded, but Hg(3) can not be described in this fashion because the two short Hg–O bonds are not trans to one another. Bond-valence sum calculations indicate that these longer interactions are important for stabilizing a divalent oxidation state for all three Hg centers, with values ranging from 1.75-1.82. In addition to these bond-valence sums, the absence of short Hg···Hg contacts indicates that this is not a Hg(I) compound. This is important because charge balance considerations point to the presence of a mixture of hydroxo and oxo groups in these layers.

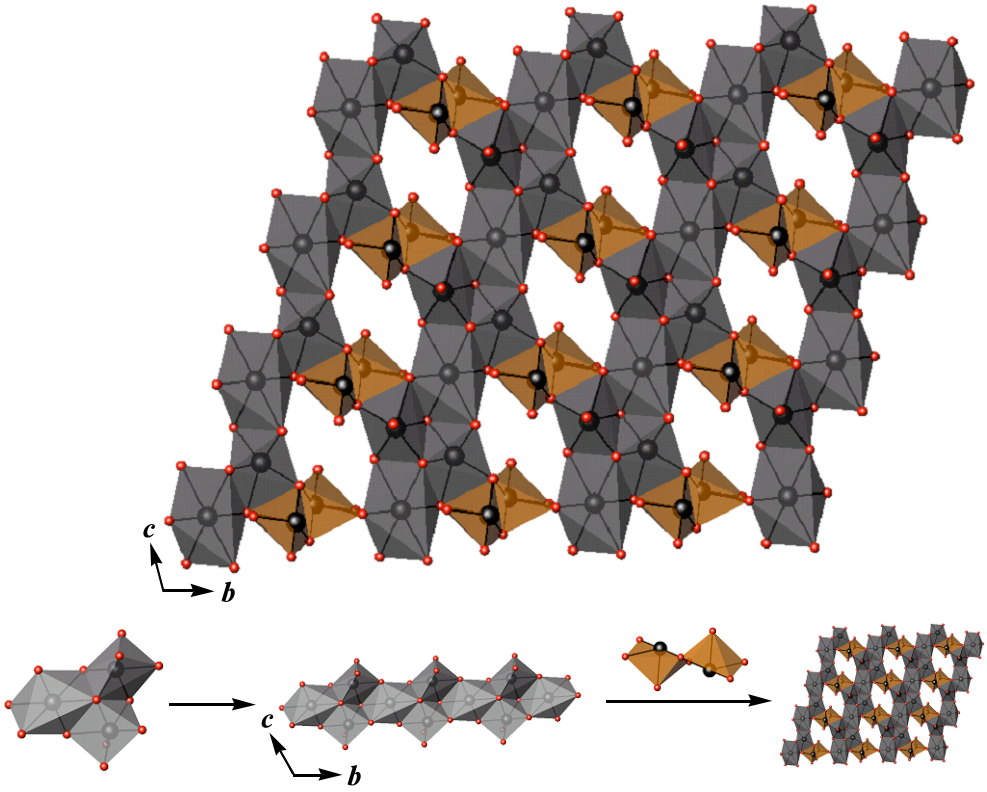

Figure 3.9.4. 2D plane constructed from $^{2}_{\infty}[Hg_5O_2(OH)_5]^{2+}$.

There are three crystallographically unique mercury centers. One and half of the mercury centers are five coordinate with distorted square pyramidal coordination geometries, and Hg–O bond lengths from 2.018(14) to 2.074(13) Å. The other mercury centers is six-coordinate, adopting a distorted octahedral geometry with long interactions along one axis, and Hg–O bond lengths of 2.130(12) and 2.595(12) Å. Hg(1) and Hg(2) have bond-valences of 1.45 and 1.36, respectively. This value is substantially greater than that expected for Hg^{+}. Hg(3) has a bond valence sum of 1.76. One could argue that the coordination environments and charges for Hg(1) and Hg(2) are most similar to that of Hg(I) compounds, and that Hg(3) is most similar to a Jahn-Teller distorted Hg(II) center. However, a better description is that this is an intermediate oxidation state compound, and that formal integral oxidation states do not apply.

3.9.2 Raman Spectroscopy.

The Raman spectrum of HgUAs-1 is shown in Figure 3.9.5. The band at 804 cm^{-1} is attributed to the υ_1 symmetric stretching mode for the UO_2^{2+} unit. The empirical relationship provided by Bartlett and Cooney ($R = 106.5[\nu_1(UO_2)^{2+}]^{-2/3} + 0.575$ Å) enables us to calculate the U=O bond lengths in uranyl units of HgUAs-1 using the Raman shift of the uranyl symmetric stretching vibrations [R(Å)/ν_1(cm^{-1})] = 804 cm^{-1}, yielding a bond length of 1.804 Å, which is reasonably consistent with the corresponding average single crystal data of 1.820(15) Å. Bands observed lower than 300 cm^{-1} are assigned to the ν_2 (δ) UO_2^{2+} (ν (U-O) and δ (U-O) vibrations) as well as the Hg–O bonds. The bands surrounded the 884 cm^{-1} and 842 cm^{-1} are assigned to the AsO_4^{3-}

antisymmetric stretching modes. The AsO_4^{3-} symmetric stretching mode is found at 628 cm^{-1}. The bands surrounded at the mode at 507 cm^{-1} can be assigned to AsO_4^{3-} bending.

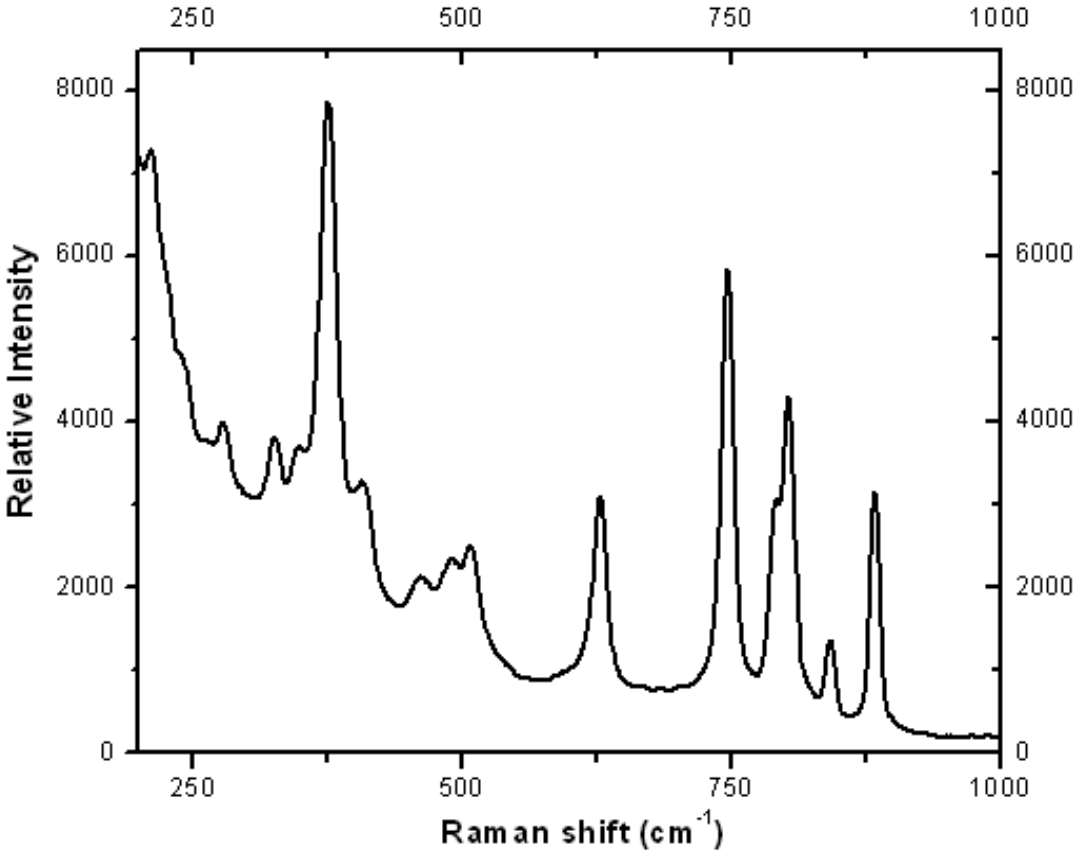

Figure 3.9.5**.** Raman spectrum of $[Hg_5O_2(OH)_4][(UO_2)_2(AsO_4)_2]$ (HgUAs-1).

3.9.3 Fluorescence Spectroscopy**.**

Fluorescence from uranyl compounds can be identified from the vibronic fine-structure characteristic of the UO_2^{2+} moiety (Shown in Chapter 1.6.2). Uranyl fluorescence typically has a characteristic six peak spectrum relating to the $S_{11} \rightarrow S_{00}$ and $S_{10} \rightarrow S_{0v}$ ($v = 0–4$) electronic and vibronic transitions, and for $UO_2(NO_3)_2 \cdot 6H_2O$ the most intense peak ($S_{10} \rightarrow S_{00}$) is position at 508 nm (Shown in Chapter 3.3.3). The vibronic

transitions for HgUAs-1 are somewhat broad, and five transitions are discernable, as shown in Figure 3.9.6.

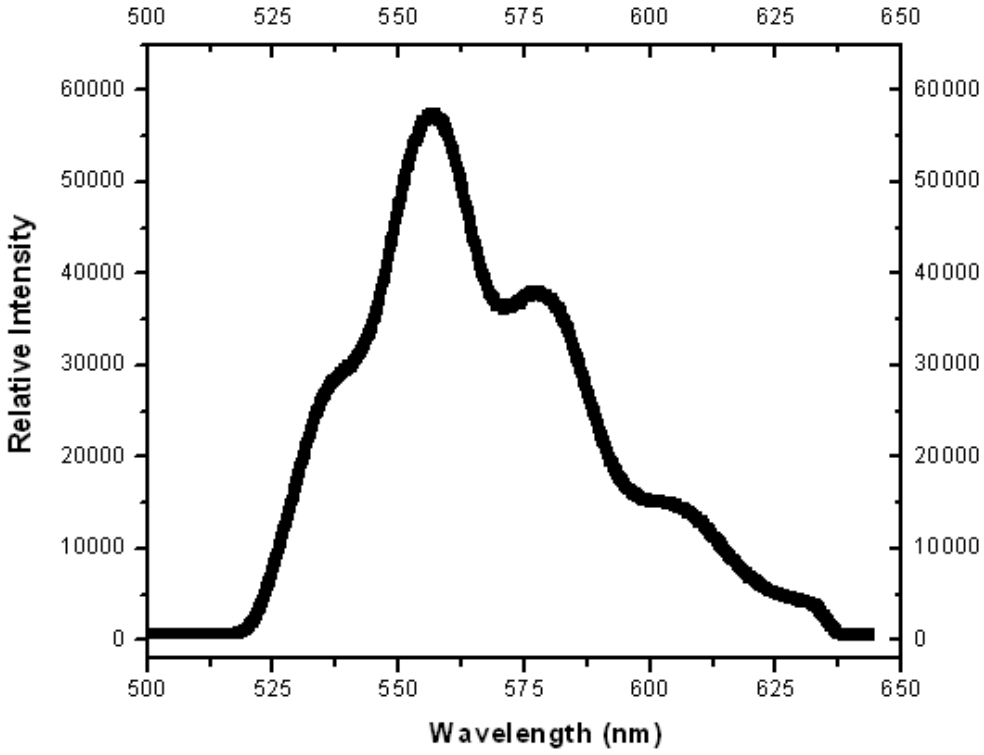

Figure 3.9.6. Fluorescence spectrum of $[Hg_5O_2(OH)_4][(UO_2)_2(AsO_4)_2]$ (HgUAs-1).

3.10 $[Zn(2,2'\text{-bpy})]_2[UO_2(HPO_4)_3]$ (ZnUP-1)

3.10.1 Structural features.

The structure of ZnUP-1 is complex. The metal centers are found as $[UO_7]$ pentagonal bipyramids, $[ZnN_2O_2]$ highly distorted tetrahedra, and $[ZnN_2O_3]$ distorted trigonal bipyramids. The uranyl moieties are bound by both bridging and bridging/chelating phosphate anions. The phosphate groups further ligate two different zinc centers. Zn(1) is bound by phosphate groups to the periphery of the chains, whereas Zn(2), found as $[ZnN_2O_3]$ units, is located within the chain and is an integral feature of chain propagation. The basic repeating unit for ZnUP-1 is shown in Figure 3.10.1.

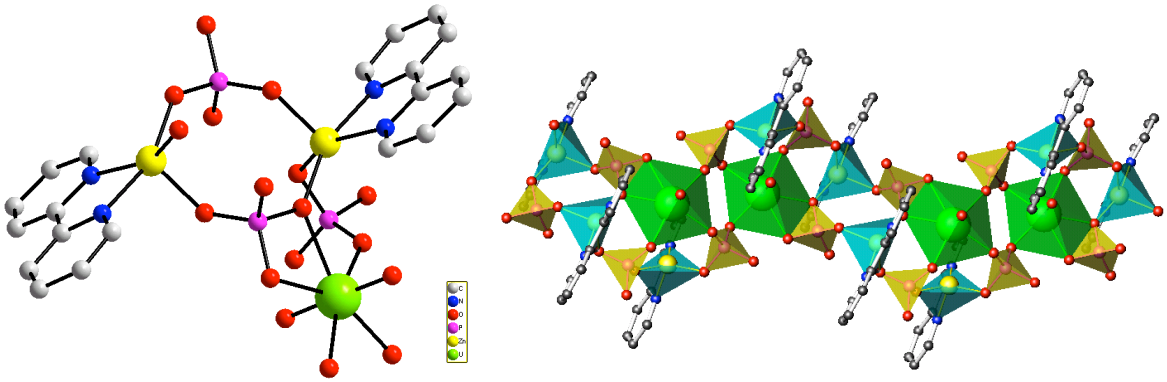

(a) (b)

Figure 3.10.1. A depiction of the basic repeating units for $[Zn(2,2'\text{-bipy})]_2[UO_2(HPO_4)_3]$ (ZnUP-1).

The 2,2'-bipy molecules lie perpendicular to the chains and are loosely π-stacked with 2,2'-bipy molecules from neighboring chains with a stacking distance of approximately 3.48 Å. A view of packing of the chains is shown in Figure 3.10.2.

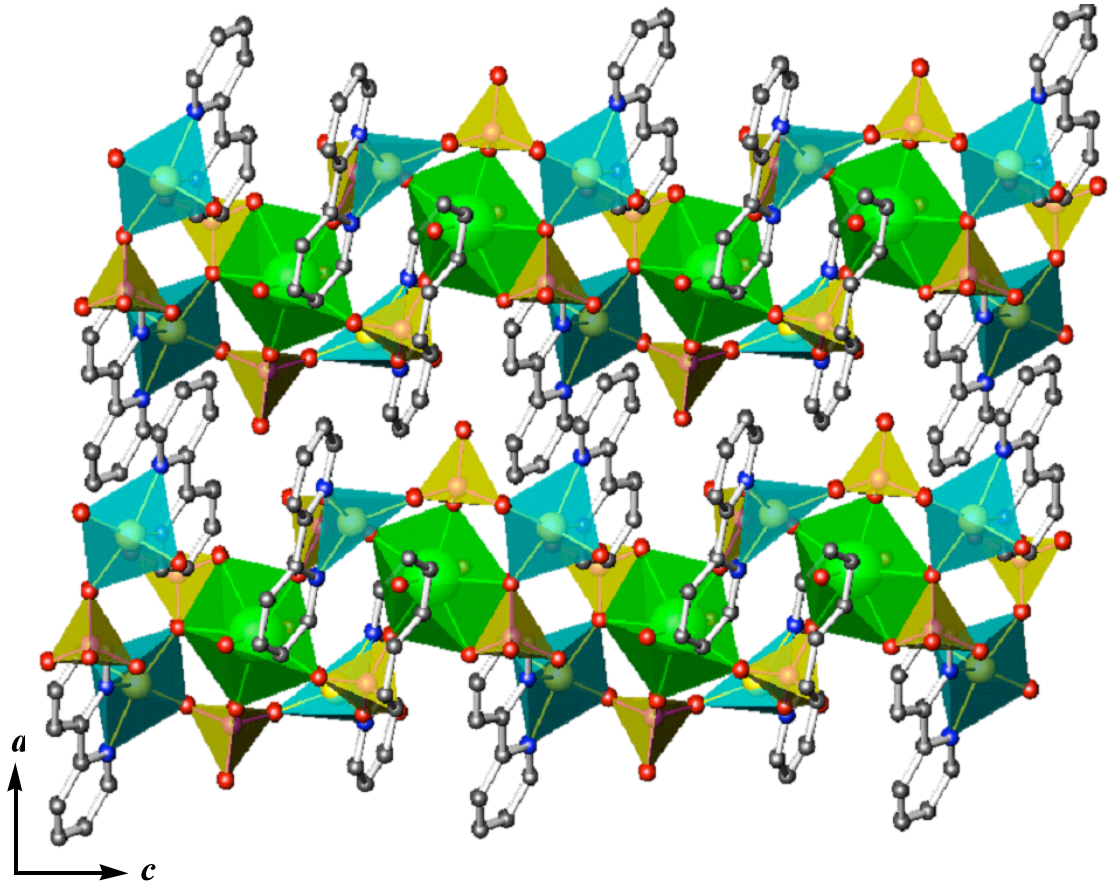

Figure 3.10.2. A view of packing of the chains in $[Zn(2,2'\text{-bipy})]_2[UO_2(HPO_4)_3]$ (ZnUP-1).

The UO_7 pentagonal bipyramid is composed of a central uranyl, UO_2^{2+}, cation with normal U≡O bond distances of 1.776(3) and 1.797(3) Å. The five equatorial U-O distances range from 2.294(3) to 2.484(3) Å. Taken together, these distances result in a bond-valence sum of 6.0. The Zn(1) atom is bound by one 2,2'-bipy molecule and two

phosphate anions to create [ZnN_2O_2] highly distorted tetrahedra. Zn(1)-N bond distances are 2.061(4) and 2.102(4) Å. The Zn(1)-O distances are 1.929(3) and 1.946(3) Å. Zn(2) is found as [ZnN_2O_3] distorted trigonal bipyramids, where the Zn(2) center is bonded to one 2,2'-bipy molecule and three phosphate anions. Zn(2)-N bond distances are 2.085(4) and 2.130(4) Å; whereas the Zn(2)-O distances are slightly shorter and range from 1.959(3) to 2.036(3) Å. There are three crystallographically unique phosphate anions. Each of these anions has three short P-O bonds, which average 1.521(3) Å for the three anions, and one long P-O bond of 1.575(3) Å. The length of the long bond is consistent with this oxygen atom being protonated, which also allows the compound to achieve charge neutrality.

3.10.2 Raman Spectroscopy.

The Raman spectra were collected on a Renishaw inVia Raman microscope spectrometer, as shown in Figure 3.10.3. Raman band at 799.0 cm^{-1} is attributed to the υ_1 symmetric stretching mode for the $(UO_2)^{2+}$ units. The empirical relation by Bartlett and Cooney ($R = 106.5[\nu_1(UO_2)^{2+}]^{-2/3} + 0.575$ Å) enable us to calculate the U-O bond lengths in uranyl using Raman shift (cm^{-1}) of the uranyl symmetric stretching vibrations [R(Å)/ $\nu_1(cm^{-1})$]: 1.812 Å / 799.0, which close to the single crystal data of 1.797 Å. The bands at 1027 cm^{-1} are assigned to the split ν_1 $(PO_4)^{3-}$ symmetric stretching vibration and ν_3 antisymmetric stretching vibration respectively. And the weak band at 367 cm^{-1} is attributed to split, doubly degenerate ν_2 $(PO_4)^{3-}$ bending vibrations. Bands of very low intensity in the 575-655 cm^{-1} region are attributed to the split, triple degenerate ν_4 $(PO_4)^{3-}$ bending modes. Bands observed lower than 300 cm^{-1} are assigned to the ν_2 (δ) $(UO_2)^{2+}$ (ν (U-O) and δ (U-O)) vibrations.

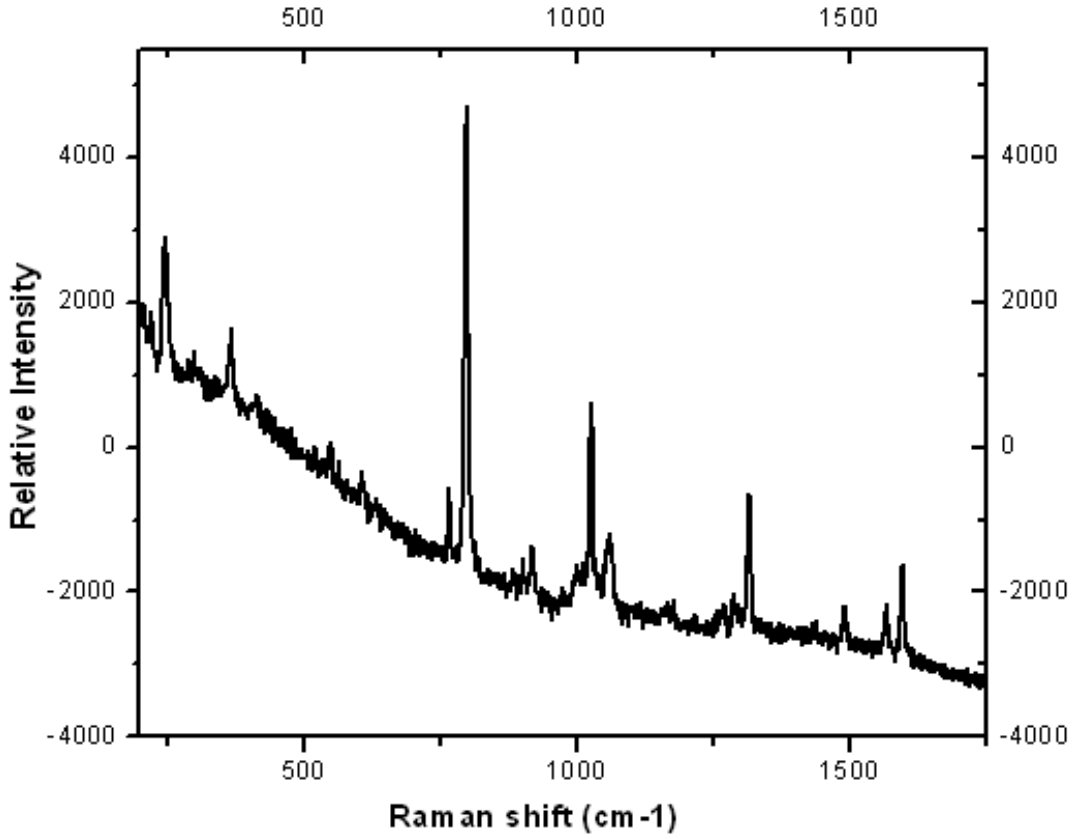

Figure 3.10.3. Raman spectrum of $[Zn(2,2'\text{-bipy})]_2[UO_2(HPO_4)_3]$ (ZnUP-1).

3.10.3 Fluorescence Spectroscopy.

The fluorescence spectroscopy of $[Zn(2,2'\text{-bipy})]_2[UO_2(HPO_4)_3]$ (ZnUP-1) shows in Figure 3.10.4. The intensity multi-peaks at 526, 543, 568 and 596 nm ascribed to the vibronic of uranyl cation. Uranyl fluorescence typically has a characteristic six peak spectrum relating to the $S_{11} \rightarrow S_{00}$ and $S_{10} \rightarrow S_{0v}$, where $v = 0\text{-}4$, electronic transitions, and for $UO_2(NO_3)_2 \cdot 6H_2O$, the most intense peak ($S_{10} \rightarrow S_{00}$) is position at 508 nm (Shown in Chapter 3.3.3). The intensity bands of emission spectrum in ZnUP-1**,** which shows the red shift, is the results of vibronic electronic transitions and 2,2'-bpy ligand excitation.

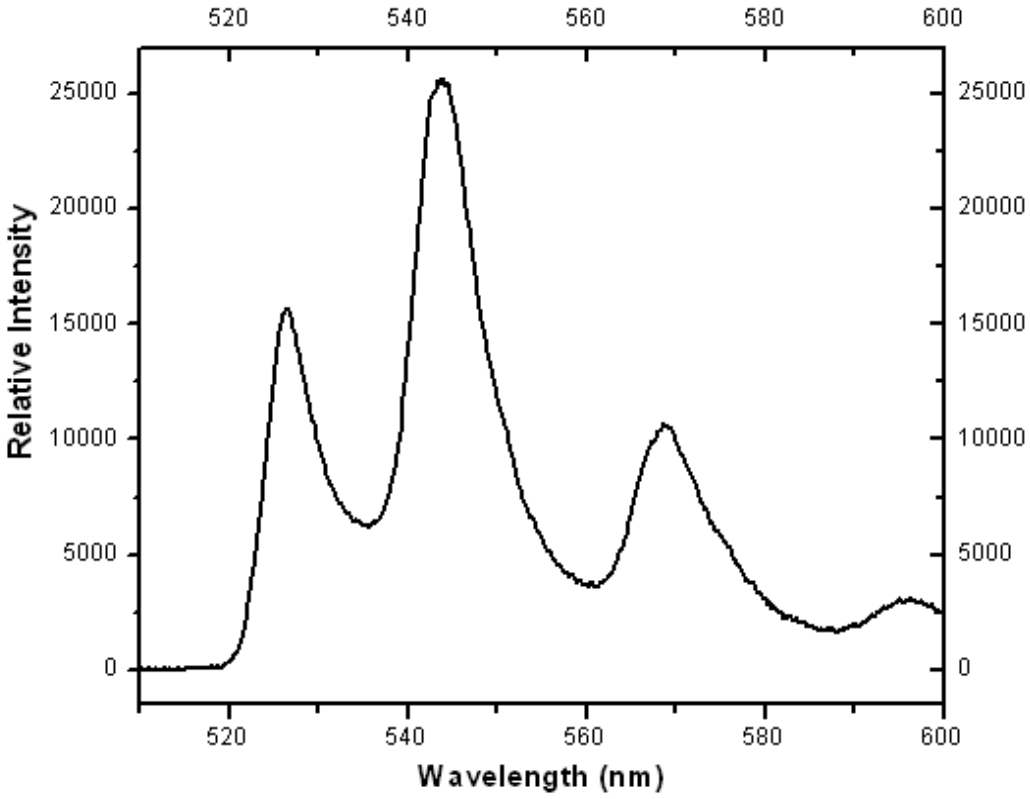

Figure 3.10.4. The fluorescence spectrum of $[Zn(2,2'\text{-bipy})]_2[UO_2(HPO_4)_3]$ (ZnUP-1) showing fine-structure in its emission peaks assigned to vibronic coupling for the UO_2^{2+} moiety and 2,2'-bpy ligand excitation.

3.11 $[H_2bipy]_2[(UO_2)_6Zn_2(PO_3OH)_4(PO_4)_4]\cdot H_2O$ (ZnUP-2)

3.11.1 Structural features.

ZnUP-2 possesses an open-framework structure consisting of UO_7 pentagonal bipyramids that are linked into edge-sharing dimers that are joined together by ZnO_4 and PO_4 tetrahedra. Intersecting channels occur along the *a*, *b*, and *c* axis. These channels house the diprotonated 4,4′-bipyridyl cations and water molecules and are approximately 5.6 × 8.7 Å. Various views of this structure are shown in Figure 3.11.1. The basic building units are shown in Figure 3.11.2. The view down the *a* axis shows something peculiar about the channels that extend in this direction in that they appear to be void spaces. We suspect that disordered water resides in these channels, but these are not resolved in the structure. The Checkcif program notes that there are very large void spaces in the structure, which was investigated further using PLATON. This calculation reveals 20% void space in the structure.

There are three crystallographically unique uranium centers in the structure of ZnUP-2. Each of these units contains a nearly linear uranyl, UO_2^{2+}, core. The U≡O distances within the uranyl cations average 1.771(8) Å; whereas those in the equatorial plane are considerably longer and average 2.394(8) Å. These bond distances are typical for uranyl polyhedra, and can be used to calculate bond-valence sums of 6.08, 5.97, and 5.91 for U(1), U(2), and U(3), respectively, which is consistent with the expected oxidation state of U(VI) in UO_2^{2+}.The single zinc center is found as a ZnO_4 distorted

tetrahedron with Zn–O bond distances ranging from 1.908(7) to 1.974(7) Å; yielding a reasonable value for Zn(II) of 2.10. The P–O bond distances average 1.533(10) Å. However, this average encompasses both short and long P–O bonds. For example, the P(1)–O(2) bond is 1.503(8) Å, and the oxygen atom is terminal. This linked and be described as P=O. This contrasts sharply with the long P(1)–O(1) of 1.583(10) Å, which is also terminal, and most likely represents a P–OH bond.

The structure of ZnUP-2 shares some common structural building features with previous members of the UO_2^{2+}/M/PO_4 series (Shown in Chapter 1.3). The most obvious similarity is found in the edge-sharing dimers of UO_7 pentagonal bipyramids that are linked by phosphate anions. This unit is also found in $Cs[UO_2Ga(PO_4)_2]$ and $Cs_4[(UO_2)_2(GaOH)_2(PO_4)_4]\cdot H_2O$ (Shown in Chapter 1.3.1). ZnUP-2 differs from these aforementioned compounds in two respects. First, the dimers form sheets (shown in Figure 3.11.3) instead of chains that are linked by a second set of dimers that are composed of the third crystallographically unique uranium center. What makes ZnUP-2 especially different from $Cs[UO_2Ga(PO_4)_2]$ and $Cs_4[(UO_2)_2(GaOH)_2(PO_4)_4]\cdot H_2O$ is the absence of metal-containing one-dimensional chains. Rather here there are small clusters containing two Zn centers and seven phosphate anions. Finally, there is an expansion of the intersecting channels needed to accommodate the larger $[H_2bipy]^{2+}$ cations versus those where alkali metals are employed. We will demonstrate shortly that these larger channels do not equate with improved properties, a common myth perpetuated in the literature on open-framework compounds.

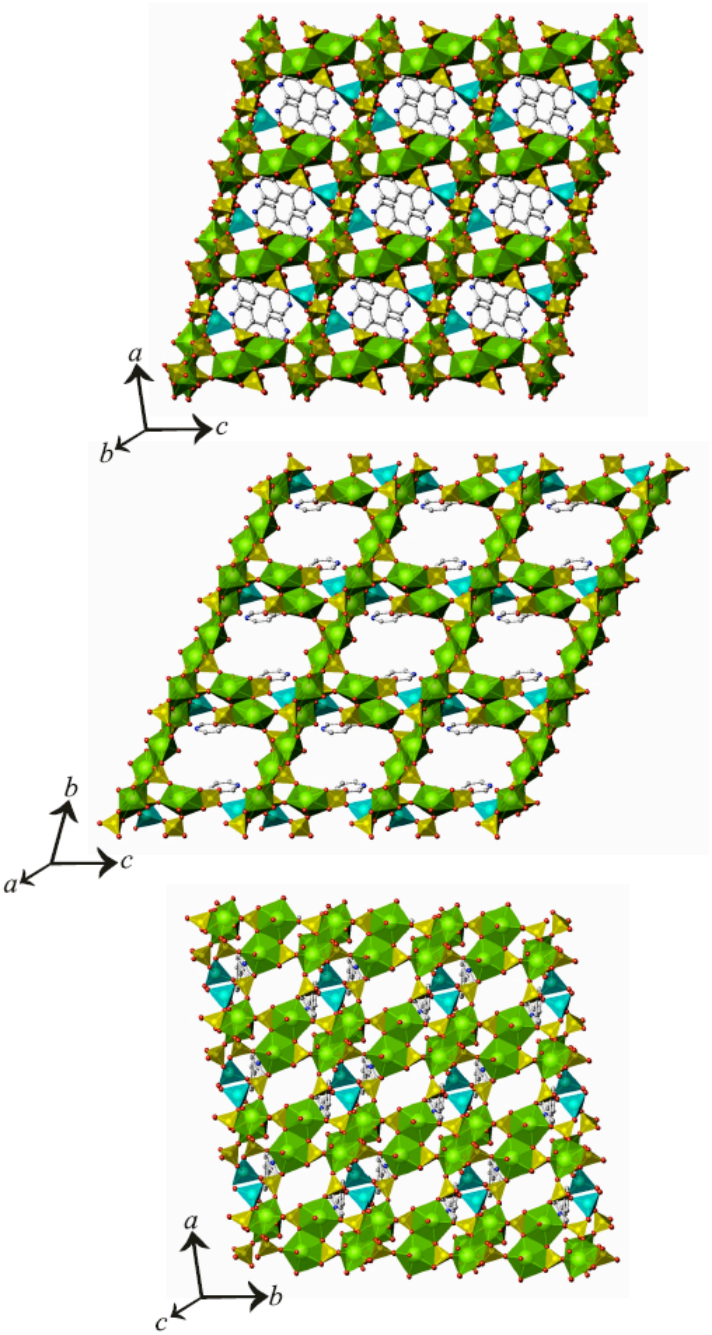

Figure 3.11.1. Three views of the open-framework structure of $[H_2bipy]_2[(UO_2)_6Zn_2(PO_3OH)_4(PO_4)_4]\cdot H_2O$ (ZnUP-2). UO_7 = green, ZnO_4 = light blue, PO_4 = yellow.

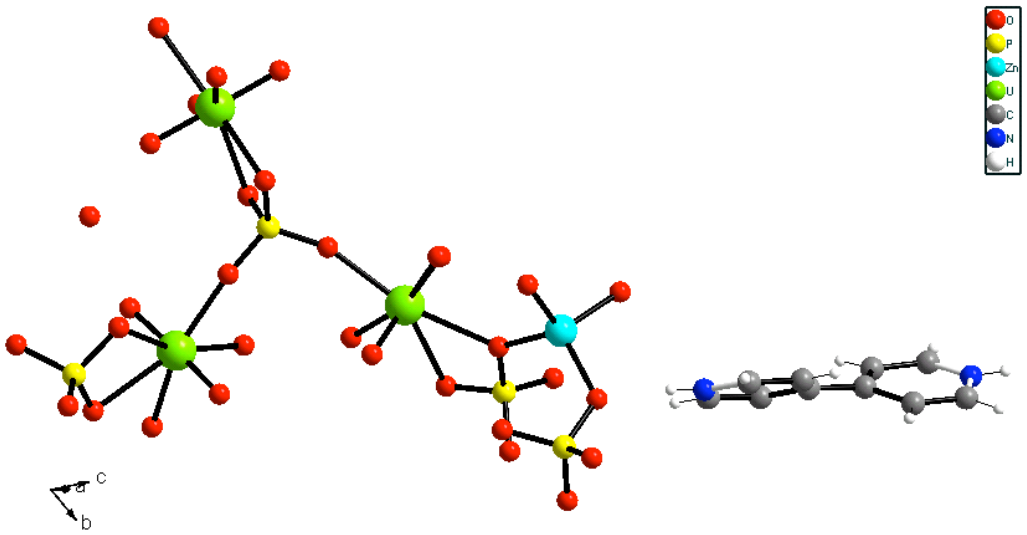

Figure 3.11.2. A depiction of the basic building units in $[H_2bipy]_2[(UO_2)_6Zn_2(PO_3OH)_4(PO_4)_4]\cdot H_2O$ (ZnUP-2)

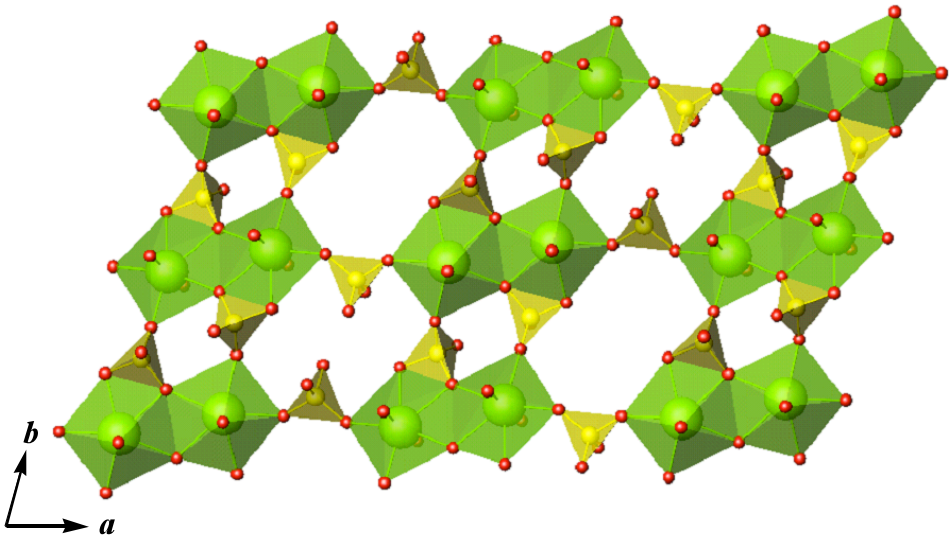

Figure 3.11.3. A view of the [*ab*] plane showing the two-dimensional sub-structure constructed by uranyl phosphate dimers in $[H_2bipy]_2[(UO_2)_6Zn_2(PO_3OH)_4(PO_4)_4]\cdot H_2O$ (ZnUP-2).

3.11.2 Raman Spectroscopy.

The key feature in the Raman spectrum of ZnUP-2 is the band at 833 cm^{-1}, which is attributed to the υ_1 symmetric stretching mode for the UO_2^{2+} units. The UO_2^{2+} bending mode is found at much lower frequency, in this case at 213 cm^{-1}. The presence P–O stretching modes from the phosphate anions are also readily observed by Raman spectroscopy with a feature at 1030 cm^{-1}, which assigned to an anti-symmetric stretching mode. A weak band at 402 cm^{-1} is attributed to PO_4^{3-} bending vibrations. The Raman spectrum of ZnUP-2 is shown in Figure 3.11.4.

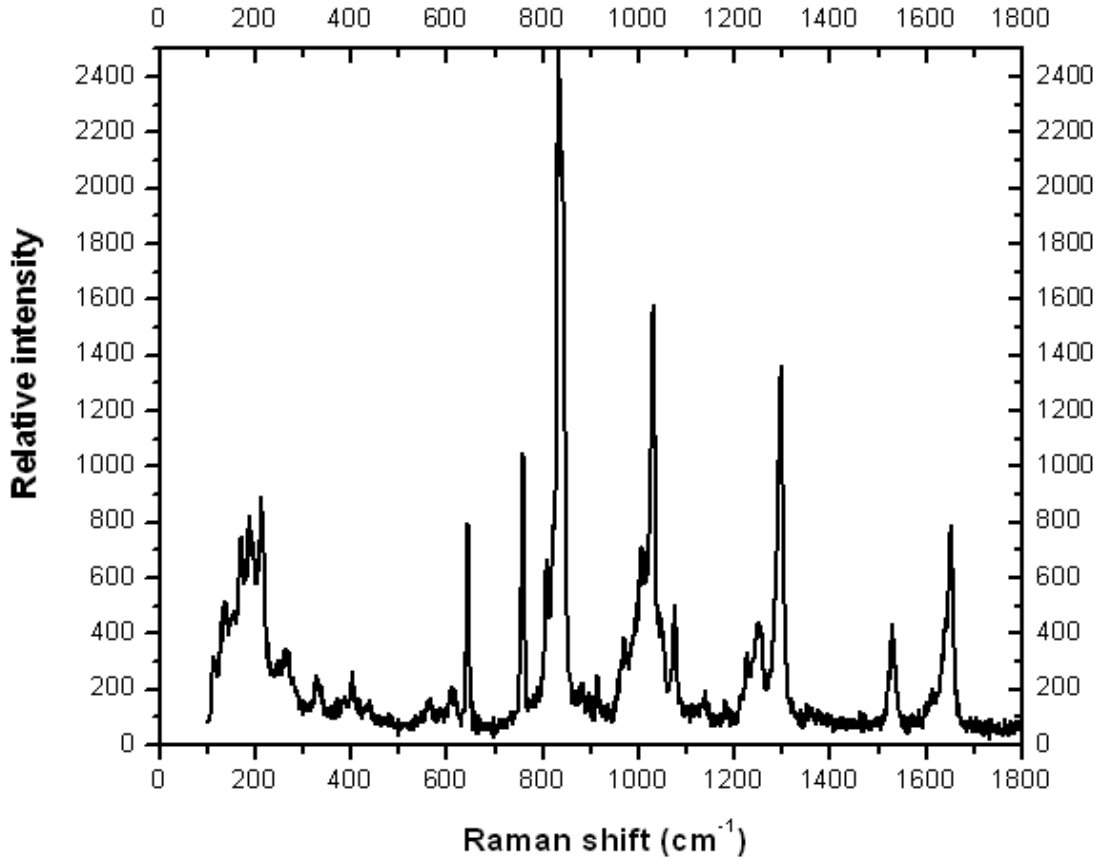

Figure 3.11.4. The Raman spectrum of $[H_2bipy]_2[(UO_2)_6Zn_2(PO_3OH)_4(PO_4)_4]\cdot H_2O$ (ZnUP-2).

3.11.3 Ion-Exchange Studies.

The ion-exchange properties of ZnUP-2 were evaluated to determine whether the $[H_2bipy]^{2+}$ cations can be exchanged for Na^+, K^+, Ca^{2+}, Sr^{2+}, and Ba^{2+} cations. X-ray powder diffraction patterns after ion-exchange has taken place show that replacement of the 4,4′-bipyridyl cations by alkali and alkaline-earth metal cations results in the rearrangement of the framework, as shown in Figure 3.11.5. This is especially pronounced with K^+. This type of structural rearrangement has been previously noted in uranyl phosphates. These results sharply contrast with ion-exchange studies on $Cs[UO_2Ga(PO_4)_2]$, $Cs_4[(UO_2)_2(GaOH)_2(PO_4)_4]\cdot H_2O$, and $A_{3.48}[(UO_2)(VO)_4H_{1.52}(PO_4)_5]$ (A = K, Rb) where the basic framework remains intact after ion-exchange (Shown in Chapter 1.3.3). It may well be that uranyl phosphate frameworks with large pores are not stable when the organic cations are exchanged.

3.11.4 Fluorescence Spectroscopy.

The fluorescence spectra of $[Ag(4,4'\text{-bipy})]_2[(UO_2)_2H_3(PO_4)_3]$, $Ag(2,2'\text{-bipy})(UO_2)(HPO_4)(PO_4)$ and $[Zn(2,2'\text{-bipy})]_2[UO_2(HPO_4)_3]$ compounds exhibited substantial differences in their emission properties (Shown in 3.5.3, 3.6.3 and 3.10.3 respectively). As shown in Figure 3.11.6, ZnUP-2 shows fine-structure in its emission with peaks at 535, 555, and 582 nm assigned to vibronic coupling typical for the UO_2^{2+} moiety.

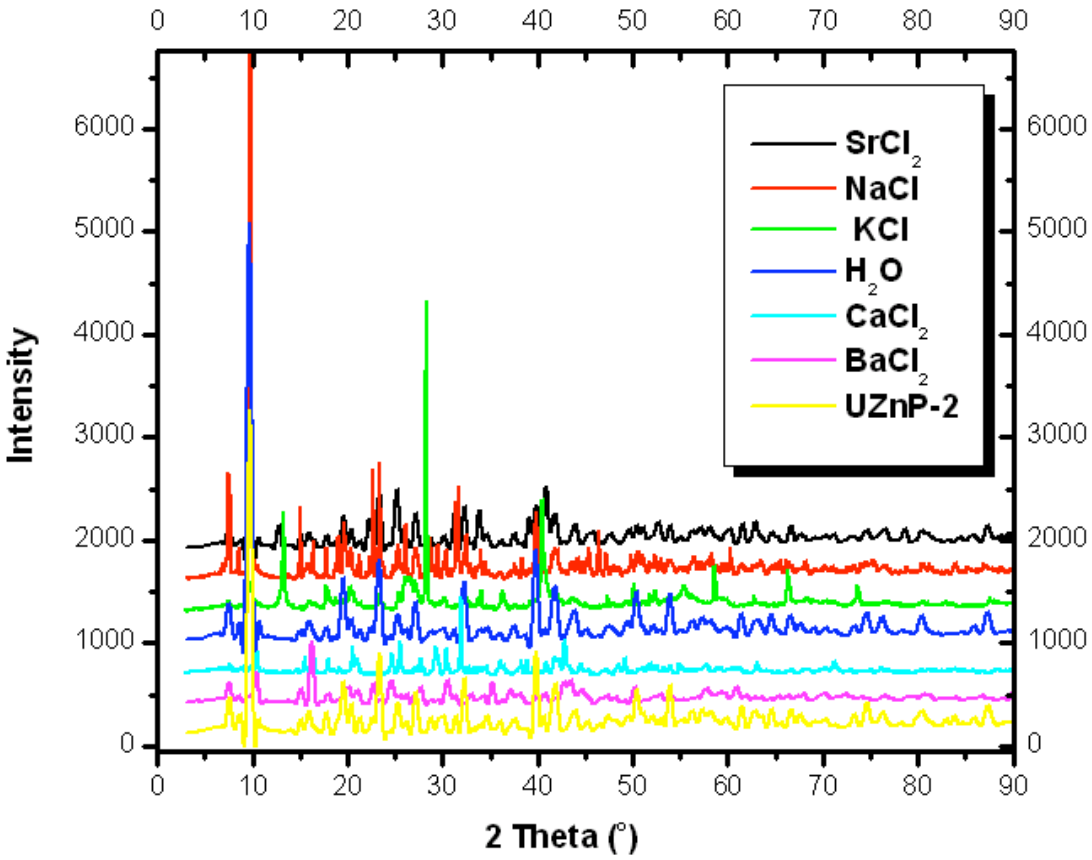

Figure 3.11.5. X-ray powder diffraction patterns after ion-exchange has taken place show that replacement of the 4,4′-bipyridyl cations by alkali and alkaline-earth metal cations results in the rearrangement of the framework in $[H_2bipy]_2[(UO_2)_6Zn_2(PO_3OH)_4(PO_4)_4]\cdot H_2O$ (ZnUP-2).

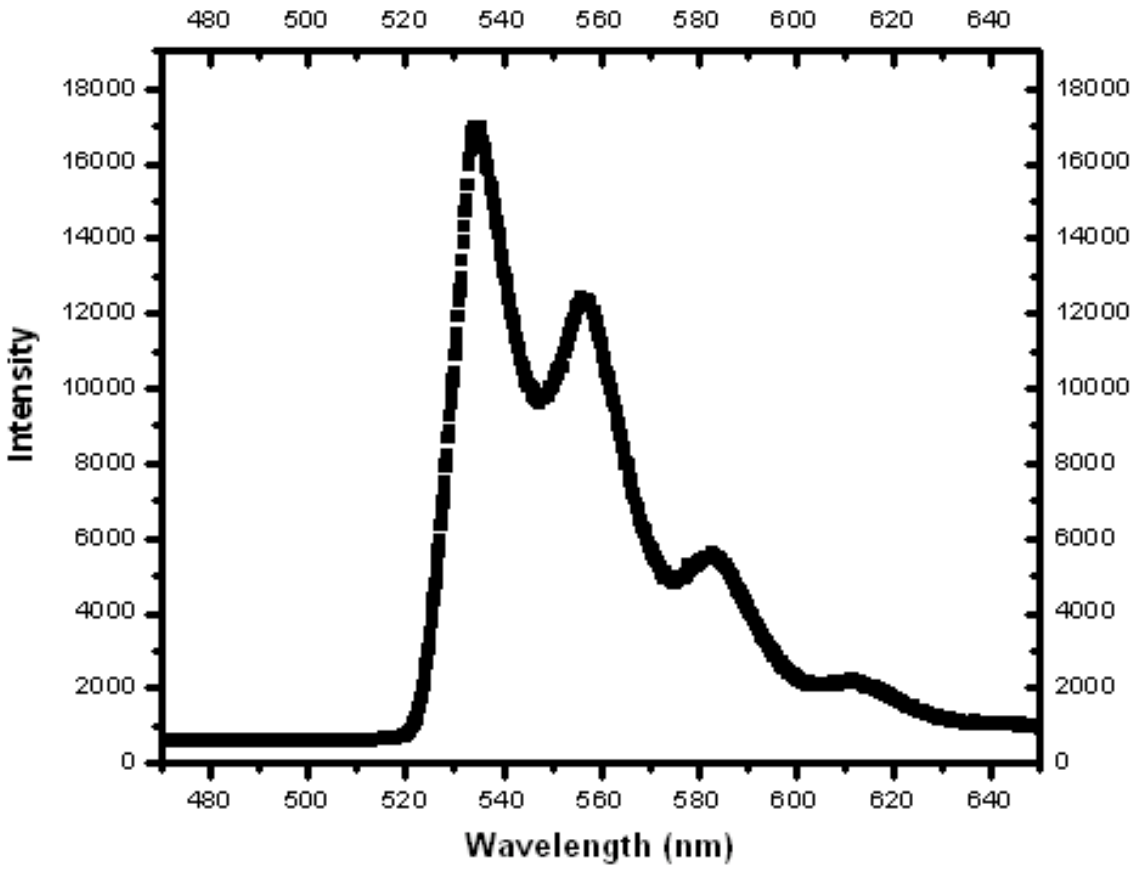

Figure 3.11.6. The fluorescence spectrum of $[H_2bipy]_2[(UO_2)_6Zn_2(PO_3OH)_4(PO_4)_4]\cdot H_2O$ (ZnUP-2) showing fine-structure in its emission with peaks at 535, 555, and 582 nm assigned to vibronic coupling for the UO_2^{2+} moiety.

3.12 $K_2[UO_2Co(PO_4)_2] \cdot H_2O$ (CoUP-1)

3.12.1 Structural Features of $K_2[UO_2Co(PO_4)_2]\cdot H_2O$.

The structure of CoUP-1 consists of a three-dimensional framework that is constructed from two intersecting one-dimensional substructures. The first of these substructures are chains of uranyl phosphate that are fashioned from edge-sharing dimers of UO_7 pentagonal bipyramids that are bridged by phosphate anions. These chains extend down [1 0 1], and are shown in Figure 3.12.1.

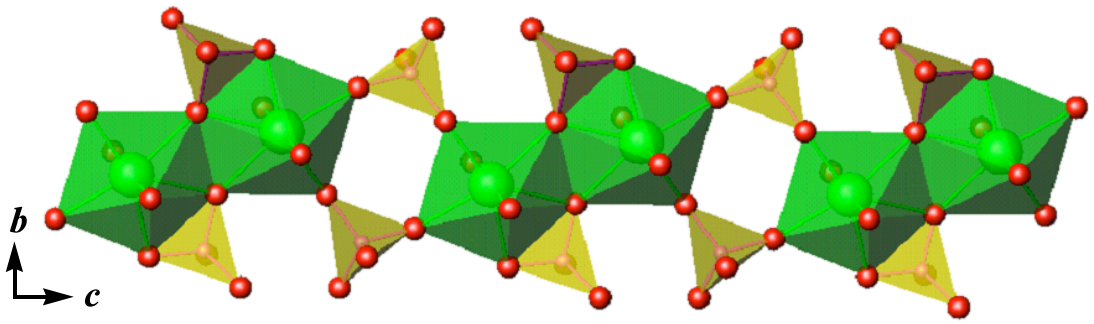

Figure 3.12.1. A view of the uranyl phosphate chains that are fashioned from edge-sharing dimers of UO_7 pentagonal bipyramids that are bridged by phosphate anions in $K_2[UO_2Co(PO_4)_2]\cdot H_2O$ (CoUP-1).

Similar chains have been observed in $Cs_4[(UO_2)_2(GaOH)_2(PO_4)_4]\cdot H_2O$ (UGaP-1) and $Cs[UO_2Ga(PO_4)_2]$ (UGaP-2) (Shown in Chapter 1.3.1). These chains are linked with chains of Co(II) phosphate (depicted in Figure 3.12.2) containing tetrahedra Co to yield a

somewhat open three-dimensional network with channels that occur along the *c* axis that are occupied by K^+ cations and water molecules, as is shown in Figure 3.12.3.

The U≡O bonds that make up the uranyl unit have distances of 1.781(4) and 1.800(4) Å. The U−O distances in the equatorial plane show substantial variability and range from 2.265(4) to 2.502(4) Å. Using these bond distances a bond-valence sum of 6.06 was calculated for U(1), which is consistent with U(VI). The four Co−O bond distances occur from 1.952(4) to 1.971(4) Å, and with a bond-valence sum of 1.92, indicate the presence of Co(II). The bond angles, which are given along with selected bond distances indicate a distorted tetrahedra environment for the Co center. The two K^+ cations, K(1) and K(2) are present in ten- and eight-coordinate environments, respectively, with $K^+\cdots O$ contacts ranging from 2.841(4) to 3.298(4) Å for K(1), and 2.685(4) to 3.211(5) Å for K(2).

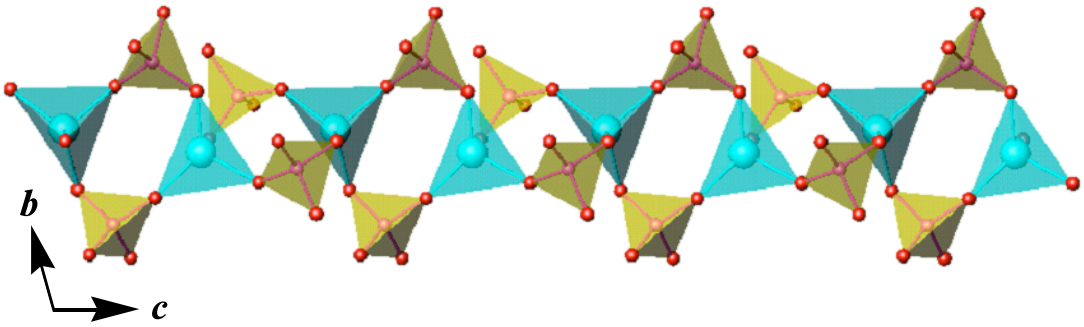

Figure 3.12.2. A depiction of the Co(II) phosphate chains that extend along the *c* axis in $K_2[UO_2Co(PO_4)_2]\cdot H_2O$ **(**CoUP-1**).**

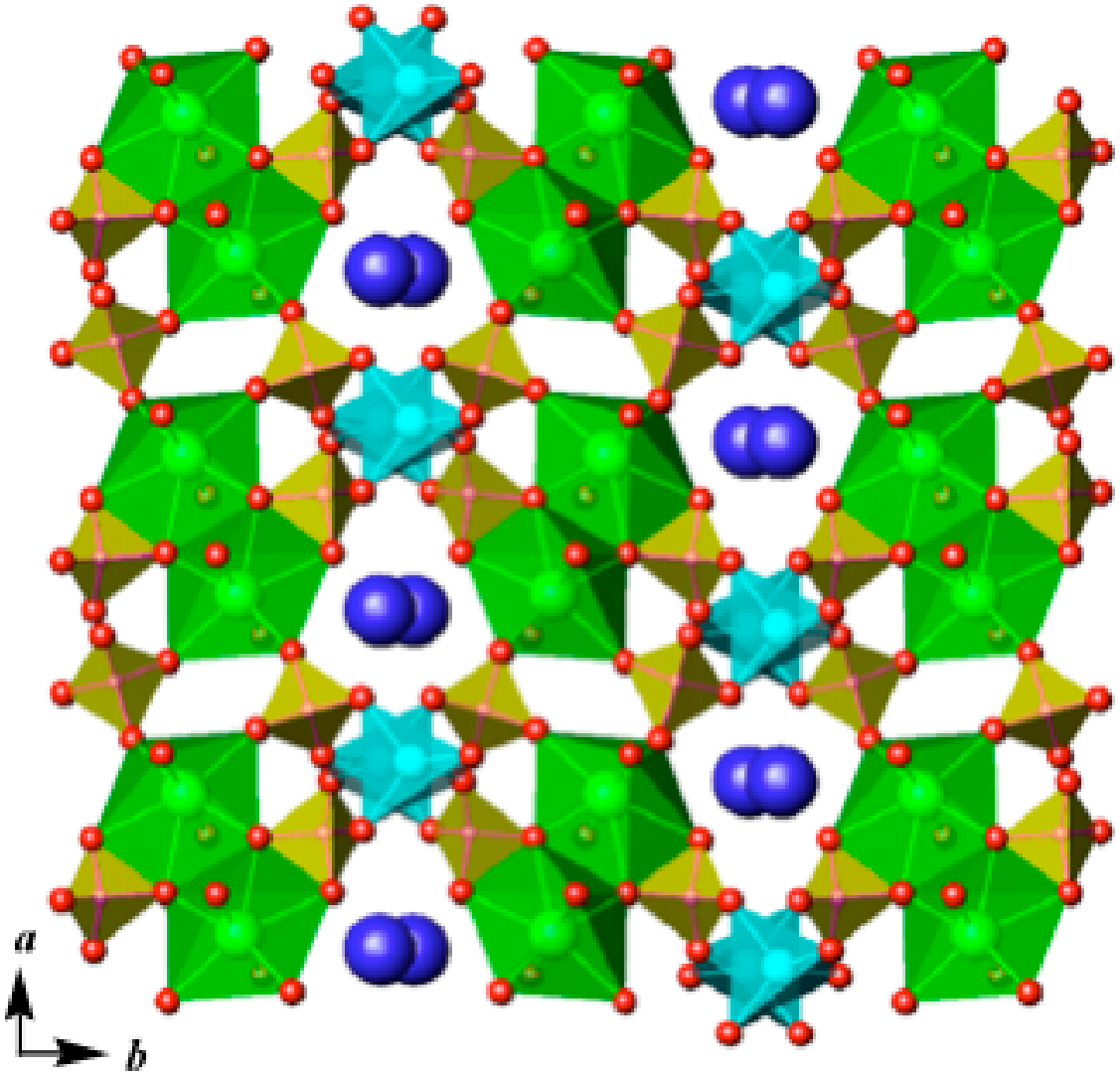

Figure 3.12.3. An illustration of the three-dimensional structure of $K_2[UO_2Co(PO_4)_2]\cdot H_2O$ **(**CoUP-1**).** The channels are occupied by K^+ cations and water molecules.

3.13-3.16 $Zn(OH)_2[(UO_2)_8O_4(SO_4)_4] \cdot 14H_2O$ (ZnUS-1); $[Co(OH)_2]_3[(UO_2)_8O_4(SO_4)_4] \cdot 2H_2O$ (CoUS-1); $[Ni(OH)_2]_3[(UO_2)_8O_4(SO_4)_4] \cdot 10H_2O$ (NiUS-1); $[Ni(OH)_2][(UO_2)_4O_2(SO_4)_2] \cdot 8H_2O$ (NiUS-2)

3.13-3.16.1 Structural features of Zippeite-sheet $[(UO_2)_8O_4(SO_4)_4]$.

All four of the compounds investigated contain the well-known Zippeite-type sheet as originally described by Vochten (Shown in Chapter 1.2.3), formed by zigzag chains of edge-sharing uranyl pentagonal bipyramids, and the chains are connected *b* the sharing of vertices between the bipyramids and sulfate tetrahedra, such that each sulfate tetrahedron is linked to four different bipyramids, as shown in Figure 3.13-3.16.1.

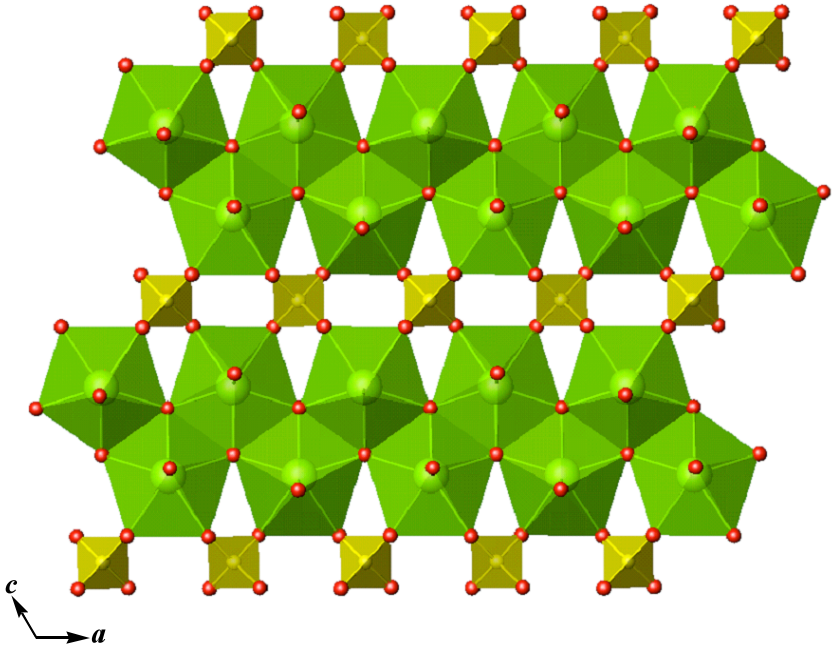

Figure 3.13-3.16.1. The Zippeite-sheet $[(UO_2)_8O_4(SO_4)_4]$ found in ZnUS-1, CoUS-1, NiUS-1 and NiUS-2.

Burns et al. showed that although the uranyl sulfate sheets are topologically identical in each zippeite-group structure studied, the sheets in some are anhydrous, whereas in others they may contain hydroxyl groups located at equatorial vertices of the uranyl pentagonal bipyramids (Shown in Chapter 1.2.3). The interlayer configurations of zippeite-group phases are diverse, and include either monovalent or divalent cations as well as H_2O groups. Burns et al. concluded that the distribution of interlayer constituents can be rationalized on the basis of the bonding requirements of the uranyl sulfate sheets.

3.13-3.16.2 Structural features of cation structures of ZnUS-1, CoUS-1, NiUS-1 and NiUS-2.

Zn^{2+} is six coordinate with the electronic configuration of d^{10}, and adopts tetragonal bipyramids coordination geometry. The bond distances of Zn-O within the range of 2.01(3) to 2.196(14) Å are consistent with the reported structure features. The Zn^{II} tetragonal bipyramids connect to Zippeite-sheet $[(UO_2)_8O_4(SO_4)_4]$ along the equatorial positions by corner-sharing of apical oxygen atoms of uranyl pentagonal bipyramids, as shown in Figure 3.13-3.16.2.

Co^{2+} is six coordinate with the electronic configuration of $t_{2g}^5e_g^{*2}$, using distorted octahedra coordination geometry due to the Jahn-Teller effect. There are two crystallographic independent Co^{II} centers linked to each other to form a dimer as the basic unit, as shown in Figure 3.13-3.16.3. The bond distances of Co-O within the range of 1.97 (5) to 2.26(2) Å are consistent with the reported structure features. The Co^{II} dimer basic units connect to Zippeite-sheet $[(UO_2)_8O_4(SO_4)_4]$ by corner-sharing of apical oxygen atoms of uranyl pentagonal bipyramids, as shown in Figure 3.13-3.16.4.

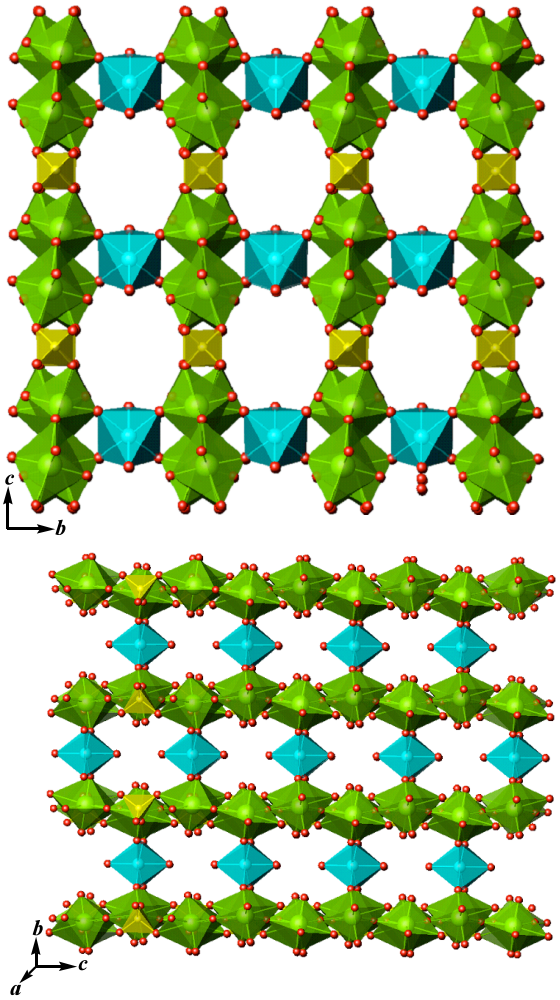

Figure 3.13-3.16.2. Various views of open-framework of compound $Zn(OH)_2[(UO_2)_8O_4(SO_4)_4] \cdot 14H_2O$ (ZnUS-1).

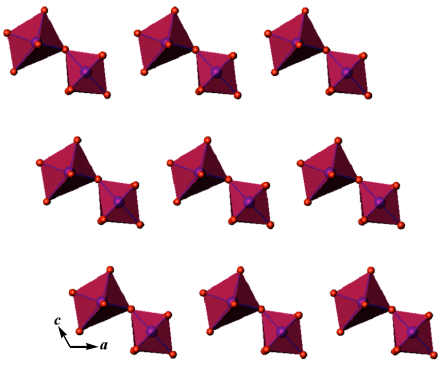

Figure 3.13-3.16.3. Two-dimension sheets constructed from distorted octahedral dimer of $[Co(OH)_2]_3[(UO_2)_8O_4(SO_4)_4] \cdot 2H_2O$ (CoUS-1).

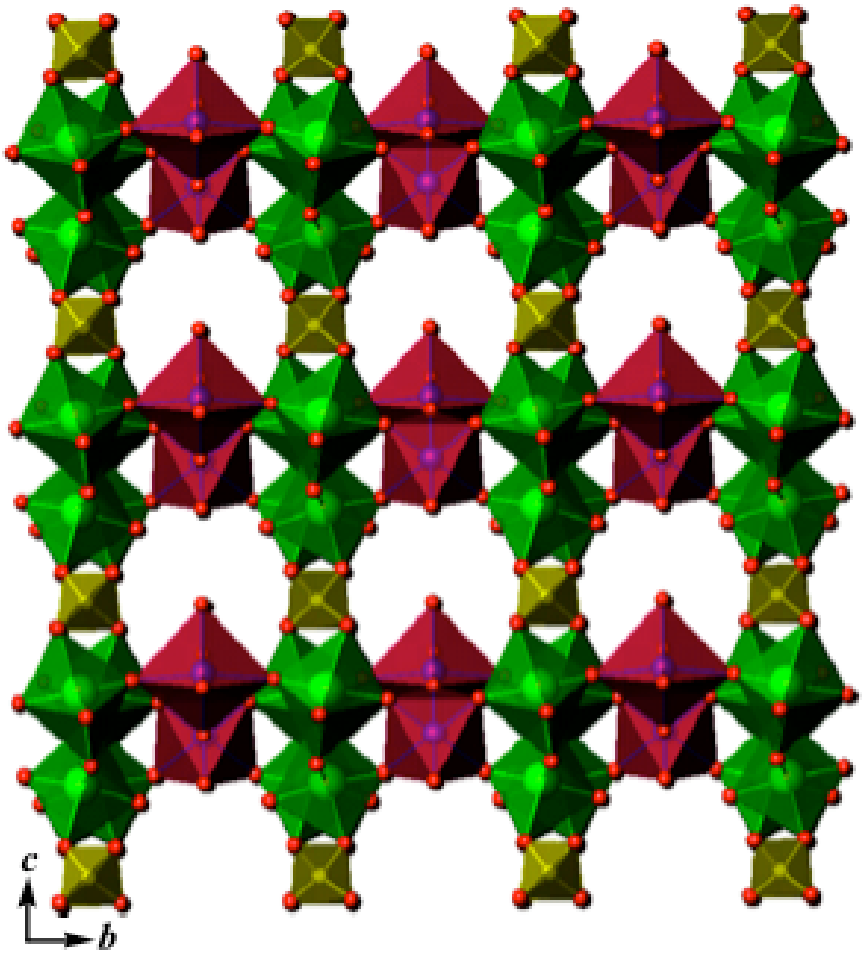

Figure 3.13-3.16.4. Open-framework of $[Co(OH)_2]_3[(UO_2)_8O_4(SO_4)_4] \cdot 2H_2O$ (CoUS-1).

Ni^{2+} is six coordinate with the electronic configuration of $t_{2g}^6 e_g^{*2}$, using tetragonal bipyramids coordination geometry. There are two crystallographic independent Ni^{II} centers linked each other to one-dimensional chain along *a* axis, as shown in Figure 3.13-3.16.5. The bond distances of Ni-O within the range of 1.961(16) to 2.21(7) Å are consistent with the reported structure features. The Ni^{II} one-dimensional chains connect to Zippeite-sheet $[(UO_2)_8O_4(SO_4)_4]$ by corner-sharing of apical oxygen atoms of uranyl pentagonal bipyramids, as shown in Figure 3.13-3.16.6.

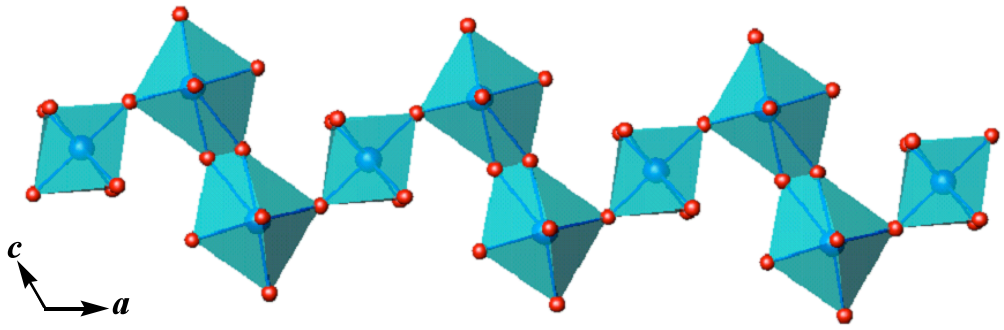

Figure 3.13-3.16.5. One-dimensional chains constructed by distorted octahedral Ni^{II} $[Ni(OH)_2]_3[(UO_2)_8O_4(SO_4)_4] \cdot 10H_2O$ (NiUS-1).

Ni^{2+} is six coordinate with the electronic configuration of $t_{2g}^{6}e_g^{*2}$, using tetragonal bipyramids coordination geometry. There is only one crystallographic independent Ni^{II} center linked to each dimer by corner-sharing, as shown in Figure 3.13-3.16.7. The bond distances of Ni-O within the range of 2.035(10) to 2.228(13) Å are consistent with the reported structure features. The Ni^{II} dimers connect to Zippeite-sheet $[(UO_2)_8O_4(SO_4)_4]$ by corner-sharing of apical oxygen atoms of uranyl pentagonal bipyramids, as shown in Figure 3.13-3.16.8.

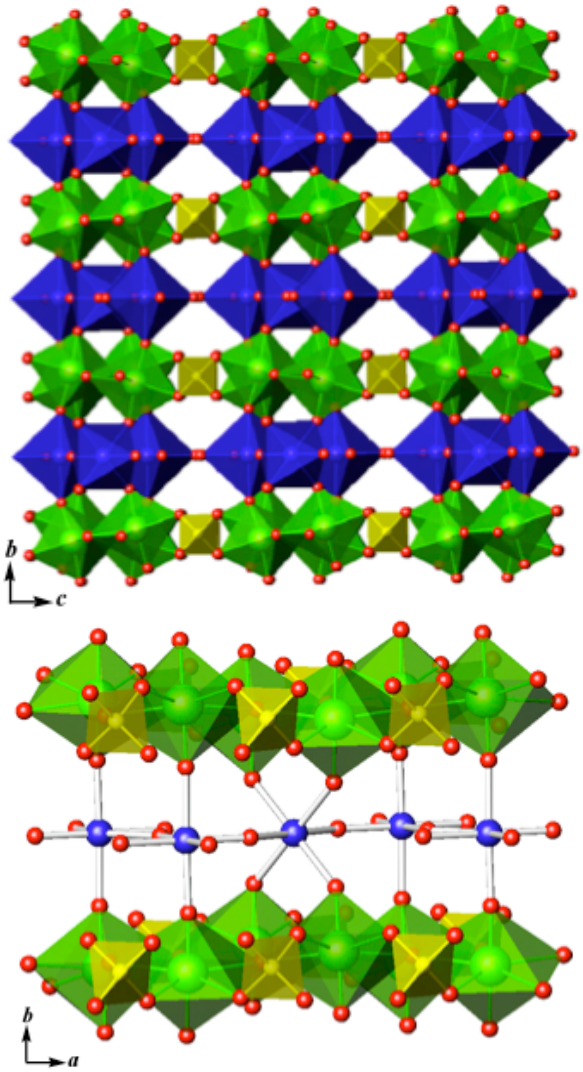

Figure 3.13-3.16.6. Open-framework of $[Ni(OH)_2]_3[(UO_2)_8O_4(SO_4)_4] \cdot 10H_2O$ (NiUS-1).

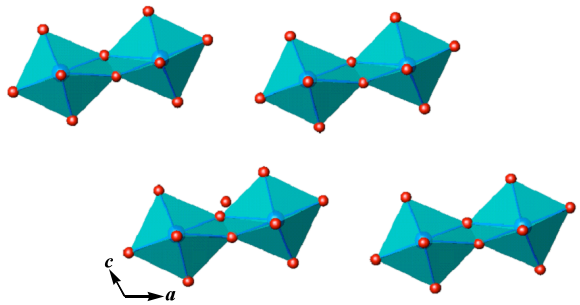

Figure 3.13-3.16.7. Layers constructed from distorted octahedra dimer of $[Ni(OH)_2][(UO_2)_4O_2(SO_4)_2] \cdot 8H_2O$ (NiUS-2).

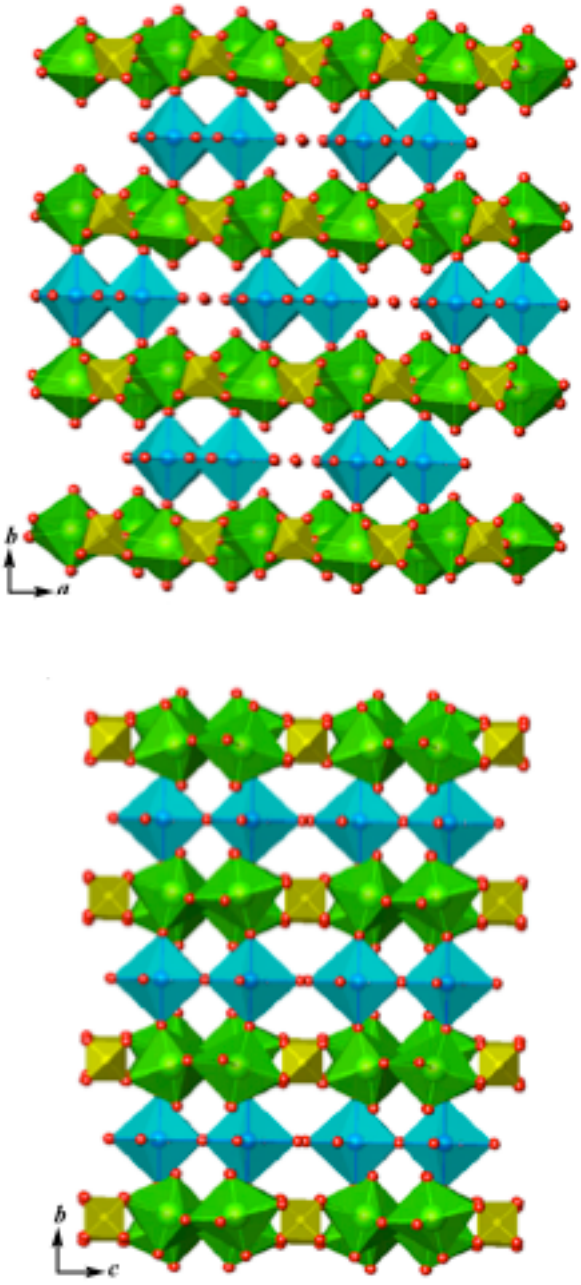

Figure 3.13-3.16.8. Open-framework of $[Ni(OH)_2][(UO_2)_4O_2(SO_4)_2]\cdot 8H_2O$ (NiUS-2).

3.17 $(UO_2)(OH)(CO_2)(C_5H_4N)$ (Uoxa-1)

3.17.1 Synthesis and structural features.

Synthesis.

Hydrothermal method has been proven to an effective to synthesized uranyl transition metal phosphates and inorganic-organic hybrid framework containing uranyl cations (Shown in Chapter 1.3). Previous reports show that the oxalate anion formation under hydrothermal conditions (Shown in Chapter 2.1) is one such example and several pathways for its formation have been proposed, including the reductive coupling of carbon dioxide, the decomposition or oxidation of an organic compound, and decarboxylation of an organic species (Shown in Chapter 1.1). The infinite structures including one-dimensional chain (Shown in Chapter 1.2.1), two-dimensional sheets (Shown in Chapter 1.2.2), and three-dimensional frameworks (Shown in Chapter 1.2.3) constructed from uranyl, UO_2^{2+} cations, have been widely reported with the potential application in radioactive materials, new selective ion-exchange materials, proton conductors, and fluorescence materials (Shown in Chapter 1.1). The three-dimensional compound $(UO_2)(OH)(CO_2)(C_5H_4N)$ (Uoxa-1) constructed from L-handed single stranded helix linked each other by oxalate anions have been synthesized under mild hydrothermal method. Single crystal structure diffraction shows that Uoxa-1 belongs to mix ligands inorganic-organic hybrid material with strong fluorescence signal including in 4,4'-bipy and *in situ* synthesized oxalate anions. It is well-known that HCN is

thermodynamically unstable, could be hydrolyzed by H_2O and $[CN]^-$ are kinetically stable enough for them to well-established. As shown in Scheme 2.1, HCN behaves as a weak acid (p*Ka* = 9.31) and is hydrolyzed in aqueous solution to $[HCO_2]^-$ which could be further coupling to oxalate anions under hydrothermal reaction.

Structural features.

Uoxa-1 possesses an open-framework structure consisting of UNO_6 pentagonal bipyramids that are linked into edge-sharing dimers that are joined together by oxalate anions. Intersecting channels occur along [0 0 1] and [1 1 1] axis. These channels house the two coordinated 4,4′-bipyridyl ligands independent of each other with the long distance of 8.91 Å and the size of channels are approximately 15.422 × 9.663 Å. Various views of this structure are shown in Figure 3.17.1. The basic building unit of Uoxa-1 is an L-handed single stranded helix constructed from edge-sharing UNO_6 pentagonal bipyramids dimers which are further linked to each other to form an open-framework by oxalate anions bridges, as shown in Figure 3.17.2. One dimensional chains constructed from edge-sharing UNO_6 pentagonal bipyramids dimers which are further linked to each other by oxalate anion bridges through edge-sharing along both [1 0 0] and [1 1 0] axis.

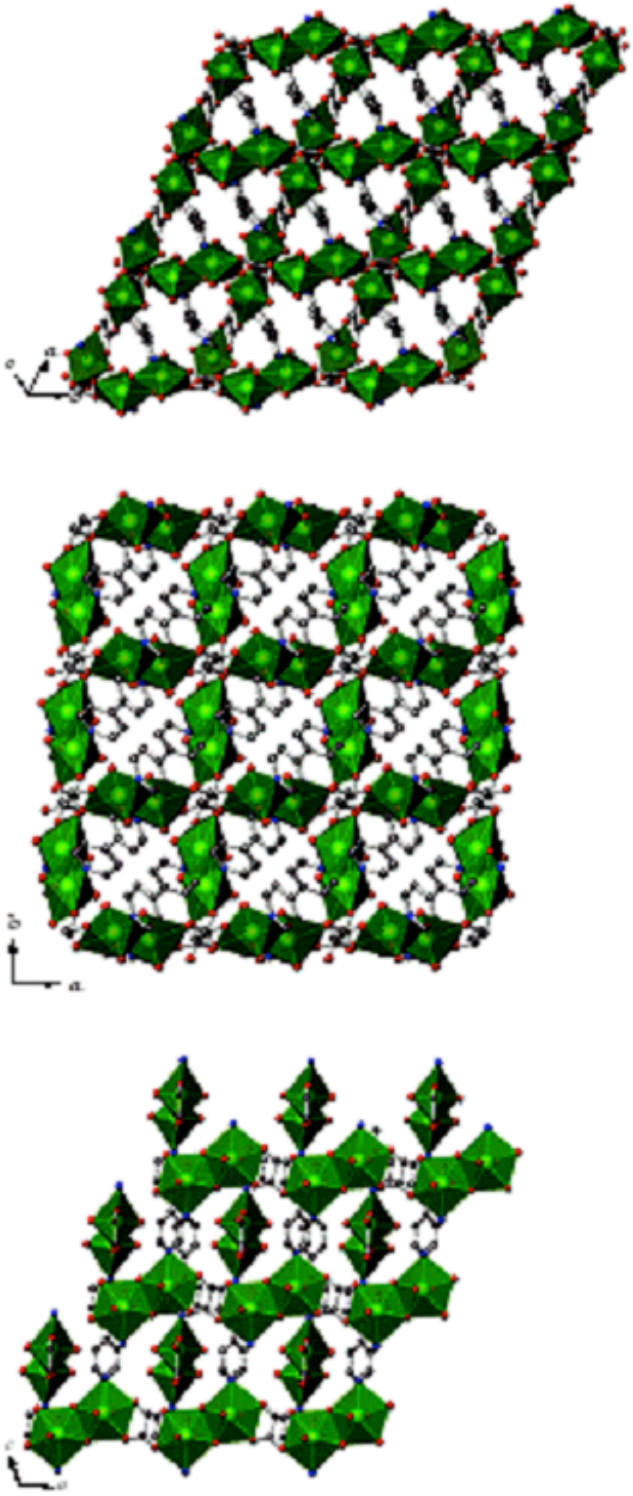

Figure 3.17.1. Three views of $(UO_2)(OH)(CO_2)(C_5H_4N)$ (Uoxa-1).

There is only one crystallographic unique uranium center in Uoxa-1. Each of these units contains a nearly linear uranyl, UO_2^{2+}, core. The U≡O distances within the uranyl cations average 1.771(3) Å; whereas those U-O bonds in the equatorial plane are considerably longer and average 2.477(3) Å consistent with the distance between uranium to diprotonated equatorial O(1) and U-N bond in the equatorial position is 2.549(4) Å consistent with the previous reports (Shown in Chapter 1.4). These bond distances are typical for uranyl polyhedra, and can be used to calculate bond-valence sums of 5.87 for U(1), which is consistent with the expected oxidation state of U(VI) in UO_2^{2+}. There is only 0.5 crystallographic unique 4,4'-bipyradine molecule and 0.5 unique oxalate molecule in structure of Uoxa-1 due to the general atom positions for *C2/c* space group. The delocalization of electron for oxalate anions lead to make average bond length for carbon oxygen double bond and single bond with the bond length 1.245 (5) and 1.267 (5) Å, respectively, and 126.7(4)^o bond angle. Each pentagonal bipyramid uranyl geometry links each other to the dimers by edge-sharing through equatorial oxygen atoms. Four oxygen atoms and one nitrogen atom which come from 4,4'-bpy ligand are locate on the equatorial plan of pentagonal bipyramide uranyl polyhedra.

As shown in Figure 3.17.2, the open-framework structure of Uoxa-1 is constructed from L-handed single stranded helix linked to each other by oxalate anions along *a* axis and *b* axis alternatively. L-handed single stranded helix, called basic units in the structure of Uoxa-1, constructed from pentagonal bipyramid UNO_6 dimers linked each other by 4,4'-bpy ligand along *c* axis.

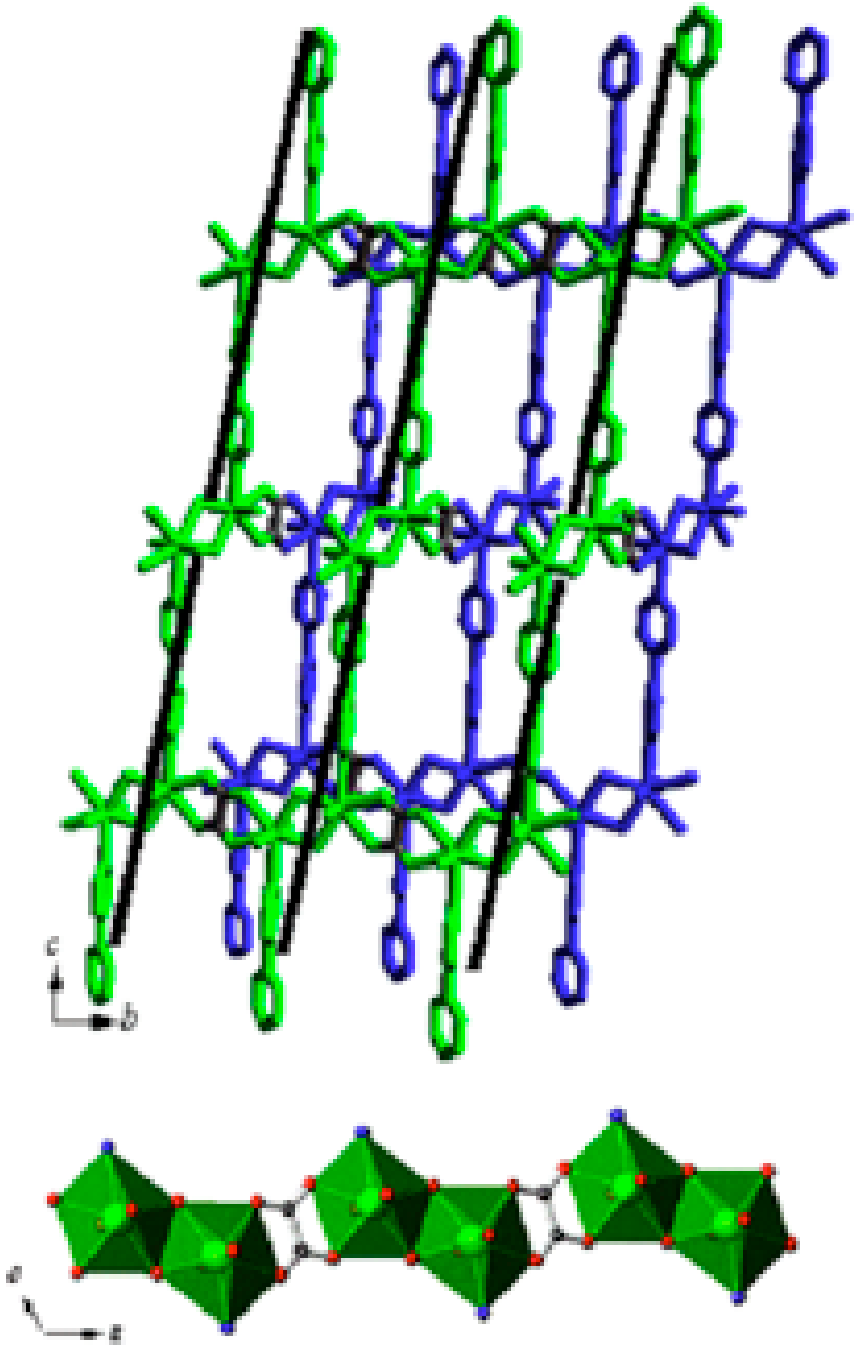

Figure 3.17.2. Open-framework constructed from L-handed single stranded helix $[(UO_2)(OH)(C_5H_4N)]^+$ each other by oxalate anions.

The L-handed single stranded helix basic units in Uoxa-1 are generated from crystallographic unique motif [$(UO_2)(OH)(CO_2)(C_5H_4N)$] by 2-fold screw axes, c-glide planes translations of *C2/c* space group, which is a centrosymmetric space group.

3.17.2 Raman Spectroscopy.

The Raman spectra were collected on a Renishaw inVia Raman microscope spectrometer, as shown in Figure 3.17.3. Raman band at 840 cm^{-1} is attributed to the υ_1 symmetric stretching mode for the $(UO_2)^{2+}$ units. The empirical relation by Bartlett and Cooney ($R = 106.5[\nu_1(UO_2)^{2+}]^{-2/3} + 0.575$ Å) enable us to calculate the U-O bond lengths in uranyl using Raman shift (cm^{-1}) of the uranyl symmetric stretching vibrations [R(Å)/ $\nu_1(cm^{-1})$]: 1.745/840, which is consistence with the single crystal data of 1.771 Å. Bands observed lower than 300 cm^{-1} (mutiple peaks surround 215 cm^{-1}) are assigned to the ν_2 (δ) $(UO_2)^{2+}$ (ν (U-O(N)) and δ (U-O(N))) vibrations. Compared to isolated oxalate molecule, the bands at 1720 cm^{-1} assigned to υ_a (C=O) stretching shift to 1621 cm^{-1} which could be assigned to υ(C-O) due to the delocalization of electron for oxalate anions consistent with single-crystal diffraction data. The intensity peak at 1301 cm^{-1} could be assigned to υ(C-C), υ(C-N), δ(C-H). Compared to calculation data, the Ring breathing peaks at 694, 737 cm^{-1} shift sharply from 674, 765 cm^{-1} because planar conjugated was broken by the lattice energy consistent with the 31^o angle of two pyridine rings in single-crystal structure.

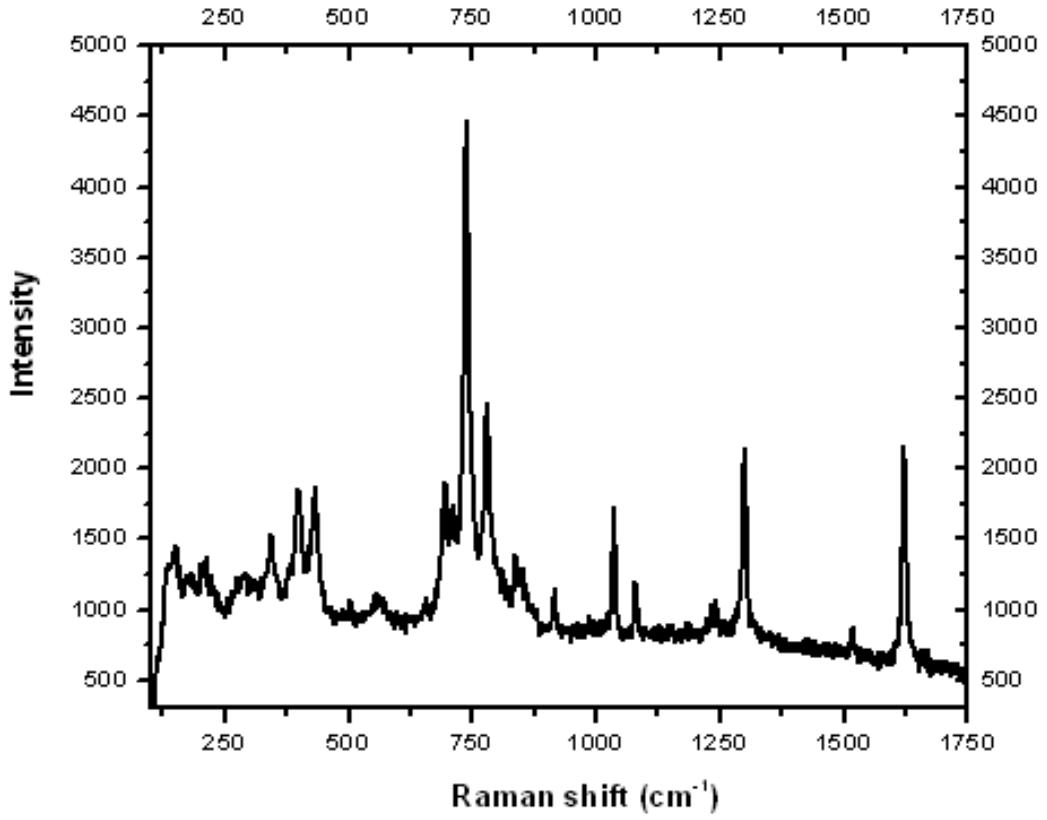

Figure 3.17.3. Raman Spectrum of $(UO_2)(OH)(CO_2)(C_5H_4N)$ (Uoxa-1).

3.17.3 Fluorescence Spectroscopy.

The fluorescence spectra of $[Ag(4,4'\text{-bipy})]_2[(UO_2)_2H_3(PO_4)_3]$, $Ag(2,2'\text{-bipy})(UO_2)(HPO_4)(PO_4)$ and $[Zn(2,2'\text{-bipy})]_2[UO_2(HPO_4)_3]$ compounds exhibited substantial differences in their emission properties because The organic ligand can exhibit the antenna effect, yielding enhanced emission by the uranyl cations (Shown in Chapter 3.5.3, 3.6.3, 3.10.3 respectively). As shown in Figure 3.17.4, Uoxa-1 shows

strong emission band with peaks at 555, and 570 nm, which is consistent with the fine-structure characteristic UO_2^{2+} moiety in aforementioned compounds.

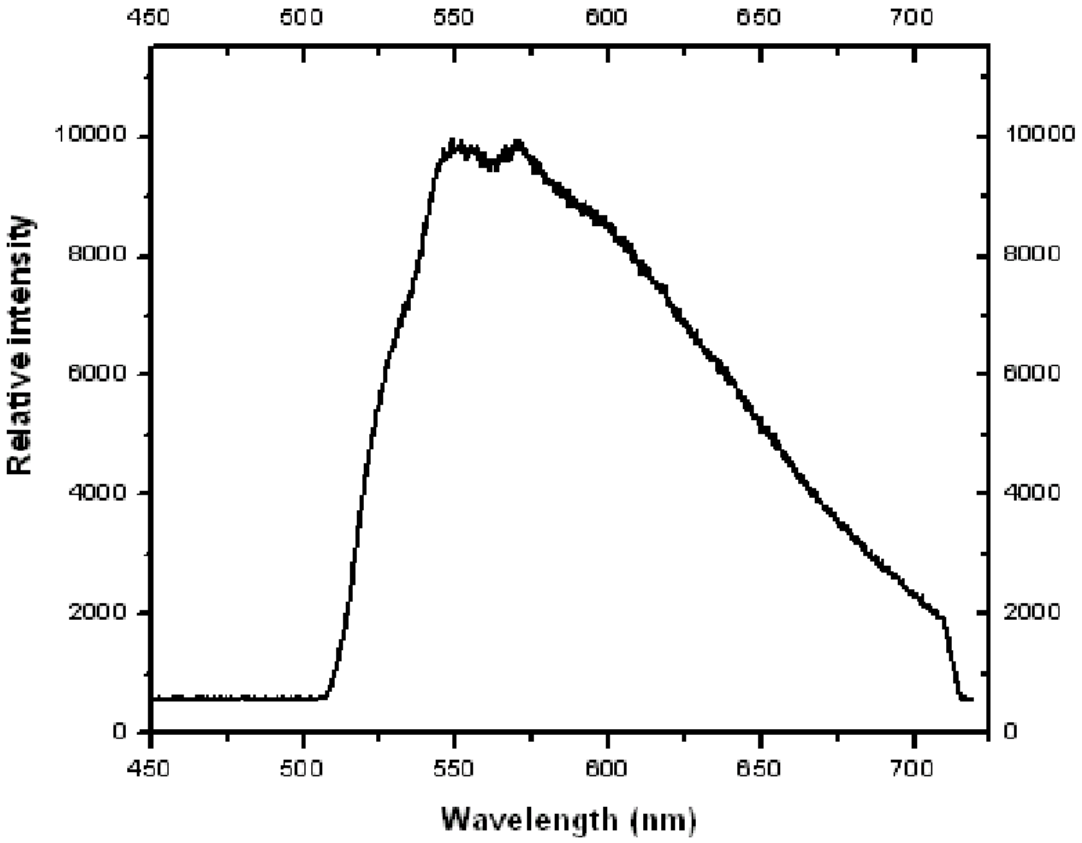

Figure 3.17.4. Fluorescence spectrum of $(UO_2)(OH)(CO_2)(C_5H_4N)$ (Uoxa-1).

3.18 $(UO_2)(OH)_2(C_5H_4N)_2$ (Ubpy-1)

3.18.1 Structural features.

Ubpy-1 possesses an open-framework structure consisting of UNO_6 pentagonal bipyramids that are linked into edge-sharing along equatorial positions into one-dimensional chains. These one-dimensional chains parallel each other occur along the *a* axis. The coordinated 4,4′-bipyridyl ligands are independent from each other with the long distance of 4.08 Å and a small angle of 3.4°, showing the weak aromatic face to face interaction between 4,4′-bipyridyl ligands come from the adjacent chains. Various views of this structure are shown in Figure 3.18.1. The basic building unit of Ubpy-1 is an one-dimensional chains constructed from edge-sharing UNO_6 pentagonal bipyramids through equatorial positions, as shown in Figure 3.18.2. One-dimensional chain constructed from edge-sharing UNO_6 pentagonal bipyramids further linked each other by weak aromatic interaction provided from adjacent chains.

There is only one crystallographic unique uranium center in Ubpy-1. Each of these units contains a nearly linear uranyl, UO_2^{2+}, core. The U≡O distances within the uranyl cations within the range of 1.783(3) to 1.793(3) Å; whereas those U-O(N) bonds in the equatorial plane are considerably longer and within the range of 2.346(3) to 2.608(4) Å consistent with the distance between uranium to diprotonated equatorial O(1) and U-N bond in the equatorial position is 2.608(4) Å consistent with the previous reports (Shown in Chapter 1.4). These bond distances are typical for uranyl polyhedra, and can be used to calculate bond-valence sums of 5.84 for U(1), which is consistent with the expected

oxidation state of U(VI) in UO_2^{2+}. There is only 0.5 crystallographic unique 4,4'-bipyradine molecule in structure of Ubpy-1 due to the general atom positions for $P2_12_12_1$ space group.

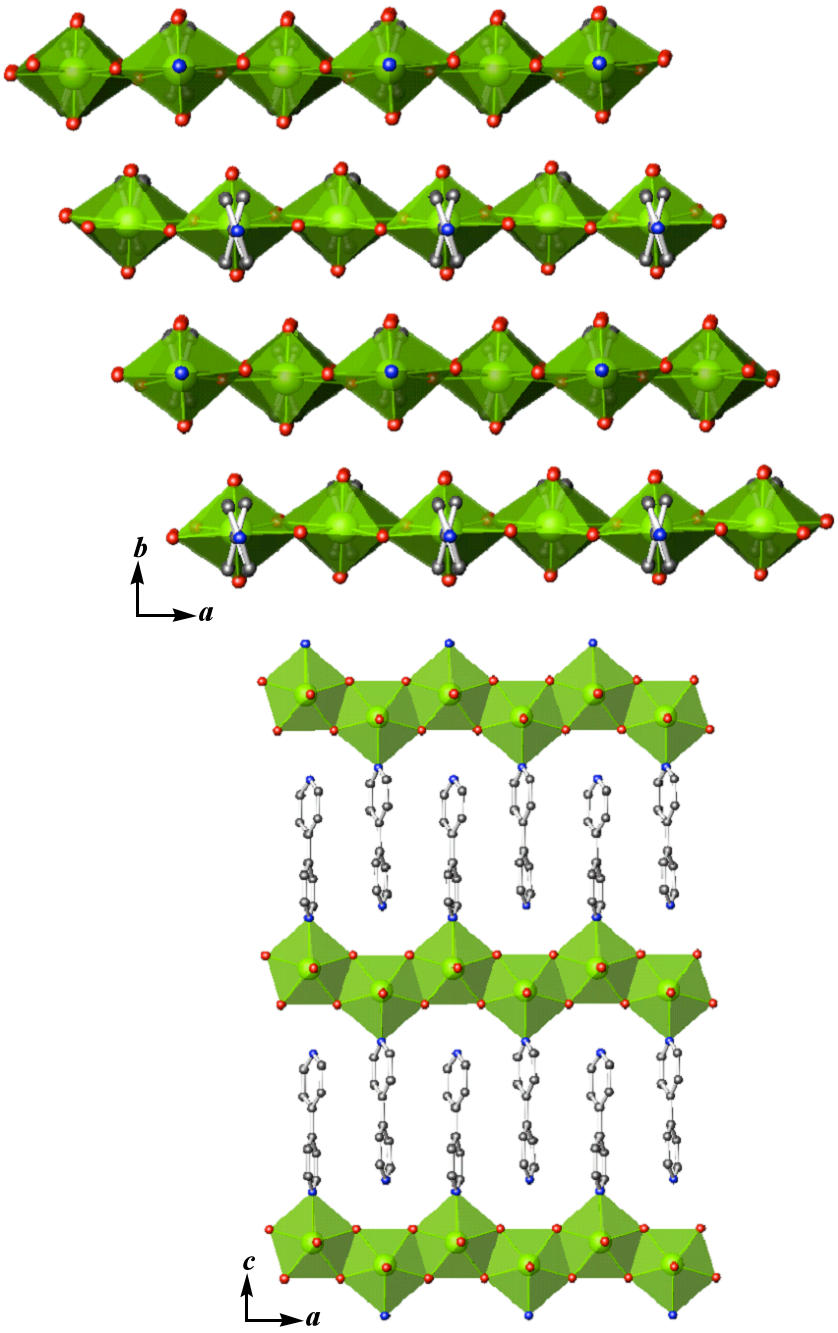

Figure 3.18.1. Two views of $(UO_2)(OH)_2(C_5H_4N)_2$ (Ubpy-1).

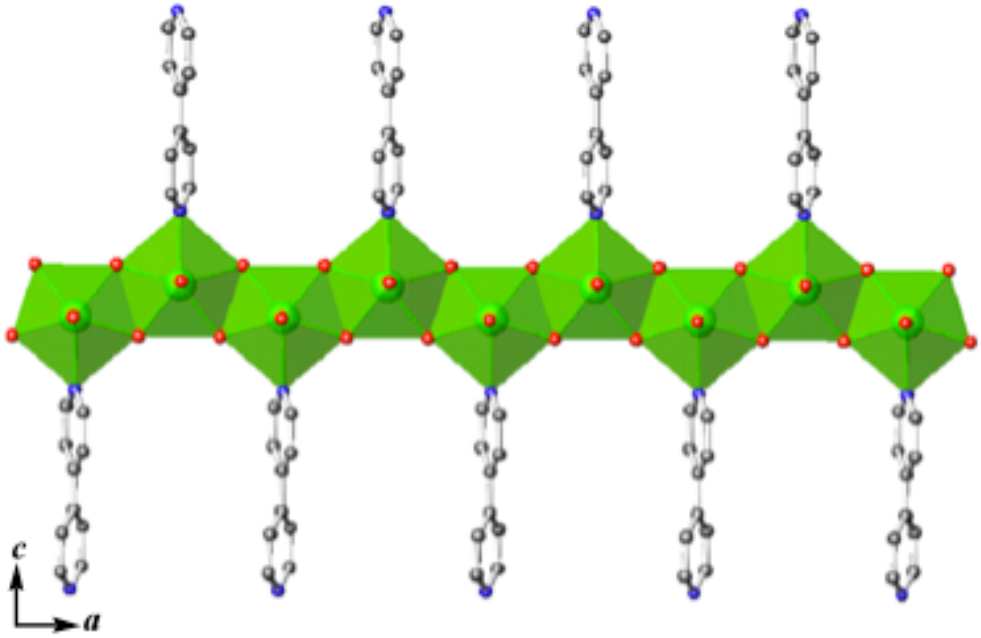

Figure 3.18.2. Structure of the basic unit of $(UO_2)(OH)_2(C_5H_4N)_2$ (Ubpy-1).

The delocalization of electrons for oxalate anions leads to an average bond length for carbon oxygen double bond and single bond with the bond length 1.245 (5) and 1.267 (5) Å, respectively, and 126.7(4)^o bond angle. Each pentagonal bipyramidal uranyl geometry links each other to dimer by edge-sharing through equatorial oxygen atoms. Four oxygen atoms and one nitrogen atom which come from 4,4'-bpy ligand are locate on the equatorial plan of pentagonal bipyramidal uranyl polyhedra.

3.18.2 Fluorescence Spectroscopy.

Fluorescence from uranyl compounds can be identified from the vibronic fine-structure characteristic of the UO_2^{2+} (Shown in Chapter 1.6.2). As shown in Figure 3.18.3, Uoxa-1 shows strong emission band with peak at 551 nm, which is consistent with the fine-structure characteristic UO_2^{2+} moiety in aforementioned compounds.

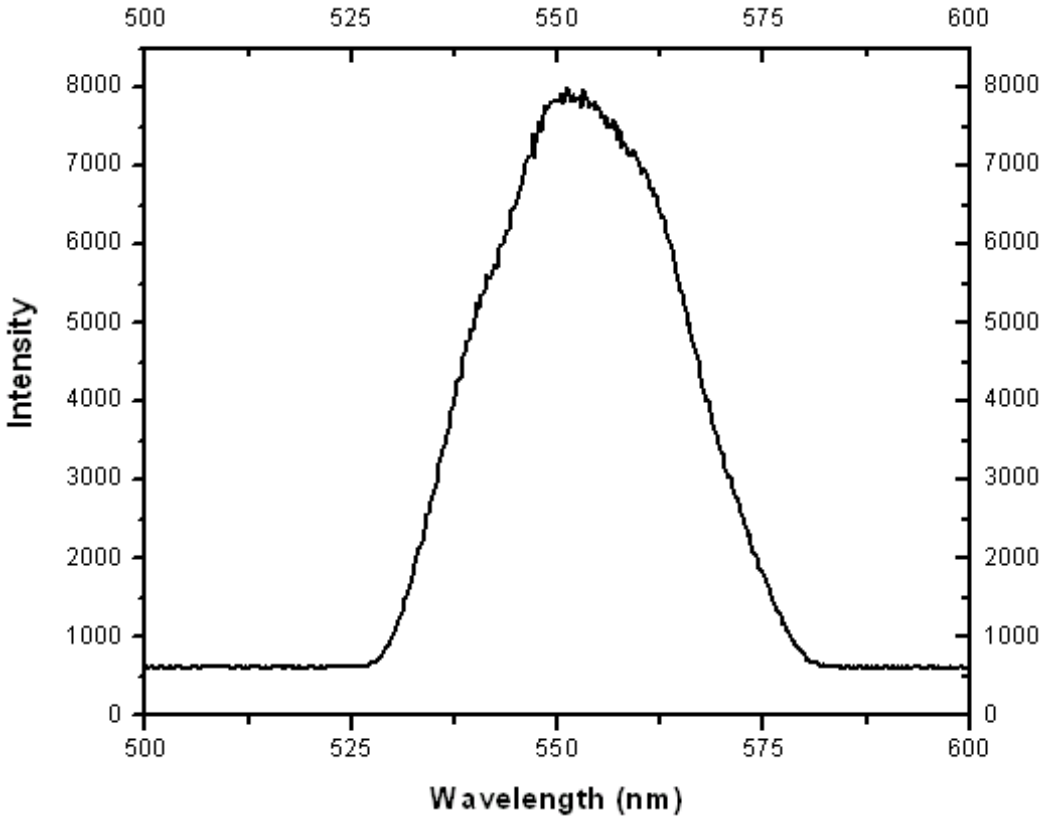

Figure 3.18.3. Fluorescence spectrum of $(UO_2)(OH)_2(C_5H_4N)_2$ (Ubpy-1).

3.19 $(C_6H_5NH)(UO_2)(PO_4)$ (Ubpe-1)

3.19.1 Structural features.

The autunite-type sheet shown in Figure 3.19.1 is formed by uranyl square bipyramids and tetrahedra that are connected by sharing vertices, such that each bipyramid is connected to four tetrahedra, and each tetrahedron is linked to four bipyramids (Shown in Chapter 1.2.2). Charge balance diprotonated organic ligands are filled with the interlayer space, as shown in Figure 3.19.2.

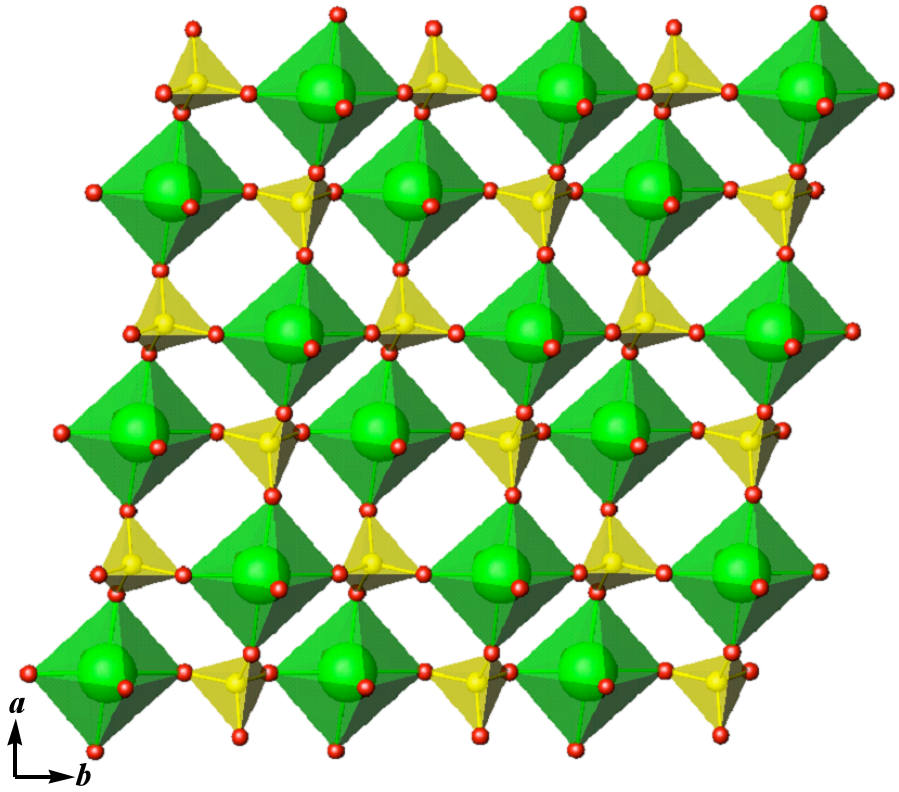

Figure 3.19.1. The autunite-type sheet found in $(C_6H_5NH)(UO_2)(PO_4)$ (Ubpe-1).

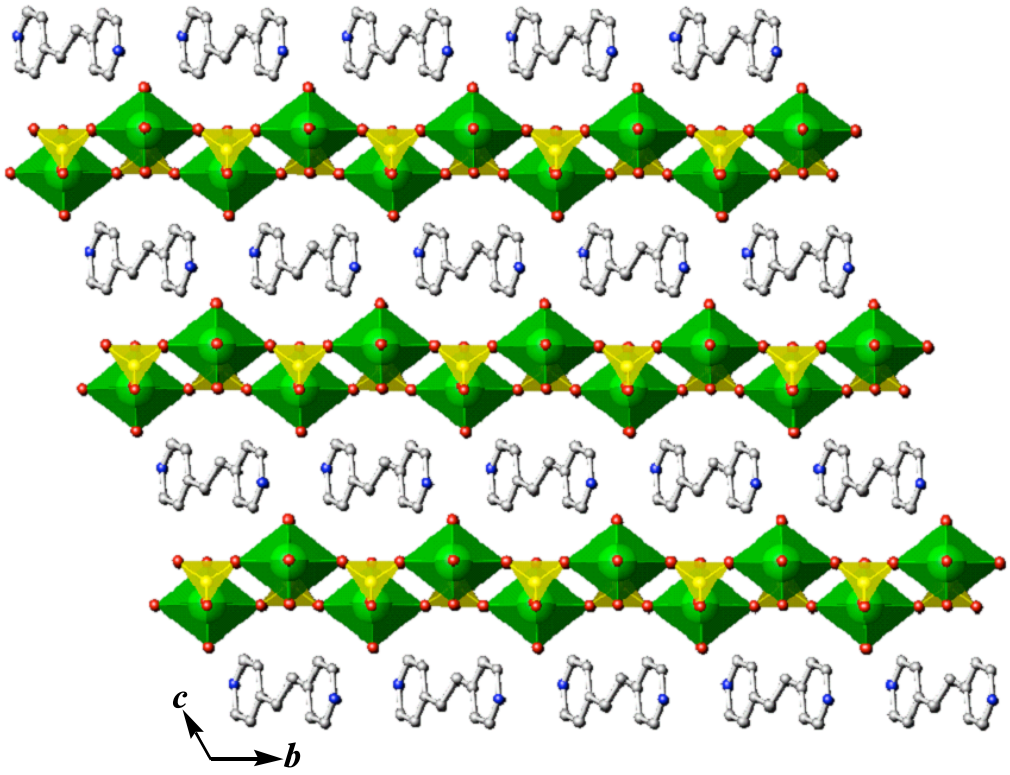

Figure 3.19.2. Packing view of the [*bc*] plane in $(C_6H_5NH)(UO_2)(PO_4)$ (Ubpe-1).

3.20–3.22 $Co(UO_2)_2(AsO_4)_2 \cdot 8H_2O$ (CoUAs-1); $Mn(UO_2)_2(AsO_4)_2 \cdot 8H_2O$ (MnUAs-1); $Cu(UO_2)_2(AsO_4)_2 \cdot 5H_2O$ (CuUAs-1)

3.20-3.22.1 Structural features of $[(UO_2)_2(AsO_4)_2)]^{2-}$.

All three of the compounds investigated contain the well-known corrugated autunite-type sheet as originally described by Beintema (Shown in Chapter 1.2.2), formed by the sharing of vertices between uranyl square bipyramids and arsenate tetrahedral with composition $[(UO_2)_2(AsO_4)_2)]^{2-}$, as shown in Figure 3.20-3.22.1.

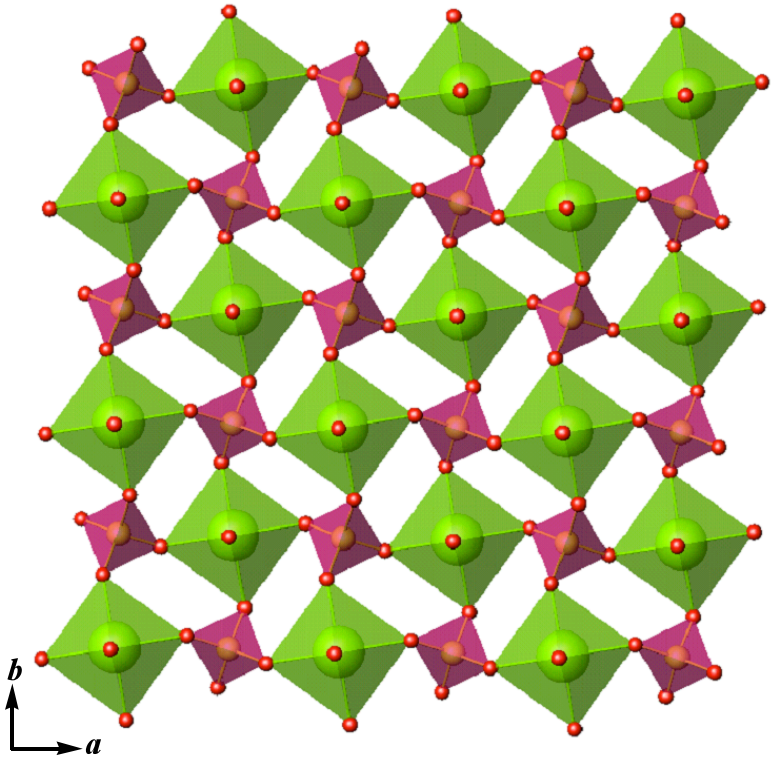

Figure 3.20-3.22.1. The autunite-type sheet found in CoUAs-1; MnUAs-1; CuUAs-1, formed by the sharing of vertices between uranyl square bipyramids and arsenate tetrahedral.

The autunite-type sheet shown in Figure 3.20-3.22.1 is formed by uranyl square bipyramids and tetrahedra that are connected by sharing vertices, such that each bipyramid is connected to four tetrahedral, and each tetrahedron is linked to four bipyramids.

3.20-3.22.2 Structural features of CoUAs-1 and MnUAs-1.

There are two crystallographic independent uranium centers in CoUAs-1 and MnUAs-1 respectively**,** each of these units contains a nearly linear uranyl, UO_2^{2+}, core. The U≡O distances within the uranyl cations within the range of 1.765(4) to 1.808(4) Å; whereas those U-O bonds in the equatorial plane are considerably longer and within the range of 2.242(4) to 2.308(4) Å consistent with the previous reports (Shown in Chapter 1.2, 1.3, 1.4 respectively). These bond distances are typical for uranyl polyhedra, and can be used to calculate bond-valence sums of 6.13, 6.13 and 6.15, 6.12 respectively, which are consistent with the expected oxidation state of U(VI) in UO_2^{2+}. There are also crystallographic independent arsenates centers in CoUAs-1, MnUAs-1 respectively. The As-O bond distances within the range of 1.676(4) to 1.689(4) Å are consistence with the expected tetrahedral AsO_4^{3-}. There is only one crystallographic independent M (M = Co, Mn) center in structure of CoUAs-1 and MnUAs-1, adopting an octahedra coordination geometry. Bond-valence sums of 2.04, 2.08 for Co^{2+} and Mn^{2+} in CoUAs-1, MnUAs-1 respectively, are consistence with the expected value of 2+. The Co (Mn) octahedral located on the both sides of the uranyl arsenates autunite anion sheets act as the surface decoration for two-dimensional structure, as shown in Figure 3.20-3.22.2.

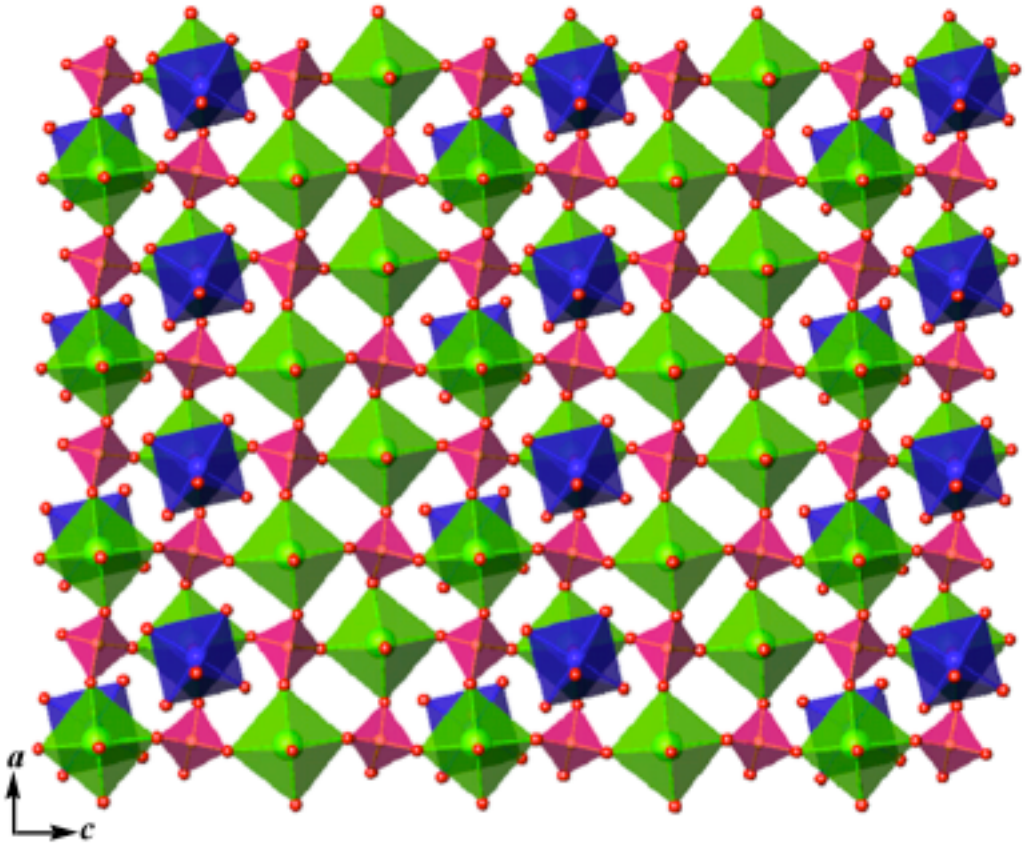

Figure 3.20-3.22.2. Decorated two-dimensional topology of $Co(UO_2)_2(AsO_4)_2{\cdot}8H_2O$ (CoUAs-1); $Mn(UO_2)_2(AsO_4)_2{\cdot}8H_2O$ (MnUAs-1).

The pack mode for CoUAs-1 and MnUAs-1 shows there is strong covalent bonding between layers. Due to the high surface Gibbs energy occurs, the orientation of arsenate is the same and the location of transition metals octahedra appears between the layers alternatively, as shown in Figure 3.20-3.22.3.

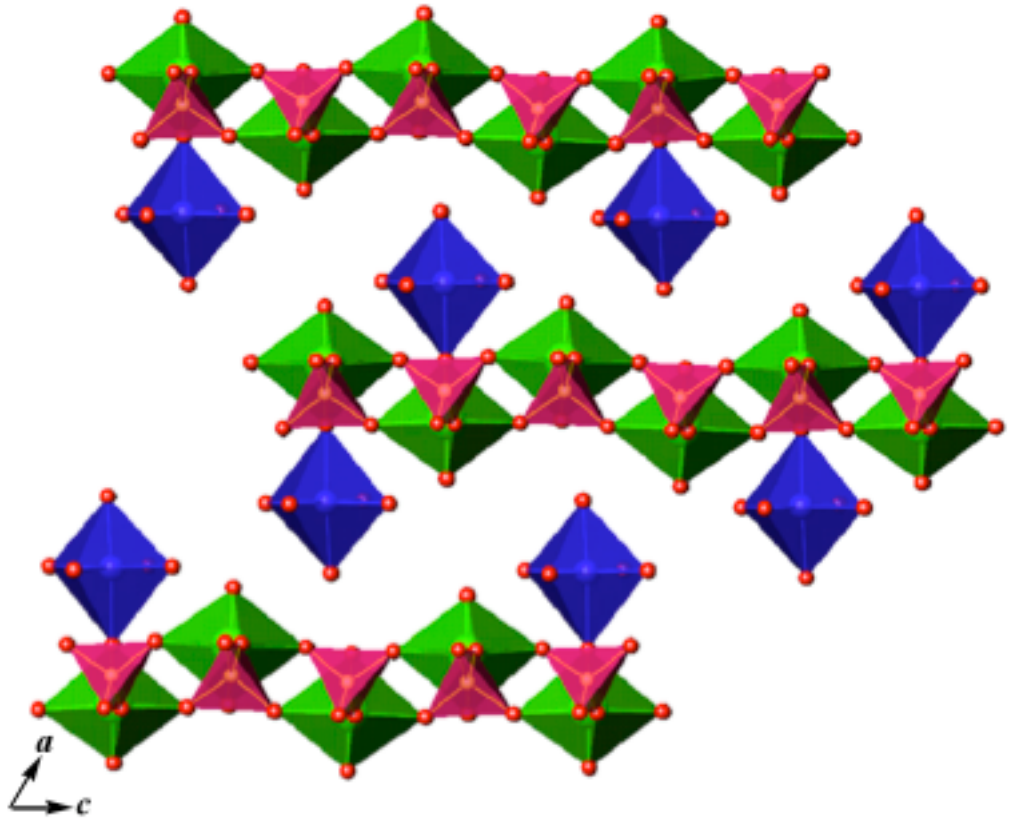

Figure 3.20-3.22.3. Three-dimensional structure of $Co(UO_2)_2(AsO_4)_2{\cdot}8H_2O$ (CoUAs-1); $Mn(UO_2)_2(AsO_4)_2{\cdot}8H_2O$ (MnUAs-1).

3.20-3.22.3 Structural Features of $Cu(UO_2)_2(AsO_4)_2{\cdot}5H_2O$ (CuUAs-1).

The structure of CuUAs-1 is different in that it shares the similar formula with compounds CoUAs-1 and MnUAs-1. But CuUAs-1 shares the common two-dimensional autunite uranyl arsenates plane with the compounds CoUAs-1 and MnUAs-1. There are two aspects which make the CuUAs-1 compound identical. First of all, each Cu^{2+} connected with apical oxygen atoms from each UO_2^{2+} square bipyramid unit, rather than every two UO_2^{2+} square bipyramide units connection. The difference space groups,

which are *P*4/nmm for CuUAs-1 and *P*$\bar{1}$ for CoUAs-1 and MnUAs-1 lead to the different decorated two-dimensional topology of $Cu(UO_2)_2(AsO_4)_2{\cdot}5H_2O$ (CuUAs-1), as shown in Figure 3.20-3.22.4. Secondly, the coordination number for Cu^{2+} is five using square planer geometry different with the octahedral coordination geometry of Co^{2+} and Mn^{2+}, as shown in Figure 3.20-3.22.5. It is important that the packing mode of compound CuUAs-1 shows the very compact 3D structure.

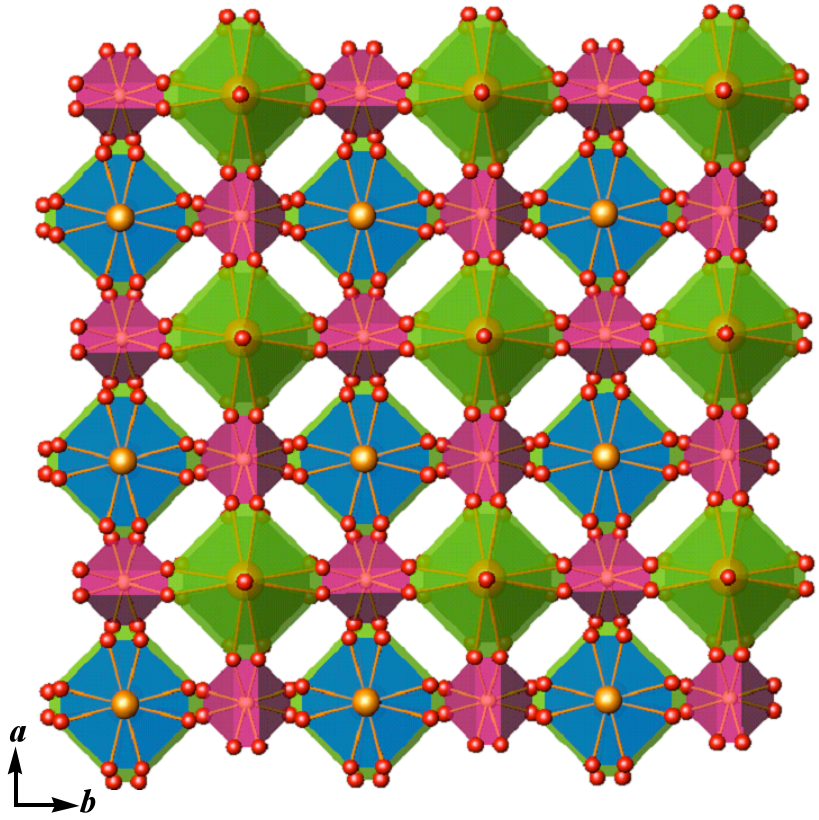

Figure 3.20-3.22.4. Decorated two-dimensional topology of $Cu(UO_2)_2(AsO_4)_2{\cdot}5H_2O$ (CuUAs-1).

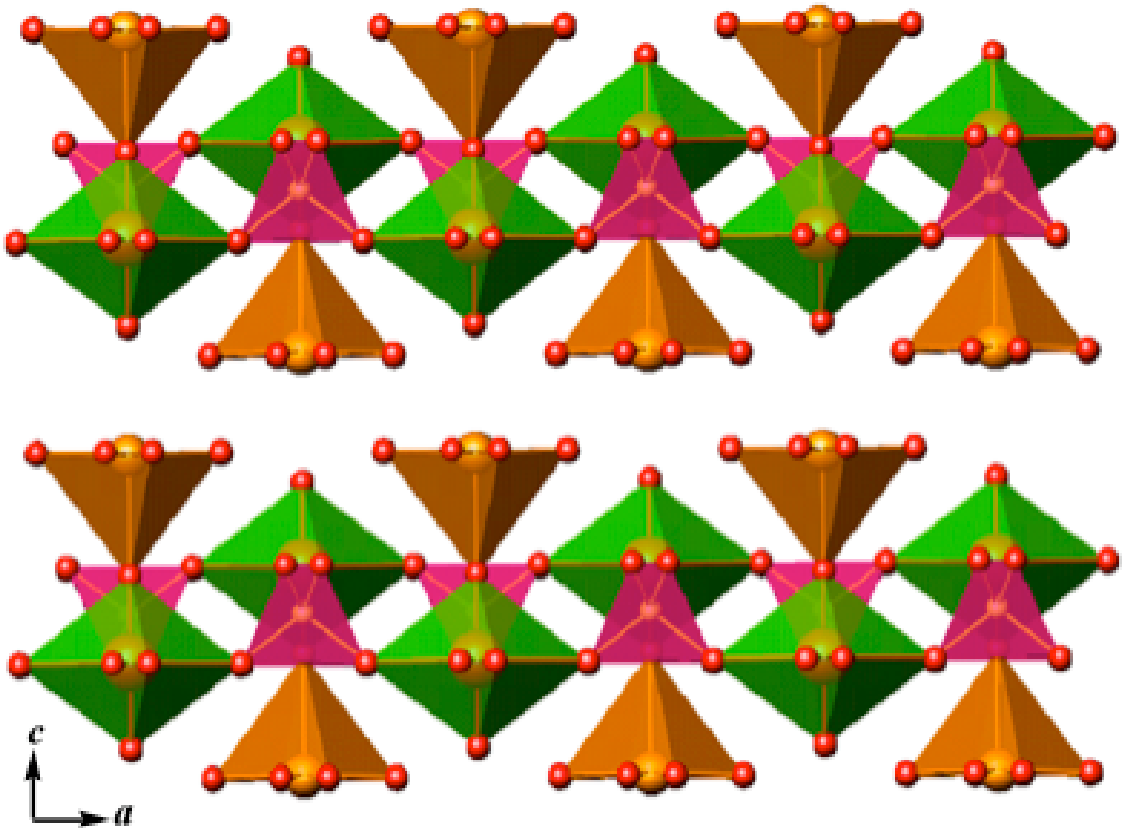

Figure 3.20-3.22.5. Three-dimensional structure of $Cu(UO_2)_2(AsO_4)_2 \cdot 5H_2O$ (CuUAs-1).

Chapter IV: Future Work

4.1 Work Review.

The convergence of greatly enhanced technologies for the detection of X-rays in single-crystal diffraction experiments created a renewed interest in the crystal chemistry of U^{6+}, and resulted in an explosion of new structures containing U^{6+}. During the past decade, known structures of uranyl compounds have more than doubled. These studies have further revealed the tremendous structural elegance, beauty, and complexity of uranyl compounds.

1. We have succeed in synthesizing open-framework $(H_3O)U_2(PO_4)_3(U^{IV}P\text{-}1)$ constructed from low-valence U(IV) hexanuclear center-missing Anderson-type cluster, building unit, by mild hydrothermal synthesis method. Most of Anderson-type polyoxometalates are bimetallic material formulated as $[Mo(W)_6MO_{26}]^{x-}$ (M = Co, Ni, Fe). Unlike the Anderson-type polyoxometalate anions, the structure features make the building unit of $U^{IV}P\text{-}1$ identical. First of all, there are only six U(IV) centers in different planes stabilized by the four capped phosphate tetrahedrons. Secondly, the two-dimensional $[U^{IV}_2O_7]^{6-}$ anion-sheet constructed from one-dimensional chains parallel each other, which are self-assembled from hexanuclear uranium(IV) basic unit, by oxygen-bridging. Thirdly, there are two kinds of phosphate tetrahedron according to their different functions, which act both as surface decoration and bridging group for $[U^{IV}_2O_7]^{6-}$ anion-sheets.

2. The 0D structures containing isolated U^{6+} polyhedra are still limited. Most of compounds based upon finite cluster constructed from uranyl coordinated with anions (CO_3^{2-}, NO_3^-, MoO_4^{2-}, CrO_4^{2-} and SO_4^{2-}) and metal such as alkali, alkali earth and transition atoms acted as the charge balance cations. It is a prospective topic for actinide sciences to find the new topologic structures constructed from limited uranyl polyhedra. Three compounds based upon limited cluster polyhedra have been synthesized by hydrothermal method in my dissertation :

   $[[Ni^{II}(2,2'\text{-bpy})_3](UO_2)(NO_3)(H_2PO_4)_2](NO_3)\cdot 3.25(H_2O)$ (NiUP-1);

   $[(UO_2)(NO_3)_2(H_2O)][C_6H_6N]$ (UNO_3-1);

   $(UO_2)(Ac)_2(2,2'\text{-bpy})$ (UAc-1).

   NiUP-1 based upon finite cluster constructed from uranyl coordinated with mixed anion groups: phosphates and nitrates. UNO_3-1 possesses a finite structure consisting of UO_8 hexagonal bipyramids that are linked into edge-sharing binuclear. The structure of UAc-1, it possesses a finite structure consisting of UO_6N_2 distorted hexagonal bipyramids edge sharing with acetate and 2,2'-bpy ligands, belong to the inorganic-organic hybrid structure.

3. The inorganic hybrid materials containing uranium and transition metals have been reported as the potential application in fluorescent spectroscopy and magnetic properties. It is a still great prospective topic to synthesis inorganic hybrid materials with novel structures under suitable conditions. A series of inorganic hybrid materials containing uranium and transition metals (Co^{2+}, Mn^{2+}, Cu^{2+}, Ni^{2+}, Zn^{2+}) have been reported in my dissertation, such as:

   $Na_2Ag_6[(AgO)_2(UO_2)_3(AsO_4)_4]$ (AgUAs-1); $Ag(UO_2)(AsO_4)$ (AgUAs-2);

$Hg_5O_2(OH)_5][(UO_2)_2(AsO_4)_2]$ (HgUAs-1); $K_2[UO_2Co(PO_4)_2] \cdot H_2O$ (CoUP-1); Transition metal zippeite (Zn^{II}, Co^{II}, Ni^{II}) ZnUS-1; CoUS-1; NiUS-1; NiUS-2; Transition metal autunite (Mn, Co, Cu) CoUAs-1; MnUAs-1; CuUAs-1.

HgUAs-1 possesses a pseudo-layered structure with $^{2}_{\infty}[Hg_5O_2(OH)_5]^{2+}$ and $^{2}_{\infty}[(UO_2)_2(AsO_4)_2]^{2-}$ layers. The latter layers consist of UO_7 pentagonal bipyramids that are linked into edge-sharing dimers that are joined together by AsO_4^{3-} tetrahedra. The former layer formulated as $^{2}_{\infty}[Hg_5O_2(OH)_5]^{2+}$ consists of three crystallographically unique mercury centers. The fluorescent spcectra show that the vibronic transitions for HgUAs-1 are somewhat broad, and five transitions are discernable.

4. Inorganic-organic uranyl carboxylates hybrid materials synthesized by hydrothermal method have been reported recently. It is first reported for inorganic-organic uranyl hybrid materials: $(UO_2)(OH)(CO_2)(C_5H_4N)$ (Uoxa-1); $(UO_2)(OH)_2(C_5H_4N)_2$ (Ubpy-1) to constructed from uranyl and bipyradine ligand. The open-framework structure of Uoxa-1 is constructed from L-handed single stranded helix linked to each other by oxalate anions along *a* axis and *b* axis alternatively. L-handed single stranded helix, called basic units in the structure of Uoxa-1, constructed from pentagonal bipyramid UNO_6 dimers linked each other by 4,4'-bpy bridge along *c* axis. The basic building unit of Ubpy-1 is an one-dimensional chains constructed from edge-sharing UNO_6 pentagonal bipyramids through equatorial positions. 4,4'-bpy ligands act as terminal group in structure of Ubpy-1.

5. The structures of $Ag(2.2'\text{-bpy})(UO_2)_2(HPO_4)(PO_4)$ (AgUP-2); $[Zn(2,2'\text{-bpy})]_2[UO_2(HPO_4)_3]$ (ZnUP-1); $[H_2bipy][(UO_2)_6Zn_2(PO_3OH)_4(PO_4)_4 \cdot H_2O$ (ZnUP-2) belonging to the bimetallic inorganic-organic uranyl transition metals compounds shows more intensity emission bands in fluorescent spectra due to the antenna ligand effect. Chelating nature of 2,2'-bipy ligands in AgUP-2 prevent the formation of a $Ag(bipy)^+$ extended substructure. The structure of ZnUP-1 is complex. The metal centers are found as $[UO_7]$ pentagonal bipyramids, $[ZnN_2O_2]$ highly distorted tetrahedra, and $[ZnN_2O_3]$ distorted trigonal bipyramids.

4.2 Future work.

Unlike U^{6+}, relatively few crystal structures have been analyzed that contain low-valence uranium. Considerable efforts have been made in synthesizing polynuclear low-valence uranium cluster structures, due to their potential applications in nuclear industry and natural environment as well as in the field of magnetic properties and catalysis. First uranium cluster containing an isopolyoxometalate Lindqvist-type core (U_6O_{13}) was reported in 2001. There are rare structures constructed from POM analogues containing low-valence uranium(IV) clusters. The successful attempts show that the variety and scope of such polynuclear compounds should be considerably enlarged by replacing the oxo group O^{2-} with the isoelectronic imido group RN^{2-} , such as the polyimido $U_7(\mu_3\text{-}N)_6(\mu_2\text{-}N)_6$ analogous to the Anderson-type POM structure. Up to date, the most applicable synthesizing methods is that the controlled hydrolysis of trivalent uranium in acetinitrile can indeed lead to the self-assembly of a large dodecanuclear discrete oxide clusters.

4.2.1 Target Compounds.

Although a varied assortment of isopolyoxometalate clusters have been reported since 19th century, all examples have been restricted to the Group 5 and 6 metals with Mo and W comprising the vast majority of derivatives. For potential extension of this chemistry to other elements, uranium may initially seem a logical candidate in three aspects. First, the comparable chemical properties to Mo and W, and has been incorporated into heteropolyanions as either U^{IV} ions or uranyl ions. Second, the structural requirements for cluster formation preclude a traditional aqueous synthesis of a homolepic isopolyoxouranate species. Third, uranium(IV) does in face share with Mo^{VI} and W^{VI} the strong M=O π bonding necessary to terminate a structure, but the dominance of the uranyl unit in aqueous media still permits oligomerization along the equatorial plane, whereas discrete cluster topologies require stable cis-dioxo geometries met by d^0 metals such as Mo^{VI} and W^{VI}.

4.2.2 Results anticipation.

A large number of prospects remain to be explored for these low-valence uranium POM analogue structures.

1. X-ray diffraction technologies reveal the novel single crystal structures.
2. Low-valence uranium materials with multi-nuclear cluster exhibit the magnetic exchange between the metal centers. The exchange parameters could be calculated by DFT or fitted from temperature-dependent magnetic susceptibility data.
3. Electron transfer phenomena between uranium centers and organic ligands can be detected by fluorescence spectroscopy.

Appendices

Appendix I: Crystallographic data for Compound 3.1-3.22

Compound	3.1 $U^{IV}P$-1	3.2 NiUP-1	3.3 UNO_3-1
Formula	$H_3U_2P_3O_{13}$	$C_{30}H_{34.5}N_7NiUP_2O_{19.25}$	$C_6H_8N_3UO_9$
Formula Mass	779.97	1174.55	504
Color and habit	green, tablet	pink, block	yellow, Plate
Space group	*C2/c* (No. 2)	*C2/c*	*P2(1)/n*
a (Å)	17.540(3)	24.1288(12)	13.2939(7)
b (Å)	6.7836(10)	13.4636(7)	5.5881(3)
c (Å)	8.0225(11)	26.0388(13)	15.4891(8)
a (°)	90	90	90
b (°)	102.408(2)	103.4420(10)	93.2420(10)
g (°)	90	90	90
V (Å^3)	932.3(2)	8227.2(7)	1148.81(10)
Z	4	8	4
T (K)	193	193	193(2)
λ (Å)	0.71073	0.71073	0.71073
Maximum 2θ (deg.)	56.66	56.6	56.64
ρ_{calcd} (g cm^{-3})	5.536	1.891	2.903
μ(Mo *K*α) (cm^{-1})	352.92	0.4554	1.4180
R(*F*) for $F_o^2 > 2\sigma(F_o^2)$[a]	0.0466	0.0319	0.0213
$R_w(F_o^2)$ [b]	0.1262	0.0899	0.0557

[a] $R(F) = \sum \left| |F_o| - |F_c| \right| / \sum |F_o|$. [b] $R_w\left(F_o^2\right) = \left[\sum \left[w\left(F_o^2 - F_c^2\right)^2 \right] / \sum wF_o^4 \right]^{1/2}$

Compound	3.4 UAc-1	3.5 AgUP-1	3.6 AgUP-2
Formula	$C_{12}H_{11}N_2UO_4$	$C_{20}H_{19}N_4Ag_2UP_3O_{14}$	$C_{10}H_9N_2AgUP_2O_{12}$
Formula Mass	544.30	1356.10	995.06
Color and habit	yellow. Plate	yellow, block	yellow, needle
Space group	*P2(1)/n*	$P\bar{1}$	$P\bar{1}$
a (Å)	7.8154(4)	7.0342(5)	9.3642(18)
b (Å)	19.0027(10)	10.6929(7)	9.8038(19)
c (Å)	10.5875(6)	11.1301(8)	10.488(2)
a (°)	90	93.682(1	100.350(3)
b (°)	95.9330(10)	106.908(1)	98.449(3)
g (°)	90	107.031(1)	93.135(3)
V (Å^3)	1563.97(15)	755.57(9)	933.6(3)
Z	4	1	2
T (K)	193(2)	193	193
λ (Å)	0.71073	0.71073	0.71073
Maximum 2θ (deg)	56.64	56.6	56.94
ρ_{calcd} (g cm^{-3})	2.312	2.974	3.536
μ(Mo *K*α) (cm^{-1})	1.0410	122.01	185.80
R(*F*) for $F_o^2 > 2\sigma(F_o^2)$[a]	0.0315	0.0382	0.0291
$R_w(F_o^2)$ [b]	0.0757	0.0967	0.0871

[a] $R(F) = \sum \left| |F_o| - |F_c| \right| / \sum |F_o|$. [b] $R_w\left(F_o^2\right) = \left[\sum \left[w\left(F_o^2 - F_c^2\right)^2 \right] / \sum wF_o^4 \right]^{1/2}$

Compound	3.7 AgUAs-1	3.8 AgUAs-2	3.9 HgUAs-1
Formula	$Na_2Ag_8U_3As_4O_{24}$	$AgUAsO_6$	$H_7Hg_5U_2As_2O_{18}$
Formula Mass	2306.71	516.82	1918
Color and habit	green, plate	yellow, plate	yellow, block
Space group	*Pmna*	*P4/ncc*	$P\bar{1}$
a (Å)	19.9048(11)	7.0929(4)	6.8229(5)
b (Å)	5.4738(3)	7.0929(4)	6.8795(5)
c (Å)	11.3704(7)	17.0159(15)	9.5959(6)
a (°)	90	90	109.4560(10)
b (°)	90	90	104.8340(10)
g (°)	90	90	93.8670(10)
V (Å^3)	1238.86(12)	856.06(10)	404.74(5)
Z	2	4	1
T (K)	193	193	193
λ (Å)	0.71073	0.71073	0.71073
Maximum 2θ (deg)	56.62	56.54	56.6
ρ_{calcd} (g cm^{-3})	6.184	4.010	2.36
μ(Mo *K*α) (cm^{-1})	311.37	249.87	713.12
R(*F*) for $F_o^2 > 2\sigma(F_o^2)$[a]	0.0474	0.0516	0.0555
$R_w(F_o^2)$ [b]	0.1494	0.1557	0.1349

[a] $R(F) = \sum \left| |F_o| - |F_c| \right| / \sum |F_o|$. [b] $R_w\left(F_o^2\right) = \left[\sum \left[w\left(F_o^2 - F_c^2\right)^2 \right] / \sum wF_o^4 \right]^{1/2}$

Compound	3.10 ZnUP-1	3.11 ZnUP-2	3.12 CoUP-1
Formula	$H_{19}Zn_2UP_3O_{14}$	$C_{10}H_{16}N_2Zn_2U_6P_8O_{41}$	$H_2K_2CoUP_2O_{11}$
Formula Mass	1001.07	2848	615.10
Color and habit	yellow, plate	yellow, tablet	blue block
Space group	$P\bar{1}$	$P\bar{1}$	$P2_1/c$
a (Å)	10.9496(8)	10.980(2)	8.1051(8)
b (Å)	11.4702(8)	13.029(3)	17.0316(18)
c (Å)	12.9805(9)	13.599(3)	7.8255(8)
a (°)	67.222(1)	62.312(3)	90
b (°)	86.708(1)	70.921(3)	105.574(2)
g (°)	66.378(1)	72.954(3)	90
V (Å^3)	933.6(3)	1604.7(5)	1040.59(18)
Z	2	1	4
T (K)	193	193	193
λ (Å)	0.71073	0.71073	0.71073
Maximum 2θ (deg.)	56.72	56.6	56.66
$\rho_{calcd.}$ (g cm^{-3})	2.423	2.938	3.913
μ(Mo *K*α) (cm^{-1})	78.99	161.14	182.92
R(*F*) for $F_o^2 > 2\sigma(F_o^2)$[a]	0.0317	0.0581	0.0250
$R_w(F_o^2)$ [b]	0.0751	0.1738	0.0650

[a] $R(F) = \sum \left| |F_o| - |F_c| \right| / \sum |F_o|$. [b] $R_w\left(F_o^2\right) = \left[\sum \left[w\left(F_o^2 - F_c^2\right)^2 \right] / \sum wF_o^4 \right]^{1/2}$

Compound	3.13 ZnUS-1	3.14 CoUS-1	3.15 NiUS-1
Formula	$H_{30}ZnU_8S_4O_{52}$	$H_{10}CoU_8S_4O_{44}$	$H_{26}Ni_3U_8S_4O_{52}$
Formula Mass	2959.85	2875.31	3002.34
Color and habit	yellow, needle	Burgundy, Block	purple, Prism
Space group	*Cm*	*Cm*	C2/m
a (Å)	8.6538(5)	8.6514(17)	8.6800(8)
b (Å)	14.1887(9)	14.134(3)	14.1579(12)
c (Å)	8.8537(6)	8.8151(17)	8.8288(8)
a (°)	90	90	90
b (°)	104.1480(10)	104.352(3)	104.362(2)
g (°)	90	90	90
V (Å^3)	1054.14(12)	1044.2(3)	1051.07(16)
Z	8	2	2
T (K)	193	193	193(2)
λ (Å)	0.71073	0.71073	0.71073
Maximum 2θ (deg.)	56.6	56.72	56.62
ρ_{calcd} (g cm^{-3})	4.429	4.785	4.854
μ(Mo *K*α) (cm^{-1})	354.60	323.85	323.47
R(*F*) for $F_o^2 > 2\sigma(F_o^2)$[a]	0.0300	0.0464	0.0483
$R_w(F_o^2)$ [b]	0.0762	0.1074	0.1223

[a] $R(F) = \sum \left| |F_o| - |F_c| \right| / \sum |F_o|$. [b] $R_w\left(F_o^2\right) = \left[\sum \left[w\left(F_o^2 - F_c^2\right)^2 \right] / \sum wF_o^4 \right]^{1/2}$

Compound	3.16 NiUS-2	3.17 Uoxa-1	3.18 Ubpy-1
Formula	$H_{18}NiU_4S_2O_{28}$	$C_6H_5NUO_5$	$C_5H_{10}N_2UO_4$
Formula Mass	1508.82	409	458.21
Color and habit	yellow, block	yellow, Block	yellow, block
Space group	C2/m	C2/c	$P2_12_12_1$
a (Å)	8.6480(8)	15.5710(10)	7.4065(4)
b (Å)	14.1375(14)	11.4461(10)	10.8441(6)
c (Å)	8.8423(9)	11.9337(11)	14.0907(8)
a (°)	90	90	90
b (°)	103.973(2)	129.970(2)	90
g (°)	90	90	90
V (Å^3)	1049.08(18)	1630.0(2)	1131.72(11)
Z	2	8	4
T (K)	193(2)	193	193(2)
λ (Å)	0.71073	0.71073	0.71073
Maximum 2θ (deg.)	56.66	28.28	56.60
ρ_{calcd} (g cm^{-3})	4.821	3.326	2.689
μ(Mo *K*α) (cm^{-1})	319.79	199.03	143.46
R(*F*) for $F_o^2 > 2\sigma(F_o^2)$[a]	0.0282	0.0226	0.0223
$R_w(F_o^2)$ [b]	0.0751	0.0536	0.0501

[a] $R(F) = \sum \left| |F_o| - |F_c| \right| / \sum |F_o|$. [b] $R_w\left(F_o^2\right) = \left[\sum \left[w\left(F_o^2 - F_c^2\right)^2 \right] / \sum wF_o^4 \right]^{1/2}$

Compound	3.19 Ubpe-1	3.20 CoUAs-1	3.21 MnUAs-1
Formula	$C_6H_6NUPO_6$	$H_{16}CoU_2As_2O_{20}$	$H_{16}MnU_2As_2O_{20}$
Formula Mass	457.11	1020.96	1016.84
Color and habit	yellow, block	pink, plate	yellow, plate
Space group	$P\bar{1}$	$P\bar{1}$	$P\bar{1}$
a (Å)	6.9442(4)	7.2023(4)	7.2235(4)
b (Å)	7.0243(4)	9.7011(5)	9.8201(5)
c (Å)	10.0830(6)	13.2381(7)	13.3068(7)
a (°)	107.0540(10)	75.6120(10)	75.1970(10)
b (°)	105.0660(10)	84.1880(10)	84.2290(10)
g (°)	92.9300(10)	81.6840(10)	81.9440(10)
V (Å^3)	449.70(5)	884.46(8)	901.52(8)
Z	2	2	2
T (K)	193(2)	193(2)	193(2)
λ (Å)	0.71073	0.71073	0.71073
Maximum 2θ (deg.)	56.58	56.56	56.54
ρ_{calcd} (g cm^{-3})	3.368	3.834	3.687
μ(Mo *K*α) (cm^{-1})	182.33	229.99	223.42
$R(F)$ for $F_o^2 > 2\sigma(F_o^2)$[a]	0.0201	0.0320	0.0299
$R_w(F_o^2)$[b]	0.0511	0.0796	0.0685

[a] $R(F) = \sum \left| |F_o| - |F_c| \right| / \sum |F_o|$. [b] $R_w\left(F_o^2\right) = \left[\sum \left[w\left(F_o^2 - F_c^2\right)^2 \right] / \sum wF_o^4 \right]^{1/2}$

Compound	3.22 CuUAs-1
Formula	$H_{10}CuU_2As_2O_{17}$
Formula Mass	971.44
Color and habit	green, plate
Space group	*P4/nmm*
a (Å)	7.1136(5)
b (Å)	7.1136(5)
c (Å)	8.7059(9)
a (°)	90
b (°)	90
g (°)	90
V (Å^3)	440.55(6)
Z	4
T (K)	193(2)
λ (Å)	0.71073
Maximum 2θ (deg.)	56.50
ρ_{calcd} (g cm^{-3})	3.624
μ(Mo *K*α) (cm^{-1})	233.28
R(*F*) for $F_o^2 > 2\sigma(F_o^2)$[a]	0.0433
$R_w(F_o^2)$ [b]	0.0954

[a] $R(F) = \sum \left| |F_o| - |F_c| \right| / \sum |F_o|$. [b] $R_w\left(F_o^2\right) = \left[\sum \left[w\left(F_o^2 - F_c^2\right)^2 \right] / \sum wF_o^4 \right]^{1/2}$

Appendix II: Selected Bond Distances (Å) and Angles (^{o}) Compound 3.1-3.22.

Compound 3.1: $(H_3O)U_2(PO_4)_3$ (U^{IV}P-1)

	Distances (Å)		
U(1)-O(1)	2.415(8)	P(1)-O(1)#6	1.549(8)
U(1)-O(1)#2	2.495(8)	P(1)-O(4)#2	1.519(9)
U(1)-O(2)	2.470(8)	P(1)-O(5)#5	1.506(8)
U(1)-O(2)#3	2.610(8)	P(1)-O(6)	1.525(7)
U(1)-O(3)	2.378(8)	P(2)-O(2)#3	1.520(8)
U(1)-O(4)	2.459(8)	P(2)-O(2)#8	1.520(8)
U(1)-O(4)#1	2.454(8)	P(2)-O(3)	1.531(8)
U(1)-O(5)	2.304(8)	P(2)-O(3)#9	1.531(8)
U(1)-O(6)	2.318(6)		

Symmetry transformations used to generate equivalent atoms: #1 x,-y-1,z-1/2 #2 -x+1/2,-y-1/2,-z+2 #3 x,-y-1,z+1/2 #4 -x+1/2,y-1/2,-z+3/2 #5 x,y+1,z #6 x,-y,z-1/2 #7 -x+1/2,y+1/2,-z+3/2 #8 -x+1,-y-1,-z+2 #9 -x+1,y,-z+5/2 #10 x,-y,z+1/2 #11 -x,y,-z+3/2 #12 x,y-1,z

Compound 3.2: $[[Ni(2,2'\text{-bpy})_3](UO_2)(NO_3)(H_2PO_4)_2](NO_3)\cdot 3.25(H_2O)$ (NiUP-1)

		Distances (Å)	
U(1)-O(9)	1.769(3)	Ni(1)-N(5)	2.092(3)
U(1)-O(10)	1.774(3)	Ni(1)-N(3)	2.092(3)
U(1)-O(8)	2.283(3)	Ni(1)-N(7)	2.093(3)
U(1)-O(4)	2.288(2)	O(1)-P(1)	1.504(3)
U(1)-O(5)#1	2.290(3)	O(2)-P(1)	1.567(3)
U(1)-O(12)	2.533(3)	O(3)-P(1)	1.569(3)
U(1)-O(11)	2.536(3)	O(4)-P(1)	1.504(3)
U(1)-N(2)	2.961(4)	O(5)-P(2)	1.504(3)
Ni(1)-N(8)	2.079(3)	O(6)-P(2)	1.556(3)
Ni(1)-N(6)	2.080(3)	O(7)-P(2)	1.559(3)
Ni(1)-N(4)	2.092(3)	O(8)-P(2)	1.506(3)
		Angles (°)	
P(1)-O(4)-U(1)	143.97(16)	P(2)-O(5)-U(1)#1	149.82(17)
P(2)-O(8)-U(1)	141.30(17)	N(2)-O(11)-U(1)	96.6(2)
N(2)-O(12)-U(1)	96.9(2)		

Symmetry transformations used to generate equivalent atoms: #1 -x+1/2,-y+1/2,-z

Compound 3.3: $[(UO_2)(NO_3)_2(H_2O)][C_6H_6N]$ (UNO_3-1)

		Distances (Å)	
U(1)-O(8)	1.767(2)	U(1)-O(2)	2.509(3)
U(1)-O(7)	1.771(2)	U(1)-O(5)	2.523(3)
U(1)-O(9)	2.362(3)	U(1)-O(3)	2.543(3)
U(1)-O(9)#1	2.391(3)	U(1)-N(1)	2.957(3)
U(1)-O(6)	2.496(3)	U(1)-N(2)	2.978(3)
		Angles (°)	
U(1)-O(9)-U(1)#1	112.10(10)	O(5)-U(1)-O(3)	60.42(9)
N(1)-U(1)-N(2)	110.71(8)	O(9)-U(1)-O(9)#1	67.90(10)

Symmetry transformations used to generate equivalent atoms: #1 -x+2,-y+1,-z+2 #2 -x+2,-y,-z+1

Compound 3.4: $(UO_2)(Ac)_2(2,2'\text{-bpy})$ (UAc-1)

		Distances (Å)	
U(1)-O(1)	1.776(4)	U(1)-O(6)	2.456(4)
U(1)-O(2)	1.772(4)	U(1)-N(1)	2.639(4)
U(1)-O(3)	2.435(4)	U(1)-N(2)	2.620(4)
U(1)-O(4)	2.471(4)	U(1)-C(12)	2.833(5)
U(1)-O(5)	2.443(4)	U(1)-C(14)	2.838(5)
		Angles (°)	
O(6)-U(1)-N(2)	67.41(12)	O(4)-U(1)-N(1)	69.88(12)
O(1)-U(1)-N(2)	77.19(15)	N(2)-U(1)-N(1)	60.87(13)
O(2)-U(1)-O(1)	179.36(16)		

Compound 3.5: $[Ag(4,4'\text{-bpy})]_2[(UO_2)H_3(PO_4)_3]$ (AgUP-1)

		Distances (Å)	
U(1)-O(3)	2.313(6)	P(1)-O(1)	1.541(14)
U(1)-O(5)#2	2.279(5)	P(1)-O(2)	1.571(12)
U(1)-O(6)#1	2.261(5)	P(1)-O(3)	1.656(7)
U(1)-O(7)	2.265(5)	P(1)-O(3)#3	1.586(7)
U(1)-O(8)	1.788(5)	P(2)-O(4)	1.551(6)
U(1)-O(9)	1.791(5)	P(2)-O(5)	1.527(5)
Ag(1)-N(1)	2.100(6)	P(2)-O(6)	1.534(5)
Ag(1)-N(2)	2.123(6)	P(2)-O(7)	1.535(6)
		Angles (°)	
O(8)-U(1)-O(9)	179.3(2)	N(1)-Ag(1)-N(2)	176.3(2)

Symmetry transformations used to generate equivalent atoms: #1 $-x + 1, -y, -z$; #2 $x - 1, y, z$; #3 $-x, -y, -z - 1$.

Compound 3.6: $Ag(2,2'\text{-bipy})(UO_2)_2(HPO_4)(PO_4)$ (AgUP-2)

		Distances (Å)	
U(1)-O(2)#1	2.282(4)	U(2)-O(11)	1.762(5)
U(1)-O(4)	2.369(4)	U(2)-O(12)	1.737(5)
U(1)-O(5)	2.497(4)	Ag(1)-N(1)	2.100(6)
U(1)-O(5)#2	2.388(4)	Ag(1)-N(2)	2.123(6)
U(1)-O(8)	2.555(4)	P(1)-O(1)	1.518(5)
U(1)-O(9)	1.766(5)	P(1)-O(2)	1.500(4)
U(1)-O(10)	1.753(5)	P(1)-O(3)	1.547(4)
U(2)-O(3)	2.454(4)	P(1)-O(4)	1.549(4)
U(2)-O(3)#4	2.373(4)	P(2)-O(5)	1.537(4)
U(2)-O(4)	2.526(4)	P(2)-O(6)	1.561(5)
U(2)-O(7)#3	2.311(4)	P(2)-O(7)	1.492(4)
U(2)-O(8)	2.385(4)	P(2)-O(8)	1.519(4)
		Angles (°)	
O(1)-Ag(1)-N(2)	148.2(2)	O(1)-Ag(1)-N(1)	137.2(2)
N(2)-Ag(1)-N(1)	73.1(2)		

Symmetry transformations used to generate equivalent atoms: #1 $-x + 2, -y + 1, -z + 1$; #2 $-x + 1, -y + 1, -z + 1$; #3 $-x + 1, -y, -z + 1$; #4 $-x + 2, -y, -z + 1$.

Compound 3.7: $Na_2Ag_6[(AgO)_2(UO_2)_3(AsO_4)_4]$ (AgUAs-1)

		Distances (Å)	
U(1)-O(4)#1	1.792(12)	U(2)-O(2)#6	2.353(9)
U(1)-O(4)	1.792(12)	As(3)-O(7)	1.677(8)
U(1)-O(1)#2	2.273(8)	As(3)-O(3)	1.684(9)
U(1)-O(1)#3	2.273(8)	As(3)-O(2)	1.685(9)
U(1)-O(1)	2.273(8)	As(3)-O(1)	1.690(9)
U(1)-O(1)#1	2.273(8)	Ag(3)-O(7)	2.440(8)
U(2)-O(6)#4	1.775(8)	Ag(3)-O(7)#6	2.440(8)
U(2)-O(6)	1.775(8)	Ag(1)-O(7)	2.376(8)
U(2)-O(3)#4	2.352(9)	Ag(1)-O(7)#9	2.376(8)
U(2)-O(3)	2.352(9)	O(7)-Ag(2)	2.274(8)
U(2)-O(2)#5	2.353(9)	O(3)-Ag(2)#8	2.561(10)
		Angles (°)	
O(7)-Ag(3)-O(7)#6	119.8(4)	As(3)-O(7)-Ag(3)	119.8(4)
O(7)-Ag(1)-O(7)#9	176.4(4)	Ag(2)-O(7)-Ag(3)	94.0(3)
As(3)-O(7)-Ag(2)	117.1(4)	Ag(1)-O(7)-Ag(3)	92.8(3)
As(3)-O(7)-Ag(1)	122.1(4)	As(3)-O(3)-U(2)	133.2(5)
Ag(2)-O(7)-Ag(1)	105.3(3)	As(3)-O(3)-Ag(2)#8	104.4(4)

Symmetry transformations used to generate equivalent atoms: #1 -x+1,-y+2,-z+1 #2 -x+1,y,z #3 x,-y+2,-z+1 #4 x,-y+2,-z+2 #5 -x+1/2,-y+2,z+1/2 #6 -x+1/2,y,-z+3/2 #7 -x+1,-y+1,-z+2 #8 x,y+1,z #9 x,-y+1,-z+1 #10 -x+1/2,-y+2,z-1/2 #11 x,y-1,z #12 -x+1,-y,-z+2 #13 x,-y+1,-z+2

Compound 3.8: $Ag(UO_2)(AsO_4)$ (AgUAs-2)

Distances (Å)			
U(1)-O(4)	1.78(2)	As(1)-O(1)#6	1.680(13)
U(1)-O(3)	1.78(3)	As(1)-O(1)#3	1.680(13)
U(1)-O(1)#1	2.320(12)	As(1)-O(1)	1.680(13)
U(1)-O(1)#2	2.320(12)	Ag(1)-Ag(1)#7	2.511(9)
U(1)-O(1)#3	2.320(12)	Ag(1)-Ag(1)#8	2.511(9)
U(1)-O(1)#4	2.320(12)	Ag(1)-Ag(1)#9	2.923(14)
As(1)-O(1)#5	1.680(13)		
Angles (°)			
Ag(1)#7-Ag(1)-Ag(1)#8	90.000(2)	Ag(1)#8-Ag(1)-Ag(1)#9	102.53(12)
Ag(1)#7-Ag(1)-Ag(1)#9	124.5(3)		

Symmetry transformations used to generate equivalent atoms: #1 x-1/2,y-1/2,-z #2 -y+1,x-1/2,-z #3 y-1/2,-x+1,-z #4 -x+1,-y+1,-z #5 -y+1,x+1/2,-z #6 -x+1/2,-y+3/2,z #7 y-1,-x+1/2,z #8 -y+1/2,x+1,z #9 -y,-x,-z+1/2

Compound 3.9: $[Hg_5O_2(OH)_5][(UO_2)_2(AsO_4)_2]$ (HgUAs-1)

Distances (Å)			
U(1)-O(9)	1.804(14)	Hg(2)-O(6)	2.074(13)
U(1)-O(8)	1.835(15)	Hg(3)-O(4)	2.130(12)
U(1)-O(7)#2	2.270(13)	Hg(3)-O(6)	2.147(13)
U(1)-O(7)	2.303(14)	Hg(3)-O(5)	2.468(13)
U(1)-O(1)#3	2.315(13)	Hg(3)-O(3)#6	2.492(12)
U(1)-O(3)#1	2.358(13)	Hg(3)-O(4)#4	2.595(12)
U(1)-O(2)#4	2.371(12)	As(1)-O(1)	1.661(12)
Hg(1)-O(5)	2.018(14)	As(1)-O(2)	1.685(12)
Hg(1)-O(5)#1	2.018(14)	As(1)-O(3)	1.692(12)
Hg(2)-O(7)	2.015(13)	As(1)-O(4)	1.718(13)
Long distances of Hg-O bonding (Å)			
Hg(1)-O(2)	3.243	Hg(2)-O(5)	2.717
Hg(1)-O(4)	2.790	Hg(2)-O(6)	2.760
Hg(1)-O(9)	2.841	Hg(2)-O(2)	2.737
Angles (°)			
O(5)-Hg(1)-O(5)#1	180.000(5)	O(3)#6-Hg(3)-O(4)#4	144.9(4)
O(7)-Hg(2)-O(6)	178.1(5)	Hg(1)-O(5)-Hg(3)	110.1(6)
O(4)-Hg(3)-O(6)	157.9(5)	Hg(2)-O(7)-U(1)#2	124.3(6)
O(4)-Hg(3)-O(5)	126.4(5)	Hg(2)-O(7)-U(1)	115.8(6)
O(6)-Hg(3)-O(5)	75.7(5)	As(1)-O(3)-Hg(3)#6	117.3(6)
O(4)-Hg(3)-O(3)#6	91.1(4)	U(1)#1-O(3)-Hg(3)#6	105.2(5)

O(6)-Hg(3)-O(3)#6	90.9(5)	Hg(2)-O(6)-Hg(3)	113.1(6)

O(5)-Hg(3)-O(3)#6	86.9(5)	As(1)-O(4)-Hg(3)	123.7(7)
O(4)-Hg(3)-O(4)#4	78.4(5)	As(1)-O(4)-Hg(3)#4	126.0(6)
O(6)-Hg(3)-O(4)#4	111.3(5)	Hg(3)-O(4)-Hg(3)#4	101.6(5)
O(5)-Hg(3)-O(4)#4	73.5(4)		

Symmetry transformations used to generate equivalent atoms: #1 -x+1,-y,-z+1; #2 -x,-y-1,-z; #3 x-1,y-1,z ; #4 -x+1,-y+1,-z+1; #5 -x,-y,-z; #6 -x+2,-y+1,-z+1; #7 x+1,y+1,z

Compound 3.10: $[Zn(2,2'\text{-bpy})]_2[UO_2(HPO_4)_3]$ (ZnUP-1)

Distances (Å)			
U(1)-O(2)	2.322(3)	Zn(2)-O(6)#2	1.959(3)
U(1)-O(7)	2.484(3)	Zn(2)-O(8)	2.036(3)
U(1)-O(8)	2.472(3)	P(1)-O(1)	1.576(3)
U(1)-O(11)	2.294(3)	P(1)-O(2)	1.531(3)
U(1)-O(12)#1	2.306(3)	P(1)-O(3)	1.520(3)
U(1)-O(13)	1.776(3)	P(1)-O(4)	1.507(3)
U(1)-O(14)	1.797(3)	P(2)-O(5)	1.579(3)
Zn(1)-N(1)	2.102(4)	P(2)-O(6)	1.495(3)
Zn(1)-N(2)	2.061(4)	P(2)-O(7)	1.521(3)
Zn(1)-O(4)	1.929(3)	P(2)-O(8)	1.542(3)
Zn(1)-O(10)	1.946(3)	P(3)-O(9)	1.570(3)
Zn(2)-N(3)	2.130(4)	P(3)-O(10)	1.536(3)
Zn(2)-N(4)	2.085(4)	P(3)-O(11)	1.525(3)
Zn(2)-O(3)	2.035(3)	P(3)-O(12)	1.517(3)
Angles (°)			
N(2)-Zn(1)-N(1)	79.11(16)	N(4)-Zn(2)-N(3)	77.49(16)
O(4)-Zn(1)-O(10)	113.87(13)	O(3)-Zn(2)-O(8)	90.08(13)

Symmetry transformations used to generate equivalent atoms: #1 $-x + 1, -y, -z + 1$; #2 $-x+1, -y + 1, -z$.

Compound 3.11: $[H_2bipy][(UO_2)_6Zn_2(PO_3OH)_4(PO_4)_4 \cdot H_2O$ (ZnUP-2)

Distances (Å)			
U(1)-O(18)	1.750(8)	P(1)-O(1)	1.583(10)
U(1)-O(17)	1.757(7)	P(1)-O(2)	1.503(8)
U(1)-O(7)	2.297(8)	P(1)-O(3)	1.528(8)
U(1)-O(12)#3	2.304(7)	P(1)-O(4)	1.538(8)
U(1)-O(3)#4	2.396(8)	P(2)-O(5)	1.556(7)
U(1)-O(4)	2.453(7)	P(2)-O(6)	1.537(7)
U(1)-O(3)	2.541(8)	P(2)-O(7)	1.507(8)
U(2)-O(20)	1.772(8)	P(2)-O(8)	1.502(8)
U(2)-O(19)	1.788(8)	P(3)-O(9)	1.568(7)
U(2)-O(16)#5	2.292(7)	P(3)-O(10)	1.534(7)
U(2)-O(11)#5	2.319(7)	P(3)-O(11)	1.528(8)
U(2)-O(5)#6	2.384(7)	P(3)-O(12)	1.503(8)
U(2)-O(6)	2.409(7)	P(4)-O(13)	1.548(8)
U(2)-O(5)	2.508(8)	P(4) –O(14)	1.540(7)
U(3)-O(21)	1.770(8)	P(4)-O(15)	1.526(8)
U(3)-O(22)	1.786(8)	P(4)-O(16)	1.527(8)
U(3)-O(14)#1	2.282(7)	Zn(1)-O(15)#1	1.908(7)
U(3)-O(8)	2.291(7)	Zn(1)-O(13)	1.944(8)
U(3)-O(10)#3	2.400(7)	Zn(1)-O(2)#2	1.947(8)
U(3)-O(9)	2.466(7)	Zn(1)-O(9)	1.974(7)
U(3)-O(10)	2.561(7)		

Angles (°)

O(15)#1-Zn(1)-O(13)	114.7(3)	O(15)#1-Zn(1)-O(2)#2	112.9(3)
O(13)-Zn(1)-O(2)#2	104.2(3)	O(15)#1-Zn(1)-O(9)	104.8(3)
O(13)-Zn(1)-O(9)	112.5(3)	O(2)#2-Zn(1)-O(9)	107.8(3)

Symmetry transformations used to generate equivalent atoms: #1 -x+1,-y,-z+1 #2 -x+1,-y+1,-z

Compound 3.12: $K_2[UO_2Co(PO_4)_2] \cdot H_2O$ (CoUP-1)

		Distances (Å)	
U(1)–O(2)	2.283(4)	Co(1)–O(8)	1.952(4)
U(1)–O(3)	2.265(4)	P(1)–O(1)	1.527(4)
U(1)–O(6)	2.502(4)	P(1)–O(2)	1.533(4)
U(1)–O(6)	2.353(4)	P(1)–O(3)	1.545(4)
U(1)–O(7)	2.369(4)	P(1)–O(4)	1.533(4)
U(1)–O(9)	1.781(4)	P(2)–O(5)	1.511(4)
U(1)–O(10)	1.800(4)	P(2)–O(6)	1.562(4)
Co(1)–O(1)	1.970(4)	P(2)–O(7)	1.538(4)
Co(1)–O(4)	1.971(4)	P(2)–O(8)	1.512(4)
Co(1)–O(5)	1.957(4)		
		Angles (°)	
O(9)–U(1)–O(10)	179.30(17)	O(4)–Co(1)–O(5)	107.31(16)
O(1)–Co(1)–O(4)	123.10(16)	O(4)–Co(1)–O(8)	106.89(16)
O(1)–Co(1)–O(5)	99.27(17)	O(5)–Co(1)–O(8)	106.95(16)
O(1)–Co(1)–O(8)	111.98(17)		

Compound 3.13: $Zn(OH)_2[(UO_2)_8O_4(SO_4)_4] \cdot 14H_2O$ (ZnUS-1)

		Distances (Å)	
U(1)-O(9)	1.847(14)	Zn(1)-O(6)#4	2.196(14)
U(1)-O(10)	1.874(19)	S(1)-O(1)	1.517(15)
U(1)-O(7)	2.26(2)	S(1)-O(2)	1.424(18)
U(1)-O(8)	2.269(14)	S(1)-O(3)	1.482(17)
U(1)-O(8)#1	2.306(16)	S(1)-O(4)	1.48(2)
U(1)-O(1)#2	2.478(15)	U(2)-O(3)#7	2.431(16)
U(1)-O(2)#3	2.501(17)	U(2)-O(4)	2.488(15)
Zn(1)-O(11)	2.01(3)	U(2)-O(5)	1.766(17)
Zn(1)-O(12)	2.017(17)	U(2)-O(6)	1.799(12)
Zn(1)-O(10)	2.133(18)	U(2)-O(7)	2.32(2)
Zn(1)-O(10)#4	2.133(18)	U(2)-O(7)#7	2.23(2)
Zn(1)-O(6)	2.196(14)	U(2)-O(8)	2.221(16)
		Angles (°)	
U(2)-O(6)-Zn(1)	140.1(8)	U(1)-O(10)-Zn(1)	139.5(9)

Symmetry transformations used to generate equivalent atoms: #1 x-1/2, -y+1/2, z #2 x,y,z-1 #3 x-1/2, -y+1/2, z-1 #4 x, -y+1, z #5 x, y, z+1 #6 x+1/2, -y+1/2, z+1 #7 x+1/2, -y+1/2, z

Compound 3.14: $[Co(OH)_2]_3[(UO_2)_8O_4(SO_4)_4] \cdot 2H_2O$ (CoUS-1)

Distances (Å)			
U(1)-O(8)	1.75(2)	S(1)-O(6)	1.45(3)
U(1)-O(10)	1.86(2)	S(1)-O(3)	1.49(3)
U(1)-O(4)#1	2.15(3)	S(1)-O(9)	1.49(3)
U(1)-O(2)#1	2.24(4)	Co(1)-O(11)#3	1.97(5)
U(1)-O(2)	2.26(4)	Co(1)-O(15)	2.043(19)
U(1)-O(3)	2.37(2)	Co(1)-O(1)	2.18(3)
U(1)-O(9)#2	2.41(3)	Co(1)-O(1)#4	2.18(3)
O(1)-U(2)	1.66(3)	Co(1)-O(14)	2.19(2)
U(2)-O(7)	1.89(2)	Co(2)-O(11)	2.03(5)
U(2)-O(4)	2.30(3)	Co(2)-O(12)	2.05(4)
U(2)-O(4)#1	2.32(3)	Co(2)-O(7)	2.05(3)
U(2)-O(2)	2.35(3)	Co(2)-O(7)#7	2.05(3)
U(2)-O(6)#5	2.51(3)	Co(2)-O(8)	2.26(2)
U(2)-O(5)#6	2.52(3)	Co(2)-O(8)#7	2.26(2)
S(1)-O(5)	1.44(4)		
Angles (°)			
U(2)-O(7)-Co(2)	140.7(10)	U(1)-O(8)-Co(2)	141.0(14)
Co(1)#10-O(11)-Co(2)	146(3)		

Symmetry transformations used to generate equivalent atoms: #1 x-1/2, -y+1/2, z #2 x+1/2, -y+1/2, z #3 x+1/2, y+1/2, z #4 x, -y+1, z #5 x+1/2, -y+1/2, z+1 #6 x+1, y, z+1 #7 x, -y, z #8 x-1, y, z-1 #9 x-1/2, -y+1/2, z-1 #10 x-1/2, y-1/2, z

Compound 3.15: $[Ni(OH)_2]_3[(UO_2)_8O_4(SO_4)_4]\cdot 10H_2O$ (NiUS-1)

Distances (Å)			
U(1)-O(1)	1.799(9)	Ni(1)-O(4)	2.016(15)
U(1)-O(3)	1.825(9)	Ni(1)-O(3)	2.153(9)
U(1)-O(2)	2.245(9)	Ni(1)-O(3)#6	2.153(9)
U(1)-O(2)#1	2.286(9)	Ni(1)-O(3)#5	2.153(9)
U(1)-O(2)#2	2.299(9)	Ni(1)-O(3)#2	2.153(9)
U(1)-O(5)#3	2.448(8)	Ni(2)-O(4)	1.961(16)
U(1)-O(6)	2.470(7)	Ni(2)-O(2W)	2.05(2)
S(1)-O(6)#4	1.480(9)	Ni(2)-O(1)#7	2.066(9)
S(1)-O(6)	1.480(9)	Ni(2)-O(1)#1	2.066(9)
S(1)-O(5)#4	1.481(9)	Ni(2)-O(1W)	2.21(7)
S(1)-O(5)	1.481(9)	Ni(2)-O(3W)	2.21(2)
Ni(1)-O(4)#5	2.016(15)		
Angles (°)			
U(1)-O(1)-Ni(2)#1	165.3(5)	U(1)-O(3)-Ni(1)	141.1(5)
Ni(2)-O(4)-Ni(1)	149.8(11)		

Symmetry transformations used to generate equivalent atoms: #1 -x+1/2, -y+1/2, -z #2 -x, y, -z #3 -x+1/2, -y+1/2, -z+1 #4 -x, y, -z+1 #5 -x, -y, -z #6 x, -y, z #7 -x+1/2, y-1/2, -z #8 -x+1, -y, -z

Compound 3.16: $[Ni(OH)_2][(UO_2)_4O_2(SO_4)_2]\cdot 8H_2O$ (NiUS-2)

		Distances (Å)	
U(1)-O(4)	1.810(5)	S(1)-O(2)	1.485(5)
U(1)-O(5)	1.815(5)	S(1)-O(2)#5	1.485(5)
U(1)-O(3)	2.230(5)	Ni(1)-O(6)	2.035(10)
U(1)-O(3)#2	2.271(5)	Ni(1)-O(5)#1	2.036(5)
U(1)-O(3)#3	2.296(5)	Ni(1)-O(5)	2.036(5)
U(1)-O(1)#4	2.445(5)	Ni(1)-O(3W)	2.05(2)
U(1)-O(2)	2.494(5)	Ni(1)-O(2W)	2.134(17)
S(1)-O(1)	1.463(5)	Ni(1)-O(1W)	2.228(13)
S(1)-O(1)#5	1.463(5)		
		Angles (°)	
U(1)-O(5)-Ni(1)	166.3(3)		

Symmetry transformations used to generate equivalent atoms: #1 x, -y, z #2 -x+3/2, -y+1/2, -z+1 #3 -x+2, y, -z+1 #4 -x+3/2, -y+1/2, -z #5 -x+2, y, -z #6 -x+2, -y, -z+1

Compound 3.17: $(UO_2)(OH)(CO_2)(C_5H_4N)$ (Uoxa-1)

		Distances (Å)	
U(1)-N(1)	2.549(4)	U(1)-O(4)	1.771(3)
U(1)-O(1)	2.477(3)	U(1)-O(5)	2.460(3)
U(1)-O(2)	2.314(3)	O(5)-C(6)	1.267(5)
U(1)-O(2)#1	2.345(3)	O(1)-C(6)#2	1.243(5)
U(1)-O(3)	1.771(3)	C(6)-C(6)#2	1.541(8)
		Angles (°)	
C(2)-C(3)-C(3)#3	121.0(3)	O(4)-U(1)-N(1)	89.98(14)
O(1)#2-C(6)-O(5)	126.7(4)		

Symmetry transformations used to generate equivalent atoms: #1 -x-1/2, -y+1/2, -z-1 #2 -x-1, -y, -z-1 #3 -x, y, -z+1/2

Compound 3.18: $(UO_2)(OH)_2(C_5H_4N)_2$ (Ubpy-1)

		Distances (Å)	
U(1)-O(2)	1.783(3)	U(1)-O(4)	2.355(3)
U(1)-O(1)	1.793(3)	U(1)-O(3)	2.356(3)
U(1)-O(4)#1	2.346(3)	U(1)-N(1)	2.608(4)
U(1)-O(3)#2	2.348(3)		
		Angles (°)	
O(4)-U(1)-N(1)	72.91(12)	O(2)-U(1)-N(1)	92.27(14)
O(3)-U(1)-N(1)	73.37(13)	O(1)-U(1)-N(1)	83.37(12)

Symmetry transformations used to generate equivalent atoms: #1 x-1/2, -y+3/2, -z-3 #2 x+1/2, -y+3/2, -z-3

Compound 3.19: $(C_6H_5NH)(UO_2)(PO_4)$ (Ubpe-1)

Distances (Å)			
U(1)-O(5)	1.778(3)	U(1)-O(2)#3	2.276(3)
U(1)-O(6)	1.816(3)	P(1)-O(1)	1.535(4)
U(1)-O(1)#1	2.247(4)	P(1)-O(2)	1.530(4)
U(1)-O(4)	2.255(4)	P(1)-O(3)	1.531(4)
U(1)-O(3)#2	2.271(3)	P(1)-O(4)	1.535(4)

Symmetry transformations used to generate equivalent atoms: #1 x+1, y, z #2 -x+1, -y+1, -z+2 #3 -x+1, -y+2, -z+2 #4 x-1, y, z #5 -x+1, -y+2, -z+3

Compound 3.20: $Co(UO_2)_2(AsO_4)_2 \cdot 8H_2O$ (CoUAs-1)

		Distances (Å)	
U(1)-O(12)	1.765(4)	As(3)-O(4)	1.679(4)
U(1)-O(7)	1.788(5)	As(3)-O(8)	1.678(4)
U(1)-O(8)#1	2.277(4)	As(3)-O(5)	1.683(4)
U(1)-O(4)#2	2.285(4)	As(4)-O(1)	1.674(4)
U(1)-O(3)	2.292(4)	As(4)-O(2)	1.680(4)
U(1)-O(9)	2.303(4)	As(4)-O(9)	1.683(4)
U(2)-O(6)	1.773(5)	As(4)-O(11)	1.689(4)
U(2)-O(10)	1.808(4)	Co(1)-O(16)	2.043(5)
U(2)-O(5)	2.242(4)	Co(1)-O(17)	2.044(4)
U(2)-O(11)#3	2.274(4)	Co(1)-O(15)	2.052(5)
U(2)-O(2)#4	2.285(4)	Co(1)-O(18)	2.081(5)
U(2)-O(1)	2.288(4)	Co(1)-O(13)	2.121(5)
As(3)-O(3)	1.676(4)	Co(1)-O(10)	2.243(4)
		Angles (°)	
U(2)-O(10)-Co(1)	179.0(2)		

Symmetry transformations used to generate equivalent atoms: #1 -x+1, -y+1, -z+2 #2 x-1, y, z #3 -x+1, -y+2, -z+1 #4 x+1, y, z

Compound 3.21: $Mn(UO_2)_2(AsO_4)_2 \cdot 8H_2O$ (MnUAs-1)

Distances (Å)			
U(1)-O(17)	1.766(4)	As(3)-O(9)	1.680(4)
U(1)-O(15)	1.804(4)	As(3)-O(7)	1.684(4)
U(1)-O(7)	2.249(4)	As(3)-O(12)	1.684(4)
U(1)-O(10)#1	2.278(4)	As(4)-O(16)	1.679(4)
U(1)-O(8)#2	2.283(4)	As(4)-O(6)	1.680(4)
U(1)-O(16)	2.291(4)	As(4)-O(8)	1.687(4)
U(2)-O(14)	1.769(4)	As(4)-O(10)	1.691(4)
U(2)-O(13)	1.780(4)	Mn(1)-O(2)	2.139(5)
U(2)-O(12)#3	2.281(4)	Mn(1)-O(1)	2.146(4)
U(2)-O(11)	2.289(4)	Mn(1)-O(3)	2.152(4)
U(2)-O(9)#4	2.297(4)	Mn(1)-O(5)	2.179(4)
U(2)-O(6)	2.308(4)	Mn(1)-O(4)	2.182(4)
As(3)-O(11)	1.676(4)	Mn(1)-O(15)	2.323(4)
Angles (°)			
U(1)-O(15)-Mn(1)	179.5(2)		

Symmetry transformations used to generate equivalent atoms: #1 -x, -y+1, -z+2 #2 x+1, y, z #3 -x, -y+2, -z+1 #4 x-1, y, z

Compound 3.22: $Cu(UO_2)_2(AsO_4)_2 \cdot 5H_2O$ (CuUAs-1)

Distances (Å)			
U(1)-O(1)	1.774(13)	As(1)-O(4)	1.677(9)
U(1)-O(2)	1.779(12)	Cu(1)-O(1W)	1.949(14)
U(1)-O(4)	2.301(11)		

Appendix III: Atomic coordinates (x 10^4) and equivalent isotropic displacement parameters ($Å^2$ x 10^3) for Compound 3.1-3.22.

- U(eq) = 1/3[U22 + 1/$\sin^2\beta$(U11 + U33 + 2U13cosβ)]

Compound 3.1: $(H_3O)U_2(PO_4)_3$ (U^{IV}P-1)

	x	y	z	U(eq)
U(1)	3458(1)	-4064(1)	9661(1)	10(1)
P(1)	3087(2)	918(3)	8181(4)	7(1)
P(2)	5000	-4138(5)	12500	8(1)
O(1)	2973(4)	-1539(13)	11286(9)	12(2)
O(1W)	-99(16)	4120(20)	7040(30)	29(6)
O(2)	4278(5)	-4648(12)	7563(10)	13(2)
O(3)	4734(4)	-2897(12)	10886(10)	14(2)
O(4)	2752(5)	-5539(12)	11690(10)	9(1)
O(5)	3461(5)	-7440(11)	9337(10)	12(2)
O(6)	3567(5)	-972(9)	8507(10)	8(2)

Compound 3.2: $[[Ni^{II}(2,2'\text{-bpy})_3](UO_2)(NO_3)(H_2PO_4)_2](NO_3)\cdot 3.25(H_2O)$ (NiUP-1)

	x	y	z	U(eq)
U(1)	3439(1)	3755(1)	99(1)	18(1)
Ni(1)	3326(1)	4908(1)	2472(1)	22(1)
P(1)	3058(1)	6356(1)	39(1)	21(1)
P(2)	1969(1)	3856(1)	153(1)	20(1)
N(1)	32(2)	4978(3)	-1749(2)	37(1)
O(1)	2429(1)	6255(2)	-193(1)	26(1)
O(1W)	668(1)	7390(3)	55(1)	29(1)
O(2)	3176(1)	7123(2)	504(1)	30(1)
O(2W)	659(2)	4364(4)	463(2)	59(1)
O(3)	3330(1)	6788(2)	-406(1)	32(1)
O(3W)	43(2)	6061(3)	532(2)	65(1)
O(4)	3355(1)	5413(2)	259(1)	28(1)
O(4W)	4156(2)	9053(3)	599(2)	26(1)
O(5)	1666(1)	2936(2)	-93(1)	32(1)
O(6)	1734(1)	4203(2)	631(1)	35(1)
O(7)	1835(1)	4675(2)	-282(1)	29(1)
O(8)	2602(1)	3734(2)	365(1)	27(1)
O(9)	3866(1)	3666(2)	750(1)	24(1)
O(10)	3041(1)	3853(2)	-563(1)	29(1)
O(11)	4217(1)	4618(2)	-242(1)	44(1)
O(12)	4281(1)	3031(2)	-199(1)	36(1)
O(13)	4885(2)	3860(3)	-523(2)	60(1)
O(14)	314(2)	4280(3)	-1490(2)	55(1)
O(15)	-387(2)	4807(3)	-2101(2)	61(1)
O(16)	202(2)	5838(3)	-1647(2)	62(1)
C(1)	3059(2)	2403(3)	1374(2)	30(1)
N(2)	4473(2)	3839(3)	-329(2)	36(1)
C(2)	2280(2)	3781(3)	3504(2)	37(1)

N(3)	3898(1)	5573(2)	2084(1)	25(1)
C(3)	2122(2)	6358(3)	1170(2)	35(1)
N(4)	3487(1)	6261(2)	2874(1)	24(1)
C(4)	2611(2)	5954(3)	1485(2)	31(1)
N(5)	2610(1)	5473(2)	1937(1)	25(1)
C(5)	2119(2)	5375(3)	2086(1)	26(1)
N(6)	2674(1)	4498(2)	2829(1)	25(1)
C(6)	3781(2)	2953(3)	2304(1)	24(1)
N(7)	3976(1)	4157(2)	3002(1)	27(1)
C(7)	3468(2)	7411(3)	3567(2)	36(1)
N(8)	3332(1)	3554(2)	2089(1)	25(1)
C(8)	2735(2)	3991(3)	3281(2)	32(1)
C(9)	3869(2)	6850(3)	2716(1)	25(1)
C(10)	2151(2)	4814(3)	2583(1)	25(1)
C(11)	3294(2)	6548(3)	3291(2)	30(1)
C(12)	4342(2)	5788(3)	1363(2)	33(1)
C(13)	4128(2)	3288(3)	2819(2)	27(1)
C(14)	4044(2)	5231(3)	1656(2)	32(1)
C(15)	4056(2)	6508(3)	2245(2)	25(1)
C(16)	3883(2)	2084(3)	2056(2)	32(1)
C(17)	2985(2)	3276(3)	1636(2)	27(1)
C(18)	3523(2)	1820(3)	1584(2)	35(1)
C(19)	4504(2)	6743(3)	1527(2)	35(1)
C(20)	1678(2)	4615(3)	2788(2)	33(1)
C(21)	4580(2)	2736(3)	3107(2)	37(1)
C(22)	4258(2)	4473(3)	3477(2)	34(1)
C(23)	4070(2)	7722(3)	2982(2)	35(1)
C(24)	3869(2)	8000(3)	3414(2)	39(1)
C(25)	4365(2)	7102(3)	1977(2)	32(1)
C(26)	1622(2)	6275(3)	1326(2)	40(1)
C(27)	1612(2)	5777(3)	1791(2)	36(1)

C(28)	4705(2)	3952(3)	3786(2)	39(1)
C(29)	4874(2)	3079(3)	3598(2)	42(1)
C(30)	1745(2)	4099(3)	3254(2)	38(1)

Compound 3.3: $[(UO_2)(NO_3)_2(H_2O)][C_6H_6N]$ (UNO_3-1)

	x	y	z	U(eq)
U(1)	2792(1)	1691(1)	6591(1)	29(1)
O(1)	513(5)	1727(2)	6522(4)	36(1)
N(1)	3424(5)	330(2)	6791(4)	31(1)
C(1)	4280(7)	82(3)	7863(5)	40(1)
O(2)	5067(5)	1656(2)	6679(4)	37(1)
N(2)	1810(5)	867(2)	4669(4)	31(1)
C(2)	4843(7)	-611(3)	7999(6)	43(1)
O(3)	3038(6)	2424(2)	8488(4)	44(1)
C(3)	4541(7)	-1064(3)	6977(6)	42(1)
O(4)	2659(5)	1302(2)	8806(4)	36(1)
C(4)	3690(7)	-811(2)	5870(5)	39(1)
O(5)	2741(5)	2949(2)	6111(4)	44(1)
C(5)	3152(6)	-118(2)	5797(5)	29(1)
O(6)	3060(5)	2254(2)	4533(3)	37(1)
C(6)	795(6)	1144(3)	3690(5)	33(1)
C(7)	141(7)	754(3)	2654(5)	38(1)
C(8)	575(7)	52(3)	2612(5)	40(1)
C(9)	1574(7)	-243(3)	3611(5)	38(1)
C(10)	2160(6)	174(2)	4652(5)	30(1)
C(11)	2588(8)	2077(3)	10577(5)	39(1)
C(12)	2775(6)	1930(3)	9231(5)	32(1)
C(13)	3088(10)	3496(3)	4127(7)	42(1)
C(14)	2962(7)	2874(3)	4972(5)	35(1)

Compound 3.4: $(UO_2)(Ac)_2(2,2'\text{-bpy})$ (UAc-1)

	x	y	z	U(eq)
U(1)	8615(1)	6212(1)	9791(1)	13(1)
O(1)	7048(2)	10462(5)	11486(2)	28(1)
O(2)	8376(2)	8408(5)	11177(2)	23(1)
O(3)	7111(2)	8617(4)	10249(2)	23(1)
O(4)	6815(2)	4472(5)	7587(2)	27(1)
O(5)	7010(2)	6254(4)	8839(2)	21(1)
O(6)	8234(2)	4252(5)	8361(2)	21(1)
O(7)	9099(2)	8768(4)	9281(2)	19(1)
O(8)	8153(2)	3661(4)	10315(2)	21(1)
O(9)	10073(2)	6223(4)	10736(2)	14(1)
N(1)	7331(2)	4973(5)	8233(2)	18(1)
N(2)	7485(2)	9226(5)	10992(2)	19(1)
N(3)	9894(2)	4206(5)	2408(2)	19(1)
C(1)	9281(3)	2306(7)	2362(2)	23(1)
C(2)	9218(3)	824(7)	3065(3)	23(1)
C(3)	9785(3)	1290(5)	3837(2)	17(1)
C(4)	10407(3)	3297(6)	3855(2)	20(1)
C(5)	10457(3)	4727(6)	3128(2)	20(1)
C(6)	9709(3)	-384(6)	4589(2)	19(1)

Compound 3.5: $[Ag(4,4'\text{-bpy})]_2[(UO_2)H_3(PO_4)_3]$ (AgUP-1)

	x	y	z	U(eq)
U(1)	1371(1)	-636(1)	-1857(1)	17(1)
Ag(1)	439(1)	-4931(1)	2842(1)	29(1)
P(1)	-1336(7)	133(4)	-4899(4)	25(1)
P(2)	6827(3)	189(2)	-1600(2)	19(1)
O(1)	-1630(20)	1347(13)	-4250(13)	41(3)
O(2)	-3558(19)	-968(12)	-5392(11)	38(3)
O(3)	356(11)	-503(6)	-4004(6)	41(2)
O(4)	6926(11)	1284(6)	-2452(6)	40(2)
O(5)	8122(8)	-657(5)	-1858(5)	26(1)
O(6)	7724(9)	889(6)	-212(5)	28(1)
O(7)	4529(8)	-695(6)	-1930(6)	33(1)
O(8)	2378(9)	1131(5)	-1452(6)	29(1)
O(9)	360(8)	-2405(5)	-2284(5)	24(1)
N(1)	-1377(9)	-4867(6)	994(6)	21(1)
N(2)	2235(11)	-4885(7)	4752(6)	27(1)
C(1)	3335(14)	-3746(9)	5552(8)	37(2)
C(2)	2262(14)	-6008(8)	5200(8)	35(2)
C(3)	3411(14)	-6031(8)	6425(8)	33(2)
C(4)	-2742(12)	-3674(7)	-643(7)	25(2)
C(5)	-1515(13)	-3754(8)	553(8)	30(2)
C(6)	4570(15)	-3702(8)	6802(8)	34(2)
C(7)	-2539(12)	-6008(7)	179(7)	24(2)
C(8)	-3810(13)	-6019(7)	-1047(8)	28(2)
C(9)	-3950(11)	-4858(7)	-1467(7)	19(1)
C(10)	4686(11)	-4853(7)	7235(7)	21(2)

Compound 3.6: $Ag(2,2'\text{-bipy})(UO_2)_2(HPO_4)(PO_4)$ (AgUP-2)

	x	y	z	U(eq)
U(1)	6994(1)	4419(1)	4647(1)	13(1)
P(1)	10423(2)	2645(1)	4410(2)	14(1)
O(1)	10881(4)	2420(4)	3063(5)	19(1)
N(1)	7480(7)	2897(7)	139(8)	36(2)
C(1)	6701(12)	1641(9)	-240(13)	56(3)
U(2)	7922(1)	471(1)	4670(1)	12(1)
P(2)	4402(2)	2114(1)	4372(2)	14(1)
O(2)	11298(4)	3830(4)	5357(5)	15(1)
N(2)	8880(6)	5467(7)	1117(6)	30(1)
C(2)	5457(12)	1406(10)	-1123(11)	51(2)
O(3)	10497(4)	1273(4)	4940(5)	16(1)
C(3)	4915(9)	2489(10)	-1636(9)	44(2)
O(4)	8780(4)	2834(4)	4295(5)	19(1)
C(4)	5711(8)	3794(9)	-1252(8)	34(2)
O(5)	4468(4)	3688(4)	4893(5)	17(1)
C(5)	6984(8)	3970(7)	-363(7)	28(1)
O(6)	3515(5)	1764(4)	2956(5)	22(1)
C(6)	7806(8)	5340(8)	88(7)	29(2)
O(7)	3785(4)	1297(4)	5263(4)	14(1)
C(7)	7501(9)	6468(8)	-505(8)	36(2)
O(8)	5974(4)	1882(4)	4258(5)	17(1)
C(8)	8263(9)	7741(8)	-5(9)	37(2)
O(9)	6426(5)	4311(4)	2947(5)	22(1)
C(9)	9363(8)	7863(8)	1049(9)	36(2)
O(10)	7495(5)	4512(5)	6340(5)	22(1)
C(10)	9649(8)	6702(9)	1573(9)	37(2)
O(11)	7829(4)	-100(5)	2966(5)	20(1)
O(12)	7999(5)	1045(5)	6347(5)	22(1)

Ag(1)	9562(1)	3455(1)	1688(1)	53(1)

Compound 3.7: $Na_2Ag_6[(AgO)_2(UO_2)_3(AsO_4)_4]$ (AgUAs-1)

	x	y	z	U(eq)
U(1)	5000	10000	5000	13(1)
U(2)	3116(1)	10000	10000	11(1)
As(3)	3478(1)	10326(2)	6800(1)	11(1)
Ag(1)	3516(1)	5000	5000	40(1)
Ag(2)	4206(1)	5338(3)	8014(2)	51(1)
Ag(3)	2500	5029(2)	7500	20(1)
Na(1)	5000	1130(20)	9494(11)	25(2)
O(1)	4171(5)	11523(17)	6162(9)	31(2)
O(2)	2826(5)	11468(17)	6032(11)	38(3)
O(3)	3470(6)	11515(19)	8166(8)	39(3)
O(4)	5000	12780(20)	4166(11)	22(2)
O(6)	3110(5)	7078(15)	9323(7)	23(2)
O(7)	3478(4)	7263(15)	6782(7)	18(2)
O(1W)	5000	10940(20)	8038(8)	15(2)
O(2W)	5000	-880(70)	9680(30)	76(11)

Compound 3.8: $Ag(UO_2)(AsO_4)$ (AgUAs-2)

	x	y	z	U(eq)
U(1)	2500	2500	563(1)	13(1)
As(1)	2500	7500	0	16(1)
Ag(1)	-4838(9)	6604(9)	1817(4)	26(1)
O(1)	4282(17)	8078(19)	-604(8)	17(3)
O(3)	2500	2500	-485(16)	27(6)
O(4)	2500	2500	1610(13)	16(5)

Compound 3.9: $[Hg_5O_2(OH)_5][(UO_2)_2(AsO_4)_2]$ (HgUAs-1)

	x	y	z	U(eq)
Hg(1)	5000	0	5000	16(1)
Hg(2)	2415(1)	-626(1)	323(1)	13(1)
Hg(3)	5690(1)	3871(1)	3202(1)	14(1)
U(1)	60(1)	-3740(1)	2092(1)	9(1)
As(1)	9360(3)	7737(3)	6044(2)	9(1)
O(1)	10390(20)	7920(20)	4691(15)	14(3)
O(2)	9388(19)	10089(19)	7363(14)	11(2)
O(3)	10766(18)	6400(20)	7009(14)	10(2)
O(4)	6821(19)	6576(19)	5260(14)	11(2)
O(5)	5400(20)	200(20)	3035(17)	19(3)
O(6)	4390(20)	2080(20)	775(15)	14(3)
O(7)	430(20)	-3200(20)	-75(16)	15(3)
O(8)	-2700(20)	-3650(20)	1545(16)	18(3)
O(9)	2770(20)	-3850(20)	2687(14)	15(3)

Compound 3.10: $[Zn(2,2'\text{-bpy})]_2[UO_2(HPO_4)_3]$ (ZnUP-1)

	x	y	z	U(eq)
Zn(1)	8875(1)	4744(1)	6468(1)	16(1)
U(1)	5735(1)	3790(1)	1430(1)	16(1)
U(2)	6764(1)	-1033(1)	4771(1)	14(1)
U(3)	6748(1)	3751(1)	5172(1)	14(1)
P(1)	7126(3)	3737(3)	-974(2)	19(1)
P(2)	6754(2)	1606(2)	4057(2)	14(1)
P(3)	6195(2)	5954(2)	5801(2)	14(1)
P(4)	9877(2)	7019(2)	4657(2)	15(1)
O(1)	6641(10)	2936(9)	-1308(8)	38(2)
O(1W)	7960(20)	546(15)	984(15)	49(6)
O(2)	8259(8)	4257(8)	-1891(7)	28(2)
O(3)	5970(8)	4638(8)	-713(7)	29(2)
O(4)	7459(7)	2948(7)	197(6)	21(2)
O(5)	5543(7)	977(7)	4599(7)	22(2)
O(6)	7891(7)	564(6)	4173(6)	16(1)
O(7)	6814(8)	2384(7)	2812(7)	26(2)
O(8)	6731(8)	2262(7)	4727(7)	25(2)
O(9)	7391(7)	4929(6)	5849(6)	17(1)
O(10)	5349(7)	5660(6)	5295(6)	18(1)
O(11)	6620(7)	7138(7)	4966(7)	19(2)
O(12)	5574(8)	5931(7)	6972(7)	26(2)
O(13)	9454(7)	6226(7)	5938(6)	20(2)
O(14)	11262(7)	7248(6)	4432(7)	19(2)
O(15)	9829(7)	6424(7)	3937(6)	20(2)
O(16)	8934(8)	8189(7)	4371(8)	28(2)
O(17)	6728(8)	4770(7)	1172(7)	25(2)
O(18)	4800(8)	2813(8)	1603(7)	29(2)
O(19)	6696(8)	-569(7)	3326(7)	22(2)

O(20)	6834(8)	-1507(7)	6205(6)	23(2)
O(21)	7522(9)	4545(7)	3744(7)	26(2)
O(22)	5998(7)	2971(7)	6629(7)	23(2)
N(1)	7847(11)	7452(10)	12614(9)	31(2)
N(2)	9511(10)	6481(9)	7694(8)	27(2)
C(1)	8956(13)	7778(12)	11852(13)	36(3)
C(2)	9281(14)	7648(12)	10837(11)	33(3)
C(3)	8432(9)	7179(9)	10614(9)	19(2)
C(4)	7250(14)	6936(11)	11397(11)	33(3)
C(5)	6985(14)	7058(13)	12439(12)	38(3)
C(6)	10439(13)	6447(13)	8136(12)	37(3)
C(7)	10103(12)	6650(15)	9115(13)	42(4)
C(8)	8798(11)	6940(11)	9589(10)	26(2)
C(9)	7854(10)	6994(10)	9085(10)	23(2)
C(10)	8223(11)	6755(10)	8131(10)	23(2)

Compound 3.11: $[H_2bipy][(UO_2)_6Zn_2(PO_3OH)_4(PO_4)_4 \cdot H_2O$ (ZnUP-2)

	x	y	z	U(eq)
Zn(1)	8875(1)	4744(1)	6468(1)	16(1)
U(1)	5735(1)	3790(1)	1430(1)	16(1)
U(2)	6764(1)	-1033(1)	4771(1)	14(1)
U(3)	6748(1)	3751(1)	5172(1)	14(1)
P(1)	7126(3)	3737(3)	-974(2)	19(1)
P(2)	6754(2)	1606(2)	4057(2)	14(1)
P(3)	6195(2)	5954(2)	5801(2)	14(1)
P(4)	9877(2)	7019(2)	4657(2)	15(1)
O(1)	6641(10)	2936(9)	-1308(8)	38(2)
O(1W)	7960(20)	546(15)	984(15)	49(6)
O(2)	8259(8)	4257(8)	-1891(7)	28(2)
O(3)	5970(8)	4638(8)	-713(7)	29(2)
O(4)	7459(7)	2948(7)	197(6)	21(2)
O(5)	5543(7)	977(7)	4599(7)	22(2)
O(6)	7891(7)	564(6)	4173(6)	16(1)
O(7)	6814(8)	2384(7)	2812(7)	26(2)
O(8)	6731(8)	2262(7)	4727(7)	25(2)
O(9)	7391(7)	4929(6)	5849(6)	17(1)
O(10)	5349(7)	5660(6)	5295(6)	18(1)
O(11)	6620(7)	7138(7)	4966(7)	19(2)
O(12)	5574(8)	5931(7)	6972(7)	26(2)
O(13)	9454(7)	6226(7)	5938(6)	20(2)
O(14)	11262(7)	7248(6)	4432(7)	19(2)
O(15)	9829(7)	6424(7)	3937(6)	20(2)
O(16)	8934(8)	8189(7)	4371(8)	28(2)
O(17)	6728(8)	4770(7)	1172(7)	25(2)
O(18)	4800(8)	2813(8)	1603(7)	29(2)
O(19)	6696(8)	569(7)	-3326(7)	22(2)

O(20)	6834(8)	-1507(7)	6205(6)	23(2)
O(21)	7522(9)	4545(7)	3744(7)	26(2)
O(22)	5998(7)	2971(7)	6629(7)	23(2)
N(1)	7847(11)	7452(10)	12614(9)	31(2)
N(2)	9511(10)	6481(9)	7694(8)	27(2)
C(1)	8956(13)	7778(12)	11852(13)	36(3)
C(2)	9281(14)	7648(12)	10837(11)	33(3)
C(3)	8432(9)	7179(9)	10614(9)	19(2)
C(4)	7250(14)	6936(11)	11397(11)	33(3)
C(5)	6985(14)	7058(13)	12439(12)	38(3)
C(6)	10439(13)	6447(13)	8136(12)	37(3)
C(7)	10103(12)	6650(15)	9115(13)	42(4)
C(8)	8798(11)	6940(11)	9589(10)	26(2)
C(9)	7854(10)	6994(10)	9085(10)	23(2)
C(10)	8223(11)	6755(10)	8131(10)	23(2)

Compound 3.12: $K_2[UO_2Co(PO_4)_2] \cdot H_2O$ (CoUP-1)

	x	y	z	U(eq)
U(1)	2047(1)	5362(1)	7075(1)	10(1)
Co(1)	-3021(1)	7711(1)	2968(1)	11(1)
P(1)	5409(2)	6306(1)	10689(2)	10(1)
P(2)	-946(2)	6512(1)	5459(2)	11(1)
K(1)	2866(2)	4903(1)	2274(2)	33(1)
K(2)	2480(2)	7275(1)	4106(2)	28(1)
O(1)	6759(5)	6489(2)	9709(5)	19(1)
O(2)	3715(5)	6076(2)	9363(5)	20(1)
O(3)	6000(5)	5601(2)	11943(5)	14(1)
O(4)	5075(5)	7023(2)	11733(5)	13(1)
O(5)	-2488(5)	6605(2)	6179(5)	18(1)
O(6)	-807(5)	5633(2)	4951(5)	15(1)
O(7)	768(5)	6622(2)	6874(5)	17(1)
O(8)	-1031(5)	7036(2)	3877(5)	17(1)
O(9)	854(5)	5061(2)	8568(5)	16(1)
O(10)	3251(5)	5678(2)	5573(5)	17(1)

Compound 3.13: $Zn(OH)_2[(UO_2)_8O_4(SO_4)_4] \cdot 14H_2O$ (ZnUS-1)

	x	y	z	U(eq)
U(1)	-6654(1)	2679(1)	-6662(1)	8(1)
U(2)	-3291(1)	2682(1)	-3282(1)	6(1)
Zn(1)	-4957(14)	5000	-4987(13)	9(1)
S(1)	-4950(10)	2515(2)	23(10)	9(1)
O(1)	-5620(19)	3157(11)	1078(17)	11(3)
O(1W)	-4700(50)	0	-5070(70)	91(14)
O(2)	-3780(20)	1915(12)	964(19)	13(3)
O(2W)	-4655(15)	0	2068(18)	31(3)
O(3)	-6200(20)	1926(12)	-991(18)	11(3)
O(3W)	-5210(40)	0	-1280(30)	153(17)
O(4)	-4220(20)	3141(13)	-940(19)	16(3)
O(4W)	-7080(40)	5000	-40(40)	77(13)
O(5)	-3228(17)	1481(12)	-2747(17)	16(3)
O(5W)	-2910(30)	5000	-30(50)	73(11)
O(6)	-3398(16)	3936(8)	-3585(17)	9(3)
O(6W)	-1768(9)	5000	-7369(9)	4(1)
O(7)	-6040(20)	2496(16)	-4050(20)	24(4)
O(8)	-3976(16)	2485(13)	-5848(19)	9(3)
O(9)	-6864(19)	1426(10)	-7241(15)	12(3)
O(10)	-6590(20)	3971(13)	-6212(18)	25(4)
O(11)	-6170(30)	5000	-3320(40)	63(9)
O(12)	-3813(19)	5000	-6717(13)	10(3)

Compound 3.14: $[Co(OH)_2]_3[(UO_2)_8O_4(SO_4)_4] \cdot 2H_2O$ (CoUS-1)

	x	y	z	U(eq)
U(1)	1244(1)	2328(1)	7312(1)	13(1)
U(2)	4612(1)	2315(1)	10714(1)	9(1)
Co(1)	4727(6)	5000	11358(6)	23(1)
Co(2)	2960(30)	0	9090(30)	15(2)
S(1)	-2040(30)	2501(3)	3950(30)	12(1)
O(1)	4700(30)	3460(20)	11130(30)	33(8)
O(2)	3920(40)	2548(19)	7990(40)	22(7)
O(3)	-780(30)	1946(17)	5050(20)	7(4)
O(4)	6880(30)	2466(18)	9800(40)	10(6)
O(5)	-3180(30)	1850(20)	3030(30)	26(7)
O(6)	-1340(30)	3170(15)	3070(30)	7(4)
O(7)	4480(20)	995(14)	10340(30)	17(6)
O(8)	1340(30)	1107(15)	7680(20)	18(6)
O(9)	-2690(30)	3040(20)	5110(30)	27(7)
O(10)	1080(20)	3584(15)	6680(20)	2(4)
O(11)	1810(70)	0	10830(60)	110(20)
O(12)	4150(30)	0	7350(40)	25(8)
O(14)	5970(30)	5000	13850(30)	34(6)
O(15)	2670(20)	5000	12100(40)	42(8)
O(16)	2440(50)	5000	9110(60)	74(17)

Compound 3.15: $[Ni(OH)_2]_3[(UO_2)_8O_4(SO_4)_4] \cdot 10H_2O$ (NiUS-1)

	x	y	z	U(eq)
U(1)	1684(1)	2318(1)	1705(1)	13(1)
Ni(1)	0	0	0	28(2)
Ni(2)	3195(6)	0	-2327(6)	32(1)
S(1)	0	2490(4)	5000	16(1)
O(1)	1831(10)	3541(7)	2278(10)	21(2)
O(2)	1021(11)	2531(6)	-897(10)	19(2)
O(3)	1561(10)	1049(6)	1334(10)	20(2)
O(4)	1180(20)	0	-1700(20)	47 (4)
O(5)	1212(9)	3111(7)	5994(8)	20(2)
O(6)	695(9)	1868(7)	3996(9)	20(2)
O(1W)	4450(90)	0	170(80)	120(30)
O(2W)	5240(30)	0	-3090(40)	108(15)
O(3W)	2040(40)	0	-4860(30)	85(13)

Compound 3.16: $[Ni(OH)_2][(UO_2)_4O_2(SO_4)_2] \cdot 8H_2O$ (NiUS-2)

	x	y	z	U(eq)
U(1)	8315(1)	2682(1)	3306(1)	8(1)
Ni(1)	8269(3)	0	2739(3)	20(1)
S(1)	10000	2558(2)	0	12(1)
O(1)	8779(5)	1958(4)	-978(5)	17(1)
O(2)	9313(6)	3189(4)	1011(6)	17(1)
O(3)	8968(6)	2520(4)	5891(6)	14(1)
O(4)	8324(6)	3948(4)	3611(6)	17(1)
O(5)	8250(6)	1440(4)	2776(6)	16(1)
O(6)	6121(12)	0	3299(12)	34(2)
O(1W)	7030(20)	0	218(15)	74(4)
O(2W)	10340(20)	0	1820(30)	116(8)
O(3W)	9420(30)	0	5060(30)	51(6)
O(4W)	10000	5000	5000	6(2)

Compound 3.17: $(UO_2)(OH)(CO_2)(C_5H_4N)$ (Uoxa-1)

	x	y	z	U(eq)
U(1)	-3042(1)	1708(1)	-4153(1)	15(1)
O(1)	-3809(3)	460(3)	-3284(3)	22(1)
O(2)	-1569(3)	2772(3)	-3660(3)	21(1)
O(3)	-3686(3)	2977(3)	-4141(4)	24(1)
O(4)	-2390(3)	393(3)	-4039(4)	23(1)
O(5)	-4900(3)	876(3)	-6108(3)	21(1)
N(1)	-1778(3)	1773(3)	-1373(4)	18(1)
C(1)	-1234(4)	805(4)	-587(5)	21(1)
C(2)	-550(4)	774(4)	914(5)	21(1)
C(3)	-385(4)	1782(4)	1688(5)	18(1)
C(4)	-974(4)	2776(4)	881(5)	19(1)
C(5)	-1663(4)	2739(4)	-643(5)	19(1)
C(6)	-5324(3)	115(4)	-5819(4)	16(1)

Compound 3.18: $(UO_2)(OH)_2(C_5H_4N)_2$ (Ubpy-1)

	x	y	z	U(eq)
U(1)	3766(1)	7447(1)	-14592(1)	14(1)
O(1)	3669(5)	9077(3)	-14381(2)	23(1)
O(2)	3845(5)	5810(3)	-14707(2)	23(1)
O(3)	728(4)	7255(3)	-14119(2)	21(1)
O(4)	6806(4)	7405(3)	-14104(2)	25(1)
N(1)	3770(6)	7325(3)	-12744(3)	20(1)
N(2)	3955(6)	7286(4)	-7706(3)	30(1)
C(1)	3348(6)	6296(4)	-12258(3)	20(1)
C(2)	3348(6)	6239(4)	-11275(4)	21(1)
C(3)	3786(7)	7283(4)	-10750(4)	18(1)
C(4)	4216(7)	8368(5)	-11252(4)	24(1)
C(5)	4191(7)	8332(5)	-12242(4)	25(1)
C(6)	4394(8)	6287(6)	-8219(4)	31(1)
C(7)	4329(6)	6221(5)	-9206(4)	22(1)
C(8)	3803(8)	7289(5)	-9692(4)	21(1)
C(9)	3380(7)	8336(5)	-9189(4)	25(1)
C(10)	3418(8)	8276(5)	-8198(4)	34(2)

Compound 3.19: $(C_6H_5NH)(UO_2)(PO_4)$ (Ubpe-1)

	x	y	z	U(eq)
U(1)	7019(1)	7088(1)	9027(1)	9(1)
P(1)	2512(2)	7487(2)	10037(1)	10(1)
O(1)	290(6)	7045(6)	9141(4)	17(1)
O(2)	2988(6)	9686(5)	11004(4)	15(1)
O(3)	2960(6)	6160(5)	11014(4)	15(1)
O(4)	3739(5)	7039(5)	8943(4)	13(1)
O(5)	7676(5)	7914(5)	10951(3)	13(1)
O(6)	6400(5)	6278(5)	7064(4)	13(1)
N(1)	-959(7)	7090(7)	15337(5)	18(1)
C(1)	583(9)	8189(8)	16441(6)	19(1)
C(2)	2335(8)	8912(8)	16181(6)	17(1)
C(3)	2423(8)	8476(7)	14765(5)	15(1)
C(4)	771(8)	7310(8)	13638(6)	18(1)
C(5)	-932(8)	6610(8)	13951(6)	18(1)
C(6)	4208(7)	9232(8)	14397(6)	17(1)

Compound 3.20: $Co(UO_2)_2(AsO_4)_2 \cdot 8H_2O$ (CoUAs-1)

	x	y	z	U(eq)
U(1)	2243(1)	7047(1)	9092(1)	8(1)
U(2)	7619(1)	8068(1)	6002(1)	8(1)
As(3)	7463(1)	6298(1)	8813(1)	8(1)
As(4)	2436(1)	8796(1)	6282(1)	8(1)
Co(1)	6696(1)	11434(1)	7363(1)	13(1)
O(1)	4496(6)	7785(5)	6155(3)	12(1)
O(2)	784(6)	8185(5)	5758(3)	12(1)
O(3)	5386(6)	7271(5)	8987(3)	14(1)
O(4)	9085(6)	6909(5)	9358(3)	12(1)
O(5)	8048(6)	6464(5)	7529(3)	14(1)
O(6)	8035(6)	6604(5)	5395(3)	14(1)
O(7)	1828(6)	8464(5)	9761(3)	14(1)
O(8)	7368(6)	4545(5)	9337(3)	14(1)
O(9)	1827(6)	8757(5)	7550(3)	13(1)
O(10)	7229(6)	9574(4)	6605(3)	14(1)
O(11)	2628(7)	10512(5)	5640(3)	16(1)
O(12)	2640(6)	5657(5)	8424(3)	17(1)
O(13)	5856(6)	13253(5)	7994(3)	18(1)
O(14)	10313(7)	4031(5)	7048(4)	21(1)
O(15)	9100(7)	10774(6)	8152(4)	24(1)
O(16)	4317(6)	12155(5)	6573(4)	22(1)
O(17)	5211(7)	10256(5)	8594(4)	26(1)
O(18)	8166(7)	12703(5)	6130(4)	21(1)
O(19)	2283(7)	12268(6)	8793(4)	30(1)
O(20)	3463(8)	5089(6)	5868(5)	28(1)

Compound 3.21: $Mn(UO_2)_2(AsO_4)_2 \cdot 8H_2O$ (MnUAs-1)

	x	y	z	U(eq)
U(1)	2385(1)	6927(1)	9002(1)	8(1)
U(2)	-2256(1)	7972(1)	5913(1)	9(1)
As(3)	2536(1)	8708(1)	6189(1)	9(1)
As(4)	-2440(1)	6214(1)	8723(1)	9(1)
Mn(1)	3273(1)	3564(1)	7610(1)	15(1)
O(1)	4826(7)	4796(5)	6319(4)	32(1)
O(2)	763(6)	4277(5)	6807(4)	29(1)
O(3)	5784(6)	2831(5)	8430(3)	25(1)
O(4)	4179(6)	1738(5)	6956(3)	22(1)
O(5)	1777(7)	2229(5)	8912(4)	27(1)
O(6)	-1897(6)	6266(4)	7458(3)	15(1)
O(7)	1992(6)	8534(4)	7473(3)	15(1)
O(8)	-4507(5)	7204(4)	8869(3)	16(1)
O(9)	4604(5)	7761(4)	5991(3)	15(1)
O(10)	-2600(6)	4505(4)	9361(3)	15(1)
O(11)	901(5)	8109(4)	5660(3)	14(1)
O(12)	2614(6)	10454(4)	5666(3)	15(1)
O(13)	-1876(6)	6584(4)	5252(3)	15(1)
O(14)	-2637(6)	9347(4)	6574(3)	17(1)
O(15)	2769(5)	5452(4)	8399(3)	14(1)
O(16)	-787(5)	6840(4)	9223(3)	14(1)
O(17)	1996(6)	8357(4)	9607(3)	14(1)
O(1W)	-3489(7)	9889(5)	9138(4)	33(1)
O(2W)	7761(7)	2724(6)	6185(4)	34(1)
O(3W)	-328(7)	10926(5)	7947(4)	27(1)

Compound 3.22: $Cu(UO_2)_2(AsO_4)_2 \cdot 5H_2O$ (CuUAs-1)

	x	y	z	U(eq)
U(1)	2500	2500	3891(1)	9(1)
Cu(1)	2500	2500	8779(5)	16(1)
As(1)	7500	2500	5000	9(1)
O(1)	2500	2500	1853(14)	14(3)
O(2)	2500	2500	5935(14)	14(3)
O(4)	5692(15)	1978(15)	3839(8)	13(2)
O(1W)	3180(30)	-150(20)	8849(9)	45(6)

Appendix IV: Bond Valence Calcualtion

The Bond valence calculations performed for the aforementioned compounds were determined using equations from reference,[1,2] as well as parameters from Burns et. al. The following general equations is used with variable defined accordingly:

$$\nu_{ij} = \exp[(R_{ij}-d_{ij})/b],$$

Where ν_{ij} is the valence of an atom determined by the bond between two atom i and j and the sum of such bonds. The variable b is the 'univeral' constant and variable Rij is the bond valence parameter calculated from observed crystal structure data. Both variables are dependent on the coordination around the uranium center and the following constants were used:

6-coordinate U6+	Rij = 2.074 Å	b = 0.554 Å
7-coordinate U6+	Rij = 2.045 Å	b = 0.510 Å
8-coordinate U6+	Rij = 2.042 Å	b = 0.506 Å

The constant dij is found in the single-crystal structure data and completes the calculations for bond valence sum.

References:

1. Brese, N. E.; O'Keeffe, M. *Acta Crystallogr.* 1991, *B47*, 192.
2. Brown, I. D. The Chemical Bond in Inorganic Chemistry: The Bond Valence Model. Oxford University Press, 2002. c) Brown, I. D.; Altermatt, D. *Acta Crystallogr*. 1985, *B41*, 244.